DISPROPORTIONATE COLLAPSE PREVENTION ANALYSES FOR MID-RISE CROSS-LAMINATED TIMBER PLATFORM-TYPE BUILDINGS

by

Hercend Mpidi Bita

B.Eng., Anglia Ruskin University, United Kingdom, 2013

M.Sc., The University of Salford, United Kingdom, 2014

A THESIS SUBMITTED IN PARTIAL FULFILMENT OF

THE REQUIREMENTS FOR THE DEGREE OF

DOCTOR OF PHILOSOPHY

in

THE FACULTY OF GRADUATE AND POSTDOCTORAL STUDIES

(Forestry)

THE UNIVERSITY OF BRITISH COLUMBIA

(Vancouver)

May 2019

© Hercend Mpidi Bita, 2019

The following individuals certify that they have read, and recommend to the Faculty of Graduate and Postdoctoral Studies for acceptance, the dissertation entitled:

Disproportionate Collapse Prevention Analyses for Mid-rise Cross-laminated Timber Platform-type Buildings

submitted by   Hercend Mpidi Bita   in partial fulfillment of the requirements for

the degree of   Doctor of Philosophy

in   Forestry

Examining Committee:

Thomas Tannert
Supervisor

Marjan Popovski
Supervisory Committee Member

Supervisory Committee Member

Perry Erwin Adebar
University Examiner

Matthias Militzer
University Examiner

Abstract

Abnormal loads which can cause initial damage may trigger collapse propagation, leading to disproportionate collapse of buildings with insufficient structural robustness. To ensure structural safety, design approaches against this catastrophic collapse are embodied within the building regulations. Nevertheless, the application of existing guidelines for disproportionate collapse prevention for mid- to high-rise mass-timber buildings -as an emerging construction method- becomes unpractical and uneconomic; and research studies in this topic are scarce.

This thesis contributes to the body of knowledge with respect to structural robustness and disproportionate collapse prevention for mid-rise platform-type cross-laminated timber buildings through analytical, numerical, and experimental analyses. Nonlinear dynamic numerical analyses, using the sudden element removal, are performed on twelve- and nine-storey buildings to study their responses after initial damage. The analytical approach applies linear-elastic static equilibrium to estimate the minimum strength, stiffness, and ductility to ensure structural robustness. From subsequent reliability analysis, the results show that without considerations of the complexities associated with disproportionate collapse, mid-rise cross-laminated timber platform-type buildings have a high probability of disproportionate collapse. A structural optimisation procedure is then proposed to achieve a target performance and ensure structural safety. From the worst-case scenario, novel connection detailing is then proposed to trigger catenary and hanging actions as collapse resistance mechanisms. The proposed detailing using steel tubes and rods is numerically investigated and optimised. Then, results from experimental tests confirm that when the tubes and rods are implemented as floor-to-floor detailing, mass-timber floor system can trigger catenary action as a collapse resistance mechanism following the loss of internal loadbearing wall.

Lay Summary

Limited damage to buildings from abnormal loadings, caused by human errors during design or construction, explosions, terrorist attacks, sabotages or natural catastrophes, are acceptable. However, since it was observed that fatalities in previous incidents were mainly caused by collapsing buildings rather than the extreme event itself, buildings must be designed to remain stable for sufficient time to allow for evacuation. The research in this thesis presents numerical analyses, analytical procedures and experimental tests to evaluate the structural performance of mid-rise timber buildings after an assumed initial damage following abnormal loadings. The findings provide design guidance which may be used by structural engineers to prevent disproportionate collapse and ensure structural safety for mid-rise timber buildings.

Preface

I, the author of this thesis, am the main investigator of this research project. Parts of this study have been published in journal papers and conference proceedings, and others are currently under review for future journal publications. I am the primary authors of all these manuscripts; and my co-authors (Dr. Thomas Tannert, Dr. Neil Currie, Dr. Marjan Popovski, Johannes A.J. Huber and Konstantinos Voulpiotis) provided guidance, technical inputs, and reviews. I was responsible for all analyses and designs, as well as conducting the experimental tests and preparing the manuscripts.

Mpidi Bita, H. & Tannert, T. (2019). Tie-force Procedure for Disproportionate Collapse Prevention of CLT Platform-type Construction. Engineering Structures 189: 195-205.

Mpidi Bita, H. & Tannert, T. (2019). Disproportionate Collapse Prevention Analysis for a Mid-rise Flat-Plate Cross-laminated Timber Building. Engineering Structures 178: 460-471.

Mpidi Bita, H., Currie, N. & Tannert, T. (2018). Disproportionate Collapse Analysis of Mid-rise Cross-laminated Timber Buildings. Structure & Infrastructure Engineering 14: 1547-1560.

Mpidi Bita, H. & Tannert, T. (2018). Numerical Optimisation of Novel Connection for Cross-Laminated Timber Buildings. Engineering Structures 175: 273-283.

Mpidi Bita, H., & Tannert, T. Experimental Study of Disproportionate Collapse Mechanisms for Mass-timber floor Systems. (Submitted).

Mpidi Bita, H., Huber, J.A.J., Voulpiotis, K. & Tannert, T. Survey of Contemporary Practices for Achieving Structural Robustness. (Submitted).

Mpidi Bita, H., & Tannert, T. Catenary Action for Cross-Laminated Timber Floor Systems. The 6th INTER Meeting, August 26-29, Tacoma, USA.

Mpidi Bita, H., Popovski, M. & Tannert, T. (2019). Experimental Study of Disproportionate Collapse Resistance Mechanisms for Mass-timber Buildings. ASCE Structure Congress, April 24-27, 2019, Orlando, USA.

Mpidi Bita, H. & Tannert, T. (2018). Alternate Load-path Analysis for Mid-rise Mass-timber Buildings. ASCE Structure Congress, April 19-21, 2018, Fort Worth, USA.

Mpidi Bita, H. & Tannert, T. (2018). Numerical Optimisation of Novel Resilient Connection for Mass-timber Buildings. World Conference on Timber Engineering WCTE, August 20-23, 2018, Seoul, South Korea.

Mpidi Bita, H. & Tannert, T. (2018). Disproportionate Collapse Investigation for Mid-rise Timber Buildings. World Conference on Timber Engineering, WCTE, August 20-23, 2018, Seoul, South Korea.

Mpidi Bita, H. & Tannert, T. (2017). Robustness of Multi-storey Timber Buildings. International Association for Bridge and Structural Engineering Symposium, IABSE, September 21-23, 2017, Vancouver, Canada.

Mpidi Bita, H. & Tannert, T. (2017). Disproportionate Collapse for Mid-rise Mass-timber Buildings. China-Canada Symposium on Structural and Earthquake Engineering. August 20-24, 2017, Vancouver, Canada.

Mpidi Bita, H., Currie, N. & Tannert, T. (2017). Reliability Analysis and Disproportionate Collapse for Multi-storey Cross-Laminated Timber Building. World Conference on Earthquake Engineering, WCEE, January 9-13, 2017, Santiago, Chile.

Mpidi Bita, H., Currie, N. & Tannert, T. (2016). Assessment of Disproportionate Collapse for Multi-storey Cross-Laminated Timber Buildings. World Conference on Timber Engineering, WCTE, August 22-25, 2016, Vienna, Austria.

Mpidi Bita, H. & Currie, N. (2015). Assessment of Disproportionate Collapse for Tall Timber Buildings. Salford Postgraduate Annual Research Conference, SPARC, May 26-28, Manchester, United Kingdom.

Table of Contents

List of Tables

List of Figures

List of Abbreviations

ALPA   : Alternate load-path analysis

ALHS   : Advanced Latin Hypercube Sampling

AS/NZ   : Australia and New Zealand Building Code

ASTM   : American Society of Testing and Materials

BCBC   : Building Code of British Columbia

CHSS   : Circular hollow steel section

CLT   : Cross-laminated Timber

CSA-O86   : Canadian Standard Association: Engineering design in wood

CSA   : Canadian Standard Association

EA   : Evolutionary Algorithm

EEEP   : Equivalent Energy Elastic Plastic

ETA   : European Technical approval of connectors

EWPs   : Engineered Wood Products

FE   : Finite element

FEA   : Finite Element Analysis

FORM   : First Order Reliability Method

GCWood   : Green Construction Through Wood

GLT   : Glued-laminated Timber (GLT)

GSA   : General Service Administration

LLRS   : Lateral load-resisting system

LHS   : Latin Hypercube Sampling

LSF   : Limits state functions

LSL   : Laminated strand lumber

LVL   : Laminated veneer lumber

MSR   : Machine stress-rated lumber

NCC   : National Construction Code

NBCC   : National Building Code of Canada

PDF   : Probability distribution function

RBDO   : Reliability-Based Design Optimisation

SG   : Stress grade for mass-timber element

SPF   : Spruce-Pine Fir lumber

STS   : Self-tapping screw

TF2000   : Timber-frame 2000 research project

TRADA   : Timber Research and Development Association

UFC   : Unified Facilities Criteria

ULS   : Ultimate limit state

VBRA   : Variance-based robustness analysis

List of Symbols

α_x	: Term related to the transverse tie (F_x) for cantilever action
a_L	: Loaded end-distance, from the centre of the tube to the edge of the mass-timber panel
β_x	: Term related to the horizontal shear (S_h) for cantilever action
β	: Reliability index
B_Y	: Vertical loads on top of the wall below the affected floor
C	: Compressive force at the root of the cantilever action
c	: Diameter of the weld-coupler area
C_f	: Cost of failure
C_o	: Cost / mass of the building
CoP	: Coefficient of prognosis
CoV	: Coefficient of variation
C_R	: Axial compression resistance of CLT wall panel
Δ	: Deformation demand of connection before fracture
δ	: Deflection demand of the CLT floor panel
Δ_1	: Applied vertical deflection at maximum compressive action
Δ_2	: Applied vertical deflection at catenary action
Δ_{lim}	: Deformation limit of connection before fracture
δ_{lim}	: Maximum allowable deflection of the CLT floor panel
Δ_L	: Maximum allowable deflection for the longitudinal direction
Δ_{max}	: Maximum allowable floor deflection at the location of the removed element
Δ_T	: Maximum allowable deflection for the transverse direction

Δ_Y	: Maximum deflection of the floor panel
δ_L	: Total axial elongation for catenary action in the longitudinal direction
δ_{Ls}	: Axial elongation at the floor-to-wall connection, for longitudinal direction
δ_{Lm}	: Axial elongation for the floor-to-floor connection, for the longitudinal direction
δ_T	: Total axial elongation for catenary action in the transverse direction
δ_{Ts}	: Axial elongation at the floor-to-wall connection, for transverse direction
δ_{Tm}	: Axial elongation for the floor-to-floor connection, for the transverse direction
D	: Considered initial damage
d_f	: Diameter of fastener (screw)
d_t	: Tube diameter
d	: Depth of the floor
$deg.$	: Degree angle
DCR	: Demand-capacity ratio
DIF	: Dynamic increase factor
DF	: Dynamic factor
DL	: Dead loads
δ_t	: Deformation at the weld-coupler area
d_r	: Steel rod diameter
E	: Young's modulus
E_{el}	: Young's modulus of steel components
$E_{el,w}$	: Elastic moduli of M_2
E_F	: Steel tube strength-loss slope
EI_{eff}	: Effective bending stiffness of CLT panels

$E_{F,w}$: Strength-loss slope of M_2

El : Loadbearing element

E_{LC} : Extreme Load combination

$E_{pl,w}$: Plastic moduli of M_2,

EQ : Equivalent static loads

EQ_{Hd} : Hold-down forces at each level from seismic analysis

$EQ_{H,sh}$: Horizontal inter-storey shear on walls from seismic analysis

EQ_L : Floor-to-floor horizontal longitudinal shear from seismic analysis

EQ_T : Floor-to-floor horizontal transverse shear from seismic analysis

$EQ_{V,sh}$: Vertical shear between walls from seismic analysis

F : Transverse tie-force at the roof of the cantilever action

F_a : Applied vertical loads during experimental tests

f_b : Bending strength of the CLT floor panels

f_C : Compressive strength of the CLT wall panels

F_{com} : Maximum load during compressive arching for all tested floor assemblies

F_{dyn} : Applied loads from dynamic analysis at global level

F_L : Longitudinal tie force for catenary action

f_L : Uniaxial compressive strength in the longitudinal direction

F_{max} : Maximum load carrying capacity for all tested floor assemblies

f_s : Shear strength of the CLT panels

F_r : Highest distributed transverse tie acting at the roof for cantilever action

$F_{T,L}$: EN1991-1-7 Basic tie strength

F_T : Transverse tie forces catenary action

f_T	: Uniaxial compressive strength in the transverse direction
F_t	: Tensile or tie force during testing
$F_{t,a}$	: Tensile or tie force hand calculations
F_{tot}	: The total capacity (F_{tot}) of the joint
F_u	: Load-carrying capacity
F_v	: Minimum vertical tie force
F_x	: Distributed Transverse tie at storey-x for cantilever action
F_y	: Capacity of connection
$F_{y,t}$	: Target yield force of steel tubes
F_X	: Maximum axial forces at the connection level
g_a	: Gravity ($10 m/s^2$)
g	: Limit State Function (g)
G	: Shear modulus
$g_j(X_i)$	: Considered Limit state function j with Xi
H	: Inter-storey height
H_i	: Considered abnormal load
I	: Any level in the building; the level of interest
IF	: Importance factor
I_p	: Polar moment of area
K	: Rotational stiffness of the connection
K_e	: Elastic stiffness of connection
K_{ser}	: Axial stiffness of the joint under service load
K_{tot}	: Total connection stiffness

L	: Longitudinal ties
L_e	: Extraordinary live load
L_{eff}	: Effective CLT floor span according to EN1995-1-1
L_L	: Single longitudinal floor span
LL	: Live load
L_s	: Sustained live load
L_T	: Single transverse floor span
M_1	: Original model of the nine-storey flat-plate CLT building
M_2	: Improved model of the nine-storey flat-plate CLT building
$M1$	: Steel properties of the overall tube
$M2$	: Steel properties between the weld-coupler
M_A	: Applied moments from the rotation of the cantilever
MBM_R	: Maximum bending moment resistance of CLT panels
$Mean$	: Mean value of the PDF
MR	: Resisting moment against M_A
M_R	: Bending moment resistance of the floor panel
MSF_R	: Maximum shear force resistance of CLT panels
n	: Provided number of fasteners
N	: Total number of storey in the building
NF	: Nonlinear factor
n:	: Storey level of the removed wall
n_P	: Total number of panels in the floor transverse direction
μ_m	: Mean value of random variable

μ	: Ductility ratio
M_Z	: Bending moment in the floor panel at the location of the removed element
n_F	: Number of layers of CLT floor panels
n_W	: Number of layers of the CLT wall panels
N_{RV}	: Total number of considered input variable
Opt-2	: Second optimised tube connection
Opt-1a and b	: First optimised tube connection
P	: Peripheral tie
P_a	: Force on the steel tube during modelling
$P[DC]$	: Probability of disproportionate collapse
$P[H_i]$	: Probability of abnormal loadings
$P[D|H_i]$	: Probability of initial damage given the abnormal load H_i
$P[F|DH_i]$	: Probability of failure propagation given D and H_i
P_e	: Probability of exceedance
R^2	: Quality of the fitted regression to the data
R	: Structural resistances
Rad	: Angle radian
R_d	: Ductility factor
R_o	: Over-strength factor
ρ_m	: Mean density of timber
s	: Number of shear planes
θ	: Rotational capability of the connections
S	: Structural demands

S_1 : Results of the static analyses of twelve-storey CLT platform-type construction

S_2 : Results of the dynamic analysis of twelve-storey CLT platform-type construction

σ_0 : Normal stress for the longitudinal layers of CLT floor panel

σ_{90} : Normal stress of the transverse layers of CLT floor panel

$\sigma_{F,w}$: Failure stress of M_2; defined as 80% the selected $\sigma_{u,w}$.

σ_{par} : Compressive stresses parallel

$\sigma_{u,w}$: Ultimate strength for M_2

$\sigma_{y,w}$: Yield strength of M_2

σ-level   : Number of standard deviations about the mean of the sample

sec   : Time seconds

SID : Superimposed dead load

S_h : Horizontal inter-storey shear

SL : Snow loads

SLS   : Serviceability limit state

S_R : Shear force resistance of the floor panel

$Stdv$: Standard deviation of the PDF

S_v : Vertical shear between the cantilever and the support sections

S_Y : Maximum applied shear forces on the CLT panel

SW : Self-weight of wood

t : Tube thickness

T : Transverse tie

τ_R : Rolling shear strength of CLT floor panels

$t_{L,F}$: Thickness of the longitudinal layers of the CLT floor panel

t_r	: Speed of removal
$t_{L,W}$	: Thickness of the longitudinal layers of the CLT wall panel
$t_{T,F}$	: Thickness of the transverse layers of the CLT floor panel
$t_{T,W}$	: Thickness of the transverse layers of the CLT wall panel
TF	: Tie-force
$Tube_1$	: Steel tube of 50.8mm diameter
$Tube_2$	: Steel tube of 76.2mm diameter
$Tube_3$	: Steel tube of 101.6mm diameter
v	: Poison ratio
U	: Total energy dissipated
V	: Vertical tie
w	: Width of individual CLT panel
w_f	: Floor load
W_{f1}	: Weight of the cantilever after wall removal
WL	: Wind load
w_s	: Design weight of a single storey under extreme load combination
x:	: Storey x within the cantilever, under design consideration
w_w	: Weight of the wall
w_f	: Design floor weight under extreme load combination
$w_{f,max}$	: Maximum floor loads of the CLT panels
X_i	: Represented an input random variable i

Acknowledgements

I wish to express my sincere thanks to my supervisor Dr Thomas Tannert for his endless support, guidance and mentorship. His advice and encouragement always helped to push my limits and maintain excellent work ethics.

My deep sense of gratitude also goes to Dr Neil Currie who cultivated this desire to pursue further studies on this topic of disproportionate collapse prevention. His advice and support always motivated me to work towards 'making the skylines of the world safer'.

Likewise, my sincere thanks to my PhD committee members Drs Marjan Popovski, Frank Lam and Carlos Ventura for their constant support in providing my research with fresh ideas. They have shared their knowledge and provided answers to keep me on the right direction.

Thanks to George Lee for his technical advices during my experimental testing, MyTiCon Connectors Inc, Simpson Strong-Tie Company Inc, and Structurlam Mass-timber Corporation for providing testing materials. I also thank my colleagues Kuldeep Kaushik, Afrin Hossain, Md Shahnewaz, Steve Jeon, Johannes Huber and Konstantinos Voulpiotis for providing reference documents that helped in my research.

Special thanks to my friends Adam Yang, Jennifer Na and Josephine Wong for always being there for me. I am deeply grateful to Alexia Cadoret for her love, sacrifices, and support every time I needed her.

Lastly, I would like to thank my parents, my brother Isaac and my family for giving me this opportunity for a better life. Their sacrifices in supporting my studies were key to my success. Even miles away, I have always felt their presence which kept me going until the end.

Dedication

To my parents, my family and Steve Wengi Boleilanga

Chapter 1: Background

1.1 Urban Population Growth and Sustainable Construction

In recent years, concerns raised with respect to the number of people in urbanised cities. Statistics have shown that in the next two decades, nearly 60% of the world's population will be living in urban areas (UN-Habitat, 2008). By the middle of the twenty-first century, population in urban cities is estimated to go from 3.4 billion in 2009 to 6.4 billion in 2050 (United Nations, 2015). The stated statistics highlight the demand for housing. Multi-storey buildings may respond to the housing demand and capitalise on dwindling city centre land availability (Ali and Moon, 2007; Green and Karsh, 2012). Consequently, the number of tall buildings for residential purposes will have to skyrocket at the same rate as the population in urban cities. Nevertheless, with the question of sustainability issues related to the construction industry, there is a need to revaluate the choice of materials for structural purposes for the new buildings. Consequently, cities like Vancouver, in Canada, stated their ambitions to target zero emissions in all new building constructions by 2030 (City of Vancouver, 2018).

Considering the advantages it offers with respect to sustainability, many authors (Green and Karsh, 2012; Ramage et al., 2017; WoodCampusUK, 2017) have proposed the shift to timber as a structural material for the construction for the forthcoming world's skyline. The use of timber is one approach to reduce greenhouse gas emissions by enabling construction of structures described as zero-carbon or carbon-negative (Ramage et al., 2017). Given its renewability and its low environmental impact, in addition to be an attractive building material, it can be argued that: "if the nineteenth century was the century of steel, and the twentieth the century of concrete, then the twenty-first century is about engineered timber (Wood Solutions, 2018). Nevertheless, with the

history of fire losses in timber buildings, area and height restrictions were imposed on buildings with combustible material by numerous building codes around the world (Buchanan et al., 2014). In the 2010 version of the National Building Code of Canada (NBCC) (NBCC, 2010a), the height of light-frame residential timber buildings was limited to four storeys.

1.2 Mass-timber Construction

Mass-timber constructions, with Engineered Wood Products (EWPs), come as an answer to not only improve the fire safety but also the overall structural performance that can push the feasible height of timber for taller buildings. In the current marketplace, mass-timber panels are Cross-Laminated Timber (CLT), see Figure 1-1a, Laminated Strand Lumber (LSL), see Figure 1-1b, and Laminated Veneer Lumber (LVL), see Figure 1-1c, whereas Glued-Laminated Timber (GLT) in Figure 1-1d are used as beams or columns. CLT is composed of several layers of lumber, typically three to nine alternating layers, glued together crosswise to their wider faces to form dimensionally stable panels that can be used as floor or wall segments. LSL are floor or wall segments manufactured from strands of wood, oriented parallel to the span direction, blended with adhesive. LVL are mass-timber panels composed of laminating veneer sheets of wood, laid in the span direction and coated with exterior-type adhesive to form floor and wall segments. GLT are lamination boards stacked up and glued together to make the total cross-section, then cut into required beam or column width.

EWPs have reliable structural material properties, with improved fire performance, and durability as compared to traditional lumbers (Green and Karsh, 2012). Recent efforts from extensive studies, confirming adequate seismic performances (Fragiacomo et al., 2011; Izzi et al., 2018; Pei et al., 2016; Popovski and Gavric, 2015) and fire (Buchanan et al., 2014; Buchanan and Abu,

2017), as well as feasibility proposals for tall buildings (Green and Karsh, 2012; SOM, 2013; Wells, 2011), helped to overcome the imposed area and height limitations for timber buildings. The Building Code of British Columbia (BCBC) in Canada was the first to allow six-storey timber buildings (BCBC, 2012). Figure 1-2 illustrates the improvements in height regulations for wood structures as per BCBC. Other Canadian provinces followed similar trends. At Federal level, Green Construction Through Wood (GCWood) program was launched to address the technical gaps preventing the construction of tall timber building in order to facilitate revision of the 2025 NBCC (GCWood, 2017). Similar changes in jurisdictions and buildings codes are observed around the world to allow the construction of tall timber buildings.

(a)   *(b)*

(c)   *(d)*

Figure 1-1: EWPs: (a) CLT; (b) LSL; (c) LVL; and (d) GLT (Photo credit Mpidi Bita)
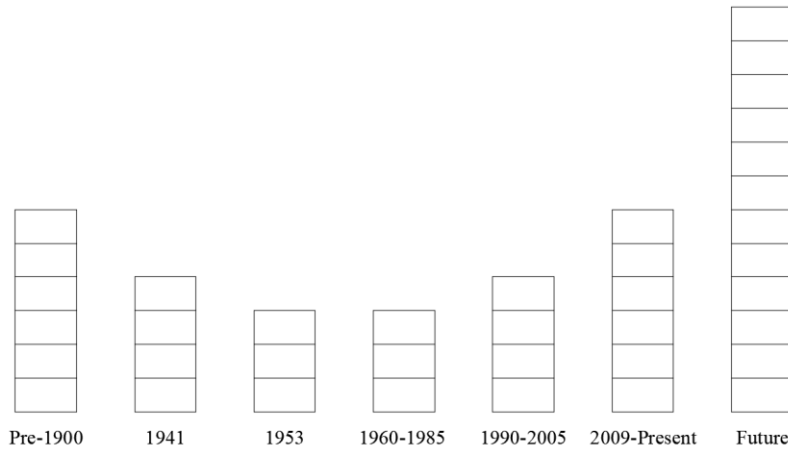
Figure 1-2: Trends towards tall timber buildings (Green and Karsh, 2012)

1.3 Typical Mass-timber Constructions

1.3.1 Platform-type Construction

A platform-type construction is composed of mass-timber walls and floor panels, e.g. CLT, LVL and LSL designed to carry gravity and/or lateral loads (Shahnewaz et al., 2018) where the floor panels act as a platform for the next level, as shown in Figure 1-3a. Typical floor-to-wall detailing for CLT platform-type construction are: self-tapping screws (STS) that connect the floors to the walls below, and angle brackets fastened with wood screws or nails that connect the floors to the walls above.

(a)   *(b)*

Figure 1-3: (a) Platform-type mass-timber building (Photo credit Lendlease); and (b) Compression perpendicular to the grain (Photo credit: Mpidi Bita)

For the floor system, the detailing can be two single span CLT panels, connected over or near the middle loadbearing wall by means of STSs; or double span CLT panel, continuous over the internal support. In both cases, the floor panels, resting on the walls to carry the gravity loads, are assumed to be simply supported. On the wall system, hold-down and angle brackets fastened with wood screws or nails are designed for uplift and shear forces, respectively, resulting from lateral loads (Popovski and Gavric, 2015; Rinaldin and Fragiacomo, 2016). Nevertheless, having the floor between the walls creates compressive stresses perpendicular to the grain of the floor panels, as shown in Figure 1-3b, which become significant with the increase in building height. Consequently, mass-timber platform-type construction is limited to ten to twelve storeys high.

1.3.2 Flat-plate Construction

A flat-plate structural system, also known as flat-slab, is a gravity load-resisting system where the mass-timber floor panels are directly supported by columns without beams. Mass-timber panels in platform-type can be used as lateral load-resisting system. From an architectural point of view, not having beams enables to have a clear storey. As shown in Figure 1-4a, the detailing can ensure

direct load transfer from the column above to the column below without affecting the floor. From a structural point of view, without the beams, the point supported floor systems behave as a two-way system (Fast and Jackson, 2017).

(a)   *(b)*
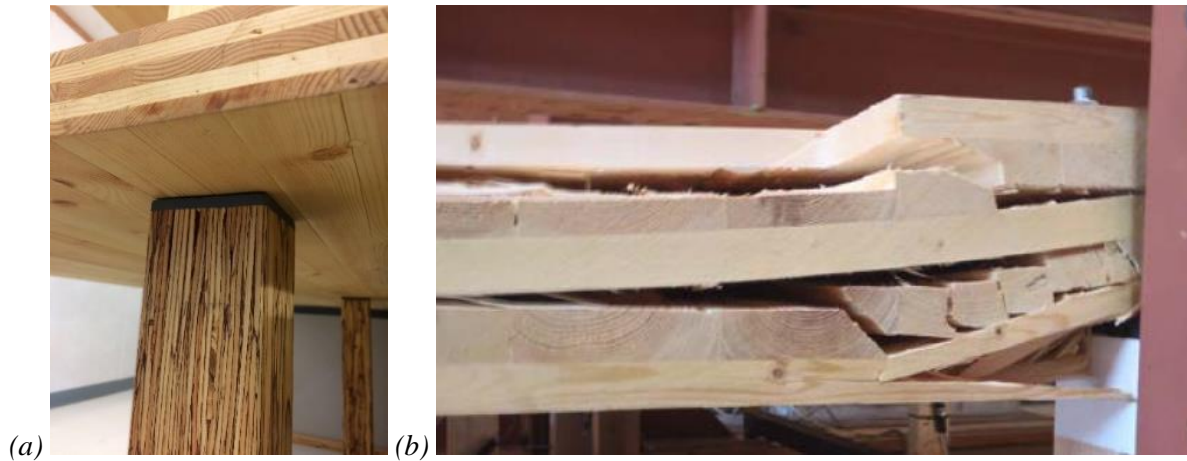
Figure 1-4: (a) Flat-plate mass-timber building (Photo credit Mpidi Bita); and (b) Rolling shear failure from experimental testing (Popovski et al., 2016) (Reprinted with permission)

Under gravity loads, analytical (Fast and Jackson, 2017) and experimental (Popovski et al., 2016) works done on flat-plate mass timber buildings demonstrated that in addition to stiffness and bending requirements, rolling shear stresses were of high concern for this structural system. For this failure mode, as shown in Figure 1-4b, the fibres of timber roll over each other due to the applied shear forces perpendicular to the grain. Nevertheless, for CLT panels, rolling shear capacities can increase with additional restraints from the compressive forces near the supports (Diestsch and Brandner, 2015). Consequently, additional considerations are required for CLT floor in flat-plate system to limit rolling shear and provide direct column-to-column load transfer.

1.3.3 Post and Beam Construction

EWPs beam and column can be used in a post and beam system as shown in Figure 1-5a. For the gravity load-resisting system, the area loads on the floor panels are transferred to the beams, then to the columns. For the lateral load-resisting system, GLT can be used to form a truss system for stability as shown in Figure 1-5b. A range of well-established connection detailing exists for mass-timber buildings in a posts and beam system; these are mainly dowel type connectors with the design given in building codes. The connections are designed for shear and axial tension/compression; and they are usually assumed to have no rotation restraints. For dowel type of connectors, detailing ensures sufficient spacing to avoid brittle wood failure (row shear, group tear-out, or net tension) and encourage ductile failure of dowels through the estimation of yield resistance.

(a)   *(b)*
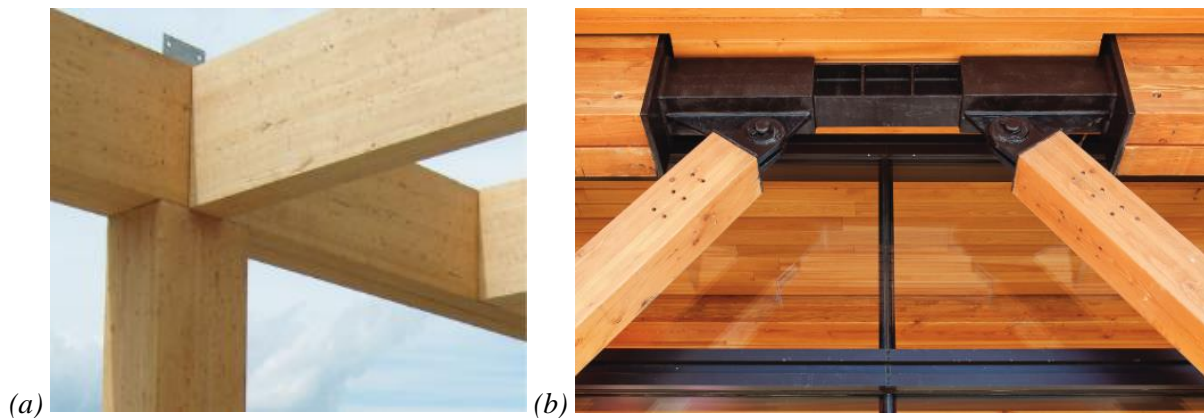
Figure 1-5: Post and beam mass-timber building: (a) Gravity load-resisting system; and (b) Lateral load-resisting system (Photo credit Matthew Millman)

1.3.4 Hybrid Mass-timber Construction

In a hybrid mass-timber construction, the structural system is composed of EWPs as well as concrete and/or steel components. Herein, the choice of material is made based on the advantages

offered by the material properties. For example, on a mass-timber building where timber is the main structural material, concrete is selected for components to take large lateral forces such as shear walls, steel for elements mainly in tension such as tension bracings/cables.

1.4 Mid and High-rise Timber Building Examples

The Stadthaus apartment building in the United Kingdom (UK), shown in Figure 1-6a, is an eight-storey timber building with CLT walls and floors (Wells, 2011). This is a platform-type construction where the floor panels are placed on top of the walls below to form a platform for the next storey. For the Stadthaus, all structural components, including stairs and elevator shafts, are made of timber. The floors are CLT panels, and the CLT walls are loadbearing designed as gravity and lateral load-resisting systems. At its completion in 2009, the Stadthaus apartment building was the world's tallest contemporary timber residential building. The same structural concept was used for the construction of the four-storey CLT Redstone Arsenal hotel in the USA, shown in Figure 1-6b. CLT are used for all exterior and interior walls, floors and roof deck. At its completion in 2016, the Redstone Arsenal hotel was the first mass-timber construction for military purposes in the USA (Wood-Works, 2016).

(a)

(b)

Figure 1-6: Platform-type construction: (a) Stadthaus (Photo credit Will Pryce); and (b) Redstone Arsenal (Photo credit Lendlease)

The Treet building in Norway, shown in Figure 1-7a, is a fourteen-storey residential building composed of GLT trusses and intermediate concrete power storeys, designed to carry the wood structure above (Abrahamsen and Malo, 2014). The trusses give the building its necessary lateral stiffness, while the power storeys carry gravity loads from the four-level residential modules above. At its completion in 2015, the Treet building was the tallest timber truss construction in the world. The Mjøstårnet in Norway, shown in Figure 1-7b, is an eighteen-storey residential and office building with GLT trusses along the facade and internal GLT beams and columns (Abrahamsen, 2017). The gravity loads are carried by beams and columns in a post-and-beam

construction. The trusses provide lateral stiffness for gravity and lateral loads; wooden floor composed of GLT beams and LVL panels are used for the floor system up to the 11th storey, and concrete decks are used for the remaining storeys. At its completion in 2019, the Mjøstårnet building was the tallest timber truss construction in the world.
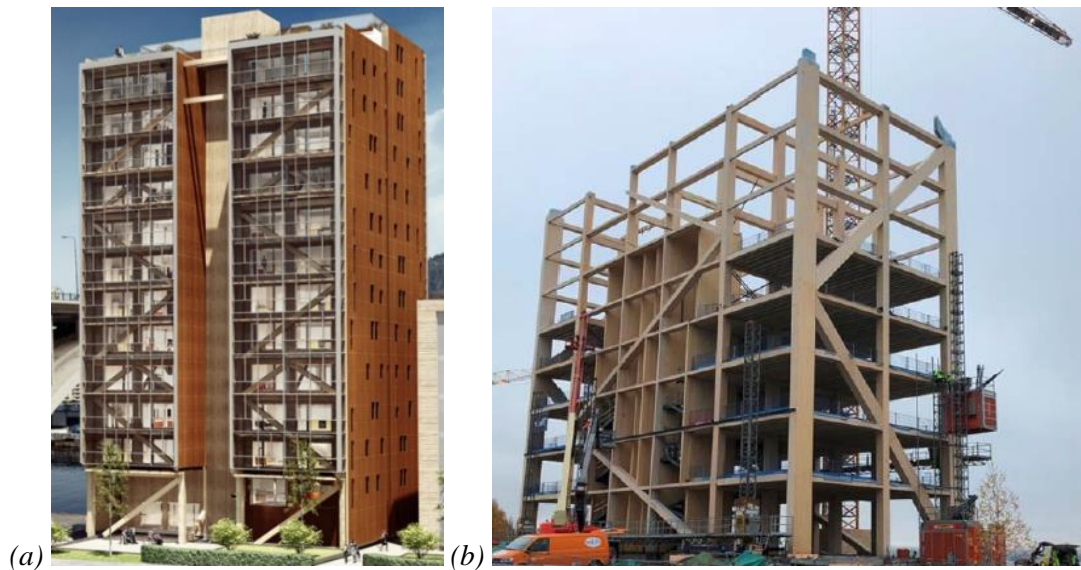
Figure 1-7: Post-and-beam construction: (a) Treet (Abrahamsen and Malo, 2014)*; and (b) Mjøstårnet* (Abrahamsen, 2017) *(Reprinted with permission)*

The Brock Commons shown in Figure 1-8a is an eighteen-storey timber-concrete hybrid building in Canada. It is composed of two concrete cores to resist the lateral loads (Fast and Jackson, 2017). The gravity load-resisting system is made of CLT floor panels resting on GLT columns, forming a point supported system also known as flat-plate construction. At its completion in 2017, the Brock Commons was the world's tallest timber hybrid building. The twenty-three-storey HoHo building shown in Figure 1-8b is a timber-concrete hybrid building in Austria (Woschitz and Zotter, 2017). The lateral load-resisting system is composed of a central concrete core. For the gravity load-resisting system, the surrounding frames with GLT columns and concrete beams carry

the CLT-concrete composite floors. At its completion in 2018, the HoHo building was the world's tallest timber hybrid building.

Figure 1-8: Hybrid construction: (a) Brock Commons(Photo credit Mpidi Bita); (b) and HoHo (Woschitz and Zotter, 2017) *(Reprinted with permission)*

1.5 Disproportionate Collapse

'Designing and building mass-timber structures also in earthquake-prone regions is no longer a domain for early adopters, but is becoming a part of regular timber engineering practice' (Tannert et al., 2018). Although high-rise buildings are gaining interest in North America and the rest of the world, there is still a big gap to cover, and more detailed analyses as well as laboratory testing are required to improve their understanding (Green and Karsh, 2012). Among the areas in need for further research, the performance against disproportionate collapse can be listed (TRADA, 2009). Initial damages from extreme or abnormal loadings not considered in the design stage have a risk of propagation, which can lead to the collapse of a significant part of the structure. As per EN1991-1-7 (CEN, 2006a), relative to the initial damage, a collapse is disproportionate when it goes beyond 15% of the floor area of the affected storey or 100m^2, whichever is less, and does extend further

than the immediate adjacent storey. Figure 1-9 shows the thresholds for permissible collapse following an initial damage, where '*el*' is the assumed initial damage and the hashed zones are illustrations of the aforementioned collapse thresholds.

(a)   *(b)*
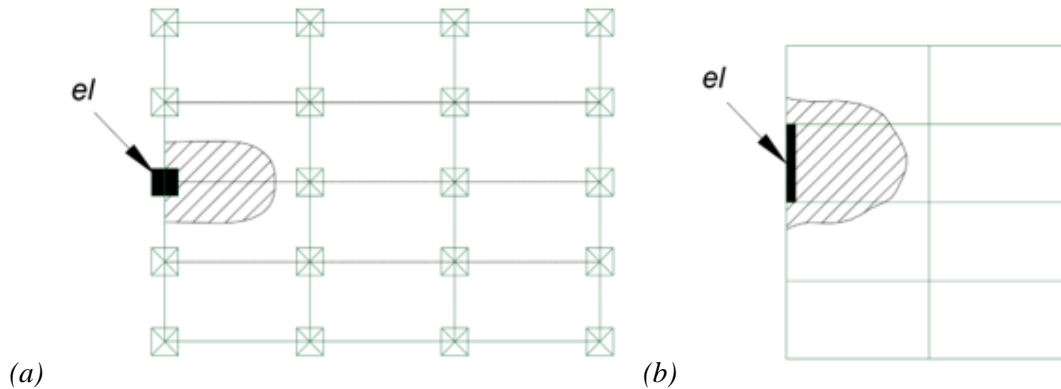
Figure 1-9: Acceptable collapse thresholds (CEN, 2006a)*: (a) Plan; and (b) Elevation*

Disproportionate collapse events have a low rate of occurrence, but they do imply serious risk for human lives (ASCE, 2013). The first of this nature was the Ronan Point apartment incident in 1968, where a gas explosion caused direct failure of a vertical loadbearing wall which in turn triggered the collapse of a major part of the building as shown in Figure 1-10a (Macleod, 2014). The collapse of the World Trade Centre, in 2001, after terrorist attack, is another example that illustrates the high risk of collapse propagation after initial damage. The collapse of the Bad Reichenhall ice area in 2006, as shown in Figure 1-10b, is the most prominent example of disproportionate collapse for timber structures. Herein, numerous causes were revealed after investigations, including manufacturing and construction errors, leading to the failure of one of the roof box-girders after heavy snow loads, which eventually propagated to the collapse of the whole structure (Winter and Kreuzinger, 2008). The aforementioned incidents show that fatalities are mainly caused by collapsing buildings or structural elements rather than the extreme loading itself.

Figure 1-10: Disproportionate collapse incidents: (a) Ronan Point apartment (Macleod, 2014)*; and (b) Bad Reichenhall ice area* (Winter and Kreuzinger, 2008)*(Reprinted with permission)*

1.6 Motivation

The load-demand placed on tall buildings and the associated risk factor are uncertain over the entire life span of the structure (Gudmundsson and Izzuddin, 2010). High-occupancy structures such as mid- and high-rise buildings, from a public safety point of view, shall be designed beyond the minimum requirements for structural stability to give sufficient time for evacuation following extreme events. Their design shall account for rigorous protections, beyond what is provided for gravity and lateral load designs (DoD, 2013). With respect to the growing interest in the use of mass-timber products for mid- and high-rise constructions, practical guidance for disproportionate collapse prevention are imminent. Although disproportionate collapse prevention analyses are well established for concrete and steel designs, being a new method of construction, there is a gap in the current knowledge of the topic with respect to timber design. Existing studies on the topic of disproportionate collapse prevention for mid- and high-rise timber buildings are scarce (Huber et

al., 2018b). Consequently, advanced analytical, numerical and experimental studies are prerequisite to understand the structural behaviour after extreme loading events.

1.7 Objectives

The main objective of this research is to study solutions that enable CLT platform-type buildings to trigger resistance mechanisms for disproportionate collapse prevention. The specific objectives are:

i) To perform a state-of-the-art review on current research studies as well as the contemporary practice on disproportionate collapse prevention for timber buildings:

- Critically review existing codes and guidelines.
- Critically review existing research studies.
- Critically review contemporary practice of applying the existing codes, guidelines and research studies.
- Advise on improvement of the existing codes and guidelines; and construct a baseline of the areas in need for further research.

ii) To assess the structural performance after initial damage of CLT platform-type construction that carry both gravity and lateral loads:

- Develop finite element (FE) model of a twelve-storey CLT platform-type building and investigate the performance after sudden loss of ground floor loadbearing walls.
- Perform a reliability analysis to quantify the probability of disproportionate collapse.
- Investigate the possible collapse-resistance mechanisms for the considered structural system.

iii)   To assess the structural performance after initial damage of CLT platform-type construction with flat-plate gravity load-resisting system:

- Develop FE model of a nine-storey flat-plate building and investigate the performance after sudden loss of ground floor columns.

- Perform a reliability analysis to quantify the probability of disproportionate collapse.

- Perform a sensitivity analysis and optimise the relevant design parameters to improve the building performance and reduce the probability of disproportionate collapse.

- Investigate the possible collapse-resistance mechanisms for the considered structural system.

iv)   To evaluate possible collapse-resistance mechanisms for CLT platform-type construction, and derive the tie-force requirements for structural integrity:

- Identify possible collapse-resistance mechanisms following different loadbearing wall removals for the considered structural system.

- Develop practical procedure of analysis and design for minimum tie-force requirements.

- Demonstrate the implementation of the proposed tie-force requirements at hand of a case-study building.

v)   To develop novel connection detailing, investigate, and optimise its performance for disproportionate collapse prevention:

- Develop a FE model of the steel tube connection and validate the performances against existing experimental test results.

- Perform sensitivity analysis and optimise the steel tube geometry and material properties to achieve a target yield force.

- Evaluate the robustness of the optimised steel tube in presence of uncertainties in the material properties and geometry.

- Propose novel connection detailing with steel tubes and rods for disproportionate collapse prevention.

vi) To perform experimental testing to investigate the collapse resistance mechanisms of mass-timber floor systems with novel tube connection detailing and compare the performance against floor systems with traditional connections:

- Evaluate ideal collapse-resistance mechanisms for different mass-timber floor systems after internal loadbearing wall removal.

- Investigate the influence of floor-to-floor connection detailing by comparing experimental test results from traditional and novel detailing.

- Propose deflection acceptance criteria to avoid disproportionate collapse for mass-timber floor systems with both conventional and novel connection detailing.

1.8 Scope and Limitations

Disproportionate collapse, once initiated, is driven by gravity (Ellingwood et al., 2007). Therefore, it is important to understand the performance of different gravity load-resisting structural systems. The scope of the research presented in this thesis focuses on two structural concepts for CLT platform-type buildings: i) with platform construction for both gravity and lateral load-resisting systems; and ii) with flat-plate construction to carry gravity loads and platform construction for lateral loads. These two concepts have shown good potential for mid- and high-rise CLT buildings for residential and office purposes.

This research is limited to CLT platform-type buildings between six and twelve storeys, without structural irregularities as defined in NBCC-2015 (NBCC, 2015). For these buildings, all structural elements are mass-timber components. The extreme events are assumed to only damage the gravity load-resisting systems, while the lateral load-resisting systems remain undamaged. In this research, structural analyses and designs for dead, live, snow and earthquake loads are performed as per NBCC-2015 and the Canadian Standard for Engineering Design with Wood (CSA-O86). The NBCC extreme loading combination is used for analysis following extreme loading events.

This research focuses on structural robustness, assumed as the best-suited approach for disproportionate collapse prevention. Here, after initial damage, the building is designed to develop alternate load-paths to prevent collapse propagation and redistribute the forces to undamaged parts. Catenary action is considered as the ideal floor system collapse-resistance mechanism to avoid debris loading, while cantilever and hanging actions are assumed ideal to prevent failure of the levels above the initial damage.

Both direct and indirect methods are utilised to assess the possible collapse-resistance mechanisms. Using 3D finite element analysis, the direct method is based on the alternate load-path analysis, with sudden element removal scenario to idealise the initial damage following the extreme event. The FE models assume wood components to remain elastic while all steel elements are modelled using nonlinear material properties. The indirect approach is a 2D linear-elastic analytical approach based on equilibrium of moments and forces. It assumes that all deformations are provided by the connections while the wood components are rigid. The developed novel connection detailing is ideal for mass-timber platform-type construction but can also be improved and adopted for other structural systems.

1.9 Outline

Chapter 2 reviews the literature with respect to disproportionate collapse prevention. Chapter 3 presents a survey that reviews the contemporary practices with respect to disproportionate collapse prevention to pinpoint areas in need for research. Chapter 4 studies the structural performance of a mid-rise platform-type CLT building after initial damage using finite element analyses (FEA). Chapter 5 studies the structural performance of a mid-rise flat-plate CLT and GLT building after initial damage, also using FEA. Chapter 6 proposes an improved analytical tie-force procedure for disproportionate collapse prevention of CLT platform-type construction. Chapter 7 presents a proposal for novel connection detailing for the considered building types, to enhance the desired collapse-resistance mechanisms, as well as numerical analyses for optimisation of the connection detailing with steel tubes and rods. Chapter 8 presents experimental tests to understand the performance of mass-timber floor systems in platform-type construction with both traditional and novel connection detailing. Chapter 9 gives the conclusions of this thesis with recommended areas for further studies.

Chapter 2: Literature Review

2.1 Introduction

In addition to gravity and lateral loads, there is a broad range of source, type, and magnitude of forces that might impact the building during its life span. According to EN1991-1-7 (CEN, 2006a), these are abnormal loadings, labelled as 'malicious actions', and considered as extreme events. Investigations on timber buildings show that human errors, during design and construction stages, are the main reasons for numerous failures observed in central Europe (Fruhwald et al., 2007; Harte et al., 2010). In these cases, ignorance or carelessness during design or construction stage is reported to be the source of inadequate structural performance. For example, after construction, many connections are found to behave differently than predicted by the design assumptions; about 11% of observed failures are caused by unexpected tensile forces perpendicular to the grain direction (Fruhwald et al., 2007). In addition, accidents, explosions, sabotage, fires, severe earthquakes and other natural catastrophes are other examples of events that can also cause significant damage to buildings (Tavakoli et al., 2012). The initial damage from these abnormal loadings may have a high risk of progression that can lead to disproportionate collapse, as defined in EN1991-1-7, and illustrated in Figure 2-1.

Abnormal load   Initial damage   Final damage
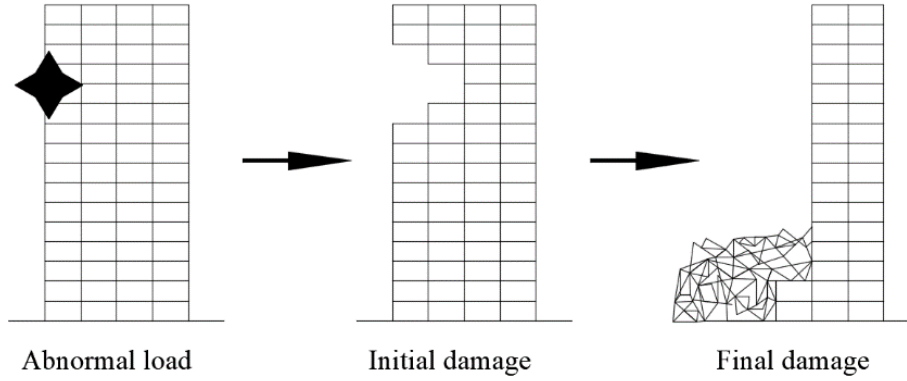
Figure 2-1: Generic illustration of a disproportionate collapse

2.2 Probability of disproportionate collapse

Equation (2.1) is utilised to quantify the probability of disproportionate collapse $P[DC]$ (Ellingwood and Dusenberry, 2005; Starossek and Haberland, 2010). In a structural design context, $P[H_i]$ is defined as the probability of exposure of a loadbearing element to a given abnormal load (H_i). $P[D|H_i]$ is the probability of initial damage (D) given the occurrence of H_i, defined as the vulnerability of the structural element. $P[F|DH_i]$ is the probability of collapse propagation or further failure (F) given H_i and D, defined as structural robustness. Deconstructing $P[DC]$ into these three components is instructive as it helps focusing on appropriate strategies for disproportionate collapse prevention: hazard prevention by reducing $P[H_i]$, initial damage prevention by reducing $P[D|H_i]$, and collapse propagation prevention by reducing $P[F|DH_i]$. Consequently, reducing $P[DC]$ may be achieved by reducing these components, assumed as statically independent, either separately or collectively (Ellingwood et al., 2007).

$$P[DC] = P[H_i] \times P[D|H_i] \times P[F|DH_i] \tag{2.1}$$

$P[H_i]$ is often assumed between 10^{-6} to 10^{-5}per year (NBCC, 2010b). From reliability analyses of the ultimate limit states given in building codes, for structural members designed to resist gravity

loads, where failure is assumed ductile, the probability of failure of the designed members under the applied forces is usually assumed in the range of 10^{-5} per year (Wang et al., 2011). For a structural system, the probability of failure is approximately one order of magnitude less ($P[D|H_i]=10^{-6}$ per year), depending on the degree of continuity between structural components and the redundancy in the system. From these assumptions, $P[F|DH_i]$ may be smaller than 10^{-2} per year (Ellingwood et al., 2007). Generally, the reliability index (β) for a safe structure is taken as 4.0, resulting to $P[DC]$ smaller than 10^{-5} per year.

Probabilistic analyses of load combinations demonstrated that the maximum structural action due to several randomly occurring independent events is when one of the actions is at maximum and the others are at their frequent values (Ellingwood et al., 1982). The total live loads (LL) on a floor system is composed of sustained (L_s) and extraordinary (L_e) live loads. L_s is normally present, whereas L_e only rises from remodelling or emergency crowding. The mean coincidence between H_i and L_e, given their respective mean rate of occurrences and durations, is negligible. Therefore, $LL = L_s$; taken as 50% of the nominal values given in design standards (Ellingwood et al., 2007). The contribution of uncertainties in the dead load (DL) is maybe assumed insignificant and decreases with increase in number of building storeys above the assumed damage; therefore, DL is taken with a factor of 1.0. Although there is less uncertainty in DL, it still remains a random variable and needs to be included if an accurate probability of collapse is to be determined. The snow (SL) and wind (WL) loads are less than their respective unities. During extreme events, SL as companion load is as specified for other load combinations (Ellingwood et al., 2007).

As disproportionate collapse is driven by gravity loads, WL is applied at each storey as 0.002 times the cumulated gravity forces from the level above, or 20% of the calculated characteristic wind

value, to account for *P-Δ* effects for stability. Consequently, the extreme load combination (E_{LC}) in this thesis, see Equation (2.2), stays in accordance to NBCC (NBCC, 2015). Equation (2.1) is also in agreement with the European EN1991-1-7 (CEN, 2006a) and the American ASCE-7 (ASCE, 2013) standards.

$$E_{LC} = 1.0DL + 0.5LL + 0.25SL \qquad (2.2)$$

2.3 Specific Design Strategies

2.3.1 Exposure ($P[H_i]$)

Thorough risk assessments help to identify foreseeable events and hazards (H_i) that may affect the building during its life span. After identifying possible threats, solutions and mitigations that reduce $P[H_i]$ may be implemented. These may include changes in building site and access, minimum stand-off distance for restricted areas, rigorous control of hazardous substances within the building, quality control and supervision during analysis, design, manufacturing and erection stages, etc. (Taylor, 1975). Nevertheless, most of these solutions do not require structural engineering expertise to be implemented (Ellingwood et al., 2007). From a structural engineering point of view, it is unpractical to control all abnormal loads given that their sources are not always anticipated. Unforeseen events, e.g. natural catastrophes, may also affect building safety. Consequently, it becomes unpractical and uneconomic to design for all abnormal loads (Lew, 2003). The probability that the designed building will actually be exposed to the assumed extreme event is low (Hamburger and Whittaker, 2004). Given these limitations, structural engineering generally focuses on vulnerability and structural robustness.

2.3.2 Vulnerability ($P[D|H_i]$)

For unforeseen events that cannot be controlled, e.g. $P[H_i]$ close to 1.0, reducing the vulnerability $P[D|H_i]$ of loadbearing elements to H_i may be done by ensuring local resistance (Starossek and Haberland, 2010). Herein, reasonable rational methods are found in the analyses and designs of the structural elements to withstand specific abnormal loads. For disproportionate collapse prevention, the key element approach consists of applying at least 34kN/m^2 in horizontal and vertical directions, one direction at the time, of a structural element as well as the attached components and connections to sustain the effects of abnormal loads (CEN, 2006a; DoD, 2013). Although the magnitude of the applied force is notionally defined, it gives reference to the applied pressure from the Ronan Point building explosion (Byfield et al., 2014; Moore, 2005). It is assumed that by designing for at least 34kN/m^2, proportionate measures have been considered for disproportionate collapse prevention (Arup, 2011). This increases local resistance, hence reducing $P[D|H_i]$ for a wide range of H_i, considering the unreasonably applied high pressure loads (Ellingwood and Dusenberry, 2005; IStructE, 2010). Nevertheless, this direct design approach which overdesigns structural elements may lead to uneconomical solutions; consequently, it is only advised as a last resort (Arup, 2011; Cormie et al., 2012).

2.3.3 Structural Robustness ($P[F|DH_i]$)

Implementing structural robustness as a property of the building, to minimise $P[F|DH_i]$, is described as the best-suited method for disproportionate collapse prevention (Ellingwood et al., 2007; IStructE, 2010; Starossek, 2006). With structural robustness, the building has the ability to withstand initial damage and stop collapse propagation by developing alternative load-paths. A building is considered robust if it is able to develop collapse-resistance mechanisms to absorb the

initial local damage without collapse. Analytical quantification of structural robustness can be based on risk analysis, reliability analysis, or deterministic analysis (Brett and Lu, 2013). Risk analysis of structural robustness is performed by modelling the total risk (Baker et al., 2008). Reliability analysis quantifies the overall system's probability of anticipated performance over the building's entire life span (Kohler, 2006).

Risk and reliability analyses are probabilistic approaches which account for the probability distribution for both exposure and overall structural system (Chen et al., 2016; Kirkegaard et al., 2011). For deterministic analysis, to obtain an acceptably low $P[F|DH_i]$, $P[H_i]$ and $P[D|H_i]$ are assumed close to 1.0 (Ellingwood and Asce, 2006; Ellingwood and Dusenberry, 2005). In other words, to meet adequate structural robustness performances, a certain amount of damage to the building may be tolerated to evaluate the solutions for collapse prevention. A deterministic analysis is recommended as best-suited to ensure robust designs against disproportionate collapse (Brett and Lu, 2013; Starossek and Haberland, 2010). Deterministic analysis ensures structural robustness by investigating the actual structural responses of the building and focusing on the structural impacts from the assumed initial damage, hence possible loss of lives, unacceptable economic and/or social losses.

2.4 Analysis Methods for Structural Robustness

2.4.1 Indirect Design Methods

Ensuring structural integrity is an indirect approach for structural robustness. With this method, the building is indirectly designed to bridge over the assumed initial damage for disproportionate collapse prevention (Starossek, 2006). Herein, the joints between the different structural components play an essential role to ensure that collapse-resistance mechanisms are triggered after

initial damage. The design accounts for sufficient strength, stiffness, and ductility at the connection level. Strength and stiffness are essential to develop the bridging capabilities after initial damage; this makes the distribution of forces from the damaged to the undamaged parts of the building possible (Schultz et al., 1977a). Ductility gains importance when the building is required to sustain large deformations without rupture while maintaining the load-carrying capacity (Byfield et al., 2014; IStructE, 2010). Ensuring minimum tie-force, as well as compatibility between the axial and vertical deformations at the connection level, is a prerequisite for structural integrity. This method may be building-specific as the anticipated resistances are based on engineering judgements without the complexities associated with modelling and analysing the building and the extreme loading itself (Arup, 2011; Ellingwood and Dusenberry, 2005).

Redundancy is also an indirect approach to ensure structural robustness. Herein, the selected structural layout has sufficient number of vertical loadbearing elements. This not only reduces the tributary area of the floor system but also provides effective direct vertical load-path to nearby columns or walls, after initial damage. Compartmentalisation is another indirect design approach for structural robustness and disproportionate collapse prevention. This is achieved by dividing the whole building into different independent structural compartments to stop collapse propagation after initial damage (Ellingwood et al., 2007). Here, local damage may be allowed to propagate within the compartment where it occurred. However, propagation across different compartments is prohibited for disproportionate collapse prevention. Compartments are created either by ensuring that certain structural components can sustain high load, e.g. carry $34kN/m^2$ to reduce $P[D|H_i]$, or by stopping load transfer, e.g. detailing fuse connections to stop continuity (Starossek, 2006). To create compartments and indirectly design for structural robustness, intermediate strong

floors are solutions for tall buildings, whereas strong walls are used for long span structures. This approach confines the collapse to a single area and ensure the survival of the remaining building.

2.4.2 Direct Design Methods

Event-dependent analysis, as a direct method to ensure structural robustness, is recommended when detailed information about the abnormal load is available, e.g. from risk-assessment of the building. The approach is practical and economical when the type of exposure and magnitude of the generated forces from the extreme events are used not only to quantify the extent of the initial damage, but to also identify alternate load-paths against disproportionate collapse. To perform an event-dependent analysis, both the abnormal loads and the building are modelled; the FE model may account for both material and geometric nonlinearities as well as dynamic behaviours for realistic and accurate responses (Gudmundsson and Izzuddin, 2010). Material and geometric nonlinearities capture axial and bending, as well as shear force and deformation demands relative to the supply from the structural elements and connections. Dynamic behaviours consider the influence of dynamic forces applied in a time history curve (DoD, 2013; GSA, 2013).

Event-dependent analysis is a load-specific design method generally used to understand the building performance following blast loads (Edri et al., 2018; Hamburger and Whittaker, 2004; Olaniyi et al., 2017). Blast loads depend on the form and shape of the building, its location relative to adjacent buildings, and the distance from the source of the blast (Gudmundsson and Izzuddin, 2010). Consequently, with the complexities related to modelling blast loads, an event-dependent analysis can only be performed when these parameters are well defined. Nevertheless, it is worth mentioning that this design approach does not consider all scenarios given the predefined parameters affecting the magnitude and modelling of the blast loads. Consequently, it may be

uneconomic when considered as a solution for disproportionate collapse for other building types and other abnormal loads.

It is not feasible to represent all abnormal loads that may impact the building, given the label of 'malicious action' according to EN1991-1-7 (CEN, 2006a). There is a broad range of source, type and magnitude of forces from vehicle impact to terrorist attacks. Compared to earthquake design for example, there is a lack of disproportionate collapse information on parameters such as source, type and magnitude of the extreme loading, as well as the size of the triggered initial damage associated with subsequent collapse. With the insufficient information, limitations and complexities to model both the abnormal loads and the considered scenarios, an event-independent design method becomes more realistic (Hamburger and Whittaker, 2004; Krauthammer et al., 2002; Lew, 2003). This is a threat-independent approach; no interest is given to the extreme loading and its probability of occurrence. Herein, the loadbearing elements are notionally deleted from their structural topology.

Although the event-independent method uses an imaginary scenario as initial damage, it enables the obtaining of a damage-to-performance correlation. In other words, it measures the structural performance of the building in terms of force and deformation demands, as well as possible collapse-resistance mechanisms following the assumed element loss. When comparing an event-dependent analysis against a threat-independent analysis, results (Gudmundsson and Izzuddin, 2010) showed that the structural performance obtained from the latter provides a suitable bound on ductility demands, hence is more suitable for disproportionate collapse investigations after extreme loadings. The alternate load-path analysis (ALPA), as an event-independent design method, often uses FE models ranging from linear static to nonlinear dynamic analyses (DoD,

2013; Stevens et al., 2003). For accurate and realistic results leading to economic designs, material and geometric nonlinearities as well as dynamic behaviours are considered (Fu, 2010; Stevens et al., 2003). ALPA quantifies the load and deformation demands on the members as well as their connections for comparison against the respective supplies, to ensure structural robustness.

2.5 Collapse-resistance Mechanisms

2.5.1 Floor System Collapse-resistance Mechanisms

In the event that a vertical internal loadbearing wall is damaged following an extreme event, to prevent debris loading on the floor below, the floor system above the damage must carry its self-weight, in addition to the imposed live or snow loads (Stevens, 2008). Analytical and experimental studies for concrete and steel buildings (Schultz et al., 1977a; Stylianidis et al., 2016) explain floor system collapse-resistance mechanisms.

The load-deformation response of an axially restrained floor system subjected to large deformations by applying a vertical force at the location of the removed internal wall or column is shown in Figure 2-2a. Initially, when the deflections are small, the floor system behaves elastically with the resistance ensured by the flexural capacity (stage 1), see Figure 2-2b. With further deflections, the system develops an arching thrust (stage 2) at the location of the applied force (F), see Figure 2-2c. When the vertical deformation (Δ_1) equals the floor depth (d), compressive arching reaches its maximum. With increasing deflections, the axial compressive forces decrease while the tensile forces in the bottom of the floor section increase. At $\Delta_1=2{\times}d$, axial compression becomes zero, and the system's response goes into a transient tensile stage (stage 3), characterised by a snap-through instability until a stable equilibrium is adopted. Provided sufficient axial capacity supplied by the floor itself and the connections' tensile resistance, increasing the deflection leads

to catenary action (stage 4), see Figure 2-2d, with any increase in floor deflection associated with a significant linear increase in its load-carrying capacity.
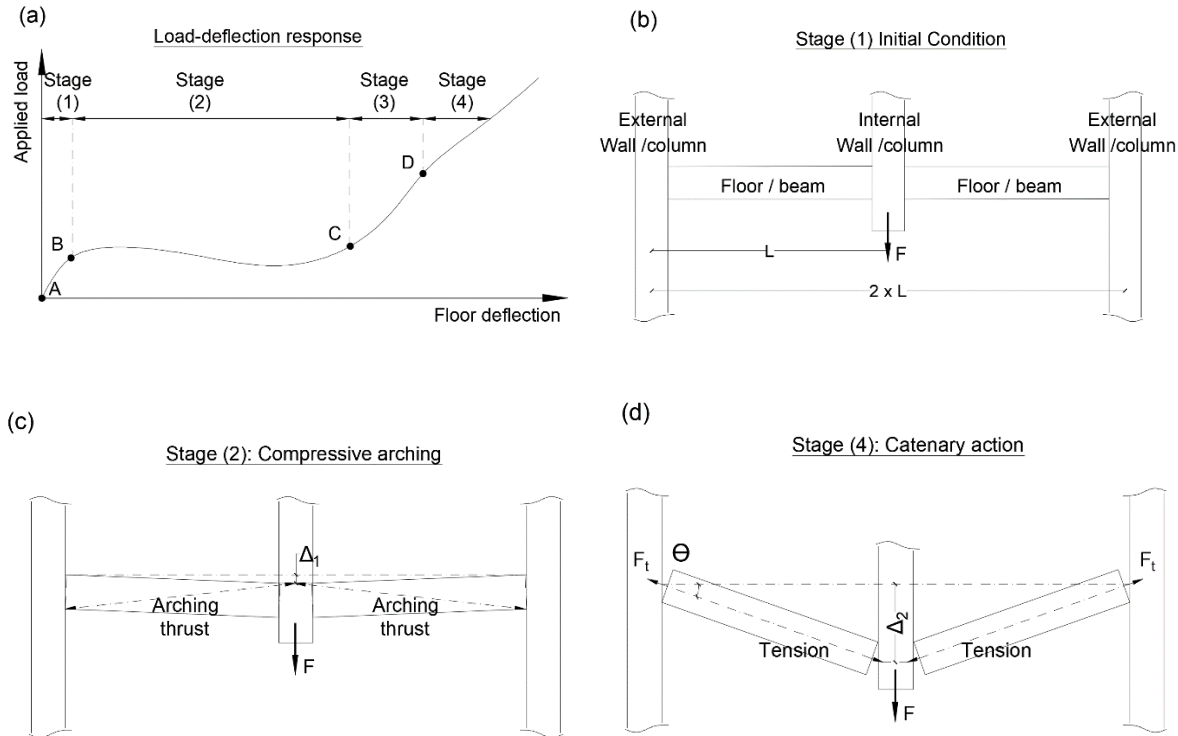
Figure 2-2: Floor system collapse-resistance mechanisms: (a) Load-deflection response; (b) Initial condition; (c) Compressive action; and (d) Catenary action (Stylianidis et al.,2016)

Catenary action is the ideal collapse-resistance mechanism for floor systems given its ability to maintain load-carrying capacity during large deformations (Schultz et al., 1977a; Stevens, 2008). The axial catenary action force is assumed to align with the floor and connection tensile forces, both located at the centroid (Stylianidis et al.,2016), see Figure 2-2d. The required tension to tie the floor system can be estimated by linear static equilibrium: applied moment for a simply supported system with mid-span point load ($M_z=F\times2L/4$) equal resisting moment ($M_r=F_t\times\Delta_2$), where F is the applied force, L is the span, F_t is the tensile or tie-force. As the catenary action is only mobilised at large (nonlinear) deflections, for concrete and steel floor systems, a reduction

factor (*NF*) equal to 0.67 is applied to the results of these linear calculations to reduce the forces and hence obtain realistic estimations (Li et al., 2011).

For laterally restrained reinforced concrete floors, Stevens (2008) estimated that catenary action develops at a deflection between 10% and 20% of *L*. For steel assemblies with welded flanges and bolted web joints, 8% of *L* was required to trigger catenary action (Khandelwal et al., 2009; Sadek et al., 2011). For reinforced concrete frames, catenary action was observed at a deformation of 18% of *L* (Main et al., 2011; Weigand et al., 2017). Consequently, The Unified Facilities Criteria (UFC 4-023-03) (DoD, 2013) requires that all floor systems be able to maintain load-carrying capacity while undergoing a rotation (θ) of 11.3*deg.* (0.20*rad.*) to ensure resistance against disproportionate collapse. This value is usually compared against the deflection obtained from FE linear static analysis of the building following the element removal, e.g. alternate load-path analysis as per UFC 4-023-03 (DoD, 2013); and represents the acceptance criterion for disproportionate collapse prevention. In other words, if the results of the floor analyses do not meet this deformation demand (deflection > than acceptance criterion), the building may exhibit high potential for disproportionate collapse under the considered element removal scenario.

2.5.2 Wall System Collapse-resistance Mechanisms

Cantilever action is developed when a building loses an external corner loadbearing element and all floors above that level must cantilever in order to prevent disproportionate collapse (Schultz et al., 1977b). For this mechanism, illustrated in Figure 2-3a, the created cantilever above the damage applies a moment, due to its weight (w_f), which must be resisted by the tie-force (F) at every storey to prevent collapse. In addition, the mechanism also creates vertical shear between the cantilever and the support section, and horizontal shear between adjacent storey levels. It is worth mentioning

that the connection detailing for these shears are important as they foster monolithic behaviour of the cantilever mechanism.

(a)

Wall assembly with ineffective panel at the nth storey

Free body diagram of cantilever mechanism

Free body diagram of support mechanism

(b)
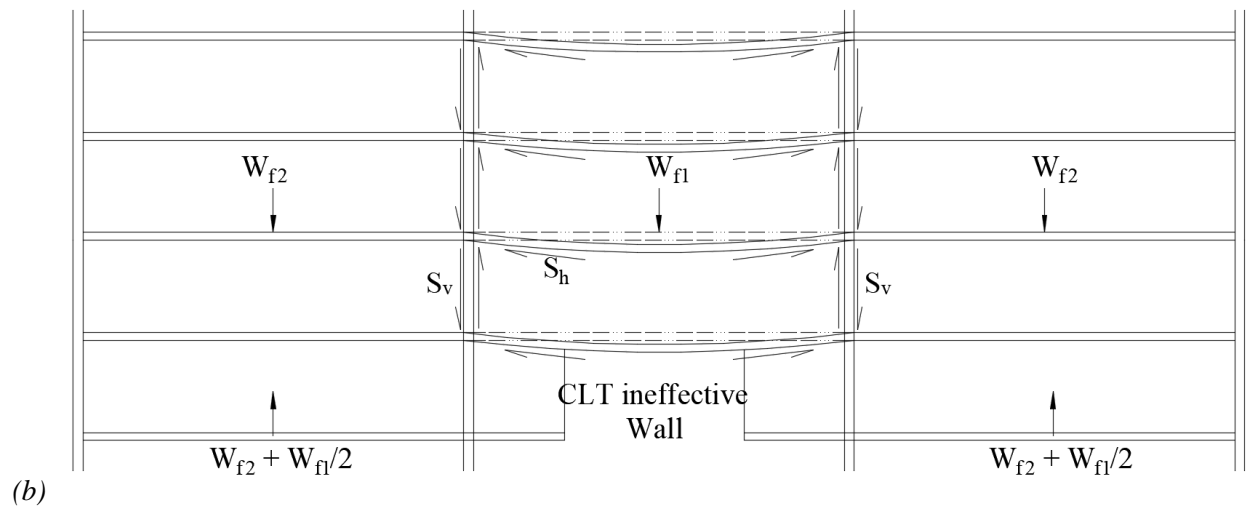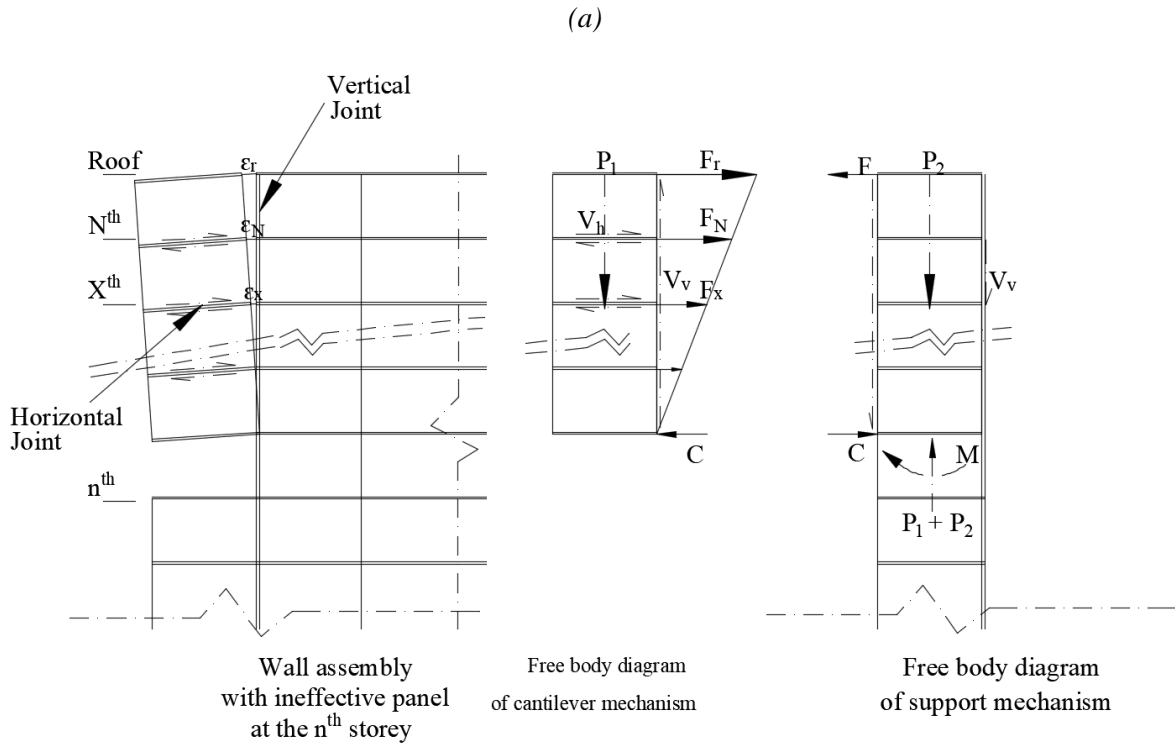
Figure 2-3: Wall system collapse-resistance mechanisms: (a) Cantilever action; and (b) Beam action (Schultz et al., 1977b)

As shown in Figure 2-3b, beam action as a resistance mechanism against disproportionate collapse is triggered after the internal or external loadbearing wall underneath becomes ineffective. This mechanism requires high in-plane stiffness in walls and adequate ties to transfer the loads to surrounding bays. The overall behaviour of beam action is identical to cantilever action (Schultz et al., 1977b). Herein, the horizontal shear between consecutive storeys and the vertical shear between the damaged and surrounding bays should be resisted to foster monolithic behaviour. Consequently, the total strength of the beam action is the sum of individual wall panels as they all act as a composite or monolithic element.

2.6 Existing Design Standards and Guidelines

2.6.1 Europe

The 'England and Wales Regulations' for designing against disproportionate collapse were introduced in 1970 following the Ronan Point incident. The included structural robustness requirements were used to describe the quality of a structure; this was the insensitivity to local failure in which modest damage causes only a similar modest change in the structural behaviour (Arup, 2011). Since then, these regulations were constantly subjected to amendments until the 2004 edition of the Approved Document A which formed the basis of the current version of the European code EN1991-1-7 (CEN, 2006a). EN1991-1-7 has a section with details for designing new buildings against disproportionate collapse. It defines the collapse thresholds and proposes strategies to ensure structural robustness depending on building categories. The extreme load combination is also in agreement with Equation (2.1). EN1991-1-7 categorisations are based on failure consequences, defined with respect to building height, occupancy level, and the intended use of the structure. No requirements are given for single-family houses not exceeding four storeys.

For residential, commercial and office buildings, lower than four storeys, minimum tie-force requirements are given to ensure effective horizontal ties, as an indirect approach to disproportionate collapse prevention. For taller buildings, between four and fifteen storeys, both horizontal and vertical ties are required for structural integrity. Alternatively, a direct approach using ALPA is recommended to ensure practical and economical solutions to bridge over the initial damage. Nonetheless, this is given without thorough procedure details. Assumed removed elements using ALPA that results in unpractical solutions may be designed as a 'key element' to reduce its vulnerability to extreme events. Above fifteen storeys, a systematic risk assessment of the building is recommended to account for all foreseen and unforeseen events. For buildings in this category, EN1991-1-7 becomes subjective as no explicit strategies are given for disproportionate collapse prevention.

2.6.2 USA

Although no specific thresholds are defined, ASCE-7 (ASCE, 2013), the design standard for civilian buildings, requires buildings to remain stable and not be damaged to an extent disproportionate to the initial failure after abnormal loads. It relies on structural integrity, by means of strength, continuity and ductility, to ensure minimum interconnectivity between structural elements. Here, it is assumed that structures designed with seismic specifications are deemed to meet structural integrity requirements. No explicit approaches and design criteria are given to meet structural integrity requirements. ASCE-7 also acknowledges that there are structures, e.g. housing a large number of persons, functioning for public safety, or those that may be subjected to intentional sabotage, that require more rigorous protections for disproportionate collapse prevention. For buildings in this category, although direct and indirect design approaches are mentioned, no explicit methods are given on how this can be implemented.

The Unified Facilities Criteria (UFC 4-023-03) (DoD, 2013; Stevens et al., 2011) and the General Service Administration (GSA) (GSA, 2013) are detailed and prescriptive guidelines for disproportionate collapse prevention for Government and Federal buildings. UFC 4-023-03 contains more details than the GSA guidelines. There are similarities with EN1991-1-7 with reference to building classifications, and design using indirect and direct design methods. The extreme load combination is also in agreement with Equation (2.1). Nevertheless, unlike EN1991-1-7, UFC 4-023-03 gives disproportionate collapse thresholds to contain the damage within the tributary area of the removed element and requires the floor directly underneath to not fail. This condition requires considerations for debris loading to prevent propagations beyond the damaged level. Furthermore, UFC 4-023-03 illustrates applications of the ALPA from linear static to nonlinear dynamic analyses, as well as worked examples for steel, concrete and lightweight timber buildings.

2.6.3 Canada

In Canada, NBCC included its first attempt to define collapse thresholds, identical to EN1991-1-7, in Commentary C of the 1977 edition. The NBCC gave reference to direct and indirect design approaches for structural robustness. The extreme load combination for disproportionate collapse included 1/3 of respective *LL* and *WL*, in addition to *DL*. After 1980, NBCC has given no direct references or clauses to disproportionate collapse (Ellingwood, 2002). Due to the fact that considerations on both probability factor and magnitude of extreme loads have become subjective, design against disproportionate collapse has turned to a matter of the designer's good practice (Gross and McGuire, 1983). Standard S850 (CSA, 2012) is the only available guidance for disproportionate collapse prevention with a scope limited to the design and assessment of buildings subjected to blast loads. These guidelines use the event-dependent approach for structural

robustness; guidance for structural integrity and event-independent approaches are heavily drawn from the UFC 4-023-03 and GSA (Driver, 2014).

NBCC-2015 assumes that buildings designed in accordance with the material design standards, the CSA Standards, would have satisfactory degree of structural integrity to localise the damage and to avoid disproportionate collapse. These references are only given in the commentary. Although the User's Guide to Commentary for Part-4 of Division B (NBCC, 2010b) acknowledges situations where special attention is required in order to satisfy structural integrity, e.g. rare loads with a probability of occurrence of 10^{-4} per year, high occupancy and high importance structures, no explicit guidance is given on how this can be achieved. Furthermore, concerns also arise for buildings with structural concepts, components and connections beyond the scope of the CSA standards. Since addressing disproportionate collapse is not a specific code requirement in Canada, safety in that aspect is left to sound engineering judgments on the part of the designer and the designer's exposure to other building code and guidance such as EN1991-1-7 and UFC 4-023-03.

2.6.4 Australia and New Zealand

In Australia, the National Construction Code (NCC) always had generic structural robustness requirement clauses similar to EN1991-1-7, but with little aids. In general, structural robustness remains an ambiguous subject and is a largely forgotten requirement (Hewson, 2016). Limited guidance can be found in Section 6 of the Australian and New Zealander code (AS/NZ 1170.0 2002) and the accompanying supplementary commentary (Australia/New Zealand Standards, 2002). AS/NZ 1170.0 2002 used for structural design action requires that all parts of the building be designed with sufficient ties capable of transmitting 5% of the ultimate dead and live loads. The application of a minimum lateral load of 1% for buildings higher than 15m (1.5% for shorter

buildings) is also required as part of the load combination. Nonetheless, the low magnitude of lateral load, smaller than design wind and earthquake load, is always neglected (Hewson, 2016). In addition, to ensure alternate load-path, the connections are required to have sufficient ductility to undergo large deformations while maintaining strength and continuity under the effect of abnormal loads. Herein, it is assumed that the material standards contain explicit considerations on how to provide such minimum strength, continuity and ductility (Arup, 2011).

2.7 Structural Robustness for Timber Buildings

2.7.1 Capacity-based Design Approach

Capacity-based design is an approach employed to guarantee building survival with low damages when subjected to high seismic loads (Follesa, 2015). Certain failure mechanisms are assumed to develop desired and safe collapse states. This approach may be considered at: i) the global; ii) the components; and iii) the connection levels, to guarantee that plastic hinges are only formed on ductile or fuse connections while brittle elements and non-dissipative connections are overdesigned to remain elastic (Follesa, 2015; Fragiacomo et al., 2011). The desired energy dissipation is only supplied by the elements designed to yield under the applied seismic loadings.

The capacity-based design approach is adopted in the CSA-O86 for seismic design considerations for CLT platform-type structures (e.g. Stadthaus apartment building). Herein, CLT floors and walls are considered as rigid bodies, overdesigned to always remain elastic. On one hand, a ductile behaviour is required at: i) the joint resisting shear between the floor and the wall above; ii) anchor or hold-down connectors resisting uplift and overturning forces; and iii) the connection against vertical shear between two wall panels. On the other hand, the members designed for over-strength are: i) joints against shear between the floor panel and wall underneath; ii) joint between adjacent

CLT floor panels; and iii) joint between perpendicular walls. This constitutes the capacity-based design consideration at global and component levels for seismic design.

2.7.2 Robust Connection Detailing

Capacity-based design principle may also be used to achieve the required structural robustness for disproportionate collapse prevention. Since the ability to stop collapse propagation depends on the weakest link, structural robustness can be achieved by ensuring adequate strength, stiffness, and ductility at connection level (Gong, 2010; IStructE, 2010). Structural detailing can ensure that the energy dissipative connections used for lateral design also have sufficient strength and stiffness in addition to the required ductility to develop disproportionate collapse resistance mechanisms. As an example, the hold-down connection may also act as a vertical tie between different wall panels, hence triggering cantilever or hanging action of the floors system to the level above. Also, non-dissipative connections, e.g. floor-to-floor connection, detailed to ensure diaphragm action should also be able to undergo large deformations in addition to strength and stiffness to develop collapse-resistance mechanisms.

The ultimate limit state design provides the required strength based on the nature of the connectors in terms of sizes, dimensions, and material properties. For this reason, traditional connections detailing using bolts, nails, and angle brackets can provide sufficient strength and stiffness for disproportionate collapse design. Design for ductility is the main difference between traditional and robust connection detailing (Gong, 2010). Usually these connection detailing are also resilient given their ability to recover their original state and performance after unloading. The significance of ductility is highlighted when the joints must withstand rigorous damages, caused by extreme loads while undergoing large deformations to allow for evacuation (Krauthammer et al., 2002). In

other words, the load-carrying capacity of the building is maintained, the system is able to bridge over the initial damage and therefore, prevent disproportionate collapse.

Obtaining robust in joint detailing demands considerations of capacity-based design at the connection level. The detailing must maximise plastic behaviour of ductile components without affecting brittle elements. Figure 2-4a shows typical failure of commercially available non-robust, also non-resilient, bracket connectors under reversed cyclic loading (Schneider, 2015; Schneider et al., 2015), idealising seismic forces on a building. The connection was designed for the required strength and stiffness according to CSA-O86. However, the lack of robustness and resilience resulted in localised brittle wood failure. In different scenarios, the deformation of the bracket connector inevitably damaged the wood as shown in Figure 2-4b. With such designs, the connection cannot be restored, and replacement can become uneconomic. Since disproportionate collapse prevention strategies require ductility in addition to strength and stiffness, there is a need to investigate commercially available connection detailing for mass-timber buildings to understand their performance in terms of structural robustness.

(a)   *(b)*
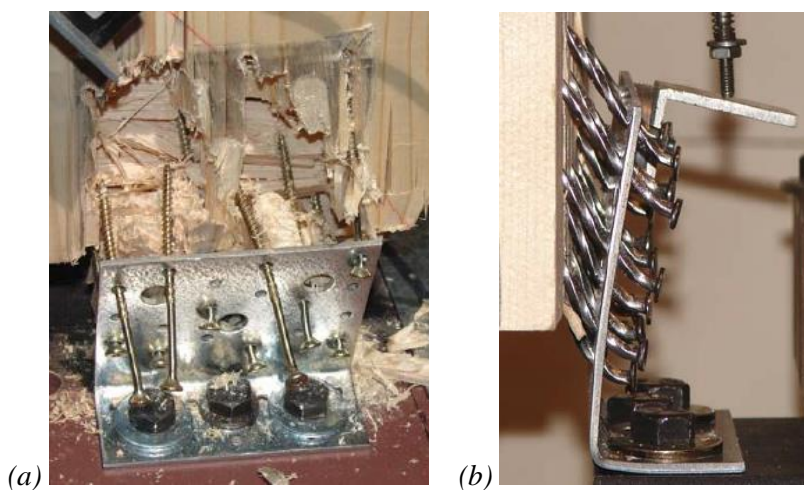
Figure 2-4: Damages of traditional non-robust and non-resilient connectors under reverse cyclic loads: (a) Brittle wood failure, and (b) Nails yielding (Schneider, 2015) *(Reprinted with permission)*

2.7.3 Existing Literature on Structural Robustness

Existing code (EN1991-1-7) and guidelines (UFC 4-023-03 and GSA) with prescriptive clauses on structural robustness and disproportionate collapse prevention are heavily drawn from experimental and numerical analyses on concrete and steel buildings. These prescriptions and recommendations are deemed uneconomic and often unpractical when implemented in mass-timber buildings (Arup, 2011; Hewson, 2016). The only available guidance on structural robustness for timber buildings was drawn from the Timber Frame (TF2000) research project carried out in the UK (Milner et al., 2003). This experimental testing was conducted on a six-storey light-frame wood building subjected to removal of wall sections. Although the results from this test led to tie-force provisions and connection detailing recommendations, it is unclear whether extrapolation is possible to other structural systems, e.g. mass-timber buildings, with different heights and proportions (Arup, 2011).

From the review article on structural robustness for timber buildings (Huber et al., 2018b), studies on the performance of mid- to high-rise mass-timber buildings when subjected to abnormal loads are scarce. An analytical example on the ALPA procedure is also provided in the UFC 4-023-03, although it is only applicable to low-rise light-frame wood buildings. Existing technical guidelines on structural robustness for CLT structures (Hewson, 2016; STA, 2017) only provide design principles without thorough investigations to ensure structural safety against disproportionate collapse. Mid- and high-rise timber buildings are a new type of construction. This lack of guidance may impede expansion of its application to post-disaster, military/federal, and tall buildings with high occupancy levels. Therefore, extensive research is currently ongoing around the world to understand the structural behaviour of mass-timber buildings after extreme events. For this building type, the focus is on the connection between different loadbearing components; as noted

from the failures observed in Europe (Fruhwald et al., 2007; Frühwald, 2011). They are critical for the overall behaviour after initial damage (Kirkegaard et al., 2011; Patel, 2014).

2.7.4 Limitations of Existing Tie-force Methods Applied to CLT Buildings

Figure 2-5a shows the possible location of ties for CLT platform-type construction: i) longitudinal (*L*) ties, connecting two floor panels in the longitudinal direction; ii) transverse (*T*) ties, running in the transverse direction of the individual panel; iii) vertical (*V*) ties, connecting two consecutive wall panels in the vertical direction; and iv) peripheral (*P*) ties running along the perimeter of the building through the external walls and floors.

(a)

(b)
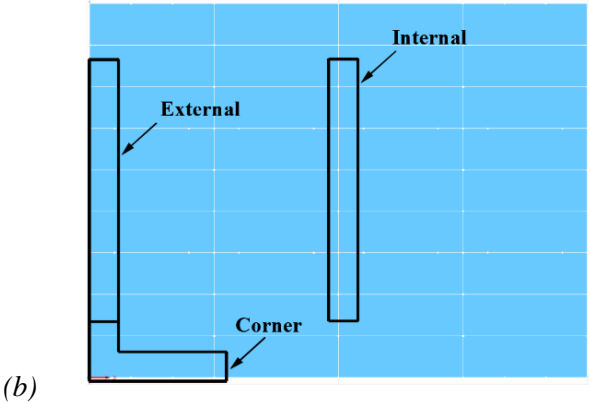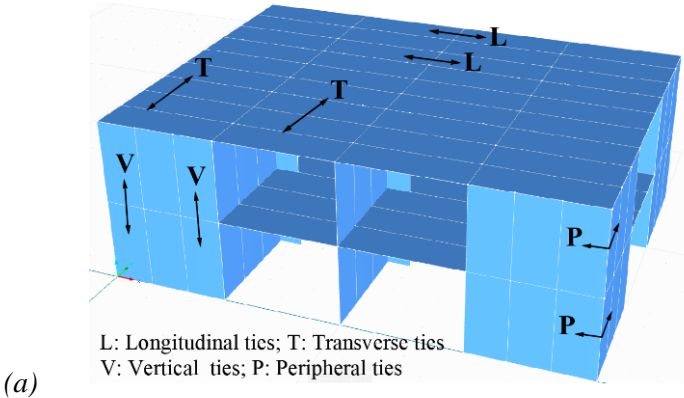
Figure 2-5: CLT building with platform-type construction: (a) Ties locations; (b) Removed wall location

EN1991-1-7 specifications for minimum internal horizontal (for both L and T) tie forces (kN) depend on the basic tie-strength ($F_{T,L}$), see Equation (2.3):

$$F_{T,L} = \min\{60\text{kN/m} ; (20 + 4 \times N)\text{kN/m}\} \tag{2.3}$$

Herein, (N) is the number of storeys and $F_{T,L}$ is empirically determined; it is assumed that a tall building collapse has more serious consequences (Li et al., 2011). Considering a simply-supported double span floor system, $F_{T,L} = 60\text{kN/m}$ is obtained from moment equilibrium after middle support removal (Stylianidis et al., 2016). In its derivation, EN1991-1-7 assumes that typical continuous floor systems have 5m span, 5kN/m^2 floor loads, and 20% of the floor span as maximum vertical defection (Li et al., 2011). While EN1991-1-7 specifies that the vertical tie-force (F_V) shall be smaller than 100kN/m for loadbearing wall systems, in the UFC 4-023-03, F_V is proportionate to the floor loads and constant throughout the height of the building (Schultz et al., 1977a; Stevens, 2008).

Li et al. (2011) discussed the limitations of the EN1991-1-7 internal tie-force prescriptions for multi-storey buildings and showed that building redundancy (and hence resistance against disproportionate collapse) increases with the number of storeys. Therefore, assuming $F_{T,L}$ to be directly proportionate to N is not always appropriate. Furthermore, the practicality of obtaining the assumed vertical deflection equal to 20% of the span (CEN, 2006a; DoD, 2013; Stevens, 2008), is questionable for wood structures. Timber is brittle in nature and there is a lack of research confirming its ability to develop the large deformations required for structural robustness (DoD, 2013). The horizontal tie-force in EN1991-1-7 and UFC 4-023-03 are considered equal for both longitudinal and transverse joints. However, for mass-timber buildings with platform-type construction, catenary action in the longitudinal and transverse direction cannot be the same given

the span difference in the two directions; e.g. mass-timber panels are only available up to 3m wide due to manufacturing limitations (Louisiana Pacific Corporation, 2018; Structurlam, 2016; Weyerhaeuser, 2018).

For mass-timber buildings with platform-type construction, considering the practical deformation limits of the connections, calculations leading to the minimum tie-force have to include the compatibility between the horizontal and vertical deformations. Furthermore, the horizontal and vertical shear forces between wall panels, important for cantilever and beam actions as collapse-resistance mechanisms, are not considered in the existing minimum tie-force guidelines. For mass-timber buildings with individual large wall panels, these shear forces may dictate the magnitude of force and deformation demands on the connections (Schultz et al., 1977a). Finally, the EN1991-1-7 tie-force requirements do not account for nonlinear and dynamic behaviours, which help obtaining better estimates of structural performance under extreme loading (Byfield et al., 2014; Ellingwood and Dusenberry, 2005). The aforementioned limitations of EN1991-1-7 and UFC 4-023-03 for tie-force requirements demonstrate that these guidelines are not suitable for mid- and high-rise CLT buildings in platform-type construction.

2.7.5 Ongoing Research on Structural Robustness

Research on structural robustness is on-going at Luleå University of Technology in Sweden (Huber, 2019, Personal communication). An accurate understanding of the mechanics of the connection detailing between the timber components is necessary for modelling anticipated resistance mechanisms. Huber et al. (2018a) analysed the role of individual components of connection details for the development of collapse-resistance mechanism in CLT platform-type buildings. The authors used FE to model the conventional detailing for platform-type construction

which is composed of STSs and angle brackets fastened with nails, see Figure 2-6. Each element followed the constitutive elastic, plastic and damage behaviours of the analytically calculated real connector. The constituent behaviour of the angle brackets was modelled in a separate FE model for each loading direction. The modelling method enabled a detailed evaluation of the failure sequence of each connector and showed that the floor-to-floor connectors tended to fail progressively in a zipper-like fashion for the studied case.
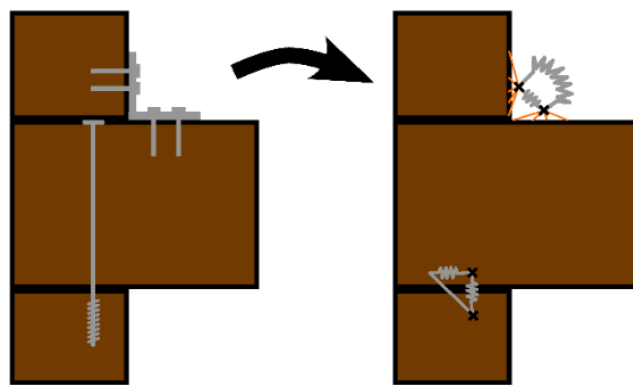
Figure 2-6: Modelling assumptions: Replacement of connection components with connector elements (Huber et al., 2018a) *(Reprinted with permission)*

For their on-going research, Huber et al. (Personal communication, 2019) investigate membrane action of the floor system and deep beam action of the wall system, in a platform-type construction. The objective of their research is to accurately model the development of alternative load-paths along the floor and wall panels. Using FE analyses, the authors use connector element type to substitute the mechanical behaviour of screws and angle brackets. The analyses performed for this investigation account for elastic, plastic, damage, and rupture in the connector elements. In the developed FE models, the authors also account for the effects of friction between the elements and for plastic crushing of the timber perpendicular to the grain in a platform-type construction. In

addition, the authors have scheduled experimental testing to investigate sections of floor-to-wall connections in a platform-type CLT building.

Structural robustness research is also ongoing at Griffith University, in Australia (Gilbert, 2018, Personal communication). Lyu et al. (2018) performed an experimental study on 2D post-and beam frames to investigate the possibilities for catenary action after quasi-static internal column removal. The test setup considered a two-span configuration, with deformations applied at the location of the removed internal column. A series of frames with T-section and double type connectors, were studied to investigate the maximum mid-span deflections and rotation supply at the supports. Observed typical failure modes were brittle wood failure under the imposed axial forces and large deformations, noted by tension perpendicular to the grain of the internal column. Adequate resistance mechanism was only triggered for the T-section, given the recorded maximum mid-span deflection and rotations at supports. The authors scheduled further testing on post-and-beam 3D 2x2 bays, see Figure 2-7b, under quasi-static edge column removal, to investigate possible collapse-resistance mechanisms accounting for 3D effects of the surrounding bays.

Figure 2-7: Test setups: 3D post-and-beam frame (Lyu et al., 2018) (Reprinted with permission)

At the Swiss Federal Institute of Technology (ETH Zurich) in Switzerland, a five-year research plan on structural robustness of mass-timber buildings is on-going in collaboration with the industry (Voulpiotis, 2019, Personal communication). The aim of the research is to investigate structural robustness for all types of mass-timber structures with emphasis on structural behaviour and reliability of buildings as well as the connections between different structural components. The research plan first examines the topic of structural robustness starting from its definition, to provide a better understanding of its application to mid- and high-rise mass-timber buildings. Thereafter, investigations based on experimental tests and numerical FE modelling are scheduled to be performed in the near future. This study attempts to provide simplifications to translate the existing knowledge of structural robustness, which is based on concrete and steel structures, to useable methodology and strategies for mass-timber practices.

2.7.6 Structural Robustness of Constructed Mass-timber Buildings

With the lack of specific guidance, solutions to prevent disproportionate collapse for mid- and high-rise mass-timber buildings are generally based on engineering judgements. For the design of the Stadthaus apartment building, the ideal design strategy against disproportionate collapse was a policy of efficient redundancy in addition to ALPA (Wells, 2011). ALPA, with single length wall removal, as per EN1991-1-7, was followed to ensure that subsequent failure did not go beyond the set collapse thresholds. In addition, the structural layout was selected for efficient redundancy: after element removal, the floor system was designed to either cantilever or span in two directions. A sufficient number of loadbearing walls of the honeycomb structural layout, with cross-walls, enabled the reduction of the tributary area and provided alternate load-paths (Wells, 2011). Furthermore, given their in-plane stiffness, CLT wall panels were designed to act as deep beam whenever the support underneath was removed.

For the Redstone Arsenal hotel, the designers used the ALPA as described in UFC 4-023-03 to ensure the distribution of forces from the assumed initial damage to the undamaged part of the structure (Wood-Works, 2016). The considered method accounted for a sudden removal of vertical loadbearing elements, to trigger dynamic behaviour on the building, and elastic linear material properties for wood components (Steimle, 2017, Personal communication). Advanced analyses on the connections were not performed as focus was on the structural performance at global level. The resulting stresses on the elements as well as their connections, considered as demands, were checked against corresponding force and deformation supplies. The design provided additional panel-to-panel straps with nails at numerous locations to act as chords and improve the structural performance. The results of the analyses showed adequate performance of the building with

respect to large deformations. The CLT wall panels also acted as deep beam for disproportionate collapse prevention (Steimle, 2017, Personal communication).

For the Treet building, ALPA as per EN1991-1-7 was followed for structural safety against disproportionate collapse (Abrahamsen and Malo, 2014). In the FE models, the main trusses were removed, one at the time, to ensure that the building could undergo large deformations with acceptable damage as per the set EN1991-1-7 thresholds. The power storeys were utilised as a compartmentalisation strategy to contain the possible collapse within a single compartment. Additionally, the concrete deck was designed to not collapse after damage to internal trusses by allowing large deformations. The flights in the main staircase, the corridor floors, and the balconies were all designed against debris loading from the level above (Abrahamsen, 2017, Personal communication). For the Mjøstårnet building, ALPA as per EN1991-1-7 was also utilised to ensure structural robustness (Huber et al., 2018a). Removals of diagonal trusses as well as the supports of the concrete floors were considered. The timber floors below the concrete floors were designed to sustain the impact of the failure of the concrete floor above. In addition, GLT columns were designed as key elements to reduce their vulnerability. The connections were designed to accommodate large deformations.

Since there are no disproportionate collapse requirements in the NBCC, the design for the Brock Commons followed EN1991-1-7 to improve structural safety after extreme events (Fast and Jackson, 2017). After the ALPA, a novel connection detailing, see Figure 2-8a, was developed to allow the column to hang on the upper levels if the support underneath was to be damaged. The column-to-column connection has a pin passing through the round hollow (HS) and solid (SS) sections, acting as a vertical tie transferring the forces to the level above through the connecting

column (Jackson, 2017, Personal communication). Furthermore, the design ensured that the CLT floor panels were double or triple-span, and the floor-to-floor joints were designed for strength and stiffness necessary for adequate structural integrity after element removal. For the HoHo building, the connections, see Figure 2-8b, were designed to provide horizontal and vertical ties (Woschitz and Zotter, 2017). The vertical ties consisted of glued-in steel rods connected to steel jackets in the concrete beams. The horizontal ties consisted of cast-in reinforcement bars between beams and floors. The ties were casted with grout on site. In addition to the ties, the design of the HoHo considered EN1991-1-7 ALPA with column loss to distribute the loads to the nearby columns via the continuous concrete beams.

(a)   *(b)*
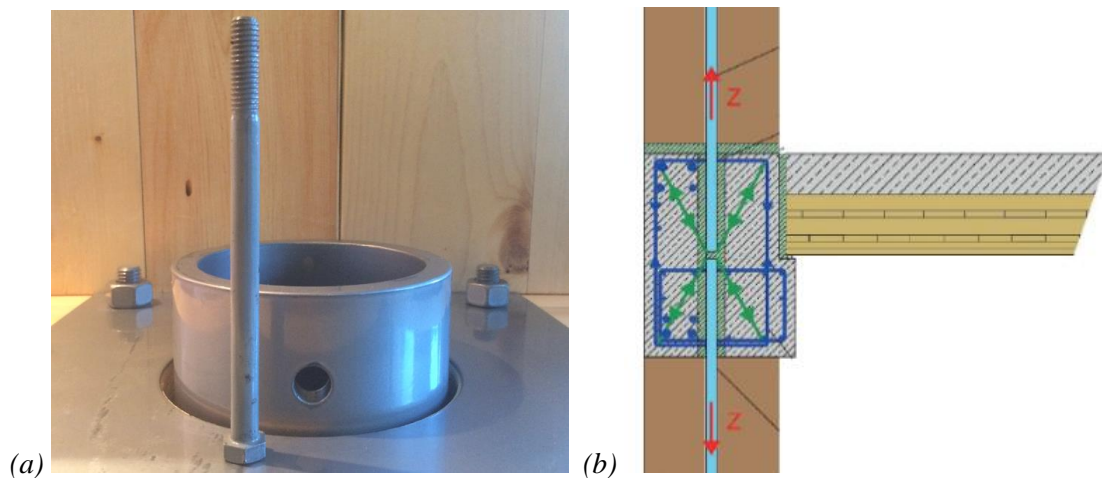
Figure 2-8: Novel connection detailing for structural robustness: (a) Brock Commons building (Photo credit Mpidi Bita); (b) HoHo building (Woschitz and Zotter, 2017) *(Reprinted with permission)*

Although different pragmatic approaches were used to provide structural robustness under extreme loading scenarios, the design of the aforementioned constructed mid- and high-rise mass-timber buildings did not account for ALPA with nonlinear dynamic analyses to obtain realistic structural behaviours and economic solutions, given the lack of data for this new construction method.

Therefore, there is a need to pinpoint the areas where further research is needed to help in the design of mass-timber buildings against disproportionate collapse.

2.8 Summary

The main summary from the state-of-the-art review is the lack of design guidance as well as code requirements for disproportionate collapse prevention for mid- and high-rise mass-timber buildings. For the considered building type, research studies on this topic are also scarce. For constructed mid- and high-rise mass-timber buildings, consideration for disproportionate collapse preventions was left to engineering judgment and best practice of the designer. In some instance, the applied solutions resulted to uneconomical designs given the considered assumptions. Therefore, there is a need for further research resulting to between approximations of the performance of mid- and high-rise mass-timber buildings with respect to disproportionate collapse prevention.

Chapter 3: Survey of Contemporary Practices for Structural Robustness[1]

3.1 Objective and Overview

An online survey was conducted to gather information regarding structural robustness and disproportionate collapse prevention in contemporary engineering practice. The objective was to investigate the factors influencing the decision for applying existing structural robustness design methods in building design in different regions and using different structural materials. The findings from the survey can inform on the development of disproportionate collapse prevention guidelines and future revisions of building codes.

3.2 Methodology

To achieve the objective, an online survey is an efficient tool to reach many individuals at a global scale, in an economical manner, compared to other methods (Wright, 2005; Van Selm and Jankowski, 2006). The automated recording in an online survey saves time, for both the issuer and the respondent, and a possible interviewer bias is eliminated (Van Selm and Jankowski, 2006). The main disadvantages of online surveys are the uncertainty regarding the validity of the collected data and the almost inevitable sampling bias (Wright, 2005; Van Selm and Jankowski, 2006). To address the latter, it is recommended to use online surveys for non-random samples of populations. Such samples may not allow for a statistical inference regarding the underlying population; however, they may be representative for a specific group (Van Selm and Jankowski, 2006).

---

[1] Materials from this chapter were submitted for Journal publication. Mpidi Bita, H., Huber, J.A.J., Voulpiotis, K., & Tannert, T. (2019). Survey of Contemporary Practices for Achieving Structural Robustness.

For this research, sampling began by inviting the initial participants via e-mail, chosen from the authors' professional networks, i.e. design engineers, and university researchers specialized in structural analysis and design. The participants were then asked to forward the invitation to their respective colleagues within their professional networks, which extended the outreach and constituted a non-random sample of participants (Kelley et al., 2003). Although the survey was anonymous, and responses were not linked to participants, the validity of the collected data was deemed acceptable as the initial participants were selected by the authors.

The survey targeted practitioners and researchers in concrete, steel and timber industries, mainly located in Europe, Canada, the USA, Australia, and New Zealand. Invitation to the survey was sent only once, without follow-up to confirm participation. Participation was primarily motivated by curiosity and willingness to share opinions. Responses were collected for six months, from May to October 2018 and responses received after that period were not considered. The number of collected answers allowed for manual checks of the soundness of the answers.

The questionnaire contained a total of 16 single-answer and multiple-answer questions; for the latter, respondents could select more than one answer. Question-6 was as multiple-answer question to allow participants to select the average size of the project in terms of height and floor area. During compilation of the received responses, for the single-answer questions, the occurrence of each answer was counted and the percentages of the total number of answers were calculated. For the multiple-answer questions, equal priority was assumed for all selected answers; answers by one respondent were uniformly weighted to avoid an overrepresentation of respondents with many answers. E.g. each alternative counted $1/n$, where n is the total number of answers by a single

respondent. For each answer alternative, the weighted answers obtained from all participants were then summed to calculate the percentage with respect to all answer options.

The considered method for data processing enabled to quantify the obtained responses and drawn conclusions that would be in line with the objective of this study. Questions 1-8 were used to create a profile of the respondents, and Questions 9-16 focused on the participants' understanding as well as practices for structural robustness and disproportionate collapse preventions. The answers were categorised with respect to the primary material and location of the respondents' projects. At the end of the questionnaire, the respondents were able to provide additional comments at the end of the questionnaire.

3.3 Results

3.3.1 Results of the Respondent Profile

Question-1 was: "Where are you based?". The proposed single answers were: i) Europe, ii) Canada, iii) USA, iv) Australia/New Zealand (Aus/NZ), and v) Other. Figure 3-1a illustrates the proportions of the received responses with respect to the respondents' location; 171 was the total number of participants to the questionnaire.

Question-2 was: "What is the main structural material used in the design or construction of your projects?". The proposed single answers were: i) Steel, ii) Concrete, iii) Timber, iv) Masonry, and v) Other. Figure 3-1b illustrates the material proportions within the defined regions, expressed as a percentage (%) of the total number of respondents per region.

(a)
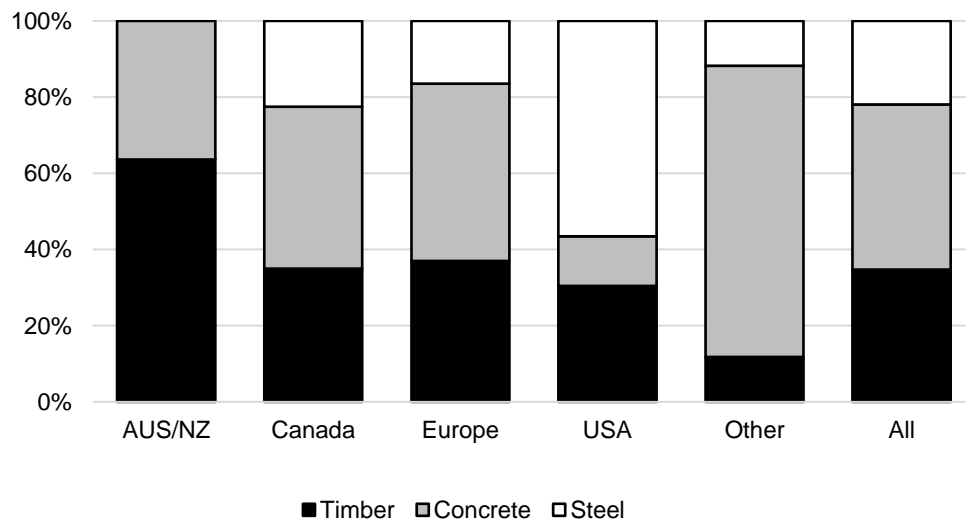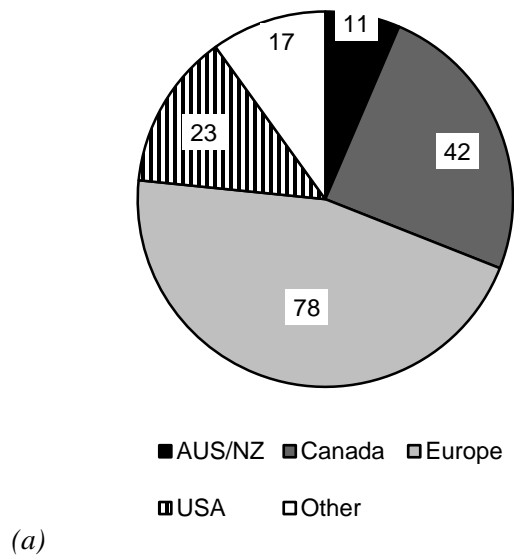
(b)

Figure 3-1: (a) Respondents' location; and (b) Primary project material split after location

Question-3 was: "What is your primary activity?". The proposed single answers were: i) Structural Engineering, ii) Architecture, iii) Fabrication, iv) Construction management, v) Business and project management, vi) Construction development, and vii) Others. Figure 3-2a illustrates the proportions with respect to the respondents' primary activity; with "All others" representing every other proposed field of expertise except structural engineering.

Question-4 was: "How many years of experience do you have in your field of practice". The proposed single answers were: i) New graduate, ii) 1-2 years, iii) 3-10 years, iv) More than 10 years, and v) I am a researcher. Figure 3-2b illustrates the proportions with respect to respondents' practical experience.

(a)

(b)
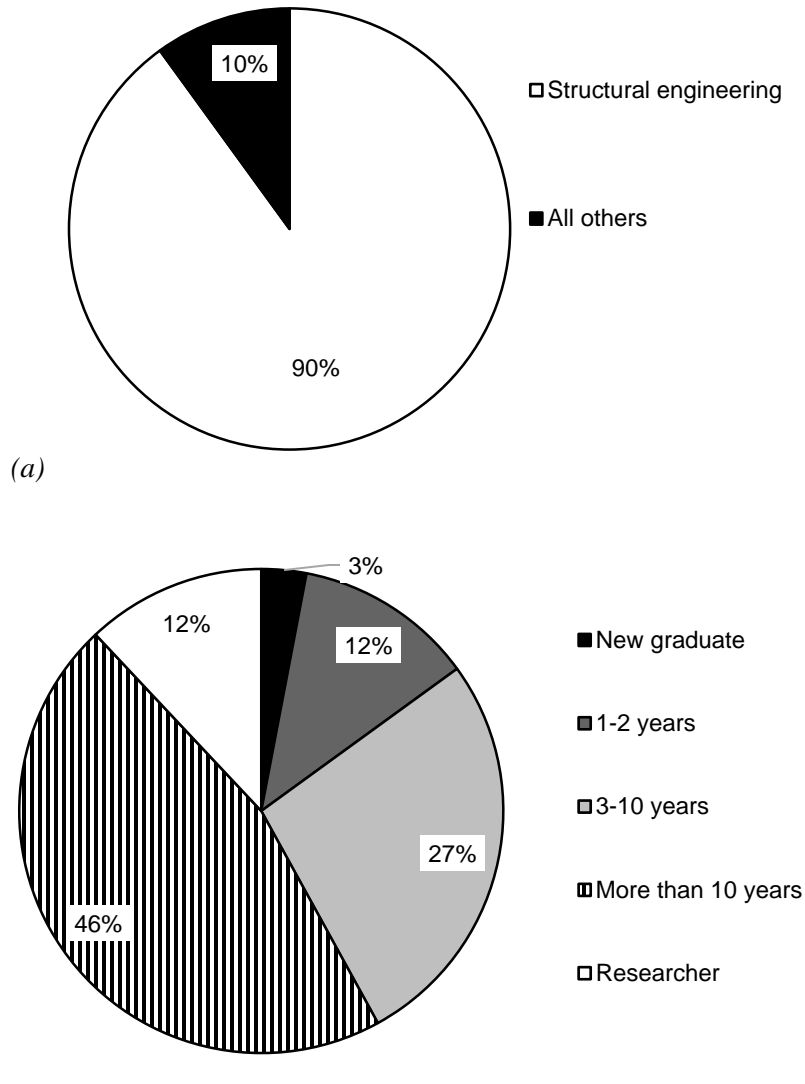
Figure 3-2: Expertise proportions with respect to: (a) Field; and (b) Experience

Question-5 was: "What type of projects do you personally mostly work on". The proposed multiple answers were: i) Residential, ii) Commercial, iii) Industrial, iv) Public, v) Military and Federal, vi)

Bridges and other infrastructure, and vii) Other. The results of the obtained proportions are illustrated in Figure 3-3a.

Question-6 was: "What is the average size of the primary project you are involved in?". The proposed multiple answers were: i) Single occupancy not exceeding 4 storeys, ii) Multiple occupancy not exceeding 4 storeys, iii) Multiple occupancy not exceeding 15 storeys, iv) Buildings higher than 15 storeys, v) Buildings with large area and significant occupancy, and vi) Other. The results of the obtained proportions are illustrated in Figure 3-3b.

(a)

(b)
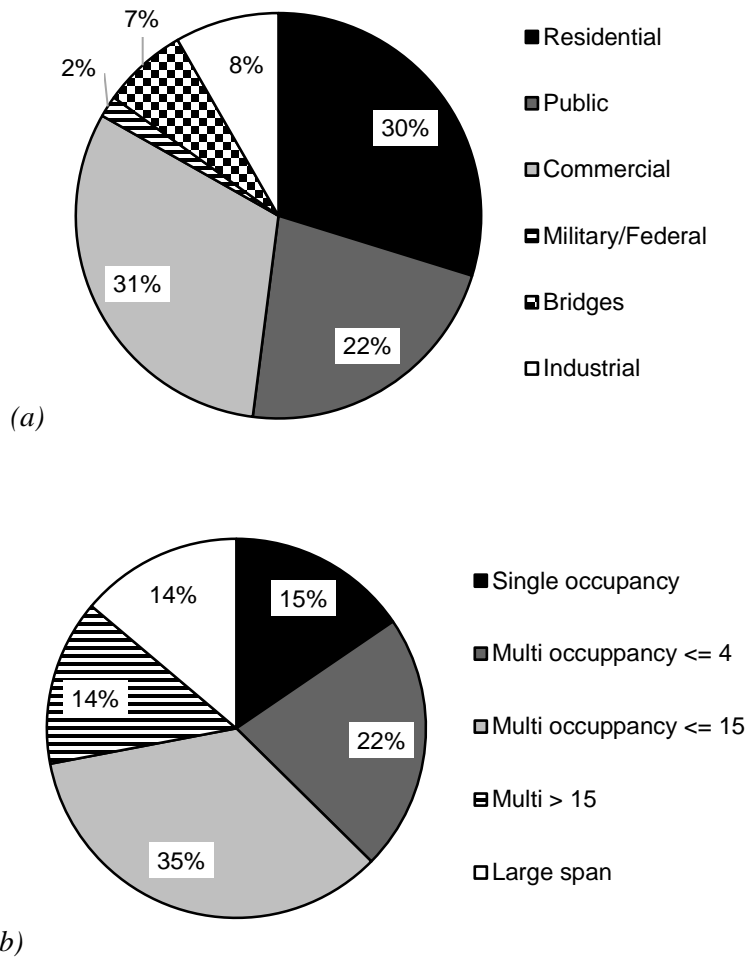
Figure 3-3: Project proportions with respect to: (a) Type; and (b) Size

Question-7 was: "How familiar are you with the concept of structural robustness and disproportionate collapse?". Responders selected one number on the scale 0-10, with 0 corresponding to '*not familiar*' and 10 corresponding to '*very familiar*'. The responses were truncated into three categories for clarity of presentation: *low* (1-4), *medium* (5-7) and *high* (8-10). Figure 3-4 illustrates the proportion of responders in each familiarity category, with respect to the primary materials as well as the participants' location.
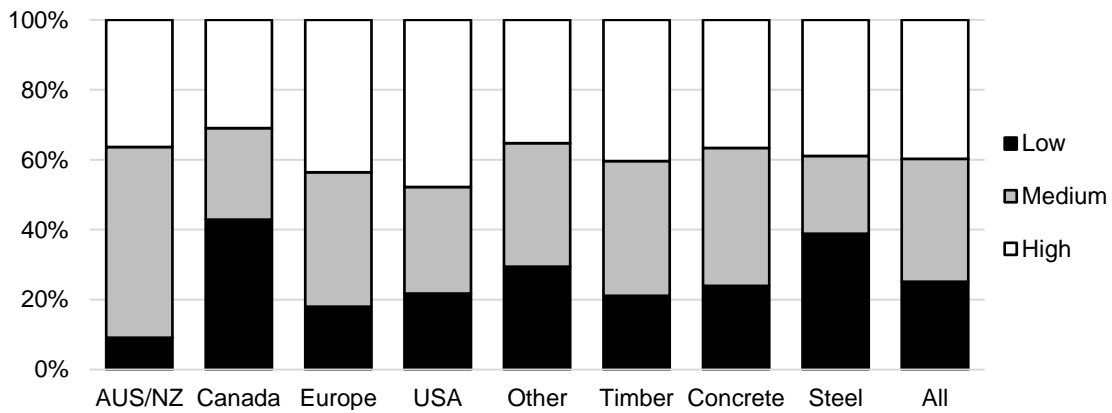
Figure 3-4: Familiarity with structural robustness with respect to the primary materials

Question-8 was: "Where did you first get exposed to the concept of structural robustness and disproportionate collapse?". The single answers were: i) University undergraduate, ii) University research; iii) Internship during studies, iv) In practice, v) Never been exposed, vi) Other. Figure 3-5 illustrates the results with respect to the location of first exposure to the concept of structural robustness.
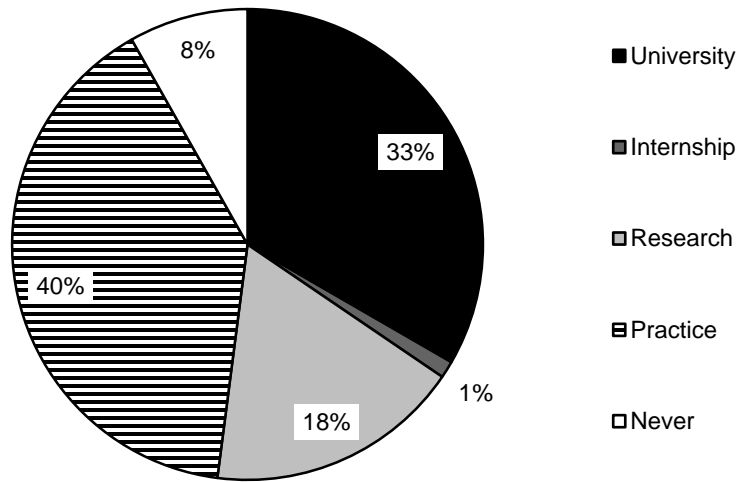
Figure 3-5: First exposure to structural robustness

3.3.2 Results of the Topic-specific Questions

Question-9 was: "Do you consider structural robustness or disproportionate collapse prevention in your designs?". The single answers were: i) "Yes", ii) "No", or iii) "Not applicable". The results are illustrated in Figure 3-6 and exclude the 'not applicable' answers which were 11 out of the 171 participants.
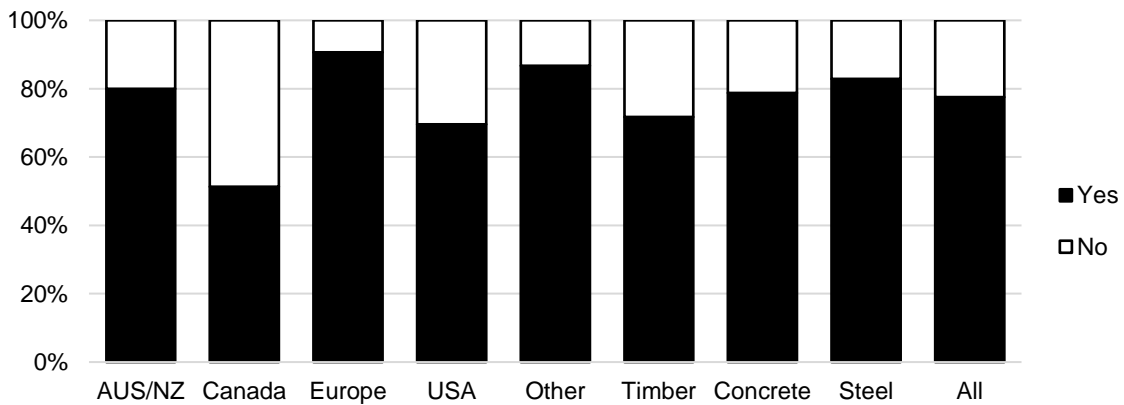
Figure 3-6: Consideration of robustness with respect to primary material and location

Question-10 was: "If you do not consider structural robustness or disproportionate collapse prevention, what are the main reasons for it? Please select the reason(s) that best apply". The multiple answers were: i) It is not a code requirement, ii) Complexity / lack of expertise, iii) Budget / cost premium, and iv) Low probability events. The results, shown in Figure 3-7, only considered participants who answered 'no' for Question-9 (36 out of 171 participants).
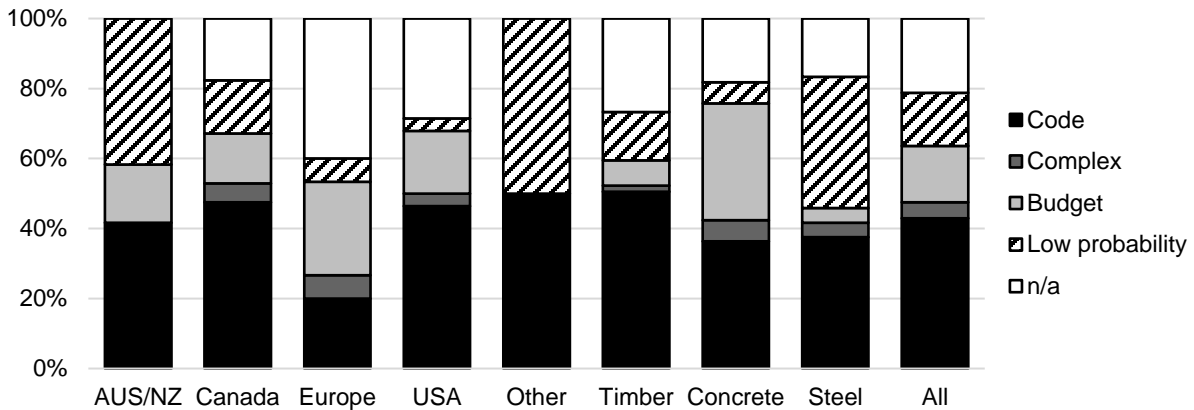
Figure 3-7: Main reasons for not considering structural robustness

Question-11 was: "If you do consider structural robustness or disproportionate collapse prevention, what are the main reasons for it? Please select the reason(s) that best apply". The multiple answers were: i) It is a code requirement (*code*), ii) Best practice depending on project (*project*), iii) Best practice regardless of project (*regardless*), and iv) I am contracted to provide expertise in structural robustness and collapse prevention (*expert*). The results for respondents who answered 'yes' on Question-9 (124 out of 171 participants), are shown in Figure 3-8.
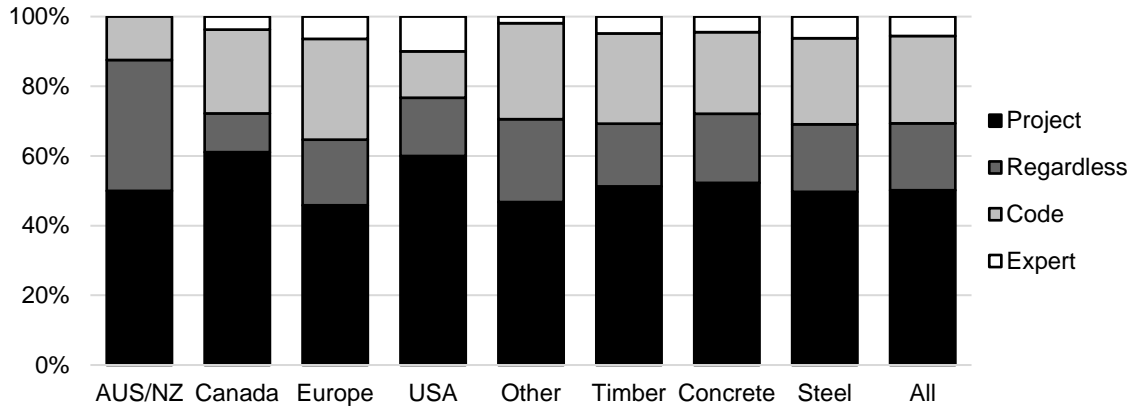
Figure 3-8: Main reasons for considering structural robustness

Question-12 was: "If you do consider structural robustness or disproportionate collapse prevention, what do you mainly design for? Please select the answer(s) that best apply". The multiple answers were: i) Human errors (in design, construction, manufacture, execution, etc.), ii) Material deficiencies and degradation, iii) Accidents (terrorism, fires, explosions, impact, sabotage, etc.), iv) Natural catastrophes (extreme earthquakes, wind, waves, etc.), and v) I consider nothing specific. Figure 3-9 shows the results for the respondents who answered 'yes' to Question-9 (124 out of 171 participants).

Question-13 was: "To what extent do you consider structural robustness and disproportionate collapse prevention in your designs?". The multiple answers were: i) Basic ALPA (linear static analysis), ii) Thorough ALPA (nonlinear and/or dynamic analysis), iii) Minimum tie-force for structural integrity, iv) Overdesign members and connections (key element design), v) Compartmentalisation/ segmentation of structure, and vi) Engineering judgements based on principles of engineering mechanics. In Figure 3-10, only the answers of the respondents who answered 'yes' to Question-9 were considered (124 out of 171 participants).
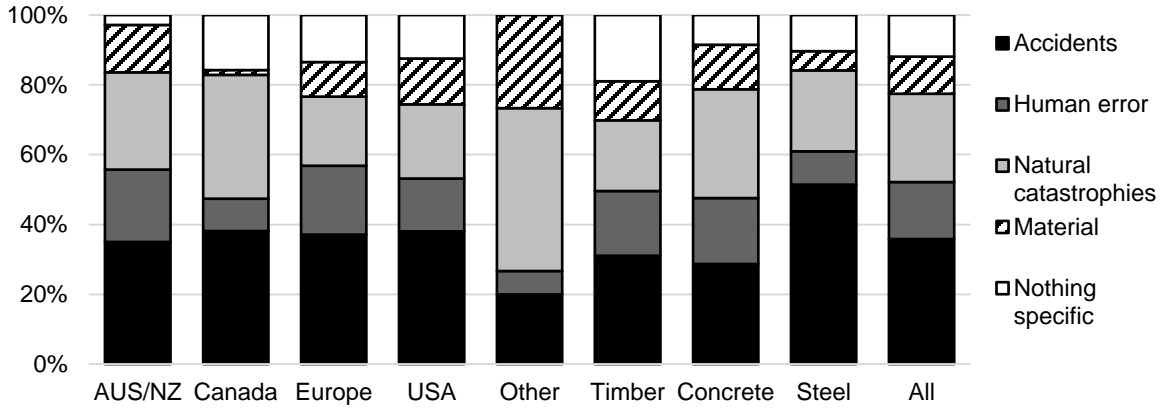
Figure 3-9: Extreme events considered in the design
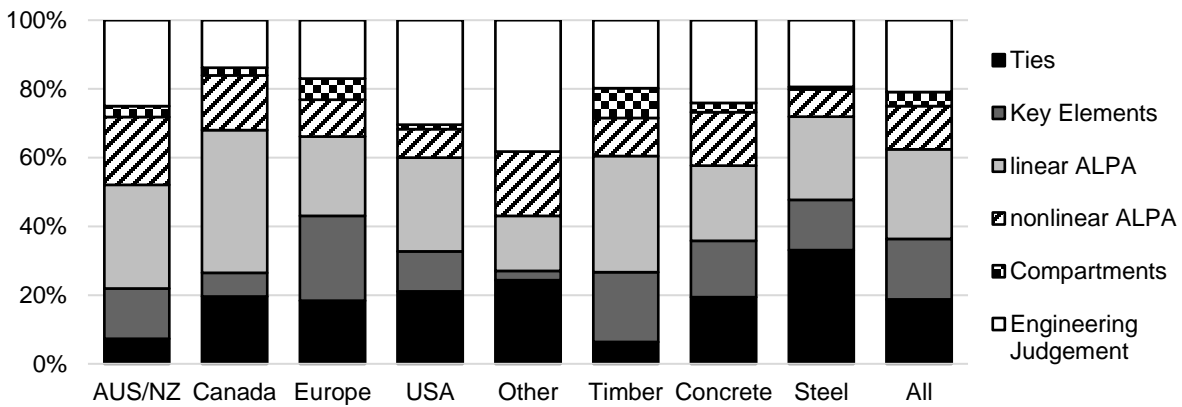
Figure 3-10: Analysis approach for structural robustness

Question-14 was: "How satisfied are you with prescriptions in the current design standards you use to meet structural robustness requirements and disproportionate collapse prevention?". Respondents selected from the scale 0-10, with 0 corresponding to '*not satisfied*' and 10 to '*very satisfied*'. The received answers accounted for all participants and were truncated into the three satisfaction categories: *not satisfied* (0-4), *fairly satisfied* (5-7), and *very satisfied* (8-10). Figure 3-11 illustrates the proportion of responders in each satisfaction category.
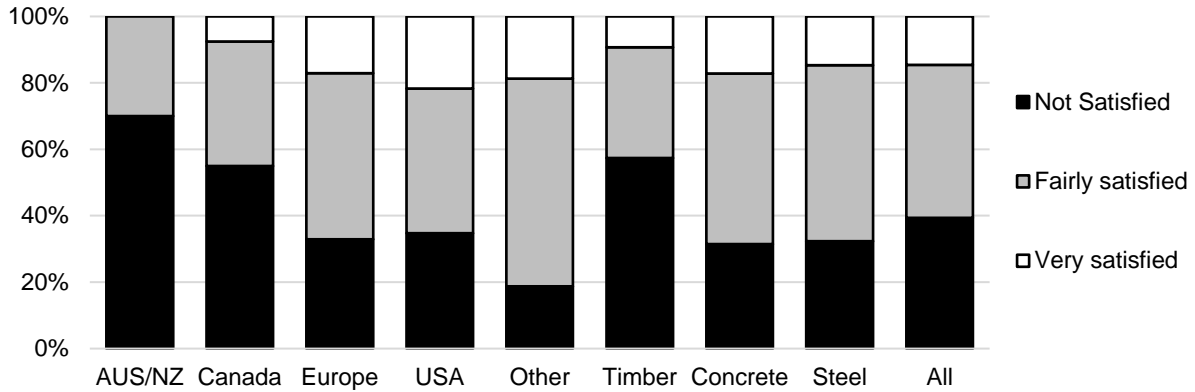
Figure 3-11: Satisfaction level with respect to location's code or guideline

Question-15 was: "What improvement(s) would you wish with respect to structural robustness and preventing disproportionate collapse?". The multiple-choice responses were: i) Prescriptive code requirements for analysis / minimum safety level for structural integrity, ii) Code recommendations or general guidelines (minimum tie-force and structural detailing, alternate load path analysis, etc.), and iii) More practical analysis examples and tutorials. The results shown in Figure 3-12, give the number of times each option was selected for all participants to illustrate individual option's popularity.
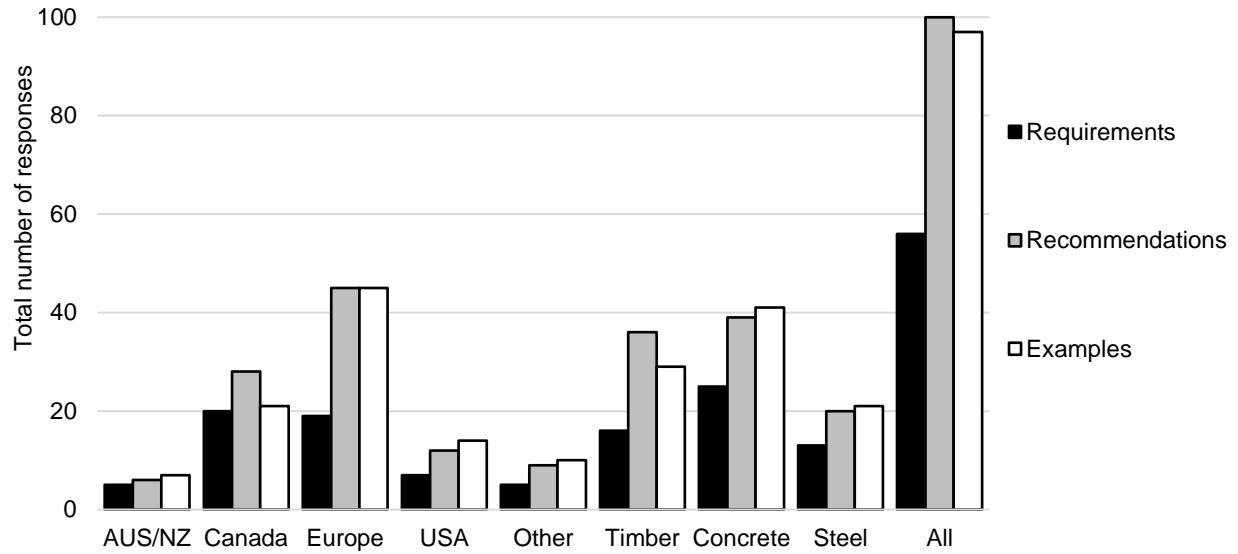
Figure 3-12: Desired improvements of the respondents

Question-16 was: "Do you recommend that the design for robustness or disproportionate collapse prevention be required/recommended for any type of building/structure or only for specific ones?". The single-choice answers were: i) All buildings/structures, or ii) Only specific buildings/structures. The results for all participants can be seen in Figure 3-13.
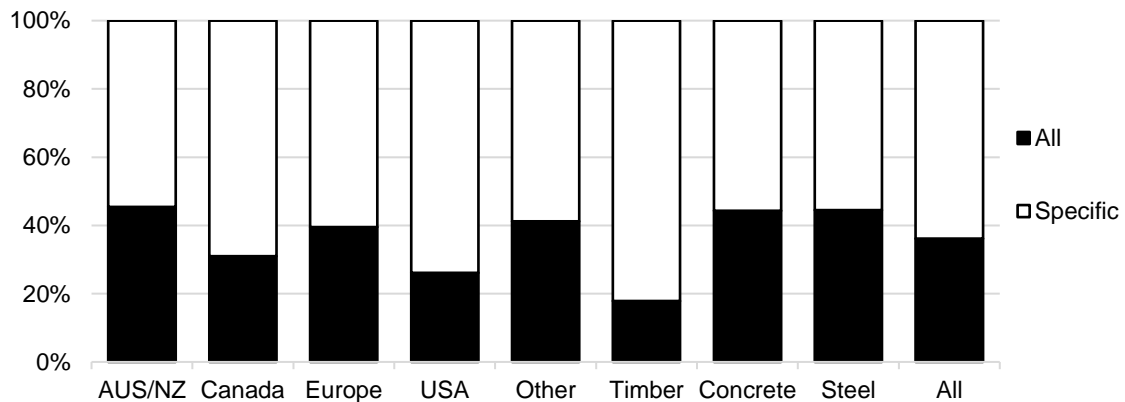
Figure 3-13: Applicability of disproportionate collapse prevention

3.4 Discussion

3.4.1 Online survey

The main advantage of the online survey was that it proved to be cost-effective and convenient to gather answers on the desired questions from individuals worldwide. Given the sampling method and the voluntariness, the survey might have attracted primarily respondents with an engineering background and an interest in the underlying topic, leading to a sampling bias. Any statistical inferences might therefore be primarily valid for the subgroup of engineers who in some way were involved with the issues of robustness and disproportionate collapse, and not for the entire structural engineering community. Considering the answers and comments of the participants, the validity of the data was evaluated to be acceptable for this thesis. If a follow-up and improvement of the survey might be issued in the future, it was recommended to improve the unambiguousness of the questions and to allow primarily single instead of multiple answers.

3.4.2 Responses on Respondent's Profile Questions

The participation from different regions constituted an acceptable estimate of the targeted stakeholder population. The large participation in Europe was because the questionnaire was circulated to several countries including the UK, Sweden, Switzerland, Germany, and Austria. The obtained balanced distribution between the participants' primary project material also enabled a comparison among them. Most respondents were structural engineers, presumably because the questionnaire was distributed within the authors' professional networks.

Given that 85% of participants had at least three years of experience, it could be argued that a good representation of the current design practice with respect to structural robustness was received.

Respondents were mostly involved in the design of buildings, mainly taller than four storeys or with large spans. This fact might have influenced their familiarity given that some codes (e.g. EN1991-1-7) require structural robustness considerations for such buildings. It seemed that familiarity with the topic was influenced by the consideration of structural robustness in the building codes. Of particular interest was the low familiarity level in Canada, where the building code does not contain requirements for structural robustness. This was also observed for respondents working with timber, for which there are no specific considerations.

3.4.3 Responses on Robustness Consideration Questions

Most survey respondents consider disproportionate collapse prevention in their designs. Because of the sampling bias discussed above, the results were skewed in favour of considering structural robustness. The high correlation between the respondents' level of familiarity and whether robustness was considered in design was expected. Most respondents who did not consider structural robustness where from Canada, when considering the location, and timber engineers, when considering the primary structural material. The main reason for these low considerations could be the lack of guidelines both in Canada and for timber. Therefore, it can be argued that the existence of guidelines increases awareness and application of disproportionate collapse prevention. However, only a large-scale survey amongst the memberships of the respective engineering associations could comprehensively address these observations.

The lack of specific code requirements was the main reason given by all participants for not considering structural robustness. Budget considerations, the low probability of an extreme event, and the complexity of designs against disproportionate collapse accounted together for only 36%. These findings suggest that apart from early adopters, mainstream changes in construction practice

are still driven by code implementations. Furthermore, five respondents commented that structural robustness is often assumed to be inherently satisfied for structures designed in high-seismic regions. Although this might be true for some cases, such a statement cannot be generalised.

The respondents who considered structural robustness did it predominantly because of best design practice, regardless the material. Interestingly, the building code only accounted for 25%, given that the lack of code requirements as the main reason for respondents to not consider robustness. This contradiction could have been caused by the fact that the respondents who considered structural robustness were also more knowledgeable in the topic. The familiarity seems to bring awareness on the topic's importance, independently of code requirements. When considering collapse prevention, for all materials, designers identified accidents and natural disasters as main causes for abnormal loads. A reason for this may be that accidents and extreme earthquakes have caused prominent examples of disproportionate collapse.

3.4.4 Responses on Robustness Design Methods Questions

Linear ALPA was identified as the most used method to ensure structural robustness, possibly because it is a simple and conservative method. The tie-force method showed some material-specific variations: although widely applied for concrete and steel structures, it was generally not used for timber structures. Given the requirements for large deformations for the safe use of the tie-force methods, it is no surprise that fewer timber designers chose this option. Engineering judgments based on the principles of mechanics are used to a considerable extent in the design for all buildings. Engineering judgement implied that either suitable code requirements from other codes or other pragmatic solutions were used to ensure robustness. Finally, key element design,

showed a high variation in its use across different regions but a rather consistent usage across the different primary materials.

3.4.5 Responses on Satisfaction of the Codes and Guidelines Questions

The survey respondents were rather dissatisfied with the current code prescriptions for structural robustness. A positive correlation between the lack of robustness code requirements and code dissatisfaction was observed, e.g. for timber, with respect to materials, and for Canada, with respect to region. Regarding the types of structure to be considered for implementing robustness, almost two thirds of the respondents noted that disproportionate collapse prevention should be considered only for specific buildings. This supports the current code categorisation into consequence or importance classes.

Regarding the improvement of robustness-related guidance, most respondents opted for recommendations and general guidance rather than prescriptive code requirements. This implies codes should provide performance-based approaches, to guide designer towards practical and economical solutions for disproportionate collapse prevention. Nonetheless, as mentioned above, the survey might have attracted primarily engineers who are knowledgeable in robustness and hence may have a better appreciation of the difficulty to provide simple, prescriptive rules. Providing specific examples and tutorials was also favoured over prescriptive code requirements; this reinforces the need for more detailed guidance on the topic. Six respondents commented on the disadvantage of prescriptive code requirements, e.g. generalised minimum tie-force requirements, as these often increase project costs without guaranteeing best solutions.

3.5 Summary

This chapter first summarised the literature with respect to structural robustness and disproportionate collapse prevention. To obtain a picture of the contemporary practice within this field, a questionnaire was conducted amongst practicing engineers. The results from 171 respondents were evaluated and pinpointed research needs and areas for improvement. From this survey, the following conclusions can be drawn:

(1) The lack of code provisions on structural robustness and design against disproportionate collapse has a detrimental effect on the consideration of structural robustness, e.g. for timber and in Canada.

(2) Building codes should include specific recommendations for structural robustness and disproportionate collapse prevention, applicable to specific building classes, as a performance-based approach.

(3) Awareness on the topic of structural robustness and disproportionate collapse prevention should be increased. This could be achieved by general guidelines, practical examples, and tutorials.

The findings on the existing practise are primarily valid for engineers who are involved with robustness and disproportionate collapse prevention. It is recognised that only large-scale surveys, with representative participations of regions and construction materials, could provide comprehensive answers on the industry-wide application of structural robustness in design and the satisfaction level concerning current building codes. Nonetheless, the findings from this survey pointed to the need for direct code requirements for disproportionate collapse preventions and practical design guidance.

Chapter 4: Analysis of a Twelve-storey Platform-type Building[2]

4.1 Introduction

Given the lack of research investigating the performance of mid-rise mass-timber buildings for disproportionate collapse prevention, there was a need to consider practical examples to illustrate analysis approaches as well as design methods in order to find practical solutions to satisfy structural robustness. In other words, illustrate analysis techniques for investigation of the structural performance of mass-timber buildings following extreme loading events.

Timber Research and Development Association (TRADA) (TRADA, 2009) published a report to illustrate the design of mid-rise CLT platform-type building under gravity and lateral wind loads, using a twelve-storey case study. From the report's conclusions, disproportionate collapse prevention analysis was among the areas recommended for further studies. Herein, thorough and detailed investigations considering the impacts of parameters such as removal of different loadbearing elements, the CLT panel layups and the connection properties, were required.

---

[2] Materials from this chapter were published in the following journal and conferences:

Mpidi Bita, H., Currie, N., & Tannert, T. (2018). Disproportionate collapse analysis of mid-rise cross-laminated timber buildings. Structure and Infrastructure Engineering. DOI: 10.1080/1532479.2018.1456553.

Mpidi Bita, H., Currie, N., & Tannert, T. (2017). Reliability analysis and disproportionate collapse for multi-storey cross-laminated timber building. World Conference on Earthquake Engineering, WCEE, January 9-13, 2017, Santiago, Chile.

Mpidi Bita, H., Currie, N., Tannert, T. (2016). Assessment of disproportionate collapse for multi-storey cross-laminated timber buildings. World Conference on Timber Engineering, WCTE, August 22-25, 2016, Vienna, Austria.

Mpidi Bita, H., & Currie, N. (2015). Assessment of disproportionate collapse for tall timber buildings. Salford Postgraduate Annual Research Conference, SPARC, May 26-28, Manchester, United Kingdom.

4.2 Objective

This chapter investigated the structural performance of a twelve-storey CLT building with platform-type construction after the loss of ground floor loadbearing walls, as initial damage following an extreme loading event. As a large panel construction, CLT buildings could only be as strong as the connection between individual loadbearing panels (Patel, 2014; Schultz et al., 1977b); 23% of structural failure in timber buildings were caused by inadequately designed and improperly fabricated joints (Fruhwald et al., 2007). Therefore, this chapter studied structural robustness by means of the rotational capabilities (θ), associated with the rotational stiffness (k) of the connections, necessary to develop collapse-resistance mechanisms. In addition to connection properties, the thickness and material properties of the CLT panels were also considered. As a further objective, a reliability analysis was conducted to compute the probability of disproportionate collapse after element removal.

4.3 Case Study

4.3.1 Building Description

The considered case study was a twelve-storey residential CLT building as proposed by TRADA (TRADA, 2009). The building was a box-shaped, in a platform-type construction identical to the Stadthaus apartment building; this was a 9m × 9m floor plan with 3m clear height, where all internal and external walls were loadbearing elements, see Figure 4-1a. As shown in Figure 4-1b, the walls were 9m long uninterrupted; the floor was double span, continuous over the internal loadbearing wall, which was placed halfway between the two external walls.
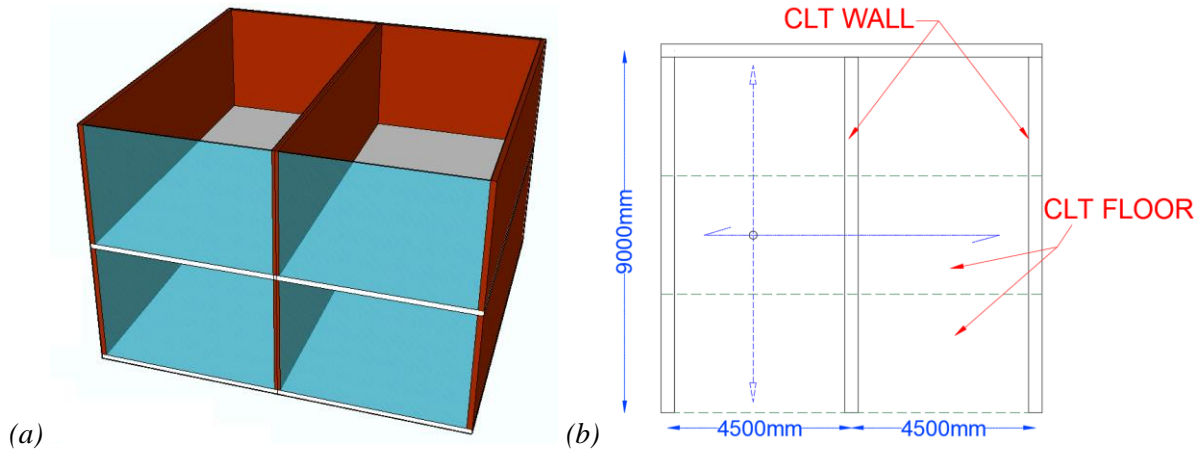
Figure 4-1: TRADA building: (a) Schematic isometric view; (b) Floor plan view

The TRADA design considered *DL*, *LL*, and *WL* to select CLT panels thicknesses and connections detailing for structural stability. *DL* was according to EN1991-1-1 (CEN, 2009) as 1.37kPa, 1.26kPa and 1.28kPa for floor, internal and external walls, respectively; the *LL* was 1.5kPa. The lateral load resisting system was designed to resist the applied *WL*, assumed to be 1.0kPa on the two orthogonal directions. Stability against overturning at the lower storey as well as the whole building was satisfied, and no additional hold-down were required. In the UK, earthquake loads were not considered for office and residential buildings. Resistance against sliding was provided by brackets at the interface with the adjacent storey or foundations. Furthermore, connections provided at the interface between perpendicular walls were also checked for lateral shear resistance; this was provided over the entire building height.

The calculations demonstrated that 126mm (floor and external walls) and 135mm thick (internal walls) 3-ply CLT panels met the EN1990 (CEN, 2006b) and EN1991 (CEN, 2009) requirements for stability as well as ultimate (ULS) and serviceability (SLS) limit states. The CLT floor panels were shown to possess adequate strength and stiffness to act as horizontal diaphragm considering that: (i) the span-to-depth ratio was less than 2:1; (ii) the span between supporting walls was less

than 12m; and (iii) the connections were designed to resist the applied horizontal shear forces. Table 4-1 presents the ratios between demands and capacities of the structural elements.

Table 4-1: Summary of design checks (TRADA, 2009)

Structural Components	Design Checks	Utilisations (%)
126mm CLT floor panel	Flexure	44
	Shear	23
	Deflection	88
	Vibration	56
135mm internal CLT shearwall	Combined axial and bending	50
	In-plane shear stress	21
	Bearing stress	138
126 mm external CLT shearwall	Combined axial and bending	85
	In-plane shear stress	12
	Bearing stress	73

Details of the full gravity and lateral designs could be found in the TRADA report (TRADA, 2009). These calculations also included the imposed limits on deflections and vibrations, according to EN1995-1-1 (CEN, 2008) from which the utilisation percentages shown in Table 4-1 were estimated. The deflection limit was taken as $l_{eff}/250$, where *leff* was 4/5 times the span according to EN1995-1-1 Annex B. The vibration checks followed EN1995-1-1 to account for transverse rigidity. Herein, the natural frequency of the floor, the maximum allowable static deflection, and the unit impulse velocity response of the floor, needed to be below their respective limits.

4.3.2 Scope and Connection Detailing

TRADA (TRADA, 2009) recommended that further checks were still needed: (i) bearing stress on CLT floor panels; (ii) disproportionate collapse as per EN1991-1-7 classifications with respect to the number of storeys and occupancy level; (iii) fire resistance; and (iv) design provisions for opening in shearwalls. The published report demonstrated the structural feasibility of the twelve-storey building under the assumed gravity and lateral loads. Therefore, the same assumptions for SLS and ULS designs were considered for the present study. The investigation presented herein only considered disproportionate collapse analysis of the case study building as recommended by UFC 4-023-03. Dynamic analyses using sudden loadbearing wall removal was performed, associated to large deformation to capture possible collapse-resistance mechanisms for disproportionate collapse prevention. The investigation presented herein was limited to mid-rise CLT buildings with platform construction which are, usually, residential, office or commercial buildings of normal or high importance according to the NBCC, or Class 2A/2B as per EN1991-1-7.

This study was based on the same layout and design as the TRADA example. The TRADA published report did not specify the CLT layup since different manufacturers could provide almost any desired layup. Herein, all panels were 3-ply CLT with equal thickness 42mm and 45mm, for 126mm and 135mm panels, respectively. The building was checked for conformity with the ULS and SLS of NBCC and the CSA-O86. It was confirmed that the capacity of the selected floor panels was adequate for gravity loads. TRADA considered wind pressure of 1.0kPa, therefore no further checks for code compliance were required as the wind loads according to NBCC were smaller. Since this investigation considered the ability to develop collapse-resistance mechanisms against disproportionate collapse following the loss of ground floor loadbearing walls, no

considerations were given on the wall-to-foundation connection detailing. This joint was restrained against translations in all three orthogonal directions.

To investigate the structural robustness of the building and its ability to develop collapse-resistance mechanisms against disproportionate collapse, the losses of the entire ground floor internal and external walls were considered as two different scenarios, according to GSA and UFC 4-023-03 guidelines. The first set-up emphasised on possible membrane and catenary actions of the floor system while the second triggered the cantilever mechanism, as explained in Chapter 5 of this thesis. It was assumed that strength, stiffness, and ductility of the connections alone controlled the overall stability of the building. The TRADA report did not detail the connections between the loadbearing components. A static analysis of the building was performed at the global level to obtain the forces at the connection level, which were then used to specify the details.

The main structural detailing of this platform-type construction, the floor-to-wall connection shown in Figure 4-2, was composed of: (i) self-tapping screws (STSs), 300mm long ASSY™ of 8mm diameter, to connect the floor to the wall below; and (ii) off-the-shelf angle brackets and regular wood screws fastened the floor to the wall above. STSs were connectors of choice for most mass-timber applications (Hossain et al., 2016); the specific products had a European Technical Approval ETA-11/0190 (ETA-11/0190, 2011). The angle brackets were 90mm wide (ETA-06/0106, 2008), 2.5mm thick without rib and were placed at 500mm centre to centre to connect the floor to the wall above. To connect the floor to the wall below, STSs were inserted at 90*deg*., with spacing of 500mm centre.
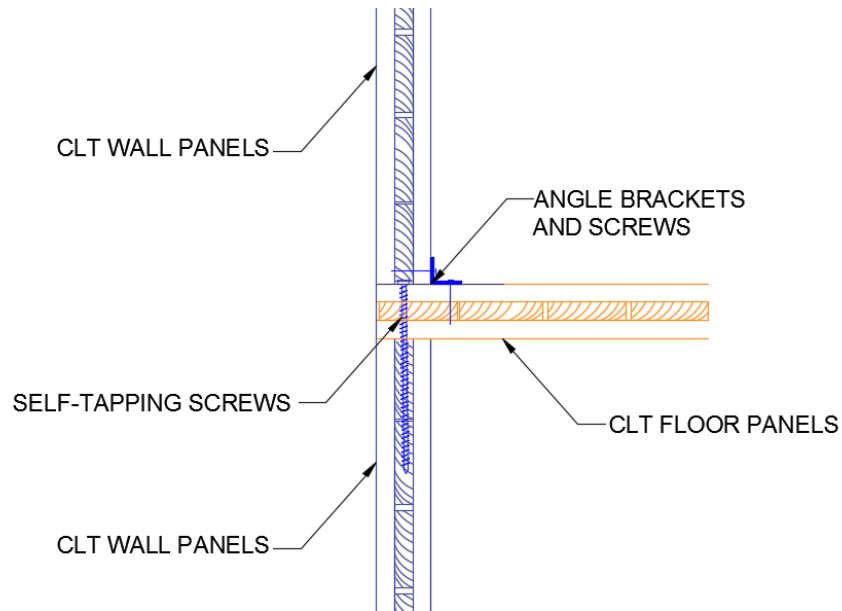
Figure 4-2: Floor-to-wall connection detailing for CLT platform-type construction

To investigate the building's behaviour at the structural (global), component (macro) and connection (micro) level, as shown in Figure 4-3, finite element (FE) analyses were performed. The commercial software package ANSYS (ANSYS, 2011) was utilised because of its capability to capture the geometric nonlinearity behaviour at every sub-step of the dynamic analysis at global level, and to model the floor-to-wall connection with screws and angle brackets in sufficient details in 3D. Therefore, this was a three-level structural idealisation, implemented at global, macro and micro levels.

(a)

Global Model

Micro Model

Macro Model

(b)
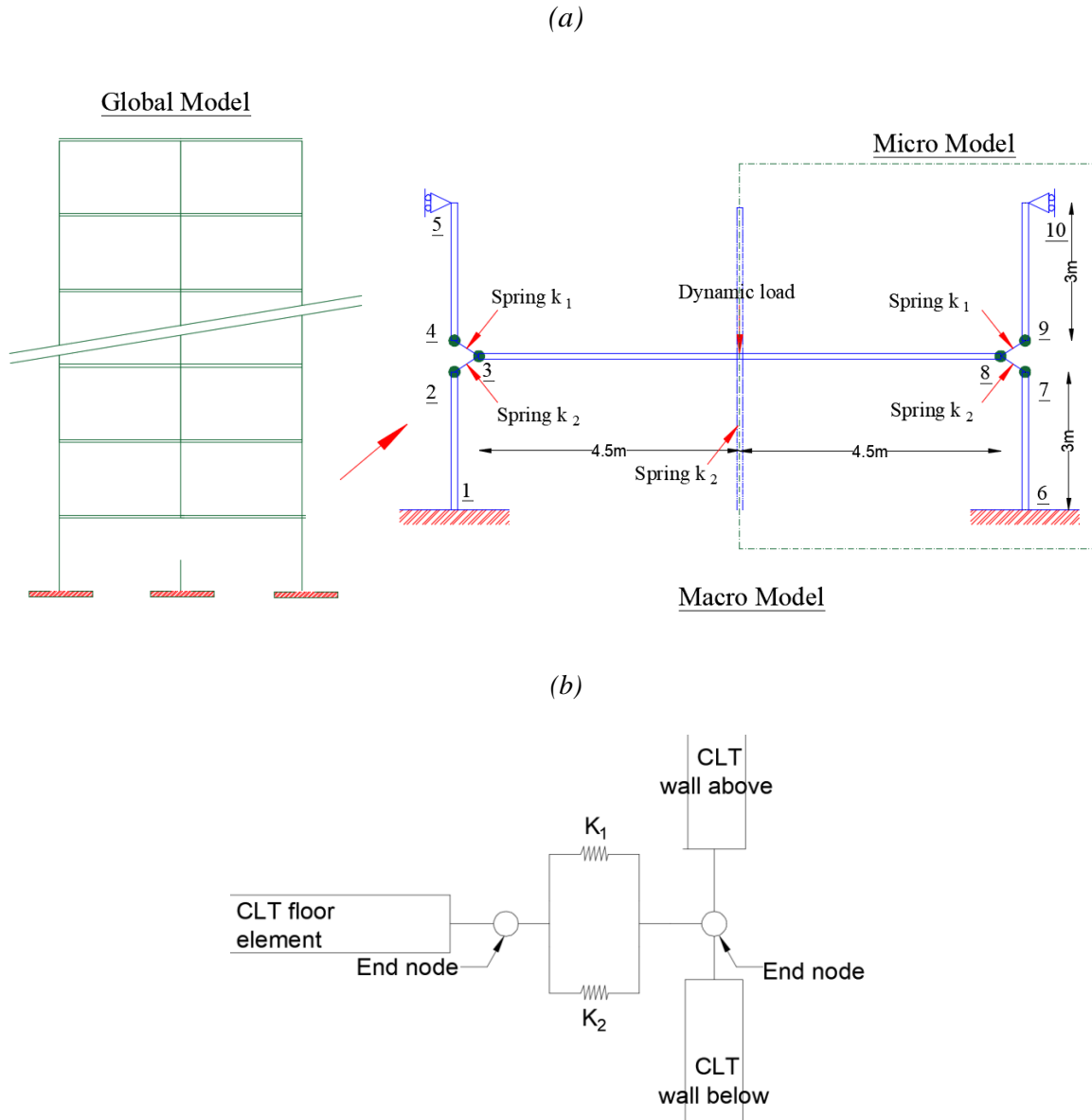
Figure 4-3: (a) Multi-level structural idealisation: Global model, Macro model, and Micro model (half of the Micro model); and (b) Micro model idealisation

4.3.3 Numerical Model Development: Global Model

Using the 3D global model, see Figure 4-4, the building behaviour after element removal was obtained from geometric nonlinear dynamic analysis. For the removal of the ground floor walls, the static case was compared to the dynamic case which accounted for the speed of removal. The

influence of the dynamic motions as compared to the linear static case, stated in UFC 4-023-03 as the dynamic increase factor (*DIF*), was assumed 2.0 for wood loadbearing walls. The static approach was identical to the TF2000 methodology (Milner et al., 2003), whereas the sudden removal triggered a dynamic response. The results from this level were considered as upper bound, in terms of force and deformation-demands on the structural components and their connections. At the global level, focus was on the resulting forces and deformations, and the ability of the building to trigger resistance mechanisms against disproportionate collapse. As a consequence, the joints were assumed to be fully fixed to allow for full force redistribution between different components.

(a)   *(b)*
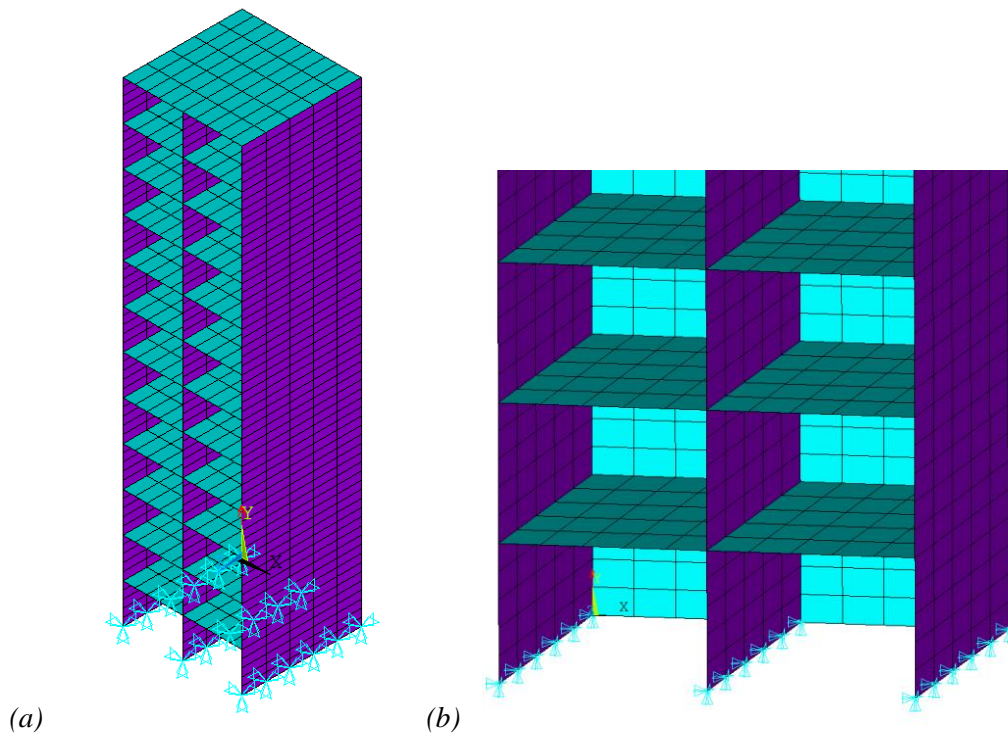
Figure 4-4: FE global model: (a) Isometric view full; and (b) Zoomed isometric view

The CLT walls and floors were idealised by 2D surface shell elements, made of different layers to represent the actual CLT layup, with linear orthotropic material properties. Table 4-2 lists the

values of the Moduli of elasticity (E), Shear moduli (G) and Poison ratios (U) for the longitudinal (L) and transverse (T) direction of timber, obtained from CSA-O86 and the wood handbook (Forest Products Laboratory, 2010). The CLT models were first verified with hand calculations for bending and shear capacities, using the shear analogy method (Gagnon and Pirvu, 2011), then validated against the experimental results of 5-ply CLT panels under four-point bending tests (Popovski et al., 2016), as shown in Appendix-A1. The floors were modelled 9m long, continuous over the internal support with no in-plane floor-to-floor connections. The top layer was longitudinal to the span direction, with the remaining layers oriented crosswise. The different layers were fully bounded and continuous along the width of the panel. Due to manufacturing limitations with respect to the width of the CLT panels (Structurlam, 2016), floor-to-floor connections were needed in the transverse direction of the building plan. With 3m as standard CLT width, three panels were needed at every floor level of the considered building in the transverse direction. The walls were 3m high continuous over their span (storey clear height).

Table 4-2: Material properties for timber elements

| Layer | E_L | E_T | G_L | G_T | ν_L | ν_T |
Direction	[MPa]	[MPa]	[MPa]	[MPa]	[~]	[~]
Longitudinal (L)	11,700	$E_L/30$	$E_L/16$	$G_{LT}/10$	0.35	0.07
Transverse (T)	9,000	$E_L/30$	$E_L/16$	$G_{LT}/10$	0.35	0.07

UFC 4-023-03 gave the locations of critical elements of the building to be removed as initial damage. To narrow down the number of analyses, the study assumed that plastic hinges and accumulated damages, e.g. during extreme earthquakes, were concentrated on the ground floor. In

addition, ground floor loadbearing wall removals resulted to high applied gravity forces above the damaged storey. In order to obtain the worst-case scenario, defined as the element failure that might trigger a disproportionate collapse, a pushover analysis was performed. Although one could have identified the internal column as the worst-case given its thickness and the applied bearing stresses from Table 4-1, both larger than external walls, a pushover analysis would help to also account for the stiffness of the connections.

The building was pushed in the direction of the three walls; a triangular displacement loads was applied on the whole building for this analysis. Although it was assumed that all three walls would be part of the lateral load resisting system, the internal wall was found to be the most critical due to its high stiffness as compared to the external ones. Figure 4-5 shows the magnitude of the base-shear recorded for both walls, external and internal, with respect to the drift.
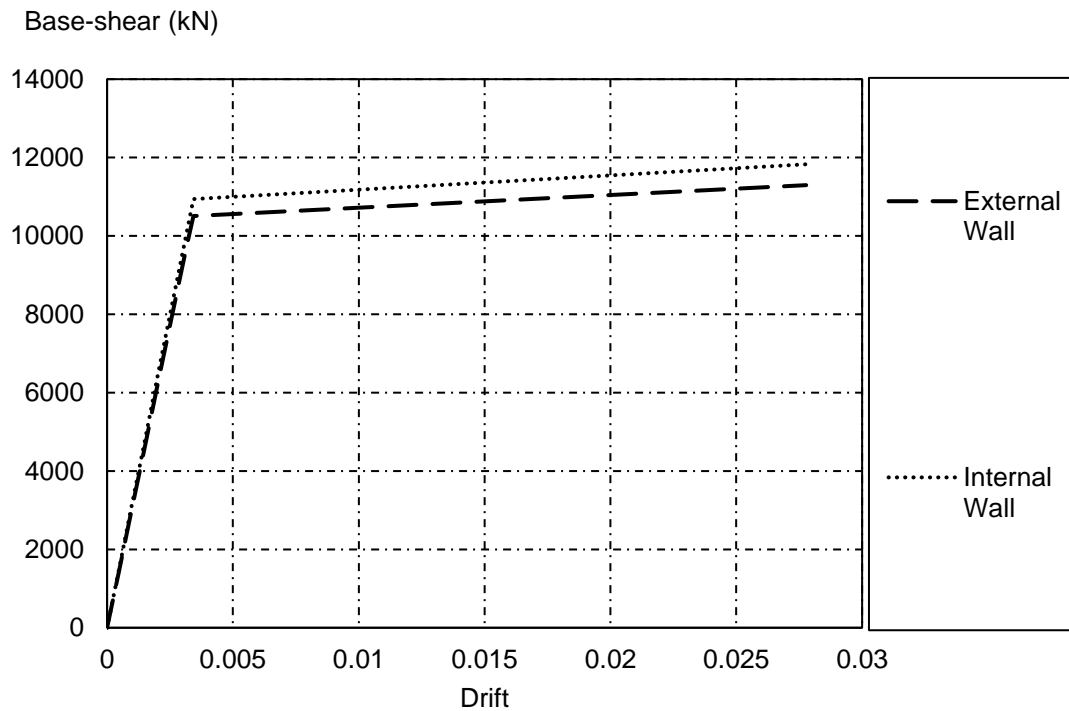
Figure 4-5: Results of pushover analysis: Base-shear vs Drift

From these results, the internal wall removal was identified as the most critical element, hence considered as the only initial damage for the macro and micro model analyses. In addition, this worst-case scenario investigated possible membrane and catenary actions as collapse-resistance mechanisms of the floor system. In this scenario, the floor panels, initially designed with a middle support at 4.5m, would span 9m continuously and be subjected to loads from all level above. The assumption was that the detailing at the location of the removed element was not designed to allow for suspension of the floor panel to the wall above, hence the floor carried its own weight plus imposed loads from the storeys above to prevent failure.

4.3.4 Numerical Model Development: Micro (connection) Model

The micro model, illustrated in Figure 4-6, was developed to study the behaviour at connection level and quantify the rotational stiffness of the detailing. The static analysis accounted for large deformations as well as material nonlinearities of the steel components whereas the timber elements remained linear. The connections were modelled in 3D to capture the contribution from the number and diameter of all screws, their embedment length as well as the dimensions of the angle brackets. The CLT panels were modelled per metre width, and only half of the span (4.5m) was considered to take advantage of symmetry.

The STSs, angle brackets and wood screws were steel with 1,000MPa (ETA-11/0190, 2011), 240MPa (ETA-06/0106, 2008) and 200 MPa as characteristic yield strengths, respectively. All CLT panels were assumed to be 3-ply with the material properties in Table 4-2. The three layers of the CLT panels were modelled using three different solid elements in the thickness direction, connected with rigid contact elements to prevent delamination. The micro model was a close representation of the joint, hence the obtained results represented the forces and deformation-

supply. From this model, it was possible to estimate the contribution of the stiffness of the connections between the floor-to-wall above (k_1) and the floor-to-wall below (k_2), separately. This model was validated against experimental studies from Gavric et al. (2014), Schneider (2015), and Hossain et al. (2016). This is also given in Appendix A.4.

The 3D model was highly nonlinear and complex; therefore, 2D models were constructed and calibrated, using the calculated k-values to mimic the same behaviour. The connection between the floor and the wall above and the wall below were represented by k_1 and k_2, respectively. Herein, the joints were idealised by the rotational springs with linear material properties, 200,000MPa and 0.3 for E and U, respectively.

(a)   *(b)*
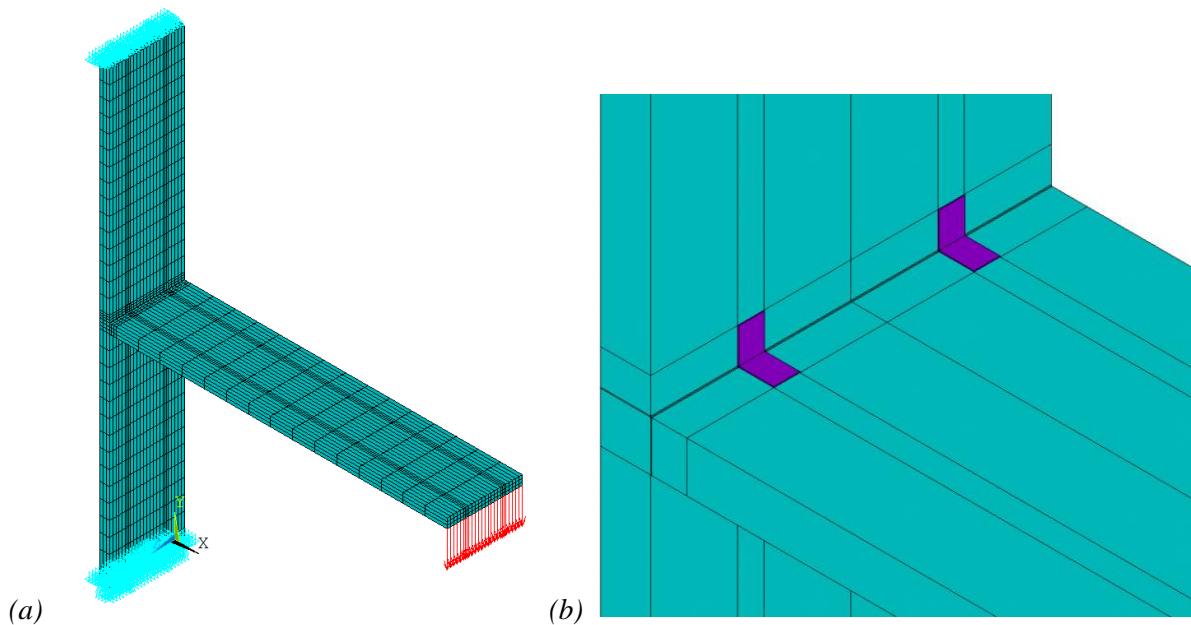
Figure 4-6: FE micro models: (a) Isometric view full; and (b) Zoomed isometric view

4.3.5 Numerical Model Development: Macro (component) Model

The calibrated 2D micro model was then extended to the 2D macro model, by symmetry. The macro model, as shown in Figure 4-7, was built with 2D shell elements, using the same

assumptions as the global model, with 3m wide CLT panels. The connections were idealised by uniaxial springs calibrated to the *k*-values as obtained from the 3D micro model and verified by hand calculations using Equation (4.1). The location of the nodes was number from 1 to 12; nodes 2, 3, and 4 (similarly 7, 8 and 9) were coincident nodes and were constrained in the two orthogonal directions to ensure identical deformations. As shown in Figure 4-3 macro model, the *DL* from the floor above were applied as favourable loads at nodes 5 and 10, as it improved stability and provided additional resistance against lateral movements of the floor panel.

The model accounted for self-weight of the CLT panels and *DL* as specified in section 4.3.1, as well as 50% of the imposed loads on the loads, as per Equation (2.2) extreme load combination. For this level of structural idealisation, to capture the in-plane floor behaviour necessary for floor system collapse-resistance mechanism, static analyses associated to large deformations and linear material properties for both structural components and their connections were performed. The forces obtained from nonlinear dynamic analyses of the global model were applied on this model, at the same location as the removed element, to investigate whether the supplied rotational stiffness was sufficient to carry the force and deformation-demands. The final failure was considered disproportionate when any of the constraints described in section 4.5 was violated.
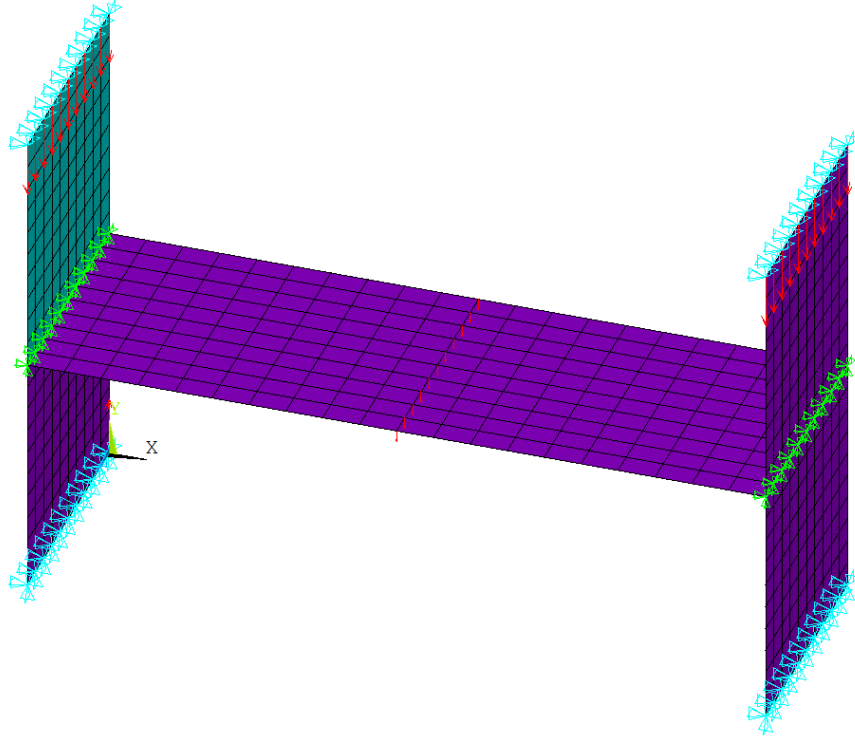
Figure 4-7: Isometric view of the macro model

The required rotational stiffness was expressed in terms of the axial stiffness (K_{ser}) under service loads, recommended from EN1995 (CEN, 2008), and calculated using Equation (4.1) multiplied by the polar second moment of area (I_p). Herein, (ρ_m) was the mean density of timber, (d_f) was the screw diameter, and (s) and (n) were the number of shear plane and screws, respectively. I_p considered the distance from the centre of the group of screws to a given fastener in the two orthogonal directions. K_{ser} allowed to estimate the required number of screws. The results from Equation (4.1) helped determining the required rotational stiffness (k) that could be achieved in a real construction; and therefore, set the limit values for what was deemed practical.

$$K_{ser} = \sum_{i-1}^{s}\sum_{j-1}^{n} \rho_m^{1.5} \times \left(\frac{d_f}{23}\right) \tag{4.1}$$

4.4 Nonlinear dynamic analysis

Nonlinear dynamic analysis was conducted to investigate the dynamic response of the building after element removal, following the UFC 4-023-03 and GSA recommendations. This analysis was only performed at the global level to define the upper bounds for disproportionate collapse prevention as described in section 4.3.3. Modal analyses were required to estimate the fundamental periods of the damaged structure without the internal or external ground floor wall. The critical Rayleigh damping ratio was assumed to be 5%, typical for timber structures (Gagnon and Pirvu, 2011). The results, which captured the modes with vertical motions around the removed element, were used to calculate the mass and stiffness coefficients of the Rayleigh damping used for the dynamic simulations. Thereafter, a static analysis of the global model, with Equation (2.2) extreme load combination, was performed to obtain the forces at the top of the removed elements; this is considered as load-step zero from Figure 4-8.
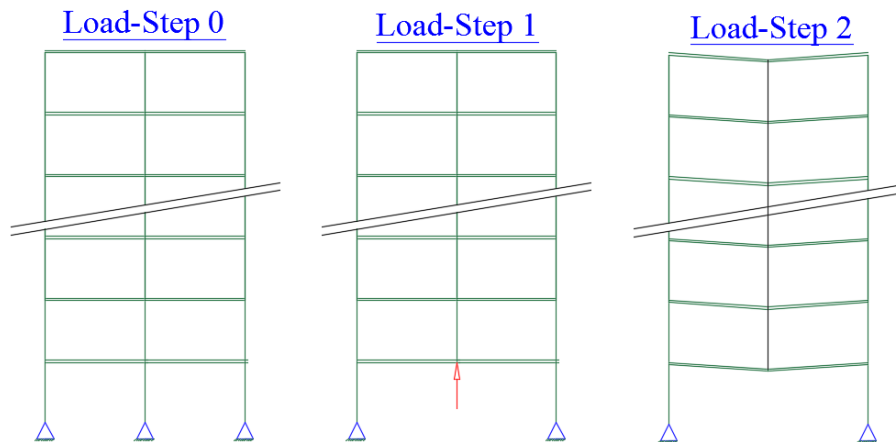
Figure 4-8: Load-steps for the dynamic analysis

Using the same global model but without the internal ground floor loadbearing wall, these forces were applied in the opposite direction, as the first load-step of the dynamic analysis to simulate

the static condition. The maximum deformations and forces on all components and their connections were checked to ensure that they were identical to the ones obtained from the undamaged building with internal wall. Then, these forces were deleted to mimic the speed of removal of the loadbearing element, as the second load-step. For the third step, the building damped the energy released from the previous step until static equilibrium was restored.

A range of removal speeds was used, keeping in mind that quicker removals led to higher dynamic effects. According to UFC 4-023-03 and GSA, the dynamic behaviour could cause up to twice the deformations obtained from the static analysis (DIF=2.0). Different speed of removal idealised possible different extreme events that the structure might be exposed. UFC 4-023-03 and GSA recommend a removal time of less than 1/10 of the period associated with the mode shape that exhibits vertical movements around the removed structural element. For initial analysis, the speed of removal (t_r) was assumed to be 0.001 seconds (*sec*) to meet the UFC 4-023-03 and GSA specifications.

4.5 Sensitivity Analysis

After understanding the structural behaviour after the defined internal loadbearing loss, a sensitivity analysis was performed at the macro level to evaluate the impact of connection stiffness, floor and wall panel thicknesses, as well as material properties of the selected CLT panels. The relevant input parameters that influenced the structural responses were defined as: (1) the stiffness of the connection between the floor and the wall above (k_1); (2) the stiffness of the connection between the floor and the wall below (k_2); (3) the stress grade of the CLT panel (*SG*) according to CSA-O86 (herein for simplicity, wall and floor panels were of the same *SG*); (4) the number of layers of the CLT floor panels (n_F) (herein an uneven number of layers with alternating

orientation); (5) the thickness of the longitudinal layers of the CLT floor panel ($t_{L,F}$); (6) the

thickness of the transverse layers of the CLT floor panel ($t_{T,F}$); (7) the number of layers of the CLT

wall panels (n_W); (8) the thickness of the longitudinal layers of the CLT wall panel ($t_{L,W}$); and (9)

the thickness of the transverse layers of the CLT wall panel ($t_{T,W}$). A boundary condition was that

for all CLT panels, the longitudinal layer thickness was always at least as big as the transverse

thickness. These parameters and their ranges are summarised in Table 4-3.

Table 4-3: Parameters ranges for sensitivity analysis

Parameters	Ranges / Values
k_1	From micro model [kNm/rad]
k_2	From micro model [kNm/rad]
SG	E_1, E_2, E_3, V_1, V_2 [-]
n_F	3, 5, 7, 9 [-]
$t_{L,F}$	30, 35, 40, 45 [mm]
$t_{T,F}$	15, 20, 25, 30, 35 [mm]
n_W	3, 5, 7, 9 [-]
$t_{L,W}$	30, 35, 40, 45 [mm]
$t_{T,W}$	15, 20, 25, 30, 35 [mm]

The response of the structure at the macro level was measured in terms of: (1) the bending moment

of the floor panel at the location of the removed element (M_Z); (2) the maximum deflection of the

floor panel (Δ_Y); (3) the maximum applied shear forces on the CLT panel (S_Y); (4) the maximum

axial forces at the connection level (F_X); and (5) the vertical loads on top of the wall below the

affected floor (B_Y) coming as compression forces on the wall below. Figure 4-9 illustrates the

locations where the response outputs were recorded from the component macro model.
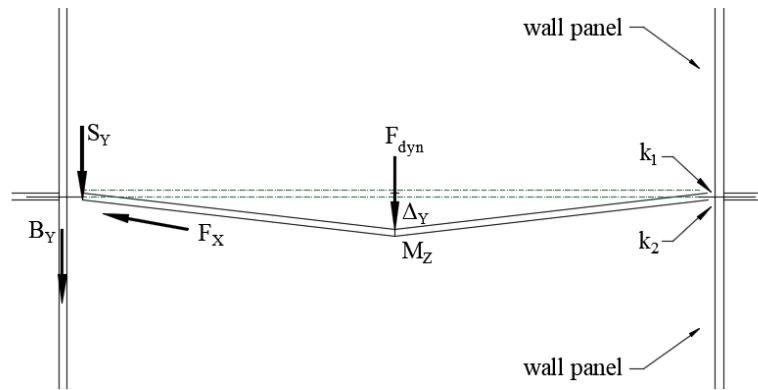
Figure 4-9: Location of design outputs

A series of constraints were defined such that the whole structure was deemed to have failed if one constraint was violated. These constraints were to keep M_Z, S_Y, and B_Y below their respective resistances M_R, S_R, and C_R. The capacities of the panels, for all SG and panel dimensions, in terms of bending, shear, and compression, were estimated using the shear analogy methods as per CSA-O86. For all defined SG, Table 4-4 lists the expected mean values for bending, shear, and compressive strength, estimated from the 5th percentile of the nominal values given in CSA-O86, as well as the corresponding E-values.

In addition, Δ_Y should be kept below the maximum deformation (Δ_{max}) allowed for floor system collapse-resistance mechanism. Stevens (2008) recommended limit deflections to 10% of the double span for catenary action. Herein, 500mm was used as thresholds for disproportionate collapse, which was around 5% of the double span after element removal. The set deflection limits accounted for the feasibility of obtaining such deformation for the considered building, given the new double span as well as the brittle nature of timber components. Also, since the floor system collapse-resistance mechanism depended on the axial forces, tying the floor to the connecting external walls, the focus of this analysis was to keep F_X small, as the proposed connections were primarily designed for shear, with low axial resistance. In the sensitivity study, 3,000 analyses

86

were run to account for different permutations of the input parameters. Advanced Latin Hypercube Sampling (ALHS) (Most and Will, 2012) was applied to determine the importance factor (*IF*) for all input parameters for subsequent structural optimisation at the macro level. The *IF* for a given random variable was calculated as the difference between the full polynomial regression model and the reduced polynomial regression model, the latter defined without the considered random variable.

Table 4-4: Material properties with respect to SG (CSA, 2016)

Stress grade	Longitudinal				Transverse
	Young's modulus [MPa]	Bending strength [MPa]	Shear strength [MPa]	Compressive strength [MPa]	Young's modulus [MPa]
E_1	11,700	33.60	0.60	23.00	9,000
E_2	10,300	28.45	0.75	21.60	10,000
E_3	8,300	20.70	0.50	18.00	6,500
V_1	11,000	11.90	0.75	16.70	10,000
V_2	9,500	14.00	0.60	13.70	9,000

4.6 Parameter Optimisation

To optimise the structure using the estimated *IF*, 13,900 analyses of the building at component level were performed. For these analyses, input parameter, see Table 4-3, with significant impact (*IF*>0.1) on the structural responses were automatically filtered, with more permutations for parameters with the highest *IF*. The objective of this analysis was to find the optimum values that would enable to carry the applied loads from analysis at global level by developing the floor system collapse-resistance mechanisms while meeting all the set constraints. Here, the smallest F_x was desired to reduce the cost of the connection. The selection of the input parameters for the best design targeted the smallest commercially available thickness of the CLT panel resulting to lighter building (lighter building results to smaller foundations). In addition to having the smallest F_X, the

analysis considered a Reliability-Based Design Optimisation (RBDO) to minimise the mass of the building (C_o), by varying the CLT layer thickness, number of CLT layers, as well as the joint rotational stiffnesses for collapse-resisting mechanisms; hence the probability of failure ($P[DC]$) times the cost of the failure (C_f). Equation (4.2) illustrate the RBDO:

$$\text{Best Design} = \text{Min } (C_o + P[DC] \times C_f \mid \text{constraints}) \tag{4.2}$$

Both sensitivity analysis and optimisation were carried out using the commercial optimisation software OptiSlang (Dynardo, 2017), and used the Metamodel of Optimal Prognosis algorithm to obtain the coefficient of prognosis (CoP). The CoP was expressed in percentage (%), and it represented the accuracy of the estimation, considering the IF of all input parameters.

4.7 Variance-based Robustness and Reliability Analysis

Since not all uncertainties encountered in the design and analysis stages could be reduced solely by high accuracy in modelling, it was appropriate to utilise probability-based methods to assess such uncertainties and quantify their effects on the outcomes of structural analysis. Stochastic analyses would relate uncertainties of the input variables to the response variabilities, both described in terms of probability metrics such as distribution functions. Standard approximation methods, such as the First Order Reliability Method (FORM), are implemented in the stochastic analysis software OptiSlang (Dynardo, 2017). Utilising the same tool for sensitivity, optimisation, variance-based robustness and reliability analyses allowed to reduce the number of random variables for the reliability analysis, as well as concentrate random sampling in the region which contribute most to the total failure probability.

The structure was optimised at the component level to carry the load obtained from analysis at the global, which was proportional to the speed of removal. Since this was an event-independent scenario, considerations of different removal speeds resulted in different forces magnitudes. In reliability analysis, uncertainties could be categorised as either aleatory (natural randomness that cannot be reduced) or epistemic (lack of knowledge that can be reduced) (Tannert and Haukaas, 2013). Due to the natural randomness of dynamic behaviours after element loss, the applied loads were accounted in the analysis as aleatory uncertainties. Epistemic uncertainties also stemmed from the fact that numerical models could neither fully represent the actual structure nor completely capture its real behaviour (Yin and Li, 2010).

In this study, the variability in the estimation of the connection stiffness were considered as epistemic uncertainties, given that the parameters were calibrated using observations from the micro model and Equation (4.1). The variability of timber as a natural material was related to both aleatory and epistemic uncertainties. This research assumed that extensive testing of CLT panels, in addition to rigorous CLT production quality control procedure, would reduce this variability. Therefore, the strength and stiffness properties of the CLT were also considered epistemic uncertainties from the fact that numerical models only captured part of the real behaviour (the material models were based on a limited number of tests) (Yin and Li, 2010).

A Variance-based Robustness Analysis (VBRA) investigated the effects of random uncertainties on the variability of the structural responses (Most and Will, 2012). The robustness analysis estimated the sigma (σ) level, which was the number of standard deviations about the mean value, for all defined structural responses with respect to the probability distribution function (PDF) obtained from varying the input uncertainties. A σ-level of 4.0 was often required for an acceptable

level of safety (Most and Will, 2012). The probability of exceedance (P_e) of the constraints could be estimated from the σ-level. The robustness analysis also required an ALHS with 3,000 as the chosen sample size.

In addition to the input parameters from the sensitivity analysis, the following uncertainties that influence the structural response were considered: (10) the modulus of elasticity of the longitudinal layers of the CLT panels (E_L); (11) the modulus of elasticity of the transverse layers (E_T); (12) the bending strength of the CLT floor panels (f_b); (13) the shear strength of the CLT panels (f_s); (14) the compressive strength of the CLT wall panels (f_C); (15) the stiffness of the floor-to-wall above connection (k_1); (16) the stiffness of the floor-to-wall below connection (k_2); and (17) the applied loads from dynamic analysis at global level (F_{dyn}). In these calculations, however, the *DL* and *LL* were assumed to be deterministic given that most of the variability was due to the speed of the element removal.

For both VBRA and FORM, the set limits state functions (LSFs) were identical to the constraints defined in the sensitivity analysis. Specifically, the LSFs (g) were the disproportionate collapse thresholds. A basic reliability problem was considered; failure occurred when $g \leq 0$, defined as the resistance (R) minus demand (S). From Equation (4.3), the R were established as M_R, S_R, C_R, and Δ_{max}; and their respective S were taken as M_Z, S_Y, B_Y and Δ_Y. For VBRA, the consideration of the LSFs was a component reliability problem; the σ-level dealt with a single LSF at the time. With the LSFs considered separately, the results of the variance-based robustness analysis would be whether the optimised structure would be safe (robust) or unsafe (non-robust), in presence of the given uncertainties in the model:

$$g = R - S \qquad (4.3)$$

In FORM, all four LSFs had to comply with the condition $g>0$ for the structure to be considered safe; and failure was defined when one, or more than one LSF was violated ($g \leq 0$). In other words, although the LSF was formulated individually, all four LSFs were considered as a series system when evaluating structural safety as shown in Equation (4.4):

$$g(X_i) = \min (g_j(X_i)); \; i=1 \ldots N_{RV} \text{ and } j=1 \ldots 4 \qquad (4.4)$$

Where X_i represented an input random variable i ($i=1 \ldots N_{RV}$), N_{RV} was the total number of considered input variable (herein = 8) and $g_j(X_i)$ was the considered LSF j ($j=1 \ldots 4$). Correlations between the LSFs were not considered; instead the algorithms implemented in OptiSlang considered input correlations of the defined random variables (with respect to the mean, coefficient of variation, and distribution type) which implied output correlations (e.g. M_R depended on the E_L, E_T and F_b; whereas the demand M_z depended on F_{dyn}). This approach led to one compound LSF; therefore, FORM results gave a single reliability index (β) used to estimate a single probability of disproportionate collapse $P[DC]$ as in Equation (4.5):

$$P_f = \Phi(-\beta) \qquad (4.5)$$

Tests on small clear wood specimens showed high variabilities in strength properties of wood (Jessome, 1977). For EWPs such as CLT, these variabilities were reduced through the homogenisation during the production process, where defects were either removed or distributed (Thelandersson and Larsen, 2003). The coefficient of variation (CoV) of the Young's modulus of tested CLT depended on the panel width; for 960mm wide panels, it was determined that CoV was 6% (Joebstl et al., 2006). The variability of CLT strength properties depended on tested panel

thickness, layup, width, strength of individual boards, moisture content and fabrication process (Steiger and Gulzow, 2009). From the different tested CLT products, the CoV for f_b ranged from 10-14%, the CoV for E ranged from 4-10%. From investigations of the in-plane f_s of the CLT panels (Joebstl et al., 2008), it was found that the CoV were between 3-16% depending on the panel layup. Other studies (Brandner et al., 2016) found that the CoV for f_s ranged from 5-10%, again depending on width, thickness and gap width between the boards. Tested CLT panels made of hardwood species birch also found CoV for E_L, f_b, f_s, and f_c as 4, 11, 9 and 7%, respectively (Jeitler et al., 2016).

In the present study, the variance-based robustness and the reliability analysis were performed on the optimised structure of the case-study building, using Canadian made CLT for which there was no data available for the strength and stiffness CoVs. However, the literature review revealed that the CoVs for strength and stiffness properties of European CLT were around 10% or smaller, depending on a series of individual parameter. Therefore, a normal PDF with 10% CoV was considered for all CLT material properties, assuming the 5th percentile was 87% of the nominal values given in the CS-O86, see Table 4-5. Although material parameters were assumed as normally distributed random variables, limits were imposed to ensure that no negative values were selected.

Table 4-5: Uncertainties for reliability analysis at component level

Variable	Description	PDF type	Mean	CoV (%)	Min (MPa)	Max (MPa)
E_L	*E*-value for longitudinal layers	Normal	As per Table 4-4	10	7,502	15,900
E_T	*E*-value for transverse layers	Normal	As per Table 4-4	10	5,770	12,230
F_b	Bending strength	Normal	As per Table 4-4	10	21.50	45.60
F_s	Shear strength	Normal	As per Table 4-4	10	0.38	0.81
F_c	Compressive strength	Normal	As per Table 4-4	10	14.73	31.22
k_1	Stiffness of floor-to-wall above	Normal	From optimisation	10	-	-
k_2	Stiffness of floor-to-wall below	Normal	From optimisation	10	-	-
F_{dyn}	Applied force	Lognornal	From global model	100	-	-

The stiffness of the floor-to-wall above as well as the floor-to-wall below were also defined as normal PDF with their mean values obtained from the optimised structure. It was found that the estimation using Equation (4.1), considering the changes in screw diameter and CLT density, were within 10% of the values obtained from the micro model, considering identical changes. Therefore, a *CoV* of 10% was also deemed acceptable for k_1 and k_2. Performed experimental tests on off-the-shelf angle brackets and screws had *CoV* in the same range (Schneider et al., 2015). The mean value of the applied forces was obtained from 30 different analyses at the global level, with the speed of removal ranging from 10^{-5} to $10^{-2}sec$. It is worth mentioning that, for the considered building, these ranges accounted for both static and maximum dynamic effects, with slowest removal mimicking simple element removal with *DL* and *LL* only. The forces obtained following

the considered range of speed removal was defined as a PDF, with a *CoV* of 100% calculated from the magnitude of the forces obtained from the different removal speeds.

4.8 Results and Discussion

4.8.1 Nonlinear Dynamic Analysis of Global Model

Modal analyses for internal and external ground floor loadbearing walls removal, estimated the natural frequency of the building to 0.6Hz. The frequency of the mode shape with vertical deformations around the removed element, as illustrated in Figure 4-10a and b for internal and external wall removal scenarios, respectively, was 6.1Hz. For the static analysis, Figure 4-11a, b and c illustrate the deflected shape of the building in the initial stage, after internal wall and external wall removals, respectively. For the considered case study building, downward forces were 1,546kN and 1,260kN right on top of the internal and external ground floor walls, respectively. The structural elements to be removed were replaced by these forces, acting upwards at the same location, in order to mimic the normal static case (load-step 1) during dynamic analysis.
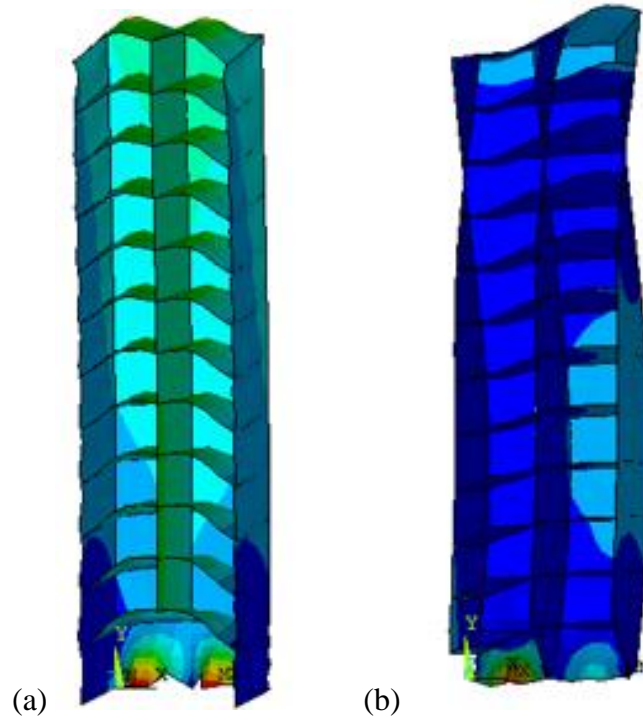
Figure 4-10: Mode shapes: (a) Internal removal; and (b)External removal
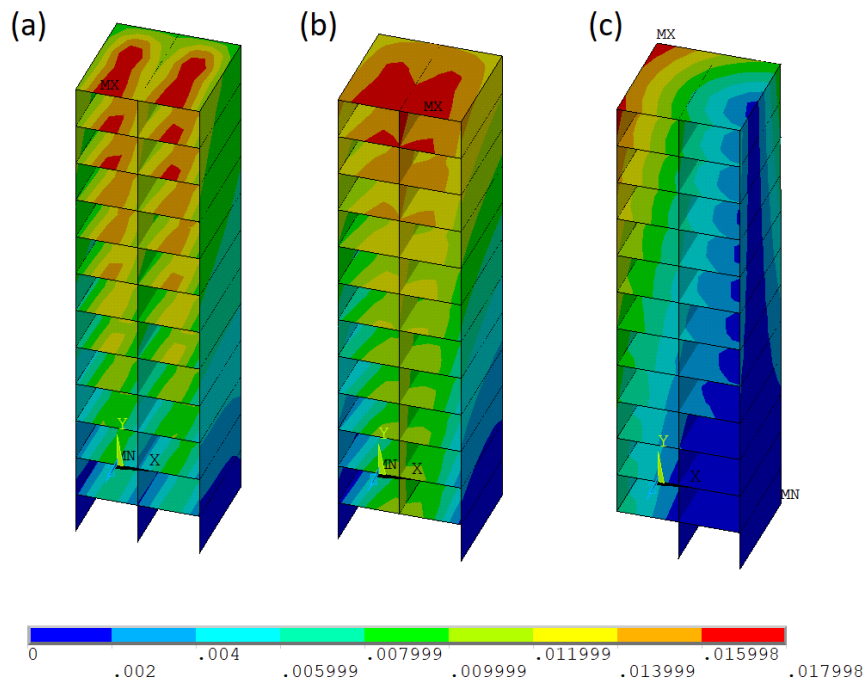
Figure 4-11: Deflected shapes under gravity: (a) Initial condition; (b) Internal wall removal; and (c)

External wall removal (units are in m)

Figure 4-12 illustrates all four load-cases required to perform the nonlinear dynamic analysis for sudden element removal. The displacement was recorded at the location of the removed element, relative to the initial position of the floor (before removal). For the nonlinear stage, as shown in Figure 4-12, the quicker the removal, the stronger the dynamic motions, which led to higher imposed deformations and consequently larger forces on the members. Furthermore, it was noted that for $10^{-3}sec$ or quicker, 5% critical damping would not be sufficient for good structural resilience. The existence of moment reversal observed in the results highlighted concerns on designing members and connections for dynamic loadings, even though the building was not subjected to seismic loads.
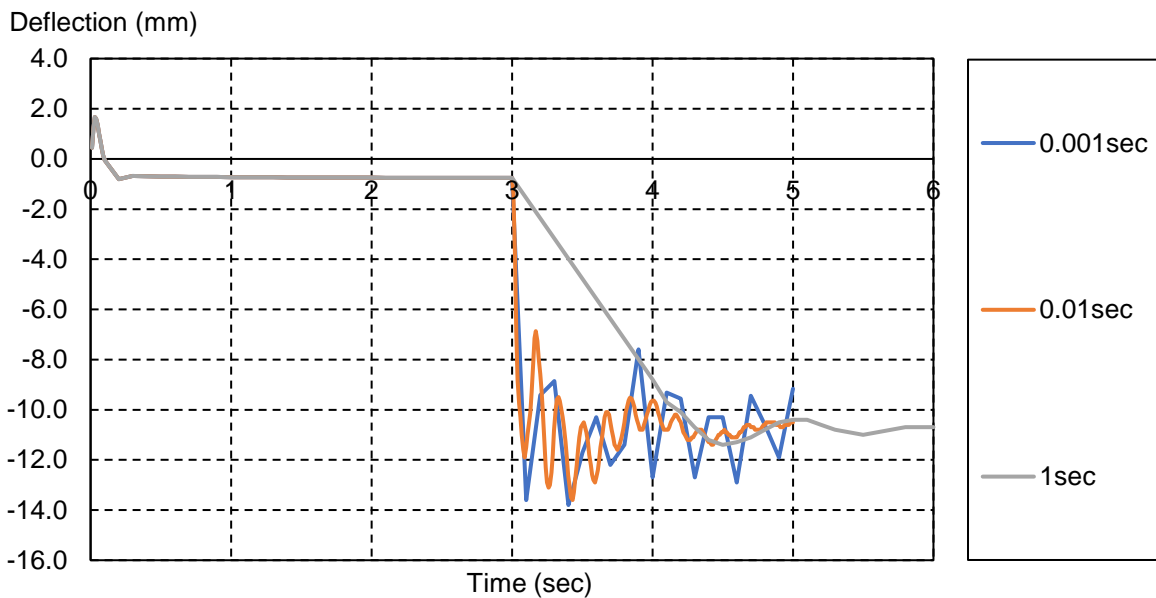
Figure 4-12: Effects of removal speed (t_r)

The results of the static analyses (S_1) were compared against the outcomes of the dynamic analysis (S_2). Since no importance was given to the extreme loading itself, the speed of removal (t_r) was initially assumed to be $10^{-3}sec$, to meet the UFC 4-023-03 and GSA specifications. Figure 4-13 and Figure 4-14 show the maximum forces obtained after the loss of the internal and external walls,

respectively, for the two cases (S_1 and S_2). Force distribution occurred and the loads on top of the removed elements decreased drastically, from the values obtained after analyses of the complete structure before initial damage. One could assume that after removal, each floor tried to carry its own loads to relieve the damaged area; hence increasing the tie-force at connection level. Furthermore, the outcomes of this study showed that S_2 were about 1.5 higher than S_1, hence agreeing with the *DIF* recommended in the literature (DoD, 2013).

The floor design had to consider not only the downward vertical forces but also the dynamic upward loads. Depending on *t*, uplift forces from S_2 at the location of the removed element were as high as 300% of the values obtained from S_1. The axial or tie-force at the connections for S_2 was about ten times higher than the results from S_1, in order to develop collapse-resistance mechanisms; this was observed for both internal and external wall removals. The noted increase of forces raised concerns as the proposed detailing was primarily designed for shear to resist lateral loads according to CSA-O86 and, therefore, was not able to carry axial forces higher than 60kN per panel width, as per EN1991-1-7 prescriptions. Furthermore, out-of-plane shear forces at wall-to-floor connections increased from 3kN for S_1 to 189kN for S_2 in the case of internal wall removal. This emphasised on the need for correct structural layout, with return walls, and new structural detailing for disproportionate collapse prevention.
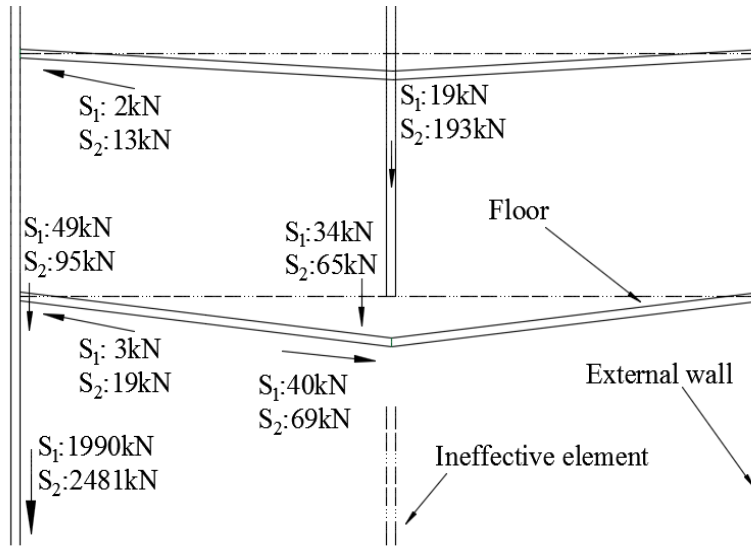
Figure 4-13: Results of internal wall removal
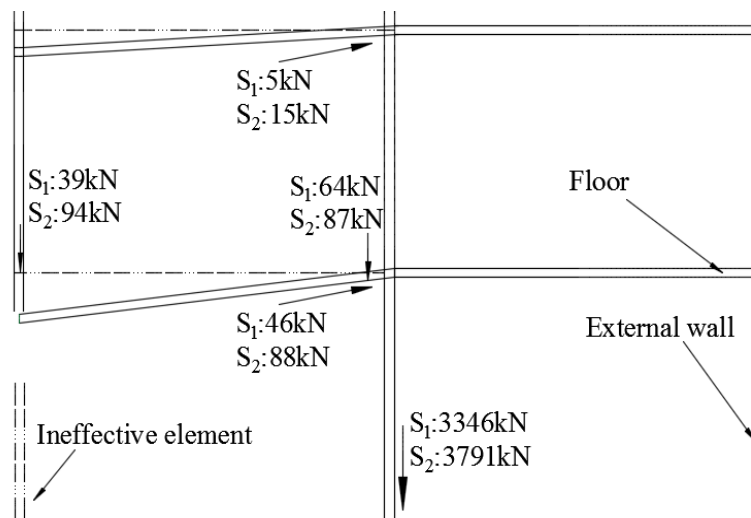
Figure 4-14: Results of external wall removal

For internal wall removal, the building's response also highlighted the need to design the floor system for twice its original length. Herein, catenary action was the collapse-resistance mechanism for disproportionate collapse prevention. The continuous floor carried 193kN at mid-span, from S_2 for the considered removal time ($t=10^{-3}sec$). A lognormal PDF was obtained with t from 10^{-5} to $10^{-2}sec$, with a mean value of 265kN and 100% *CoV*. This PDF was used to assign the random

variable F_{dyn} for the reliability analysis at the component level or the macro model. The upper limit values of the PDF, obtained from $t=10^{-4}sec$, was 423kN.

4.8.2 Analysis of the micro and macro models

From the 3D micro model, under the applied forces, the maximum floor rotation was 1.14rad. Here, the model exhibited convergence problems highlighting possible failure. These excessive deflections were not possible for the considered building. Figure 4-15a and b show the observed failure modes of the micro model. The applied floor rotation caused excessive bending of the angle brackets; this was the primary failure mode. Albeit the high applied stresses, the angle brackets themselves did not fail. Failure first occurred at the lower row (from the bottom) of screw fastening the brackets to the wall, due to pull-out force demands. High shear stresses were also observed from the first row (from the wall) of screws fastening the brackets to the floor panel.

The 3D micro model also highlighted wood failure at the floor rotation point. Herein, high compression stresses perpendicular to the floor grain were observed. Under this 'sandwich' detailing, these compression stresses on the floor panel became significant with the increase in the applied vertical (favourable) loads from the level above. Although failure was not observed, high stresses were also noted on the STSs connecting the floor to the wall below, at higher floor rotation. The obtained deformed shape showed bending of the STSs, as well as high pull-out forces. Furthermore, STSs crushed the wood around them in row-shear as the floor deformation increased; this was noted by high stresses on the connecting wood elements.
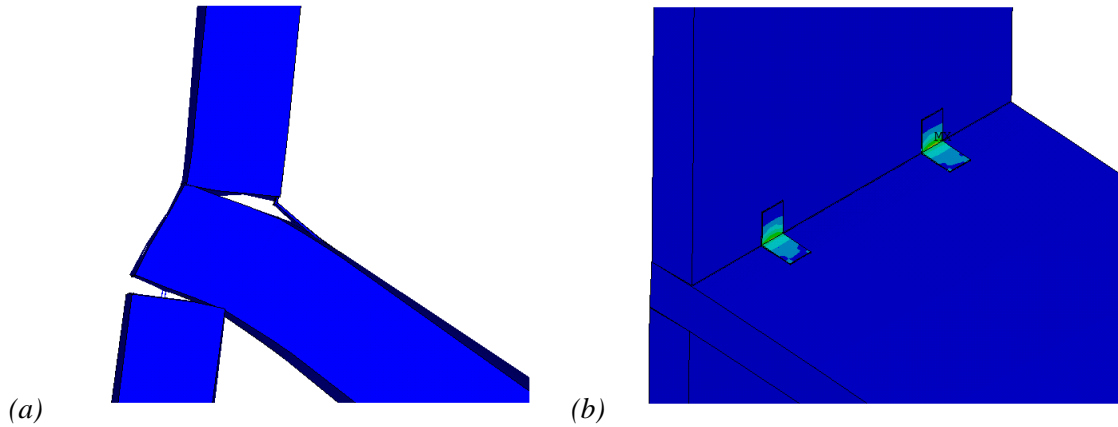
Figure 4-15: Failure of micro model: (a) Section view; and (b) Isometric view

In the 3D model, it was observed that the provided joint detailing could only carry about 44% of F_{dyn} obtained from the nonlinear dynamic analysis at the global level. Figure 4-16 shows the overall deformed shape of the 3D micro model when subjected to 1kN/m, as total load along the width, at the location of the removed internal loadbearing wall. This approach enabled to estimate k_1 and k_2 for validation. The result of the static analysis gave a value of 211 and 359kNm/rad for k_1 and k_2, respectively. These k-values were used to calibrate equivalent 2D micro models.

2D macro models, see Figure 4-17, were constructed with the obtained k_1 and k_2 values from micro model, as rotational stiffness at the floor-to-wall joints. It was observed that, when the k-values were below 10^3kNm/rad, the building was not able to carry the full force (F_{dyn}=193kN, at $t=10^{-3}sec$) due to excessive rotations and high F_X demands. The full force could only be applied if k_1 and k_2 values were increased above 10^6kNm/rad. Nonetheless, beyond 10^6kNm/rad rotational stiffness, the connection could be assumed fully rigid, and negligible changes in F_X were observed.
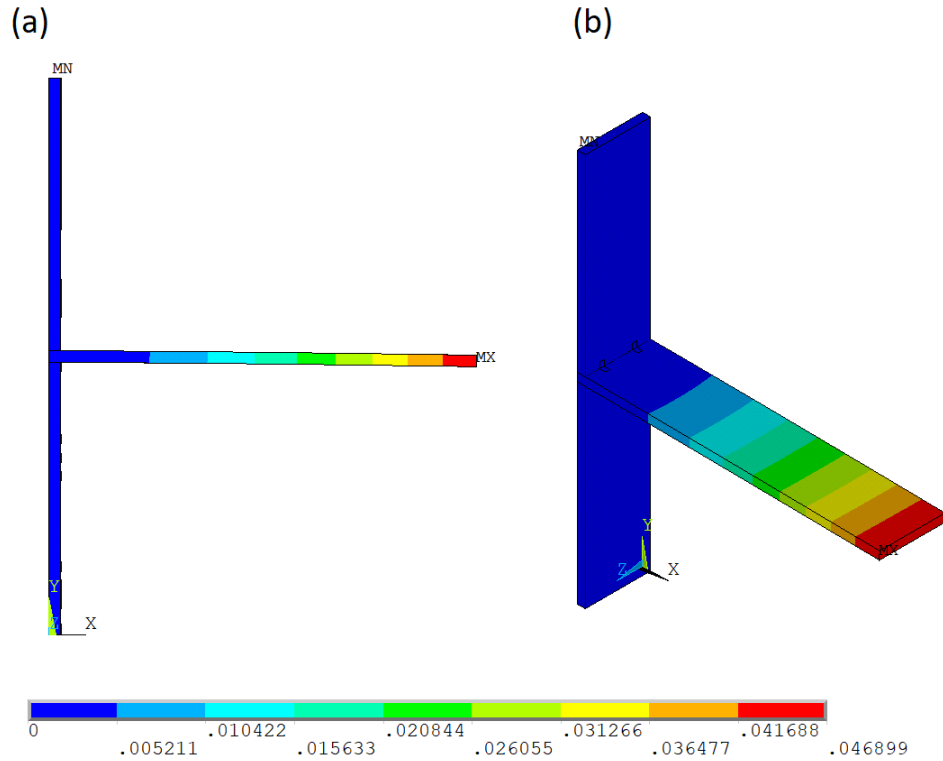
Figure 4-16: Deformed shape of the micro model: (a) Section view; and (b) Isometric view (in m)

Using the axial stiffness under the service loads, expressed in terms of K_{ser} from Equation (4.1), it was found that at least 81 screws, representing a rotational stiffness 10^5kNm/rad, would be required along the width of the panel for k_2, and assuming k_1 remained constant, to carry F_{dyn}=193kN. This requirement was deemed not practical. To obtain realistic or pragmatic number of screws, the required rotational stiffness needed to be between 1kNm/rad and 10^3kNm/rad. Therefore, these values were assumed as ranges for both k_1 and k_2 for subsequent analyses.

Assuming thresholds as defined in section 4.5, the analysis at the component level confirmed that the building was prone to disproportionate collapse. With the supplied connection stiffnesses, failure was observed due to the applied bending moments at mid-span (M_Z=868kNm, M_R=196kNm; S_Y=118kN, S_R=135kN; B_Y= 436kN, C_R=3,320kN; Δ_Y=453mm, Δ_{max}=500mm). It

could be argued that the new span of 9m became unpractical given the CLT panel thickness and layup. Furthermore, the results confirmed that the floor system was not able to develop catenary action as a collapse-resistance mechanism. Therefore, it also confirmed that 10% of the span for catenary action suggested in the literature (Stevens, 2008) was not practical for the considered mass-timber floor systems. Deflections greater than 500mm could only be attained by incorporating some sort of plastic hinge at the location of high bending moment, e.g. addition of floor-to-floor connection with high strength, stiffness, and ductility to carry the tie-force demands.
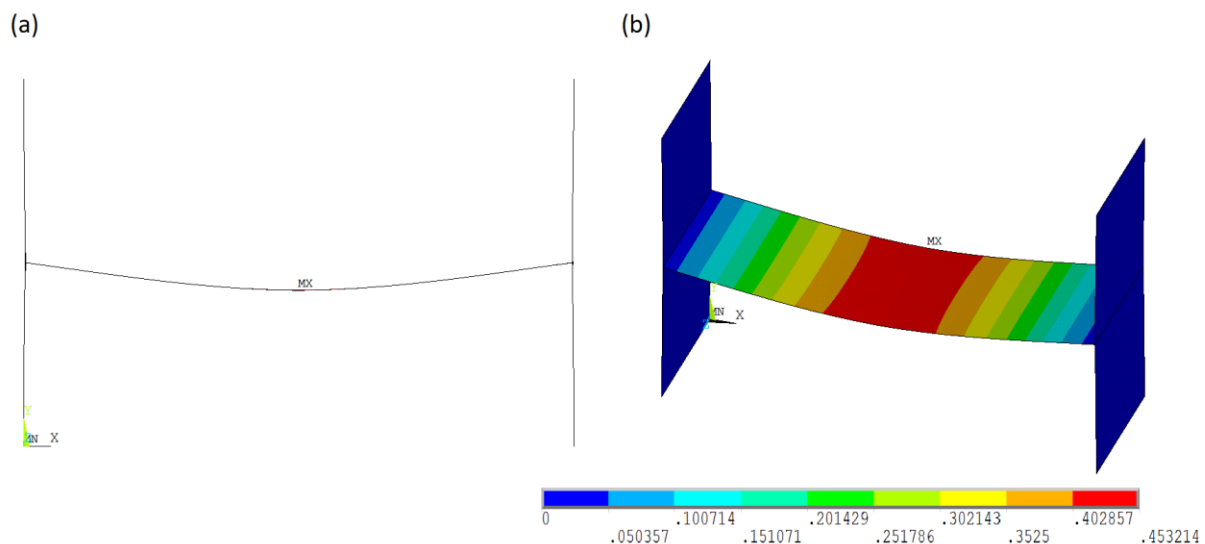
Figure 4-17: Deformed shapes of macro model: (a) Section view; and (b) Isometric view (in m)

4.8.3 Sensitivity Analysis

The results of the sensitivity analysis showed that applied mid-span bending moment and deflection on the floor panel caused failure in 85 and 35% of the sample size, respectively. This highlighted the need to incorporate a connection detailing at the location of the removed element, that could help developing plastic hinges to enable large deformations while maintaining load-carrying capacity. Table 4-6 shows how each input parameters influenced each structural response,

102

before optimisation. All responses had at least 96% *CoP*, hence confirming the accuracy of the estimations with respect to the *IF*. The results showed that, for both floor and wall panels, the main parameter was the CLT thickness, expressed as the number of plies. M_R and M_Z were the main cause of observed structural failures, *SG* was the second most important parameter. The joint stiffness k_1 and k_2 mainly influenced the values of the axial forces F_X, with the latter having the highest *IF*. Considering the thickness of the panel, the size of the longitudinal layers always had more influence compared to the thickness of the transverse layers.

Table 4-6: Results of the sensitivity analysis

Structural responses	*IF* of input parameters [%]									*CoP*
	k_1	k_2	*SG*	n_F	$t_{L,F}$	$t_{T,F}$	n_W	$t_{L,W}$	$t_{T,W}$	[%]
M_R	-	-	9	53	7	3				100
M_Z	-	-	9	53	7	3				100
S_R	-	-	4	72	6	5	-	-	-	100
S_Y	-	-	-	85	7	6	-	-	-	100
$\varDelta_y$	1	-	1	70	7	3	-	-	-	97
C_R	-	-	6	-	-	-	64	13	1	99
B_Y	-	-	-	-	-	-	79	10	8	100
F_X	1	6	-	31	4	2	8	2	1	96

4.8.4 Parameters Optimisation

The best stress grade was CSA-O86 E_1 for all CLT panels, due to its high strength. No analysis with 3-ply CLT panels was successful, regardless of the selected stress grade and layer thickness. For 5-ply CLT panels, Design #1 (see Table 4-7) was the best design out of a total of only 5

successful parameter combinations with 5-ply that met all constraints. Nevertheless, Design #2, with 7-ply, was selected as optimum design considering both RBDO and the requirement to have the smallest tie-forces at the floor-to-wall connections. To meet all constraints, floor panels of at least 200mm thick were required. For 5-ply panels, both transverse and longitudinal layers had to be 40mm. This thickness could only be reduced if the number of plies was increased; however, this would not lead to economic designs considering the objective of using the smallest panel thickness.

Table 4-7: Selected design from optimisation of macro model

Design №	Joints [kNm/rad]		CLT floor panel [mm]				CLT wall panel [mm]			
	k_1	k_2	n_F	$t_{L,F}$	$t_{T,F}$	Total	n_W	$t_{L,W}$	$t_{T,W}$	Total
1	120	530	5	40	40	200	7	40	20	220
2	1	1,000	7	35	20	200	3	30	15	75

Thicker walls increased the favourable loads acting on top of the wall above. This provided additional constraints ('sandwich' detailing) against axial pulling or pushing of the floor panels under the applied loads (F_{dyn}); thus, limiting mid-span deflection of the floor and improved in-plane stability of the overall system. The need of having thicker walls could be avoided by having floor panels with more plies in the longitudinal direction, which provided higher bending resistance. Design #2 required commercially available 3-ply wall panels with 7-ply floor panels. Nevertheless, it would be ideal to maintain the wall thickness as 126mm, as described in section 4.3.1, to meet the design for gravity and lateral loads. Furthermore, Design #2 confirmed k_1 should be kept to its minimum, based on lateral design; k_2 should be kept to its maximum to develop catenary action of floor panels as a collapse-resistance mechanism. For both cases, possible

bending or buckling of the external walls below could occur when meeting the floor panel deflection demands. Additional considerations would be required to prevent failure in these situations.

Positive axial force on the floor-to-wall connection meant that for the deflected shape at component level, the external walls, both above and below the affected floor system, would be pulled inward creating tensile axial forces on connections. Negative axial compressive forces, as obtained from the optimised design, were opposite and pulled the walls outwards. These behaviours, resulting to positive or negative axial forces, were affected by the magnitude of the considered rotational stiffness k_1 and k_2. When the latter was kept closer to its minimum (1kNm/rad) and the former closer to its maximum (10^3kNm/rad), the resulting tie-forces were positive, meant that off-the-shelf angle brackets and screws contributed the most to the resistance by pulling of the screws on the wall part of the connection, and shearing on the floor part of the connection. Since neither timber nor the proposed connection detailing were good in tension, it could be argued that applying negative axial forces would be the ideal behaviour. Herein, possible shearing of the screws on the floor parts of the connection, and compression at the top fibre of the floor panels at the location of high bending moment, were the anticipated failure modes. Both failure modes were ductile behaviours, acting in advantage of Design #2 as the optimum design.

4.8.5 Robustness and Reliability Analyses

The results of the variance-based robustness evaluation gave a $CoP > 97\%$ for all input parameters and responses. F_{dyn} from the nonlinear dynamic analysis at global level was identified as the most influential variable with an $IF > 90\%$. Although the material properties mainly influenced the panel resistances, they had a small IF for the analysis in general. Table 4-8 presents the results of the

variance-based robustness analysis, in terms of σ-level and P_e. The *CoV* given in Table 4-8 identifies the changes of the considered structural response with respect to the changes on the defined uncertainties. The results showed that only the applied deflection at mid-span (Δ_Y) and the compressive forces on the wall underneath (B_Y) were robust; with σ-level higher than 4.0. The main concerns were with respect to the bending moments on the floor; there was 32% of chance to violate the corresponding LSF. The structure was prone to disproportionate collapse with $M_Z > M_R$ identified as the primary cause of failure. Considerations of the floor-to-floor connection with adequate strength, stiffness, and ductility would be the main solution.

Table 4-8: Results of the variance-based robustness evaluation

Response	*CoV* [%]	σ-level	P_e [%]	Robustness
M_z	99	0.04	32.00	Not Robust
S_y	62	3.18	1.60	Not Robust
Δ_y	75	5.72	0.33	Robust
B_y	17	12.80	0.03	Robust

The results of the reliability analysis confirmed the outcomes from the robustness analysis. Among 93 designs, the design point corresponded to $F_{dyn} = 93$kN. Herein $\beta = 0.46$, giving a probability of disproportionate collapse $P[DC] = 32\%$. Such high $P[DC]$ obtained at component level was directly related to high chances of disproportionate collapse at global level for the twelve-storey CLT platform-type construction, in the event of sudden loss of the internal ground floor loadbearing wall. CLT floor system did not have adequate rotational stiffness at the connection to avoid disproportionate collapse. This highlighted safety concerns regarding the design of mid-rise CLT buildings with platform-type construction.

4.9 Summary

This chapter demonstrated how a three-level structural idealisations FE analyses could be used to investigate the probability of disproportionate collapse. Herein, a twelve-storey CLT building with platform-type construction, following the sudden removal of internal and external ground floor loadbearing walls, was considered as case study. Nonlinear dynamic analyses were performed at the global level to capture the overall structural performance under the applied extreme loads. This was followed by a sensitivity analysis in order to optimise the structure at component level. Thereafter, a variance-based robustness analysis was considered to estimate the vulnerability of the optimised structure in the presence of uncertainties in the applied loads, which was affected by the speed of element removal, material and connection properties. Finally, reliability analysis was performed to compute the probability of disproportionate collapse for the optimised structure. This chapter can be summarised as follows:

(1) At global level, slowly removing loadbearing elements, resulting in a static behaviour, is not sufficient; the analysis needs to capture both dynamic behaviour and nonlinearities. For the presented case study building, the forces from the dynamic simulation are about 1.5 higher than the outcomes from static analysis.

(2) Since the nature and the probability of extreme events are unknown, understanding the structural behaviours under different extreme loads is of higher importance. The importance of overdesigning the structural elements cannot be overstated to account for bigger range of events susceptible to occur during the lifetime of the building.

(3) The tie-force necessary to trigger collapse-resistance mechanisms may be higher than what traditional self-tapping screws and angle brackets can supply. Therefore, there is a need to develop novel connection detailing with sufficient strength, stiffness, and ductility.

(4) The design of buildings under extreme loading situations shall account for force reversal in all removal scenarios, and twice the original floor span, for internal wall removal. For the latter, the main causes of failure are the applied bending moment and deflection at the location of the removed element.

(5) Optimisation shows that CLT panel shall be at least 200mm thick, regardless of the number of plies, with E_1 as stress grade, to satisfy serviceability and ultimate limit states, as well as disproportionate collapse prevention requirements for quicker element removal.

(6) The results show that in presence of uncertainties in the material properties, connection stiffness, and speed of removal, the case study building has a probability of collapse as high as 32% at component level if simply designed to be code compliant without specific considerations of the complexities associated for disproportionate collapse prevention.

Chapter 5: Analysis of a Nine-storey Flat-plate Building[3]

5.1 Introduction

The increasing availability of EWPs along with innovative structural systems and connection detailing are listed among the factors behind the promotion of mid- and high-rise timber constructions (Green and Karsh, 2012; Wells, 2011). Since this building category often uses new structural systems, in the same motivation as Chapter 3 of this thesis, application of deterministic analyses for structural robustness by means of a case study was also considered for the present chapter.

The considered building was a nine-storey flat-plate construction, a structural system identical to the Brock Commons (Fast and Jackson, 2017), although here the lateral load-resisting system is composed of CLT wall panels. Mass-timber flat-plate structural system are proven to perform well under gravity load, nevertheless thorough analyses are still required to understand their performance following extreme loading events, especially the behaviour of critical connections for collapse-resistance mechanisms.

---

[3] Materials from this chapter were published in the following journal and conferences:

Mpidi Bita, H., & Tannert, T. (2019). Disproportionate collapse prevention analysis for mid-rise flat-plate cross-laminated timber building. Engineering Structures 178: 460-471.

Mpidi Bita, H., & Tannert, T. (2018). Disproportionate collapse investigation for mid-rise timber buildings. World Conference on Timber Engineering, WCTE, August 20-23, 2018, Seoul, South Korea.

Mpidi Bita, H., & Tannert, T. (2018). Alternate load-path analysis for mid-rise mass-timber buildings. ASCE Structure Congress, ASCE, April 19-21, 2018, Fort Worth, USA.

Mpidi Bita, H., & Tannert, T. (2017). Disproportionate Collapse for mid-rise mass-timber buildings. China-Canada Symposium on Structural and Earthquake Engineering. August 20-24, 2017, Vancouver, Canada.

Mpidi Bita, H., & Tannert, T. (2017). Robustness of multi-storey timber buildings. International Association for Bridge and Structural Engineering Symposium, IABSE, September 21-23, 2017, Vancouver, Canada.

5.2 Objectives

The primary objective of this chapter was to perform a nonlinear dynamic ALPA on a nine-storey flat-plate CLT building. Herein, sudden loss of ground floor columns, one at a time, was considered to estimate the demand-capacity ratio (*DCR*) on the structural members and their connections, for each removal scenario. The second objective was to perform a reliability analysis to quantify the probability of disproportionate collapse *P*[*DC*], for the worst-case *DCR* removal scenario, in presence of uncertainties in the loading, material properties, and geometry of the building. With high *P*[*DC*] following the worst-case removal scenario, the third objective was to identify the relevant design parameters to improve building performance, hence, to reduce *P*[*DC*] by maintaining structural safety after element removal.

5.3 Case Study Building

5.3.1 Description

A nine-storey case study residential CLT building with flat-plate floor system and floor plan as shown in Figure 5-1a, was studied. The gravity system was composed of CLT floor panels, directly resting on a total of 19 GLT columns. A column grid of 2.2×4.0m similar to the one of the Brock Commons building was chosen with 8m long floor panels, double span (continuous over internal loadbearing wall), and continuous over the middle supports to allow the panels to behave in a two-way system under gravity loads. The lateral load-resisting system (LLRS) was composed of a CLT core, where individual panels were three storeys tall, with 3.5m storey height. The CLT floors

were assumed to act as rigid diaphragm, transferring the horizontal loads to the CLT core through the detailing explained subsequently.
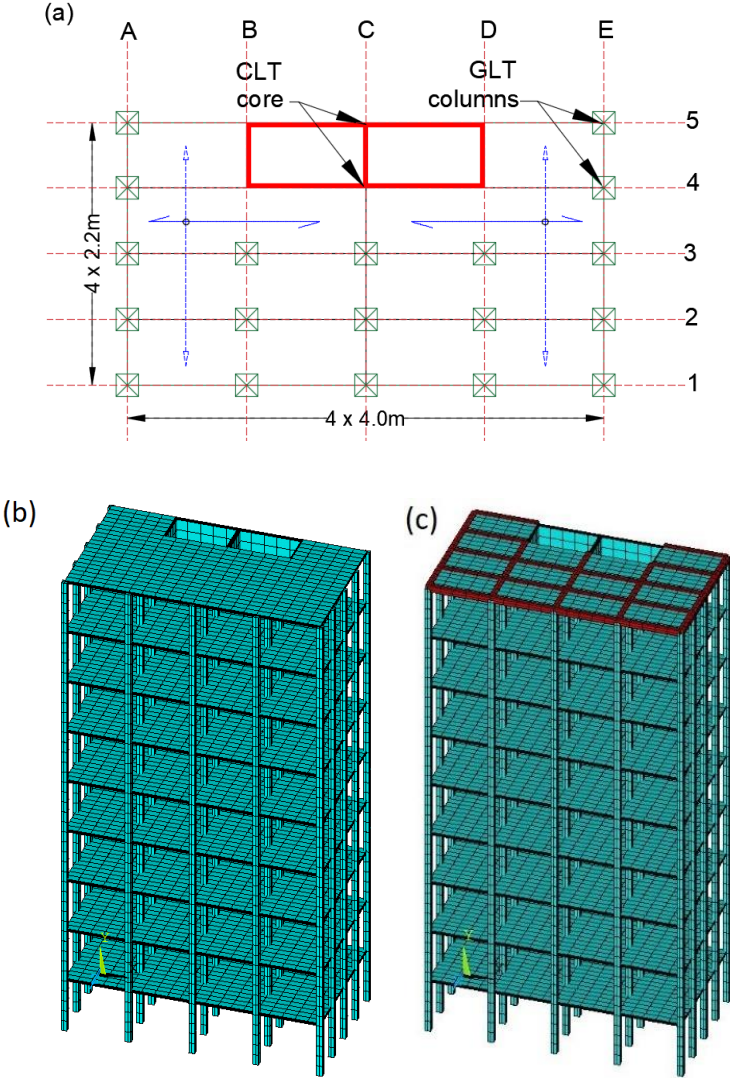
Figure 5-1: Case study building: (a) Building floor plan; (b) Isometric view of numerical original (M_1) model; and (c) Isometric view of numerical improved (M_2) model

For this study, using an advanced numerical model with respect to connection details and material properties, the building's structural performance following sudden removal of ground floor columns was investigated, accounting for dynamic behaviours as well as material and geometric

nonlinearities, as recommended by UFC 4-023-23. Taking advantage of symmetry, only the columns on gridlines A, B and C were considered for the nonlinear dynamic ALPA (Ojective-1). The removal scenarios were grouped into six categories: (i) corner (columns A-1, A-5); (ii) penultimate (A-2, A-4, B-1); (iii) near penultimate (B-2); (iv) edge (A-3, C-1); (v) near edge (C-2); and (vi) internal (B-3, C-3) columns.

For this study, two different models were built: (i) the originally proposed case study building (M_1), as shown in Figure 5-1b; and (ii) the improved model (M_2), as shown in Figure 5-1c. The latter was built after obtaining a high $P[DC]$ from the reliability analysis of the former. For M_2, a beam system was added at the top floor level, highlighted by the red lines in Figure 5-1c. The connection properties, as well as the geometry of the additional beams for the improved model, were redefined after optimisation.

5.3.2 Structural Designs: Gravity and Lateral Load-resisting Systems

The nine-storey building was designed for normal importance category according to NBCC-2015, for a location in Vancouver (Canada). *LL*, *SL*, and superimposed dead load (*SID*) were 1.9kN/m^2, 1.8kN/m^2, and 1.0kN/m^2, respectively. The weight of all timber elements was 4.2kN/m^3; the total *DL* accounted for both *SID* and self-weight. A 5-ply CLT panel, E_1 CSA-O86 stress grade (Canadian Standards Association, 2017), composed of 35mm thick layers, with the properties listed in Table 4-2, was used to carry the imposed gravity loads for the considered limit. The GLT columns were Spruce-Pine 12c-E (Canadian Standards Association, 2017), with a cross-section of 365×380mm (with the cross-section based on the bearing requirement of the point supported CLT floors), a Young's modulus of 9,700MPa, and a compressive strength of 25.2MPa.

For the gravity load design, the double span continuous point supported CLT floor panels and the GLT columns were designed for ULS and checked for SLS according to CSA-O86. For the 5-ply CLT panel, utilisation of 48%, 74%, 55% and 74% were obtained for the flexure, shear, deflection, and vibration checks, respectively. For GLT column, at the ground floor level, 37% utilisation was obtained for compression + biaxial bending requirements. As explained before, the study focused on the deformations of the connections and the CLT panels as disproportionate collapse thresholds. Therefore, the selected column cross-section resistance was anticipated to always exceed the demands even after load distribution; hence their sizing did not impact the ALPA.

For the core, 7-ply CLT panels with the individual layers 35mm thick were used, with the properties as given in Table 4-2. For seismic design, a response spectrum analysis, based on multi-model response spectra, was performed. The Vancouver-2015 design spectrum, with peak ground acceleration of $0.369g$, for 2% in 50 years probability, was used. Herein, the lateral loads were generated separately for each relevant eigenvalue and excitation direction and then combined with the requirement to consider multiple modes to reach at least 90% mass-participation in each direction. Class-C was the considered soil type; and 3% viscous damping.

Conservatively, it was assumed that the LLRS had no moderately ductile connection; therefore, the seismic forces were calculated using $R_dR_o = 1.3$ (Canadian Standards Association, 2017). R_d and R_o represent the ductility and over-strength factors, respectively. The first mode of vibration corresponded to a period of $1.04sec$ an acceleration of $0.42g$, and a mass participation of 67%. After 10 modes of vibration, the total mass participation was 94% and 92%, resulting in base-shears of 910kN and 890kN, for the longitudinal and transverse directions, respectively. The building was torsionally insensitive; the maximum inter-storey drifts in the longitudinal and

transverse directions were 19mm and 16mm, respectively, both below the 2.5% limits as per NBCC.

5.3.3 Structural Designs: Connection Detailing

Figure 5-2 illustrates the location of the connections in the building isometric view and plan. With a single wall panel spanning three storeys, the horizontal wall-to-wall joints between two vertical panels were designed as elastic, with full moment and force transfer. These moments connections could be achieved using glued-in steel rods (Zhu et al., 2017) or glued-in steel plates (Zhang et al., 2018). The corner and vertical wall-to-wall panel joints were also designed elastically for full force transfer using half-lap joint in combination with STSs (Hossain et al., 2018, 2016).

The other connection detailing were identical to the ones implemented for the Brock Common building (Fast and Jackson, 2017). Assuming a rigid diaphragm behaviour, both transverse and longitudinal floor-to-floor joints were detailed as surface splines with two rows of 80mm long 8mm diameter STSs, as shown in Figure 5-3a. For lateral load transfer from the diaphragm to the core at every level, Simpson Strong-Tie 'strong-drive' connectors (Simpson Strong-Tie, 2017), 100mm wide by 12.5mm thick, were used. For the floor-to-core connection, the CLT panels rested on 29mm thick steel ledger angles, with two rows of steel bolts loaded laterally to fasten the panel, as shown in Figure 5-3c.
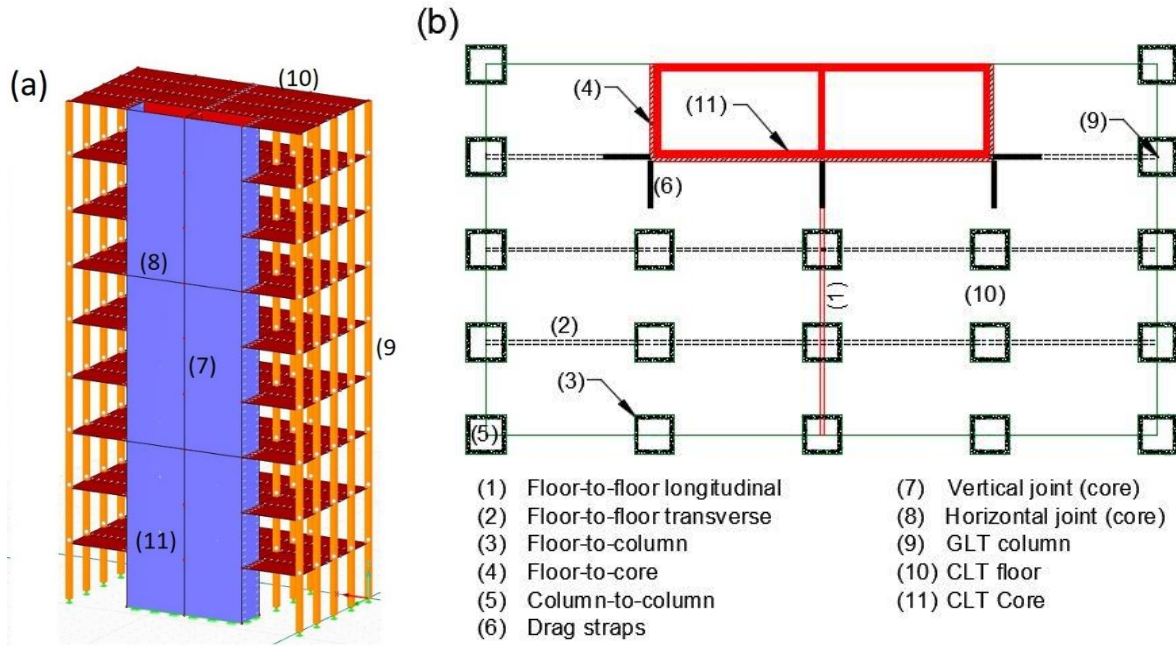
Figure 5-2: Main structural elements shown in: (a) Building isometric view; and (b) Floor plan

(1) Floor-to-floor longitudinal
(2) Floor-to-floor transverse
(3) Floor-to-column
(4) Floor-to-core
(5) Column-to-column
(6) Drag straps
(7) Vertical joint (core)
(8) Horizontal joint (core)
(9) GLT column
(10) CLT floor
(11) CLT Core
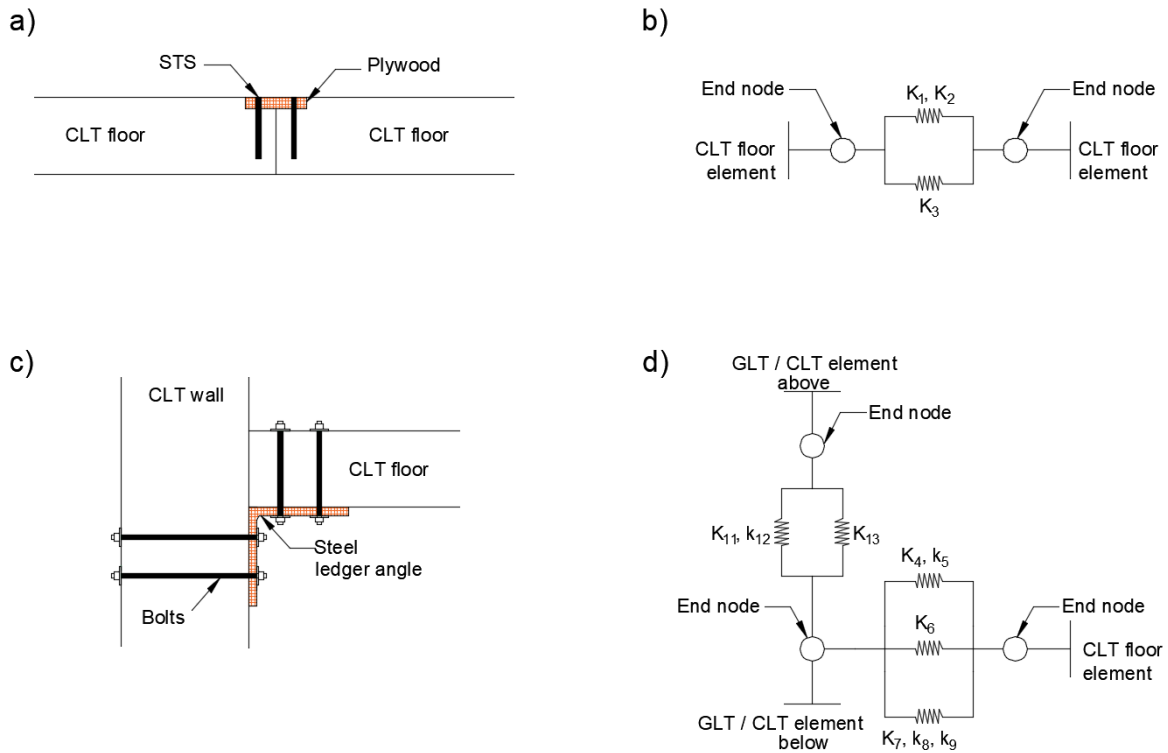
Figure 5-3: Floor-to-floor spline connection: (a) Sketch, (b) Springs idealisation; and Floor-to-steel ledger angle: (c) Sketch, (d) Springs idealisation

115

The chosen column-to-column and column-to-floor detailing followed the description in Figure 5-4 to provide direct load transfer, while avoiding compression perpendicular to the grain stresses and reducing rolling shear stresses in the CLT panels, making the design adequate for both gravity and lateral loads. Herein, as explained in section 2.7.6, steel pin passing through the round hollow (HS) and solid (SS) sections acted as vertical tie triggering hanging action of the floor panel on the column above if the column underneath was removed. All bolts were 25.4mm in diameter; all steel components were 350MPa weldable steel, with Young's modulus (E_{el}) and Poisson's ratio assumed as 200,000MPa and 0.3, respectively.
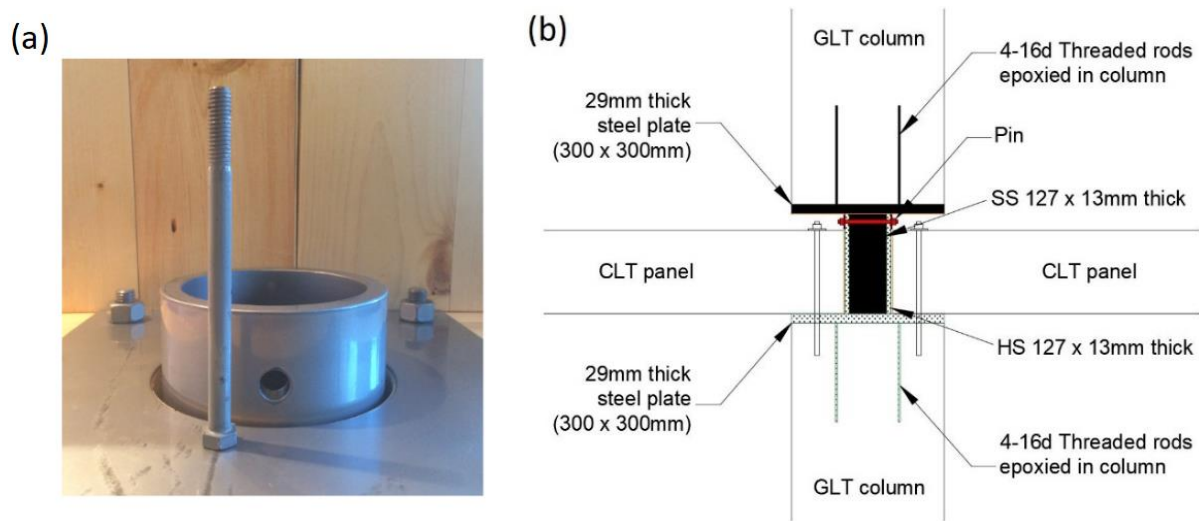
Figure 5-4: Column-to-column detailing: (a) Photo (Photo credit Mpidi Bita); (b) Schematic representation (Fast and Jackson, 2017)

5.4 Alternate Load-path Analysis (ALPA)

5.4.1 Structural Component Modelling

The nine-storey building shown in Figure 5-1b was modelled in ANSYS (ANSYS, 2011), given its ability to record every load-step during the nonlinear dynamic analysis. The NBCC extreme

load combination, given in Equation (2.2), accounting for 100% *DL*, 50% *LL* and 25% *SL*, was considered for ALPA. After the sudden element removal, the program was set to continue upon initial non-convergence, with the maximum number of equilibrium iteration set to 200; and the analysis used ramped loading with a 0.5*sec* time step. The GLT columns were represented by two-node beam elements (Beam-188), with six degrees of freedom at each node, and a uniform cross-section and elastic orthotropic material properties, as listed in Table 4-2.

Wall and floor panels were modelled using four-node shell elements (Shell-181) with both membrane and bending stiffness, using material properties listed in Table 4-2. The cross-sections were defined according to the CLT layup, with the top layer longitudinal to the span direction, and the remaining layers oriented crosswise; the layers were fully bonded, and uniform along the width of the panels. The results of quasi-static testing (see Appendix A.1) (Popovski et al., 2016) to estimate the stiffness, strength, and failure modes of point supported CLT floors, were used to validate the modelling assumptions. The performance and obtained failure modes (combination of rolling shear and compression stresses perpendicular to the grain) were also in agreement with the experimental testing performed by (Hochreiner et al., 2014). The meshing of a single shell and beam element generated six nodes for computational efficiency, resulting in a mesh-independent structural performance. Herein, a sensitivity analysis was carried out to confirm that the selected mesh size was acceptable, and negligible change in the results was observed after refining the mesh.

5.4.2 Connection Modelling

The joint between all structural components were idealised by uniaxial spring elements, (Combin-39 and Combin-14) for nonlinear and linear behaviours, respectively. With this approach, it was

possible to model the contribution of the individual springs to the connection behaviour. This approach helped to overcome the need for a three-level structural idealisation, as performed in the previous Chapter 3. Furthermore, mimicking connections using spring elements drastically reduced the computational effort for complex and accurate connection modelling, and also enabled a good representation of the performance of the building at the global level, after the extreme loading scenario (Byfield et al., 2014). The location of springs followed the description in Figure 5-2. The base of the CLT core, and the horizontal wall-to-wall joints between the vertical CLT panels, were coupled using rigid constraints to mimic moment connections. This assumption was made due to the lack of test data on the stiffness of these connections for CLT shearwalls and was expected not to affect the presented ALPA, as the removal of LLRS elements was beyond the scope of this thesis. The same assumption was considered for the corner and vertical joints between adjacent walls.

In Figure 5-3b and d, the circles represented the end nodes of all elements meeting at the joint. As shown in Figure 5-3b, for the floor-to-floor joint, the end nodes of the two floor segments were linked using two nonlinear springs for horizontal shear of the STSs in the two orthogonal directions (k_1 and k_2), and one nonlinear spring for the vertical direction (k_3) assumed as pure withdrawal of STSs between two panels. Herein, no interaction was assumed between the shear and withdrawal resistance of the STSs; the resistance in a given direction would be triggered independently, with respect to their demands. As illustrated in Figure 5-3d, the floor-to-column connection was represented by two nonlinear springs (k_4 and k_5) for the horizontal shear in both directions provided by the bolts, one linear spring for bearing (compression) and uplift (tension) resistances (k_6), and three linear rotational springs (k_7, k_8 and k_9) to control rotations about the three orthogonal axes. The same configuration was defined for the floor-to-core connection; drag straps were idealised

118

by linear springs (k_{10}). The column-to-column joint was idealised by two linear springs (k_{11} and k_{12}) to account for the horizontal restraints from the HS and SS in the two directions, and one nonlinear spring (k_{13}) to mimic bearing on the steel plates and tension resistance for hanging action provided by the steel pin.

5.4.3 Spring Properties

Realistic results using ALPA for timber structures can be achieved by assuming elastic material properties for timber members, nonlinear material models for connections, and geometric nonlinearities (Thelandersson and Honfi, 2009). For the present study, only spring behaviours which contribute to the catenary and hanging actions (collapse-resistance mechanisms also explained in Chapter 5) of the CLT floor panels, as shown in Figure 5-5a, were assigned nonlinear properties. The capacity of a single STSs in shear was obtained from experimental tests performed by (Hossain et al., 2018, 2016). In addition, the capacity of STSs in pure withdrawal was calculated using CSA-O86 provisions for lag screws, assuming an end-grain resistance factor of 0.7. The lateral resistance of a single bolt was estimated using the Johansen's yield equations as per CSA-O86. For all connections, multiplying the calculated resistance of a single screw/bolt by the provided number of fasteners (n) gave the total capacity (F_{tot}) of the joints, which was then checked against the respective demands recorded after gravity and seismic analyses of the building. Given the high probability of disproportionate collapse observed in the results, group effects as a function of the number of fasteners, were deemed not to have impacted the conclusions and were therefore not considered.
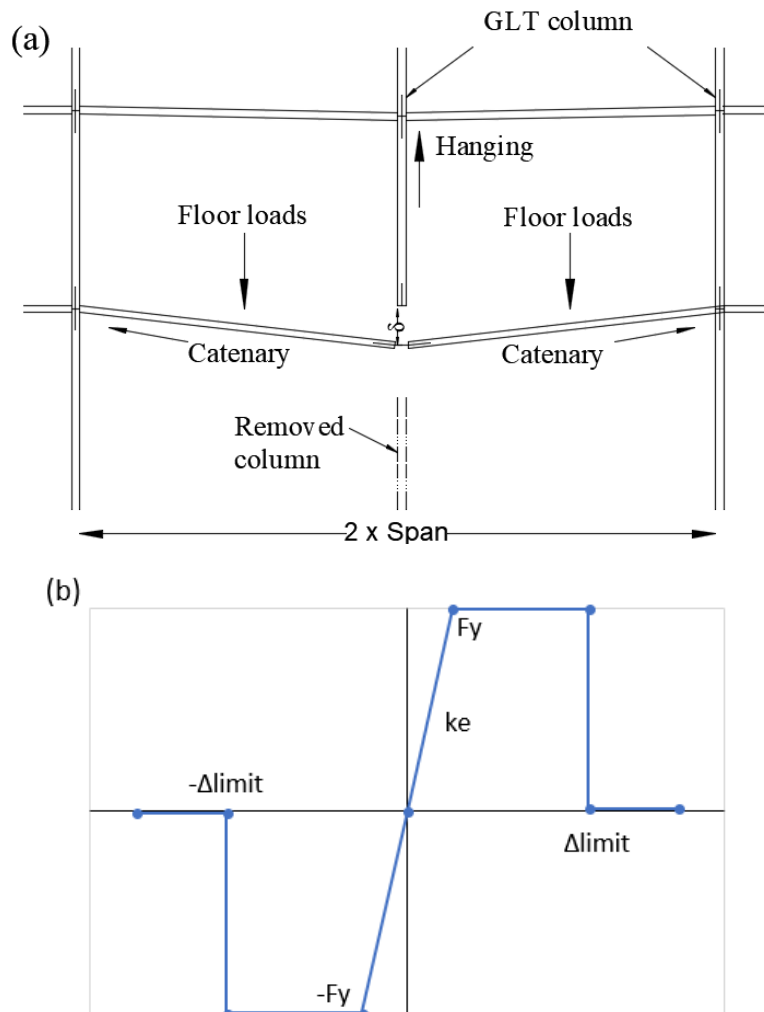
Figure 5-5: (a) Catenary and hanging actions; and (b) Force-deformation model of nonlinear springs

The elastic stiffness and the rotational stiffness of a single bolt, used for one shear plane steel-to-timber connection (floor-to-column, floor-to-core, and drag straps), was computed based on the slip modulus (K_{ser}) at serviceability limit state, given in Equation (4.1). K_{ser} was calculated per shear plane per fastener under service loads (CEN, 2008). For timber-steel connections, the stiffness was doubled assuming that only the timber deformed. Previous research (Ceccotti and Follesa, 2006; Follesa, 2015) demonstrated that these estimates are acceptable for CLT connections given the lack of experimental data for verification. As explained by (Follesa, 2015),

the total stiffness of the connection, for a given number of fasteners, was then calculated as $K_{tot} = n \times K_{ser}$.

The elastic bending stiffness of the pin was a function of its Young's modulus, its cross-sectional area, and its length (Hoogenboom and Spaan, 2005). The elastic shear stiffness of a single STSs in a surface plywood spline connection was obtained from the Equivalent Energy Elastic Plastic (EEEP) curves (American Society for Testing and Materials, 2011) of the experimental testing performed by (Hossain et al., 2016). The behaviour under bearing/uplift, as well as the shear stiffness of the column-to-column connections, were idealised by a spring of infinite stiffness.

Table 5-1 gives the properties used for the FEA: capacity (F_y), elastic stiffness (K_e), and behaviours for a single spring with F_y and K_e obtained by dividing the total capacity (F_{tot}) and stiffness (K_{tot}) of the connection, respectively, by the number of springs in the considered joint direction. Nonlinear material properties were defined by the force-deformation model shown in Figure 5-5b, setting F_y as yield point. Herein, positive and negative forces were assigned for compression and tension behaviours, respectively. The nonlinear springs were elasto-plastic; defined to break after reaching their deformation limits (Δ_{lim}), which mimicked spring failure criterion. Δ_{lim} was only defined for the floor-to-floor (k_1, k_2, k_3), floor-to-column and floor-to-core (k_4, k_5), and the column-to-column pin (k_{13}) nonlinear spring connections.

Table 5-1: Spring properties for FEA models

Components	Behaviours	F_y	k_e	IF (%)
Floor-to-floor *(k₁, k₂)*	Shear	100kN	30kN/mm	2
Floor-to-Floor *(k₃)*	Withdrawal	30kN	10kN/mm	-
Floor-to-column *(k₄, k₅)*	Shear	30kN	40kN/mm	-
Floor-to-core *(k₄, k₅)*	Shear	59kN	630kN/mm	-
Floor-to-column / Core *(k₆)*	Bearing / Uplift	-	10^{10}kN/mm	-
Floor-to-column *(k₇, k₈, k₉)*	Rotation	-	40kNmm/rad	23
Floor-to-core *(k₇, k₈, k₉)*	Rotation	-	4×10^8kNmm/rad	23
Drag strap tie *(k₁₀)*	Shear	-	60kN/mm	-
Column-to-column *(k₁₁, k₁₂)*	Shear	-	10^{10}kN/mm	-
Column-to-column *(k₁₃)*	Bearing	-	10^{10}kN/mm	-
Column-to-column *(k₁₃)*	Tension / Pin	10kN	25kN/mm	56

5.4.4 Disproportionate Collapse Thresholds

The connections between CLT panels govern the shearwall deformations, while the CLT panels themselves could be assumed as rigid bodies (Canadian Standards Association, 2017; Gavric et al., 2015). The same assumptions were considered for possible catenary and hanging actions: the connections would supply the deformation-demands, required to trigger the collapse-resistance mechanisms, whereas the CLT panels would remain elastic to avoid brittle failure (Ellingwood et al., 2007; Jorissen and Fragiacomo, 2011). For the considered building, these assumptions were confirmed after observing that the deformations of the CLT panels relative to their span and width were negligible. Therefore, the thresholds or LSFs defining disproportionate collapse were: (i) the

maximum allowable deflection (δ_{lim}) of the CLT panels at the location of removed element before brittle failure, and (ii) the maximum allowable plastic deformation (Δ_{lim}) of the connection before fracture.

The analyses considered a series system, defined in such a way that a global collapse occurred when a single LSF was violated. In other words, the deformation capacities, δ_{lim} and Δ_{lim}, should always be bigger than the respective demands, δ and Δ (Stevens et al., 2011). For each removal scenario, the deformation demands on the CLT (δ) and the connections on the bay surrounding the removed elements (Δ) were recorded and compared against the respective allowable deformations δ_{lim} for CLT, and Δ_{lim} for connections. With this approach, the demand-capacity ratio (*DCR*), defined as the ratio between the demands (δ and Δ) and the respective limits (δ_{lim} and Δ_{lim}), was calculated separately for each CLT panel, and connections. This method determined whether a given CLT panel or connection around the removed element would prevent failure failure under the considered scenario. Hence this approach checked for possible collapse propagation to undamaged parts of the building. A *DCR* > 1.0 at the storey above the removed element and/or the immediate adjacent was deemed disproportionate to the considered initial damage (DoD, 2013; Sørensen, 2011).

Experimental shear tests for STSs (Hossain et al., 2018, 2016) and bolts (Peixoto et al., 2017), with similar material properties and dimensions, estimated Δ_{lim} to 25mm and 5mm for STSs and bolts, respectively. Using the CSA-O86, the maximum allowable stresses before CLT failure were: (i) the normal stress for the longitudinal layers (bending + tension/compression components: $\sigma_0 = 28.2\text{MPa} + 15.4\text{MPa} / 19.3\text{MPa}$); and (ii) the normal stress of the transverse layers ($\sigma_{90} = 7.0\text{MPa} + 3.2\text{MPa} / 9.0\text{MPa}$). Exceedance of rolling shear strength ($\tau_R > 0.5\text{MPa}$) near the supports was

considered as a local failure. This study focused on the maximum deformations applied on the CLT panels at the location of the removed elements, measured before exceeding the stress limits, to define the disproportionate collapse deformation thresholds. For all considered removal scenarios, the deformation limit (δ_{lim}) was obtained by deleting the vertical element from the building, without dynamic effect, and applying a vertical downward displacement at the same location until brittle CLT failure (stress exceeding σ_0 or σ_{90}) was observed. Therefore, the exceedance of δ_{lim} represented a global failure.

5.5 Reliability Analysis

To address the second objective, a reliability analysis was performed to estimate $P[DC]$ following the column loss, given the uncertainties present in the modelling parameters. Probability-based methods allowed to quantify the effects of uncertainties on the structural response after element removal. Using their respective distribution functions, input uncertainties and subsequent response variabilities could be related. Herein, FORM, implemented in OptiSlang (Dynardo, 2017), was used. This enabled to quantify $P[DC]$ for both the Original (M_1) and Improved (M_2) models, given the considered LSFs.

In FORM, the considered LSF (g) defined failure or non-failure using Equation (4.3), where the resistance (R), defined by δ_{lim} or Δ_{lim}, was influenced by the material properties the element cross-section as well as the connection strength and stiffness. The demand (S), defined by δ or Δ, was influenced by the uncertainties of loads DL, LL, SL, and the column removal speed (t_r). The FORM results were given in terms of the reliability index (β), which was the distance from the origin of the standard space and the design point defined as the point in the failure domain with highest probability density (see Equation (4.5)).

Herein, disproportionate collapse occurred when a single or both LSF was violated ($g \leq 0$). Although the two LSFs were defined individually, a single $P[DC]$ was obtained and a series system was used to evaluate structural safety using Equation (4.3): $g(X_i) = \min g_j(X_i))$; i=1- N_{RV} and j=1- M, where Xi represented an input random variable, N_{RV} was the total number of considered input variables (herein = 15), and $g_j(X_i)$ was the considered LSF j and M was the number of LSFs (herein = 2). Furthermore, only the worst-case element removal with the highest *DCR* was considered, assuming that hanging and catenary actions were the only relevant collapse-resistance mechanisms for all removal cases. Herein, estimating the effects of uncertainties using worst-case column loss alone could be applicable for the remaining scenarios. Table 5-2 summarises the considered parameter uncertainties, along with their assumed PDF, μ_m and *CoV*.

100 analyses were performed using Latin Hypercube Sampling (LHS) (Dynardo, 2017; Most and Will, 2012) to determine the individual influence of uncertainties present within both loading and resistance parameters, on subsequence structural performance (*R* and *S*), and hence quantify their respective impacts in terms of importance or influence factor (*IF*). Herein, different permutations of input parameters were considered for *IF* estimation. This was the variance-based robustness analysis as described in Chapter 3.

Since ALPA is an event-independent approach, different removal speeds (t_r) imposed different deformations, hence idealising different extreme events as described in Chapter 3. To account for both static and dynamic element removal, *t* was varied from 5*sec* to 0.001*sec* (as per UFC 4-023-03 and GSA). A uniform PDF was defined to assign the same probability of occurrence for all *t*-values. The probability model for the loads were defined from the NBCC load factor calibration (Bartlett et al., 2003). As explained in section 4.7, from previous research (Jeitler et al., 2016;

Jessome, 1977; Joebstl et al., 2008; Steiger and Gulzow, 2009), the PDFs and *CoV*s assumed herein for CLT and GLT were acceptable, as defects in EWPs are removed or distributed during the production process.

Table 5-2: Parameter uncertainties considered for reliability analysis

	Parameter	PDF	Mean (μ_m)	*CoV* (%)	*IF* (%)
Loading	Removal speed (t_r)	Uniform	2.5*sec*	58	17
	Dead load ($DL + SID$)	Normal	$4.2kN/m^3 + 1.0kN/m^2$	10	23
	Live load (LL)	Normal	$1.9kN/m^2$	20	39
	Snow load (SL)	Normal	$1.8kN/m^2$	17	-
Material	*E*-longitudinal (E_L)	Lognormal	11,000MPa	5	12
	E-transverse (E_T)	Lognormal	9,000MPa	5	5
	E-steel (E_{el})	Lognormal	200,000MPa	2	-
	Floor-to-floor (k_1-k_3)	Normal	Table 5-1	10	-
	Floor-to-column (k_4-k_9)	Normal	Table 5-1	10	-
	Floor-to-shearwall (k_4-k_9)	Normal	Table 5-1	10	-
	Column-to-column (k_{13})	Normal	Table 5-1	10	-
	Drag straps (k_{10})	Normal	Table 5-1	10	-
Geometry	Thickness CLT layer	Normal	35mm	1	-
	Width column	Normal	350mm	1	-
	Depth column	Normal	350mm	1	-

For steel, the variability was based on the review provided by (Hess et al., 2002). Timber connection tests, performed by (Zhu et al., 2017) for glued-in rods, (Zhang et al., 2018) for hold-downs, (Hossain et al., 2018, 2016) for STSs, (Schneider et al., 2018) for tube connections, gave *CoV* in the range of 10%. The stiffness estimations of the off-the-shelf angle brackets and wood screws were within 10% of the results presented in Chapter 3. The aforementioned experimental and numerical investigations allowed to assume a *CoV* = 10%, given that the connections were tested under the same configurations with all materials delivered from the same manufacturer. Furthermore, it was assumed that rigorous production quality control procedures would result in a normal PDF and *CoV* = 1% for CLT and GLT cross-sectional dimensions. Therefore, for the analyses of case study building, the assumed distribution parameters were deemed acceptable.

5.6 Sensitivity Analysis and Optimisation

With a high *P*[*DC*], considerations for structural improvements were imperative. Since the performance against failure depended on the connection detailing, a sensitivity analysis was performed on the worst-case removal scenario of the Original (M_1) model (Figure 5-1b) to identify the critical parameters that influence the structural robustness. To address the third objective, a numerical optimisation was conducted to obtain the spring's capacity (F_y) and stiffness (K_e) required to satisfy their respective demands and enhance alternative load-paths. To develop resistance mechanisms against disproportionate collapse, the most important spring parameters after optimisation were used in Improved (M_2) model, see Figure 5-1c. Here, their optimum values were used as input in M_2 to demonstrate improvements in the structural performance compared to the M_1 model.

Both sensitivity analysis and optimisation, also described in section 4.5 and 4.6, respectively, were performed using OptiSlang. They both utilised the defined series LSF system to evaluate the structural performance, given in terms of *DCRs*. ALHS was used to scan the design span and 250 analyses were performed to account for all possible permutations of connection parameters, with ranges restrained within the defined probability models. The output, given in terms of *IFs*, quantified the importance of each input parameter; and the *CoPs* evaluated the accuracy of the results. For optimisation, the Evolutionary Algorithms were utilised to scan the design space, composed of 10,000 analyses, and to obtain the capacity (F_y) and stiffness (K_e) of the important connections (those with $IF > 1\%$) required to build the M_2 model and avoid disproportionate collapse ($DCR \leq 1.0$) for all considered removal scenarios.

5.7 Results and Discussion

5.7.1 ALPA: Maximum Allowable Deflection for CLT Panels

For all cases, the obtained CLT floor failure sequence was first exceedance of rolling shear strength (τ_R) at the nearest column supports, followed by the exceedance of the normal stresses parallel (σ_0) and perpendicular to the grain (σ_{90}), in agreement with previous experiments (Hochreiner et al., 2014; Popovski et al., 2016). Table 5-3 includes the values of the deformation limits (δ_{lim}), considered as thresholds for CLT floor panel deformations, and obtained after applying vertical static downward displacement at the location of the removed column until brittle CLT failure was observed. In other words, brittle failure was assumed to occur when the applied bending + compression/tension stresses in the longitudinal or transverse layers of the CLT panel exceed their stress limits.

Table 5-3: Applied deformations and residual strengths

Scenarios		Gridlines	δ_{lim} (mm)	Original M_1		Improved M_2	
				δ_{M1} (mm)	DCR_{M1} (~)	δ_{M2} (mm)	DCR_{M2} (~)
1	Corner	A-1	32	36	1.13	9	0.28
		A-5	34	29	0.85	10	0.29
2	Penultimate	A-2	15	34	2.27	8	0.53
		A-4	13	30	2.31	8	0.62
3	Near Penultimate	B-1	21	38	1.18	11	0.52
		B-2	15	36	2.40	12	0.80
4	Edge	A-3	25	35	1.40	9	0.36
		C-1	28	35	1.25	11	0.40
5	Near Edge	C-2	12	34	2.80	12	1.00
6	Internal	B-3	10	28	2.80	10	1.00
		C-3	10	22	2.20	9	0.90

Considering δ_{lim} from the different removal scenarios shown in Table 5-3, the floor-to-core joints provided strong translation and rotation restraints. On one hand, these line supports caused shear and bending failure in the transverse direction under small deformations ($\delta_{lim} = 10$mm for columns on gridlines B-3 and C-3), given the short panel width. On the other hand, these supports enhanced the resistance in the longitudinal direction, noted with the removal of column A-5 ($\delta_{lim} = 34$mm). The existence of multiple bays in the transverse direction and the transverse floor-to-floor connections resulted in higher resistance with large deformations by enabling adequate load distribution from the damaged areas to the undamaged parts of the building. This was noted by comparing δ_{lim} for the removal of penultimate columns (A-2 and A-4) against corner column (A-1 and A-5), where higher δ_{lim} was obtained for the latter cases.

Deformation limits (δ_{lim}) of 15m and 12mm were observed for near penultimate (B-2) and near edge (C-2) column removals, respectively. Although the floor-to-floor joints provided possible collapse-resistance mechanisms, the size of the damaged area and the low deformation and

moment resistance capabilities of the floor-to-column connections reduced the panel's δ_{lim}, given that this was a point supported floor system. Furthermore, the use of continuous CLT panels aided in the load distribution to undamaged parts of the structure as shown for penultimate column removal B-1 ($\delta_{lim} = 21$mm). Nevertheless, this distribution was limited by the low bending capacity of the panels. The existence of floor-to-floor connections at the location of possible maximum bending moments after element removal also aided in the load distribution by allowing higher deformations, as noted for edge column A-3 and C-1 removal ($\delta_{lim} = 25$mm and $\delta_{lim} = 28$mm, respectively), depending on the connection total capacity.

5.7.2 ALPA: Alternate Load-paths

Collapse-resistance mechanisms to provide alternative load-paths after column removal were catenary action, as shown in Figure 5-5b, and hanging action and horizontal tie, as shown in Figure 5-6a. In Figure 5-5a, the applied floor loads to avoid debris loading were transferred to the supports on either side through catenary action triggered by the floor-to-floor connections. In Figure 5-6a, the column-to-column connections, enabling hanging action as a collapse-resistance mechanism, redistributed the loads from the damaged first level to the upper floors. As shown in Figure 5-6b, the vertical forces on these connections increased from the ground level to the top floor. These vertical forces which cumulate at the roof level, needed to be horizontally transferred to the CLT core through horizontal ties. For horizontal tie forces, a triangular distribution was assumed, with the highest magnitude on the top floor. At every floor level, the horizontal ties, provided by the floor-to-floor (k_1, k_2), and floor-to-column / floor-to-core (k_4, k_5, k_7, k_8, k_9) joints, enabled this horizontal distribution.
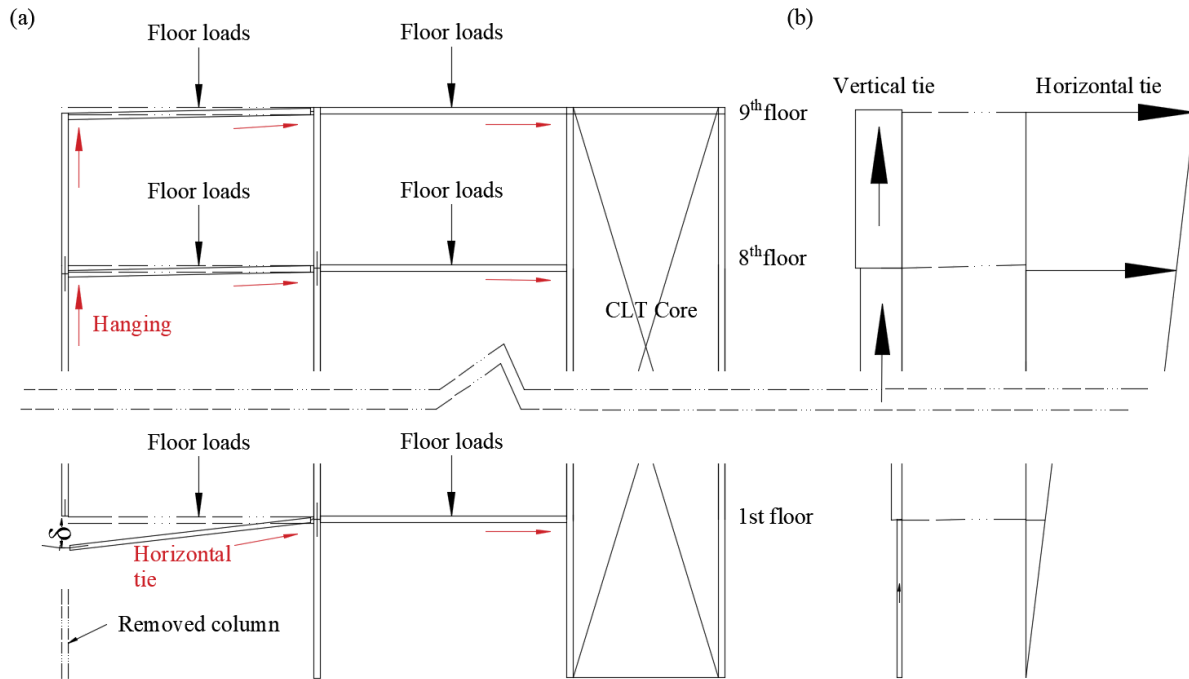
Figure 5-6: Alternative load-path: (a) Hanging action and tie-force; and (b) Idealised forces

The proposed original (M_1) structural system with point supported floor panels was not appropriate for the anticipated force distribution to fully engage the connections in resisting global collapse. Although the applied deformations (~6mm) on the floor-to-floor spline STSs connections were below Δ_{lim}, the deformations recorded on the floor-to-column bolt joints (~8mm) exceeded Δ_{lim}. These observations demonstrated that the original detailing was not sufficient to prevent collapse of the building.

5.7.3 ALPA: Speed of Removal

The speed of element removal (t_r) influenced the observed deformations. Static removal, which mimicked vertical settlement of the floor at the location of the deleted column occurred for $t \geq 5.0 sec$. The shorter the time (t_r), the higher the dynamic effects on the mode, due to the additional inertial forces on the building. Figure 5-7 shows the recorded deformations following column C-2

removal from the Original (M_1) building. For the time control to ensure that peak values were recorded for every load-step up to 30*sec* after element removal, the time-step size was defined to 0.5*sec*, with the maximum and minimum values set to $10^{-5}sec$ and 0.5*sec*, respectively. For assumed static removal ($t = 5sec$), the building was already unsafe with respect to the applied deformations (δ) on the CLT panels at the location of the removed element, with $DCR_{M1} = 1.33$. Although the applied deformations on the floor-to-floor connections could be ignored, the deformations on the floor-to-column also highlighted failure, with $DCR_{M1} = 1.2$. In other words, failure beyond the damaged area led to disproportionate collapse.

Displacement (δ)
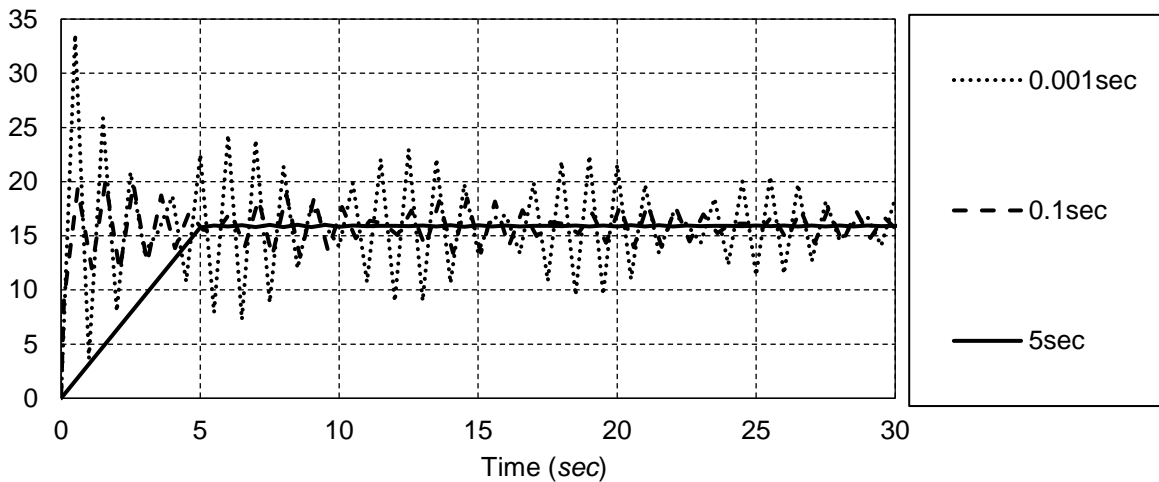
Figure 5-7: Effects of speed of element removal

For quicker removal, $t < 5sec$, dynamic effects were introduced; however, for $t > 0.1sec$, the results were not significantly different from the static case. Dynamic effects led to higher CLT deflections beyond the defined limits: $DCR_{M1}=1.67$ and $DCR_{M1}=2.80$ for $t = 0.01sec$ and $t = 0.001sec$, respectively. These analyses confirmed that UFC 4-023-03 assumptions that the dynamic response was twice the static response for the considered case study building. In addition, for sudden

element removal ($t \leq 0.001 sec$) as recommended in UFC 4-023-03 and GSA, 3% viscous damping ratio was insufficient to restore the static equilibrium of the building $30 sec$ after element removal.

5.7.4 Nonlinear Dynamic Analysis – Original (M_1) Model

The results of the nonlinear ALPA performed on the M_1 case study building, obtained after a removal time $t = 0.001 sec$, which corresponded to the GSA and UFC 4-023-03 to trigger dynamic structural response, are summarised in Table 5-3. Collapse occurred for all removal scenarios except corner column A-5 where the line supports provided by the floor-to-core connection as well as the existence of multiple bays in the transverse direction, helped reducing the vertical deformations after removal. For column B-1 removal, the applied bending moments dictated failure with τ_R and σ_0 almost simultaneously, considering the new double span CLT floor. The worst-cases were column B-3 and C-2 removals, with $DCR_{M1} = 2.80$. Failure was caused by the high area loads after element removal. Figure 5-8a, b and c show the deformed shape of the building after removal of column A-1, B-1 and C-2, respectively. Although load distribution from the damaged to the undamaged parts of the building occurred, especially in the transverse direction, the observed failures were localised within the damaged bays. For all cases, the entire bay from the ground to the top floor collapsed ($DCR_{M1} > 1.0$) after element removal, which can be defined as disproportionate collapse.
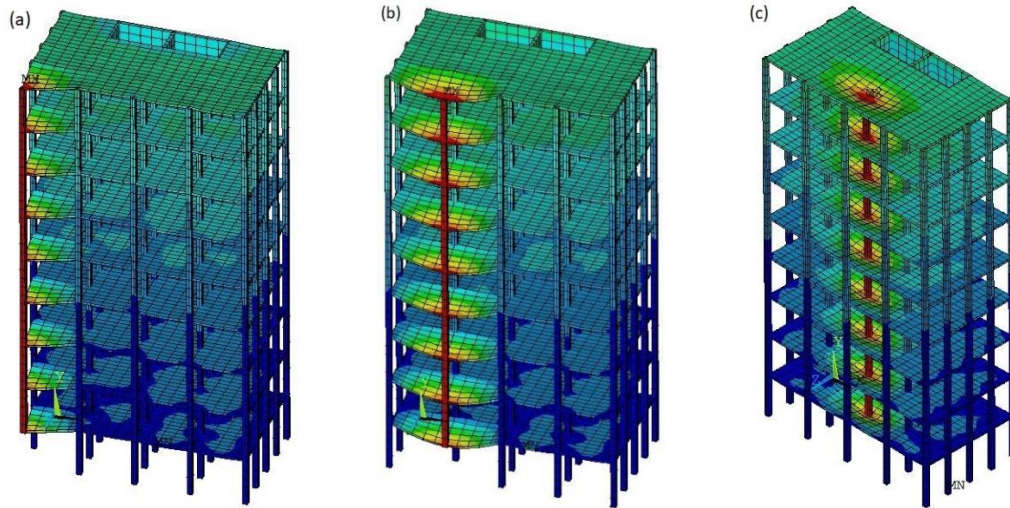
Figure 5-8: Deformed shape after column removal: (a) Column A-1; (b) Column B-1; and (c) Column C-2

5.7.5 Reliability Analysis – Original (M_1) Model

With sudden removals highlighting high disproportionate collapse potential, a reliability analysis, to estimate effects of uncertainties present with the applied loads, material properties, and geometry of the model, would be required for all cases. Nevertheless, this study assumed that the estimation of these effects using worst-case internal column B-3 ($DCR_{M1} = 2.80$) removal scenario alone could also be applicable for the remaining cases, assuming the same resistance mechanisms.

Table 5-2 shows the results of the 100 analyses, given in terms of importance factor (IF), performed to estimate the influence of uncertainties on the original (M_1) model. Herein, the loadings were identified as the most influential variables on the applied deformations (LSFs: $\delta \leq \delta_{\lim}$ and $\Delta \leq \Delta_{\lim}$ for safety). The live loads (LL) plus snow loads (SL), dead loads (DL), and the removal speed (t_r), had an IF of 39%, 23%, and 17%, respectively, with a $CoP = 88\%$ confirming the accuracy of the results. The fact that only quicker t-values influenced the dynamic structural responses resulted in low IF, whereas LL, SL, and DL had significant impacts on the analyses,

regardless the selected t-values. With respect to the material properties uncertainties, for both CLT panels and connections, E_L and E_T were the only important variables, with $IF = 12\%$ and 5%, respectively. E_L and E_T influenced the two-way bending capacities in the longitudinal and transverse direction, respectively. The CoV assigned to the connections uncertainties and the geometric uncertainties did not influence the structural performance.

In presence of the defined uncertainties, none of the 100 performed analyses satisfied the LSFs ($\delta \leq \delta_{lim}$ and $\Delta \leq \Delta_{lim}$). The main concern was on the applied deflection (δ) of CLT floor panels after element removal. On all floors above the removed element, δ was recorded from 11mm to 28mm for all analysis which were beyond the threshold ($\delta_{lim} = 10$mm). Using FORM, the probability of disproportionate collapse ($P[DC]$) was 0.998 for internal column B-3 removal. This high collapse probability meant that disproportionate collapse would almost certainly occur following the removal of internal column.

5.7.6 Sensitivity Analysis

A sensitivity analysis was performed on the case study Original (M_1) building to estimate the critical connections helping towards disproportionate collapse prevention, after the removal of internal column B-3. With respect to the defined LSFs, the most important connections were: (i) the column-to-column enabling hanging action (k_{13}); (ii) floor-to-column / floor-to-core rotational resistance (k_7, k_8, k_9); and (iii) floor-to-floor axial and shear resistance (k_1, k_2), enabling catenary action. As shown in Table 5-1, the obtained IF was 56%, 23%, and 2% for k_{13}, k_7-k_9, and k_1-k_2, respectively, with $CoP = 84\%$ confirming the accuracy of the performed analyses.

The other connections, such as STSs withdrawal (k_3), floor-to-column axial (k_4), shear (k_5), and bearing/uplift (k_6), drag straps (k_{10}), and column-to-column shear (k_{11}, k_{12}), had no impact on the

collapse resistance mechanism that helped towards maintaining δ and Δ below δ_{lim} and Δ_{lim}, respectively. After element removal, the new load-path for robustness directed the loads from the damaged floor to the levels above, through k_{13}. These loads cumulated at the top floor, before being transferred to the CLT core using the CLT panels, the floor-to-floor, floor-to-column, and floor-to-core connections. Nevertheless, given the high in-plane shear force demands between the CLT panels, in addition to the insufficient rotational stiffness of the floor-to-column, large deformations beyond δ_{lim} were recorded on the floors above the damage, after element removal. The floor-to-column connections k_7-k_9 had low strength, stiffness, and ductility to meet the rotation demands. Furthermore, with the continuous CLT floor panels, it was noted that the bending moment resistances of the panels were smaller than the demands from the new double span, causing global CLT brittle failure.

5.7.7 Structural Optimisation – Improved (M_2) Model

For the improved model (M_2), the column-to-column tension stiffness (k_{13}) was increased to 500kN/mm, twenty times stronger than the Original M_1 supply. The rotational stiffness of the floor-to-column (k_7-k_9) was increased to 4×10^8kNmm/rad, the same value as the floor-to-core. Novel detailing to provide high axial stiffness at the column-to-column and rotational stiffness for the floor-to-column would be required to meet these stiffness demands, given that existing connections were not adequate. All other connection stiffnesses were kept as given in Table 5-1. In addition, assuming a triangular horizontal tie-force distribution as shown in Figure 5-6b, to tie the structure back to the CLT core by transferring the loads from column to the core, steel beams (350×347mm W-section) were added on the top floor level as shown in Figure 5-1c. The main beams were continuous in the longitudinal direction; and the secondary beams were simply supported in the transverse direction. With the steel beams connected to the columns, transferring

shear and axial loads only, and the CLT floor panels on top of the beam, a post-and-beam concept was created at the top floor. This concept for M_2, instead of exclusively relying on the point supported flat-plate as with M_1, was anticipated to not only help the axial load transfer to the core, but also reduce the deflection of the continuous CLT floors.

Figure 5-9 compares the deformed shape of the top floor, obtained for the Original (M_1) against the Improve (M_2) models, after worst-case internal column B-3 removal. Comparing M_1 to M_2, it can be seen that the damage, initially localised for M_1, was well distributed to the undamaged parts of the building with the addition of beams in the M_2 model. The high bending moments, shear, and axial resistances of the selected steel beam resulted in a reduction of the applied maximum deflection, keeping δ below δ_{lim}. The results of the nonlinear dynamic ALPA for all column removal scenarios for the improved model (Improved M_2) are listed in Table 5-3. The applied CLT deflections (δ_{M2}), obtained for all removal scenarios, did not result in global CLT brittle failure; and all connections deformations were below their respective Δ_{lim} ($DCR_{\text{M2}} \leq 1.0$). For the worst-cases column B-3 and C-2 removals ($DCR_{\text{M2}} = 1.0$), smaller deflections (δ) were recorded at storeys above the damaged floor level (with all $DCR_{\text{M2}} \leq 1.0$), confirming that the initial damage did not lead to a disproportionate collapse.
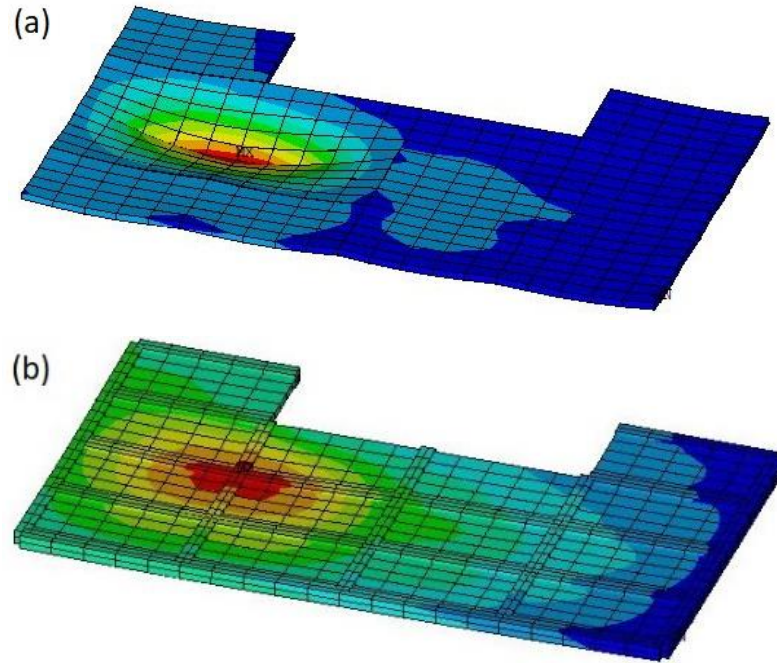
Figure 5-9: Top floor deformation after column B-3 removal: (a) M_1 model; and (b) M_2 Model

5.7.8 Reliability of Improved (M_2) Model

Figure 5-9b shows how the steel beam on the top floor enhanced the catenary action of the CLT floor panels in two-way, distributing the loads from the damaged area to the undamaged parts of the building. The maximum shear loads and bending moments of the beams, at the location of the removed element, were 110kN and 210kNm, respectively. The recorded tie forces in the beams, transferring the loads back to the core, were 20kN each, for the longitudinal and transverse directions. The addition of the beams, especially in the transverse direction, helped with respect to bending and shear. Therefore, the post-and-beam concept at the top floor, in addition to increasing the stiffness for k_{13} and k_7-k_9, were necessary for adequate structural robustness. Analysing the results of the nonlinear dynamic analysis in terms of applied vertical forces above the removed columns, the need to design the CLT floor panels and steel beam, as well as their connections for force reversal became evident. It was also noted that the magnitude of the forces, to be transferred

138

to the level above, increased for M_2 as the column-to-column (k_{13}) connection became stiffer and more effective.

In presence of uncertainties in the applied loads, material properties, and element geometries, all 100 analyses satisfied the defined LSFs ($\delta \leq \delta_{lim}$ and $\Delta \leq \Delta_{lim}$ for safety), with the applied deflections at the location of the removed elements ranging from 4mm to 9mm. From FORM, $P[DC]$ for the Improved M_2 model, following column B-3 removal, was negligible. Herein, the reliability index (β) was 8.7 signifying a robust design, capable to bridge over the damage following extreme loading, and distribute the loads from the damaged to the undamaged parts of the building. By considering steel beams on the top floor, as well as improving the column-to-column (k_{13}) and the rotation capacities (k_7-k_9) of the floor-to-column connections, the risks of disproportionate collapse were reasonably removed given the low probability. Nevertheless, given that this is a new method of construction, the practicality of obtaining the required k_{13}, and k_7-k_9 will have to be further investigated and novel connection detailing with high capacity, stiffness and ductility need to be developed. Alternatively, given the obtained β=8.7 for the M_2 model, which resulted to negligible $P[DC]$, it could be proposed to optimise k_{13}, and k_7-k_9 for a target stiffness value that would result to a $P[DC]=10^{-5}$, which is generally acceptable for building designs as mentioned in section 2.2.

5.8 Summary

The research presented in this chapter quantified the probability of disproportionate collapse $P[DC]$ of a nine-storey building with flat-plate CLT floor system, point supported on GLT columns. First, the alternate load-path method with nonlinear dynamic analysis was performed at the global level of the building, with all connections idealised as a set of independent spring

element. This helped to quantify the ratio between the resulting deformations on the CLT panels as well as connection, and the respective allowable deformation limits before failure. Thereafter, a reliability analysis was performed on the worst-case element removal to quantify $P[DC]$ given the uncertainties in the loadings, material properties, and geometry. With the obtained high $P[DC]$, a sensitivity analysis as performed to optimise the building and therefore improve the structural robustness. This chapter can be summarised as follows:

(1) The floor-to-column detailing shall minimise rolling shear failure, identified as the first failure mechanism for flat-plate system following vertical element removal, before relying on possible disproportionate collapse-resistance mechanisms.

(2) The sensitivity analysis identifies the axial tension capacity of the column-to-column, the rotational capability of the floor-to-column / floor-to-core connection, and the floor-to-floor axial and shear resistances as the most important for collapse prevention. Robust detailing was recommended to meet the strength, stiffness, and ductility demands.

(3) Hanging action, where a new load-path allows the floor to hang on to column above, is ideal for disproportionate collapse prevention. The vertical forces resulting from the hanging action, cumulating to the top floor, need to be transferred to the core using effective horizontal ties.

(4) This study demonstrates that there is a need to develop column-to-column connections for hanging actions as there is no existing detailing that can meet the demands for mid-rise mass-timber buildings. Ductility in addition to strength, and stiffness, shall be prerequisite.

(5) A post-and-beam concept can be implemented at the top floor to reduce the floor deflections after element removal and transfer the horizontal tie forces back to the core.

Chapter 6: Tie-force Procedure for Platform-type Buildings[4]

6.1 Introduction

Structural robustness, as a strategy for disproportionate collapse prevention, can be implemented using direct and indirect procedures. Applications of these procedures depend on the building's importance and occupancy (CEN, 2006a; DoD, 2013). While direct procedures, e.g. using ALPA as implemented in Chapters 3 and 4, are ideal for high important structures as well as tall buildings, indirect procedures are applicable to normal importance building. Existing code (CEN, 2006a) and guidelines (DoD, 2013) with respect to tie-force requirements as an indirect approach, e.g. Equation (6.1), were developed from analyse and testing of concrete and steel buildings. Thorough investigations are required to understand possible collapse-resistance mechanisms for mass-timber building. From this, improved tie-force requirements applicable for this construction method can be developed for pragmatic and economic solutions against disproportionate collapse. This must emphasise on the longitudinal, transverse and vertical tie-forces for structural integrity.

$$F_{T,L} = \min \ [60\text{kN/m} \ ; (20 + 4 \ \times N)\text{kN/m}] \tag{6.1}$$

6.2 Objectives

The main objective of this chapter was to propose a tie-force procedure as an indirect approach for disproportionate collapse prevention for CLT platform-type construction. The secondary

---

[4] Materials from this chapter were published in the following journal:

objectives were: i) to identify possible collapse-resistance mechanisms, after loadbearing wall removals; ii) to establish a practical procedure of analysis and design for minimum tie-force requirements, based on linear-static principles of engineering mechanics; and iii) to illustrate the implementation of the proposed tie-force procedures for CLT platform-type building at hand of a case-study building.

6.3 Improved Tie-force Method

6.3.1 Methods

The presented research implemented a tie-force method for mass-timber platform-type construction using solely engineering mechanics principles to determine the required magnitude for longitudinal (F_L), transverse (F_T), and vertical (F_V) tie forces, as well as the associated deformation compatibilities. No considerations were given to peripheral (P) tie-force, assuming that the seismic demands to ensure adequate diaphragm behaviours dictated their designs (Schultz et al., 1977a, 1977b). As per Figure 2-5b, internal, external and corner loadbearing wall removals, at any floor level of the building, were considered. The initial damage accounted for the removal of the wall equal to the inter-storey height in the direction along the height of the building, and the entire wall length in the direction along the length of the building.

As shown in Figure 6-1, typical detailing for CLT platform-type construction are: STSs that connect the floors to the walls below, and angle brackets fastened with wood screws or nails that connect the floors to the walls above. Hold-down connectors help resisting uplift forces. Figure 6-1a, shows the detailing with two single span CLT panels, connected over the middle loadbearing wall by means of STSs; and Figure 6-1b illustrates the detailing for double span.

The approach considered floor and wall resistance-mechanisms separately to ensure efficient load distribution from the damaged to the undamaged parts of the building. The collapse-resistance mechanisms were identified by equilibrium of forces and moments using linear-elastic static calculations. Consistent with the EN1991-1-7 building categorisations, this procedure was limited to residential and office mid-rise CLT platform-type construction and was implemented for buildings of up to ten storeys or 30m tall, whichever is smaller, with no structural irregularities as per the National Building Code of Canada (NBCC). For taller buildings, additional considerations might be required as different detailing might be proposed to prevent excessive compression stresses perpendicular to the grain of the CLT floor panels.

To obtain realistic structural performance for disproportionate collapse prevention following extreme loadings (DoD, 2013; Ellingwood et al., 2007), the analyses accounted for nonlinear and dynamic behaviours by means of factors. Material nonlinearity is assigned to structural elements and their connections to capture ductile behaviours. Geometric nonlinearity enables to trigger large deformations associated to the possible collapse-resistance mechanisms. A factor of 0.67 was estimated to account for both nonlinearities, and therefore reduces the structural demands (Li et al., 2011; Ruth et al., 2006). Abnormal loads may trigger dynamic inertia effects, which require considerations of damping and material strain rate effects. In general, the resulting deformations are found to be up to two times higher than those obtained from linear analyses (Stevens et al., 2011). Given that the calculations only considered linear-elastic static behaviours, a nonlinear factor (NF=0.67) (Li et al., 2011; Ruth et al., 2006) and a dynamic factor (DF=2.0) (Stevens et al., 2011) were considered. The product ($NF{\times}DF$=1.34) was included in all tie-force calculated using the proposed procedure to estimates for structural integrity, following wall removal scenarios.
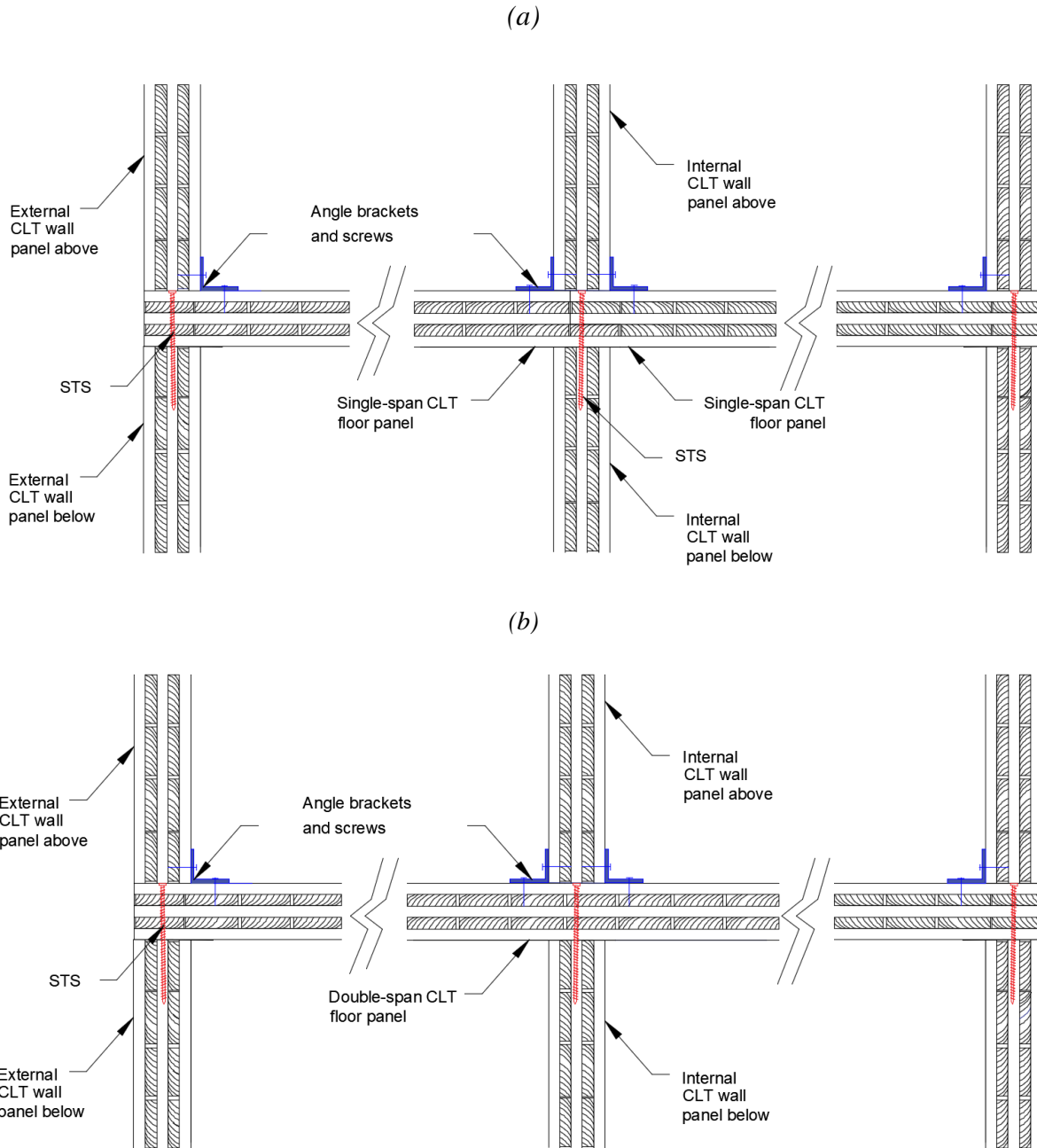
Figure 6-1: Connection detailing for platform-type CLT building: (a) Single span floor panel; and (b) Double span floor panel

The deformation and ductility supply of the connection depend on the type of connectors as well as the proposed detailing in terms of layout patterns and number of fasteners. The designer must

144

determine these parameters before applying the proposed procedure to evaluate the compatibility between the vertical and axial deformation supply and to calculate the tie forces.

6.3.2 Floor System Collapse-resistance Mechanisms: Overview

In the event that an internal or external loadbearing wall became fully damaged after an abnormal load, the floor system should carry the imposed live or snow loads in addition to its self-weight. This requirement should limit debris loads on the floors below, hence preventing collapse progression. Membrane and catenary actions are the main floor system collapse-resistance mechanisms. Herein, given that the presented procedure only considered the deformation limits, catenary action was deemed appropriate to prevent debris loading. The locations of the removed walls are illustrated in Figure 2-5b. To trigger catenary action as a collapse-resistance mechanism, F_L is assumed critical for the internal wall removal, c.f. Figure 6-2a; whereas F_T is ideal for external wall removal, c.f. Figure 6-2b. Conservatively, the contribution of the connections perpendicular to the considered direction are ignored, e.g. transverse floor-to-floor joint contributions are neglected when considering F_L, and vice-versa. The floor catenary action is a one-way system, spanning twice its original span, simply supported, and restrained in the considered direction by the adjacent panels.
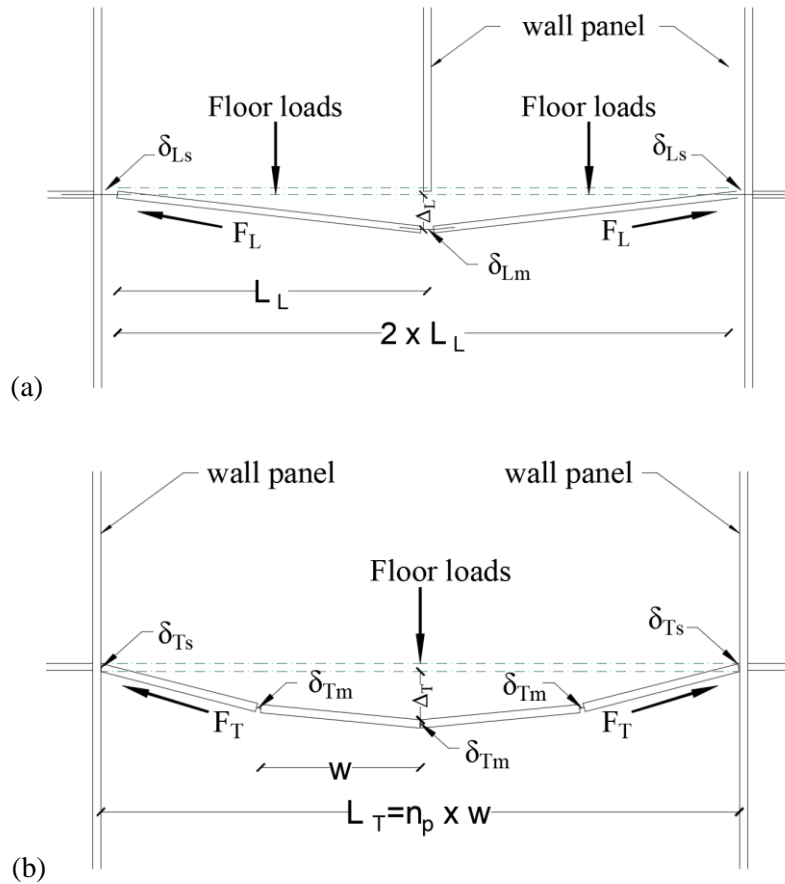
Figure 6-2: Floor system resistance mechanisms: (a) Catenary action after the loss of interior loadbearing walls; and (b) Catenary action after the loss of external loadbearing wall (as per Figure 2-5b)

6.3.3 Floor System Collapse-resistance Mechanisms: Longitudinal Catenary Action

In the longitudinal direction, the floor panels can be either two single spans with floor-to-floor connections, see Figure 6-1a, or one double span continuous over the internal wall, see Figure 6-1b. The double span CLT panel is considered as the upper bound, assuming that the maximum allowable deflection (Δ_L) is dictated by its effective bending stiffness (EI_{eff}), after internal wall removal. Using moment equilibrium, Equation (6.2), to estimate the maximum elastic capacity F_I, is derived from Figure 6-2a, given the new span ($2 \times L_L$) for continuous CLT panel:

$$F_I = \frac{w_\text{f} \times (2 \times L_I)^2}{8 \times \Delta_I}$$ (6.2)

Where $I=L$ are assumed for longitudinal and T for transverse directions, respectively. w_f is the allowable maximum floor load before CLT failure in bending or shear (governed by EI_eff) and L_L is the single longitudinal floor span. Assuming a simply supported floor system, w_f is used to estimate $\Delta_\text{L},$ the maximum elastic deflection at the location of the removed element. The deformation compatibility in Equation (6.3), obtained from the trigonometry of the catenary action, defines the total axial elongation for catenary action (δ_L) in the longitudinal direction:

$$\delta_I = 2 \times \left[L_I \times \left[\sqrt{1 + \left(\frac{\Delta_I}{L_I}\right)^2} - 1 \right] \right]$$ (6.3)

Assuming a rigid CLT panel (Canadian Standards Association, 2017), Equation (6.4) calculates δ_L in the longitudinal direction as upper bound, supplied by the deformations of the floor-to-wall connections (δ_Ls) on both sides. δ_Ls represents the individual axial yield deformation of the floor-to-wall connections as shown in Figure 6-2a:

$$\delta_\text{I} = \begin{cases} \delta_\text{Is} + \delta_\text{Is} & \text{for upper bound} \\ \delta_\text{Is} + \delta_\text{Im} + \delta_\text{Is} & \text{for lower bound} \end{cases}$$ (6.4)

The lower bound, see Figure 6-1a, is the case with two single span (L_L) CLT panels in the longitudinal direction, connected over the middle support. Equation (6.2) is still applicable, with the double span $2 \times L_\text{L}$ for catenary action. However, the deformation compatibility is affected by the presence of an additional connection at mid-span (δ_Lm); Δ_L is dictated by the axial yield deformation of δ_Lm rather than EI_eff. The deformation δ_L for catenary action in Equation (6.3) is

supplied by two floor-to-wall ($2 \times \delta_{Ls}$) and one floor-to-floor connection (δ_{Lm}), as given in Equation (6.4) for the lower bound. This procedure shows that increasing δ_L through multiple floor-to-floor connection, a larger Δ_L can be obtained and the F_L demands on the floor system can be reduced.

6.3.4 Floor System Collapse-resistance Mechanisms: Transverse Catenary Action

For the case of external loadbearing removal, with the absence of adjacent floor bay in the longitudinal direction, the floor system would have to cantilever to prevent debris loading. With 5m as minimum typical span, this approach is unpractical for CLT floor systems. The first solution is to provide a vertical support, with a connection detailing that allow the floor system to hang on the external wall. Alternatively, the existing floor-to-floor connection in the transverse direction can be used to trigger catenary action in that direction. As shown in Figure 6-2b, the span in the transverse direction (L_T) depends on the width (w) of individual CLT panel and the number of panels (n_p).

Therefore, Equation (6.2), with $I=T$, is still applicable to determine F_T; however, the distance between the outermost supports is now L_T. The individual segments, limited by the CLT panel width (w), decrease the magnitude of F_T compared to F_L. Equation (6.3) is also used to define the deformation compatibilities in the transverse direction. The total axial deformation in the transverse direction (δ_T) is supplied by all existing floor-to-floor joints (δ_{Tm}), depending on n_p, and the two floor-to-wall joints (δ_{Ts}). Given the multiple connections, with Equation (6.4), large Δ_T is obtained; which consequently decreases F_T.

6.3.5 Overview Wall System Collapse-resistance Mechanisms

After the loss of a loadbearing wall, the floor system prevents debris loading on the floor below by means of catenary action. However, for the floor levels above the damage, wall system collapse-resistance mechanisms are required to prevent collapse progression. The locations of the walls to be removed are illustrated in Figure 2-5b. As shown in Figure 6-3a, cantilever action is triggered for corner wall removal, at any storey level (n). The weight of the 'new' cantilever (W_{f1}) above the removed element applies a moment (M_A) about point C. The force-couple of the tie-force (F) at the roof, and the compressive force (C) at the root of the cantilever, resist M_A. The rotation of the cantilever due to gravity creates a horizontal shear force (S_h) between the adjacent storeys, and a vertical shear force (S_v) between the cantilever and the adjacent support bays or section where the axial forces are transferred. As this procedure assumes that the transverse ties (T) transfer the loads after external wall removal, at every level, the ties shall also be sized to resist F or F_T, whichever is greater.
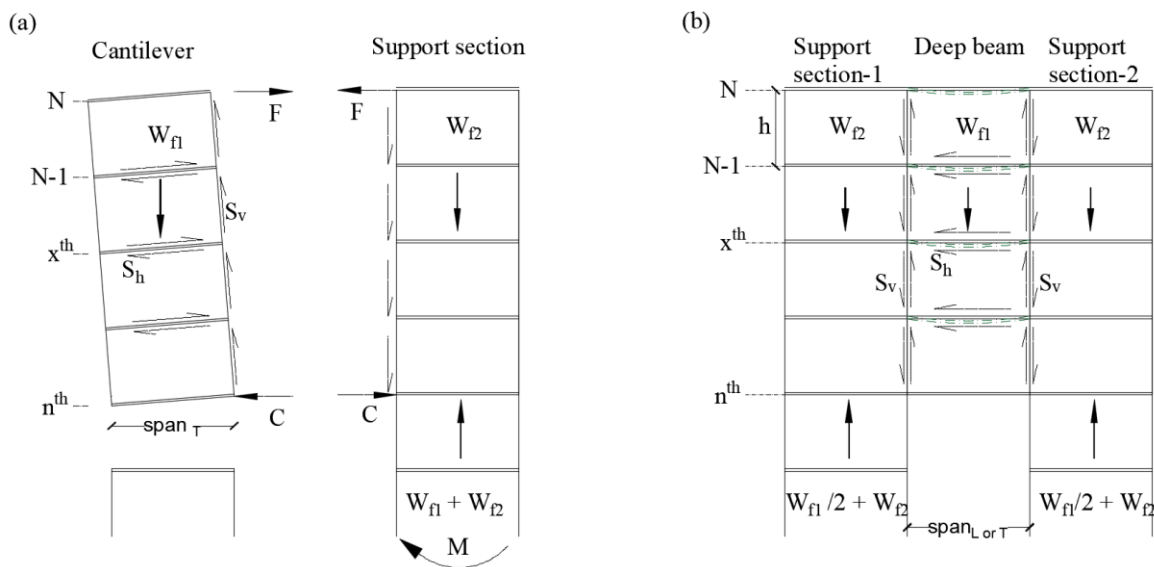
Figure 6-3: Wall system resistance mechanisms: (a) Cantilever action; (b) Beam action

Figure 6-3b shows that for any other wall removal scenario, but corner walls, beam action is the ideal collapse-resistance mechanism given the existence of bays on either side to provide vertical supports. Then, the CLT panel' in-plane bending stiffness enables the walls to act as deep beams, subject to adequate resistance against horizontal shear between consecutive panels. The forces (S_h and S_v) required to trigger beam action as a collapse-resistance mechanism are identical to those determined for the cantilever action. However, when compared to beam action, the cantilever collapse-resistance mechanism only has one support to resist M_A. Given that buildings are always designed for worst-case scenarios, the forces from the cantilever action are dominant, hence dictate the design and were considered for the subsequent analyses (Schultz et al., 1977a, 1977b).

6.3.6 Transverse Tie-force and Horizontal Shear Mechanisms

The analytical formulations of the cantilever action for CLT platform-type construction, similar to precast reinforced concrete walls (Schultz et al., 1977b, 1977a), are derived from the free body diagram shown in Figure 6-3a. Herein, the procedure assumes: i) the cantilever is rigid and rotates at C, ii) the whole cantilever exhibits monolithic behaviour with no shear slip between consecutive storeys, iii) the opening of the vertical joint between the cantilever and the support section is linear and triangular from C to the roof (highest), iv) the whole cantilever is laterally restrained by the rest of the building at every storey, and v) the transverse tie forces (T) are carried by F at the roof level, distributed at every level as F_x, and zero at C. Equation (6.5) gives the applied moments (M_A) induced by the rotation of the cantilever, and Equation (6.6) the corresponding resisting moment (MR):

$$M_A = w_s \times (N - n) \times \frac{L_T^2}{2} \tag{6.5}$$

$$MR = \sum_{i=n}^{N} \left[F_r \times \frac{N-i}{N-n} \right] \times [h \times (N-i)] \qquad (6.6)$$

Where w_s is the single storey weight, (N) the number of storeys, (n) the storey level of the removed

loadbearing wall, (i) is the building level and (h) the individual inter-storey height.

Equation (6.7) gives the maximum transverse tie-force (F_r), acting at the top of the cantilever

(roof); the tie forces (F_x) at a storey-x within the cantilever are calculated using Equation (6.8).

The horizontal shear between consecutive storey (S_h) is calculated using Equation (6.9). With a

monolithic behaviour assumed for the entire cantilever, the lowest S_h is at the roof of the cantilever.

Equation (6.9) is used to estimate S_{hx} at every storey-x between the level above the removed wall

($n+1$) and the roof (N). Therefore, the biggest S_h is at the level immediately above the point C, with

its magnitude equalled to the compressive force C.

$$F_r = \frac{(N-n)^2 \times w_s \times L_T^2}{2 \times h \times \sum_{i=n}^{N}(N-i)^2} \qquad (6.7)$$

$$F_x = F_r \times \frac{x-n-1}{N-n} \qquad (6.8)$$

$$S_{hx} = \sum_{i=x}^{N} F_r \times \frac{i-n}{N-n} \qquad (6.9)$$

It is worth mentioning that the removal of a corner loadbearing wall can occur at any level within

the building height. In other words, the total number of storeys within the triggered cantilever

action (N-n), referred to as the size of the cantilever, depends on the location of the wall removal

(n). With M_A and MR depending on the size of the cantilever, Equations (6.8) and (6.9) are used

to determine F_x and S_{hx}, respectively, for every level; and the same calculations need to be

performed for every removal case. This research considers CLT platform-type construction of up to ten storeys, therefore the approach assumes nine different wall removal scenarios, e.g. from level-1 to level-9 for a ten-storey building. Consequently, the required values of F_x and S_{hx} are the maximum values obtained considering all nine removal scenarios.

Equations (6.8) and (6.9) can be rearranged in Equations (6.10) and (6.11) and further simplified by replacing the terms within the brackets with α_x and β_x leading to Equations (6.12) and (6.13), respectively:

$$F_x = \left(\frac{(N-n)^2}{\sum_{i=n}^{N}(N-i)^2} \right) \times \frac{w_s \times L_T^2}{2 \times h} \tag{5.10}$$

$$S_{hx} = \left(\frac{\sum_{i=x}^{N}(i-N)}{\sum_{i=n}^{N}(N-i)^2} \times (N-n) \right) \times \frac{w_s \times L_T^2}{2 \times h} \tag{5.11}$$

$$F_x = \alpha_x \times \frac{w_s \times L_T^2}{2 \times h} \tag{5.12}$$

$$S_{hx} = \beta_x \times \frac{w_s \times L_T^2}{2 \times h} \tag{5.13}$$

The parameters α_x- and β_x-values are computed for all considered removal scenarios; and their respective maximum are used to calculate F_x and S_{hx}. To avoid these calculations, Figure 6-4a and b illustrates the maxima α_x and β_x values, respectively, for all possible cantilever sizes that can be created after wall removal at any level, for buildings up to ten storeys. In Figure 6-4a for a building with a given number of storeys, the α_x-value can be obtained for the ith level $(N-i)$ of the cantilever from the roof (N). The number of storeys does not directly influence β_x; therefore, these values are a direct function of the cantilever size as shown in Figure 6-4b.
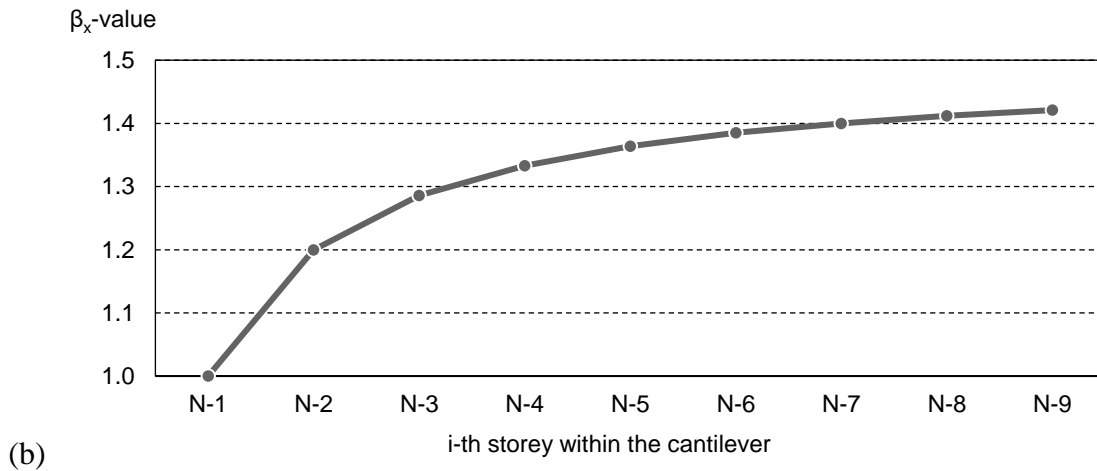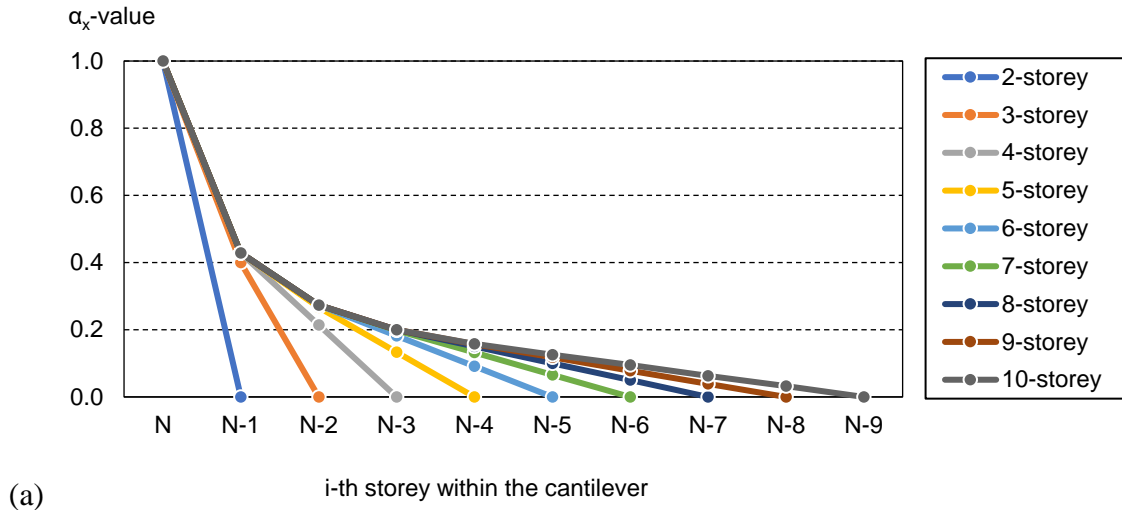
Figure 6-4: transverse tie forces at any storey for any cantilever size: (a) α_x-values; and (b) β_x-values

6.3.7 Vertical Tie-force and Vertical Shear Mechanisms

The minimum vertical tie-force (F_v), given in Equation (6.14), allows to vertically tie the wall panels between consecutive storeys, making them continuous along the height of the cantilever, for monolithic behaviour. F_v are vertical tensile forces, assumed to remain constant throughout the height provided that w_s and h are constant. F_v are designed to carry forces equal to the storey vertical loads, calculated using tributary area. As shown in Figure 6-5a, at every level, the vertical ties (V), representing the connection between two wall panels, resist S_{hx} horizontally, which varies depending on the storey level, and F_v vertically, which assumed constant throughout the height.

Both S_{hx} and F_v are important to foster monolithic behaviour of the cantilever. Equation (6.15) gives the vertical shear between the cantilever and the adjacent bays (S_v), acting as the support section receiving the tie forces. Equation (6.16) enables to estimate the size of the opening (δ_x) between the cantilever and the support section, at every level.

$$F_v = w_s \tag{6.14}$$

$$S_v = w_f \times L_T \tag{6.15}$$

$$\delta_x = \frac{x - 1}{N - 1} \times \delta_N \tag{6.16}$$

As shown in Figure 6-3a, S_v prevents downward vertical separation between the cantilever and the support section. At every floor, to carry the vertical shear created at each level, S_v remains constant throughout the height of the cantilever, assuming w_s is constant. S_v is resisted by the shear capacity of the transverse ties (F_x) at every level. Furthermore, as shown in Figure 6-5b, the opening of the vertical joint between the cantilever and the support depends on the allowable axial deformations of the transverse ties (T). With F_T assumed linear, the axial deformation is also linear, increasing triangularly from C to the top of the cantilever. The maximum horizontal deformation (δ_N) occurs for F_r at the roof level, regardless of cantilever size and number of storeys. Therefore, δ_x is the interpolated value within the distribution, at every level-x. Nonetheless, the design shall ensure that the cantilever action is compatible with the deformations required for catenary action of the floor system in the transverse direction.
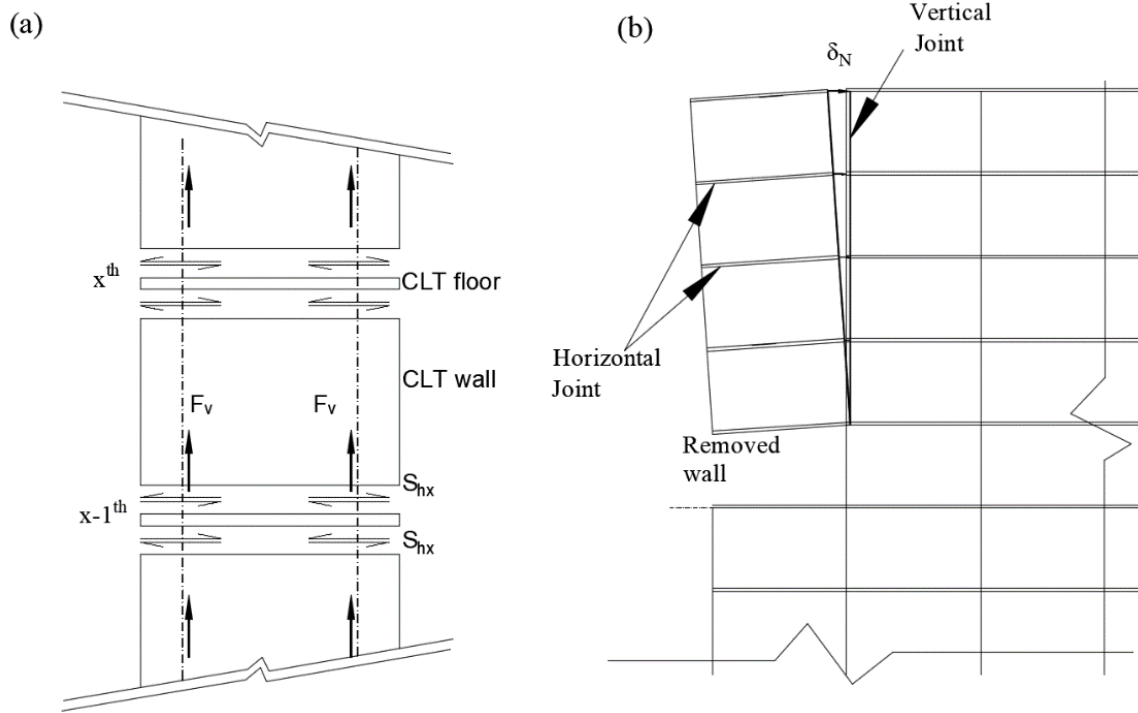
Figure 6-5: (a) Shear and tensile forces acting at the storey joints; and (b) Strain at the vertical joint

6.4 Case-study Building

6.4.1 Description

The case-study residential building was an eight-storey platform-type CLT building. The floor plan and isometric views are shown in Figure 6-6a and b, respectively. The wall gridline was 5.0×5.0m ($L_L=L_T$) and the inter-storey height (h) 3.5m. Both gravity and lateral load-resisting systems were composed of 5-ply CLT panels, with the floors directly resting on the walls. All panels were E1M5-stress grade (Structurlam, 2016) in compliance with ANSI PRG 320-2018 (American National Standards Institutes, 2018); the boards in the longitudinal and transverse directions were MSR 2100 1.8E Spruce-Pine-Fir (SPF) and SPF #3 lumber, respectively. The panels were 2.5m wide, the individual layers were 35mm thick. Under gravity loading, the CLT floor was designed as simply supported one-way system. In the longitudinal direction, the floor

155

panels were double span, continuous over the internal support, and assumed to be connected above the wall on gridline-7 using floor-to-floor joints. Due to width limitations, two CLT panels were placed between the walls in the transverse direction, connected using transverse joints. Coupled shearwalls were used as platform for the next level. In the transverse direction, 5m long simply supported GLT beams provided vertical supports for CLT floor panels in the absence of walls.

The connection detailing was as shown in Figure 6-1: i) lap joint STSs for both longitudinal and transverse floor-to-floor connection, ii) STSs for the connection floor-to-wall below, and iii) angle brackets with nails for the connection floor-to-wall above. The lap joints were composed of 8mm diameter and 90mm long, partially threaded ASSY™ Ecofast STSs (ETA-11/0190, 2011), inserted at 90deg. to the joint to obtain a moderately ductile connection. As per CSA-O86, these are connections governed by yielding failure modes with ductility ratio of at least 3.0. Experimental testing (Hossain et al., 2018, 2016) of these connections in 5-ply CLT, loaded in shear under monotonic loading, gave an average yield deformation of 6mm. The angle brackets were Simpson Strong-Tie® (Simpson Strong-Tie, 2017) AE116-R with 3.8mm diameter and 60mm long ring-shank nails. When tested in shear, these connectors have a yield deformation of 6mm (Schneider et al., 2015). In this study, the axial deformations of the angle brackets and the STSs were considered equal to their shear deformations. Hold-down connectors were provided to transfer seismic uplift forces between consecutive storeys.

To estimate the required tie-force for minimum structural integrity, hence disproportionate collapse prevention, the analyses considered removal of: i) internal wall 4/A-B, ii) internal wall 7/A-B, iii) external GLT beam 1/B-C, and iv) corner walls 1/A-B and 1-4/A simultaneously. These

removal scenarios were considered as worst cases, resulting to highest tie forces to trigger longitudinal catenary, transverse catenary, and cantilever action, respectively.
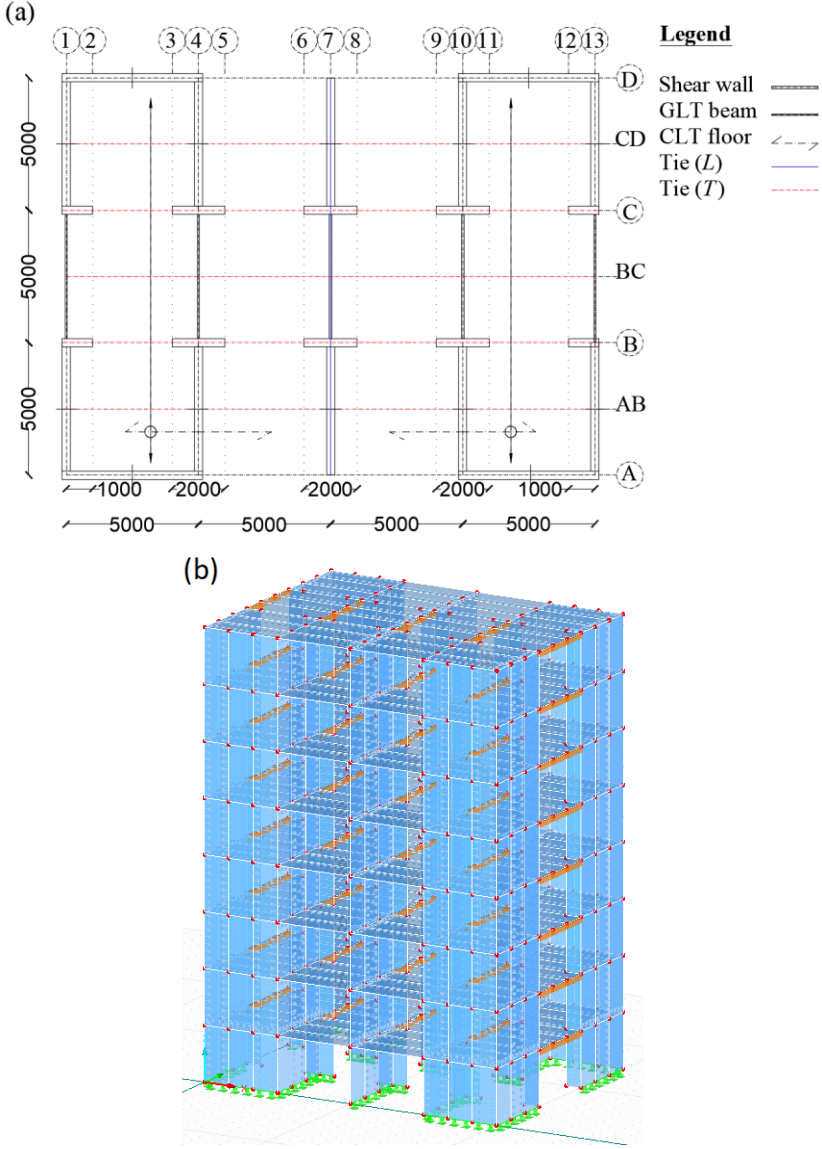
Figure 6-6: (a) Building floor plan; and (b) Isometric view of the building

6.4.2 Gravity and Lateral Designs

The building was of normal importance, for a location in Vancouver (Canada); and designed according to NBCC-2015 and CSA-O86-2014. The *LL*, *SL*, and *SID* loads were 1.9kPa, 1.8kPa, and 1.0kPa, respectively. The *DL* accounted for both *SID* and the self-weight of wood elements, assumed as 4.2kN/m^3. *EI*$_{eff}$ of the CLT panels in the major axis was 4.4×10^{3}kNm^2 per meter width. The bending moment (*MBM*$_R$) and shear force (*MSF*$_R$) resistances of the CLT panels were 94kNm and 52kN, respectively. Under gravity loads, for ultimate limit state design, the utilisation of the continuous CLT floor panels was 17%, 60%, and 17% for bending, shear, and compression, respectively. For the serviceability limit state design, the utilisation was 82% and 91% for deflection and vibration, respectively. For the GLT beams in the transverse direction, a cross-section of 215mm×304mm Douglas Fir-Larch 24f-EX was required for utilisation of 80% for both bending and shear, and 21% for deflection.

The equivalent static force procedure from the NBCC was followed to perform the seismic design of the building, using the Vancouver design spectrum. The selection of dissipative and non-dissipative connections was done according to the CSA-O86 capacity-based design approach (Canadian Standards Association, 2017). The dissipative connections (wall-to-floor panel below, vertical joints between the wall panels, and hold-downs) possessed sufficient deformation capacity to allow for rocking mechanism. The seismic forces were calculated using ductility and overstrength factors of 2.0 and 1.5, respectively (Canadian Standards Association, 2017; Pei et al., 2013). The fundamental period of the building was computed as 0.6*sec*, using the empirical formula provided in the NBCC (NBCC, 2015). The corresponding base-shear, in both directions, was 1,363kN. The building was torsionally insensitive, with the CLT floors assumed to act as rigid diaphragm.

The deflections of the CLT shearwalls were calculated assuming a rocking mechanism, for both coupled-panel and single-panel kinematic modes with additional gravity floor loads (Canadian Wood Council, 2017; Casagrande et al., 2018). The inter-storey drifts were below the NBCC limits of 2.5%, with the top storey lateral deformation of 181mm (0.64%) and 159mm (0.57%) in the longitudinal and transverse directions, respectively. Table 6-1 lists the inter-storey horizontal ($EQ_{H,sh}$) and vertical ($EQ_{V,sh}$) shears, and hold-down forces (EQ_{Hd}) for corner shearwalls 1/A-B and 1-4/A, obtained from seismic analysis (EQ), resisted at every level, and compares them against the vertical and horizontal shears required for cantilever action.

Table 6-1: Seismic (EQ) loads and tie forces (TF)

Storey level	Wall 1/A-B					
	Horizontal shear		Vertical shear		Vertical tie	
	EQ	TF	EQ	TF	EQ	TF
	$EQ_{H,sh}$ (kN/m)	S_{hx} (kN/m)	$EQ_{V,sh}$ (kN/m)	S_v (kN/m)	EQ_{Hd} (kN)	F_v (kN)
1	38.2	53.6	38.2	77	117	268
2	37.1	53.0	37.1	77	113	268
3	35.1	52.2	35.1	77	106	268
4	32.1	51.0	32.1	77	96	268
5	28.0	49.2	28.0	77	81	268
6	22.9	45.9	22.9	77	64	268
7	16.8	38.3	16.8	77	42	268
8	9.6	0	9.6	77	20.2	268

Table 6-2 gives the diaphragm shear forces at 7/A-B, resisted by longitudinal (EQ_L) STSs floor-to-floor joints; as well as at gridline AB, resisted by the transverse (EQ_T) STSs floor-to-floor joints and compares them against tie-force, horizontal and vertical shears, required to trigger catenary and cantilever actions after the specified internal, external and corner wall removals.

NBCC extreme load-combination, also given in Equation (2.2), was used for disproportionate collapse investigation. The highest floor loads (w_f) was below the roof, calculated as 2.7kN per meter width; this was used to estimate the tie-force for catenary action. For cantilever action, the weight of the storey (w_s) was 16kN/m along the transverse direction of the building, accounting for both floor and walls loads.

Table 6-2: Seismic (EQ) loads and tie forces (TF)

Storey level	Longitudinal				Transverse			
	Wall 4/A-B		Wall 7/A-B		A-B	Line-B	A-B	A-B
	EQ_L (kN/m)	F_L (kN/m)	EQ_L (kN/m)	F_L (kN/m)	EQ_T (kN/m)	EQ_T (kN/m)	F_T (kN/m)	F_x (kN/m)
1	32.7	202	27.3	148	11.2	16.8	54	0
2	31.8	202	26.5	148	10.9	16.4	54	0.8
3	30.1	202	25.0	148	10.2	15.5	54	1.5
4	27.5	202	22.9	148	9.4	14.1	54	2.3
5	24.0	202	20.0	148	8.2	12.3	54	3.1
6	19.6	202	16.3	148	6.7	10.1	54	4.2
7	14.4	202	12.0	148	4.9	7.4	54	6.6
8	8.3	163	6.9	109	2.8	4.2	40	15.3

6.4.3 Tie-Force Design: Catenary Action after Wall 4/A-B Removal

After internal wall 4/A-B removal, the CLT floor was 10m, assumed simply supported on the outer walls (1-AB and 7-AB). The maximum allowable load on the CLT floor panel ($w_{f,max}$) was 7.5kN/m, corresponding to the maximum moment and shear force resistances estimated using EI_{eff}. The maximum allowable mid-span deflection (Δ_L) of a simply supported CLT panels, calculated using $w_{f,max}$, was 223mm, representing 4.5% of L_L. Since EI_{eff} dictated failure of CLT panels under bending, the required longitudinal tie forces (F_L) for the continuous CLT floor panel, after wall 4/A-B removal, could be calculated using Equation (6.2). Nevertheless, Equation (6.2) was

rewritten as Equation (6.17) to consider both dynamic (DF) and nonlinear (NF) factors, with $\Delta_L =$ 0.045L_L; giving $F_L = 201$kN. The corresponding δ_L, calculated using Equation (6.3), was 10mm. Therefore, for compatibility between Δ_L and δ_L, 5mm was the required minimum axial deformations (δ_{Ls}) at each support.

$$F_L = 15 \times w_f \times L_L = 201\text{kN} \tag{6.17}$$

6.4.4 Tie-Force Design: Catenary Action after Wall 7/A-B Removal

After internal wall 7/A-B removal, the new CLT floor span was 10m, assumed simply supported on the outer walls (4-AB and 10-AB). For this removal scenario, the presence of longitudinal floor-to-floor joint affected δ_L. With axial deformation of STSs as well as the angle brackets and nails all assumed 6mm, $\delta_L = \delta_{Ls} + \delta_{Lm} + \delta_{Ls} = 18$mm. With the compatibility between Δ_L and δ_L, calculated using Equation (6.3), Δ_L was 300mm, representing 6% of L_L. Rewriting Equation (6.2), to account for DF and NF, F_L=148kN using Equation (6.18).

$$F_L = 11 \times w_f \times L_L = 148\text{kN} \tag{6.18}$$

6.4.5 Tie-Force Design: Catenary Action after GLT beam 1/B-C Removal

To calculate the required tie forces for catenary action in the transverse direction, removal of GLT beam 1/B-C was considered. After element loss, the CLT floor system spanned $L_T = 2 \times w$, simply supported on outer wall support (1/B and 1/C), with $w = 2.5$m. With the presence of floor-to-floor joint, $\delta_T = 18$mm; $\Delta_T = 212$mm was calculated using Equation (6.3) to account for compatibility between Δ_T and δ_T. This deflection represented 8.5% of w. To account for DF and NF, Equation (6.2) was rearranged to Equation (6.19), giving $F_T = 54$kN.

$$F_T = 8 \times w_f \times w = 54\text{kN} \tag{6.19}$$

6.4.6 Tie-Force Design: Cantilever Action after Wall 1/A-B and 1-4/A Removals

To estimate the required tie forces for cantilever action, corner walls 1/A-B and 1-4/A were simultaneously removed. Table 6-3 lists the α_x- and β_x-values (obtained from Figure 6-4a and b, respectively) along with the corresponding F_x and S_{hx} required at every level. F_x and S_{hx} were calculated using Equation (6.12) and Equation (6.13), respectively, multiplied by NF and DF to account for nonlinear dynamic behaviours. F_x was distributed along the transverse floor-to-floor connections of the floor system, whereas S_{hx} was distributed along the length of the wall between consecutive storeys. The elongation of transverse ties at the top storey (δ_N), supplied by one transverse floor-to-floor and one floor-to-wall connections, was $\delta_{Ts} + \delta_{Tm} = 12\text{mm}$. With a triangular distribution, the values of δ_x, given in Table 6-3 for every storey-x, were calculated using Equation (6.16). At each level, the vertical ties ($F_v = 268\text{kN}$) and the vertical shears ($S_v = 268\text{kN}$) were calculated using Equation (6.14) and Equation (6.15), respectively, multiplied by NF and ND. F_v was with respect to the length of the wall, whereas S_v was distributed along the height of the wall.

Table 6-3: Transverse ties and horizontal shear forces

Floor level	Transverse tie			Horizontal shear	
	α	F_x (kN)	δx (mm)	β_x	S_{hx} (kN)
1	0.00	0.0	0.0	1.40	268
2	0.05	3.8	1.7	1.39	265
3	0.10	7.7	3.4	1.36	261
4	0.15	11.5	5.1	1.33	255
5	0.20	15.3	6.9	1.29	246
6	0.27	20.9	8.6	1.20	229
7	0.43	32.8	10.3	1.00	191
8	1.00	76.6	12.0	0.00	0

162

6.5 Discussion

6.5.1 Catenary Action

The proposed approach demonstrated the importance of the compatibility between the axial deformation (δ) and the vertical deflection (Δ). Increasing δ, increased Δ, resulting to a reduction in tie-force demands at the connections. From the results of the considered case-study building, double span continuous floor system showed a tie-force increase of 40% as compared to the single span discontinuous systems with floor-to-floor joints. Therefore, floor systems allowing large δ, through additional floor-to-floor connections or ductile floor-to-wall connections, or a combination of both, were superior compared to continuous floor panels, with the performance of the latter dictated by the bending or shear capacity. Given that UFC 4-023-03 and EN1991-1-7 overestimate Δ, the minimum prescribed horizontal tie-forces of 60kN/m from Equation (6.1) were insufficient to trigger catenary action in CLT floor systems. Furthermore, the tie-force requirements for catenary action in the transverse and longitudinal direction should be considered separately, giving the spans after element removal. For the case-study building, F_L was at least 2.5 times higher than F_T. Herein, the obtained magnitude was in the same range as the existing code (CEN, 2006a) and guideline (DoD, 2013).

The floor-to-floor joints should be detailed for both tie forces, parallel to the considered direction as axial loads, and the seismic loads along the perpendicular direction as shear loads. Assuming equal axial and shear connection stiffness, in Table 6-2 the tie forces (F_L and F_T) and seismic loads (EQ_L and EQ_T) were compared for the considered case-study building. In the longitudinal direction, F_L was at least six or four times higher than EQ_L, for continuous and discontinuous floor panels, respectively. In the transverse direction, F_T was at least three times higher than EQ_T. The

results showed that additional detailing considerations were required to trigger catenary action in both directions, hence prevent disproportionate collapse. Herein, the design should separate the seismic and tie-force detailing, with additional floor-to-floor connection to carry the axial forces only. If double or triple floor panels were used, panel reinforcement, e.g. using STSs in withdrawal, at the location of high bending moments would be required. Nevertheless, it is worth mentioning that this approach increased the bending resistance rather than the maximum allowable axial deformation of the connections.

6.5.2 Cantilever Action

In Table 6-2, F_x at every level, required to trigger cantilever action, and F_T for catenary action in the transverse direction, were compared against EQ_T for diaphragm action against seismic loads. It can be seen that F_T, required to prevent debris loads on the floors below following external support removal, dictated the design. With the assumed deformations of the floor-to-floor connection for the considered case-study building, F_T was at least three times higher than EQ_T at the joints; which was also sufficient to tie the floor panels at every level for possible cantilever action after corner wall removal ($F_T > F_x$). The worst-case scenario for opening between the cantilever and the support section (δ_x) was obtained after ground-floor corner wall removal. The deformation compatibility for F_T was identical for all level, hence dictated the design when compared to δ_x. These observations showed that floor-to-floor joints should be able to carry tensile forces, to act as a tie for catenary action, and compression forces, to transfer the diaphragm forces. Additional detailing considerations would be required for the former, whereas STSs lap joint could still be used for the latter.

S_{hx} fostered monolithic behaviour between successive storey of the cantilever, therefore should be available at both the bottom, carried by the angle brackets, and the top of the storey high wall, carried by the STSs. Table 6-1 compared S_{hx} against $EQ_{H,sh}$ obtained from the seismic analysis, for the case-study building. Except at the top floor where only seismic forces were applicable, the design of the inter-storey horizontal shear was dictated by S_{hx}. S_{hx} were up to twice stronger than $EQ_{H,sh}$, with the magnitude of both forces cumulating from top to bottom storey. Herein, with additional brackets and STSs, this detailing can meet the requirements for both $EQ_{H,sh}$ and S_{hx}.

The vertical ties (F_v), required between consecutive storeys, were compared against the hold-down forces (EQ_{Hd}) from seismic analysis. Hold-down connectors, provided at both ends of the wall panels, were used to transfer F_V. Angle brackets might also be used to improve the axial capacity in order to meet high vertical tie-force demands. The in-plane tension strength of the CLT panels should be used to avoid continuous vertical ties from the lower to the uppermost floor. S_v supplied by the vertical wall-to-wall joints between the cantilever and the support section were at least twice $EQ_{V,sh}$ from seismic design, as shown in Table 6-1. With additional STSs at every level, the same detailing used for seismic loads, $EQ_{V,sh}$, could also be used for cantilever action, S_v.

6.6 Summary

This chapter presented an improved tie-force procedure based on linear-elastic principles of engineering mechanics for disproportionate collapse prevention of mass-timber building with platform-type construction. This method best-apply to residential and office mid-rise building, up to ten storeys or 30m tall, with no structural irregularities. The procedure considered internal, external and corner loadbearing walls removals at any floor level as worst-case scenarios. This chapter can be summarised as follows:

(1) For mass-timber buildings with platform-type construction, the tie-force requirements shall consider catenary action of the floors in longitudinal and transverse directions, as well as the cantilever action of walls, as separate collapse-resistance mechanisms.

(2) Tie-force requirements shall account for the compatibility between the floor panel's deflection and the connection's axial deformation. For catenary action, the existence of joints reduced the tie-force demands. Consequently, this method requires the designer to have data of the deformation supply of the proposed connection detailing.

(3) From analysis of an eight-storey CLT platform-type construction, additional considerations are required for the floor-to-floor joints given the axial demands for catenary action. The deformation demands for cantilever action can be supplied by conventional detailing. Nevertheless, additional considerations shall be given with respect to the strength demands as tie forces are found to be up to three times higher than the seismic demands. If conventional connection detailing becomes uneconomic and unpractical, novel detailing might have to be applied to provide cantilever action.

(4) This study emphasises on the need to address novel connection detailing with adequate strength, stiffness and ductility required to trigger catenary action for disproportionate collapse prevention.

Chapter 7: Novel Connection Detailing for Structural Robustness[5]

7.1 Introduction

Ensuring structural robustness is described as the best-suited approach for disproportionate collapse prevention (Ellingwood et al., 2007; IStructE, 2010). A robust building reduces $P[DC]$ by developing new equilibrium states, which consequently reduces $P[F/DH_i]$ in the event that $P[D/H_i]$ and $P[H_i]$ certainly occurred. In other words, this structural property enables the building to bridge over the initial damage from abnormal load and distribute the loads from the damaged to the undamaged parts of the building.

With the structural performance of mass-timber buildings mainly affected by the joints between the different loadbearing components, structural detailing must ensure adequate strength, stiffness, and ductility. Previous chapters demonstrated the need for novel connection detailing to enable mass-timber buildings to develop collapse-resistance mechanisms against disproportionate collapse. Given its performance steel tubes detailing, initially proposed as hold-down connector (Schneider, 2015; Schneider et al., 2018), would be investigated to further its application as horizontal or vertical tie to enhance structural robustness.

7.2 Objectives

The primary objective of this study was to optimise the geometry and material of the steel tube connector to achieve higher target yield force ($F_{y,t}$). In addition, all deformations should occur in the steel components, while stresses in the mass-timber should remain within the elastic range. The secondary objectives, contingent to the first, were: i) to understand the influence of the main parameters towards achieving an optimum detailing; ii) to evaluate the robustness of the optimised steel tube connection in presence of uncertainties associated with the geometry of the model and the material properties; and iii) propose new connection detailing with steel tubes to enhance collapse-resistance mechanisms for structural robustness.

7.3 Steel Tube Connector Description

Preliminary experimental investigations (Schneider, 2015; Schneider et al., 2018) demonstrate high strength, stiffness, and ductility of steel tube connectors (see Figure 7-1a) when used as detailing for CLT shear walls to carry large uplift forces. A circular hollow steel section (CHSS), herein referred to as steel tube, is the main component of the connection, see Figure 7-1b. The detailing is simple; the CHSS is placed inside the CLT panel into a hole of the same diameter. The components are easy to install, inspect, and potentially replace. Figure 7-1b illustrates the hold-down's main parameters: i) tube diameter *(d_t)*; ii) tube thickness *(t)*; iii) diameter of the weld-coupler area *(c)*; iv) the loaded end-distance, measured from the centre of the tube to the edge of the CLT panel *(a_L)*; and v) the steel rod diameter *(d_r)*. This detailing was essentially composed of off-the-shelf components and was therefore deemed to have negligible impact on the total cost of the project.

Schneider et al. (2018) tested the CHSS in a 3-ply CLT panel, with 35-35-35mm thick layers. A coupler area of 40mm diameter was welded at the centre of the inside of a 3.0mm thick steel tube, to enable connecting a steel rod. The circular shape allowed for a uniform distribution of forces along its circumference; and the hollow cross-section permitted large deformations, hence significant energy dissipation and ductility. In the vertical direction, the hold-down forces caused compression parallel to the grain, of the first and third CLT layers, and compression perpendicular to the grain of the second layer. The connector's loaded end-distance (a_L) was 2.5 times the tube diameter to avoid brittle wood failure.
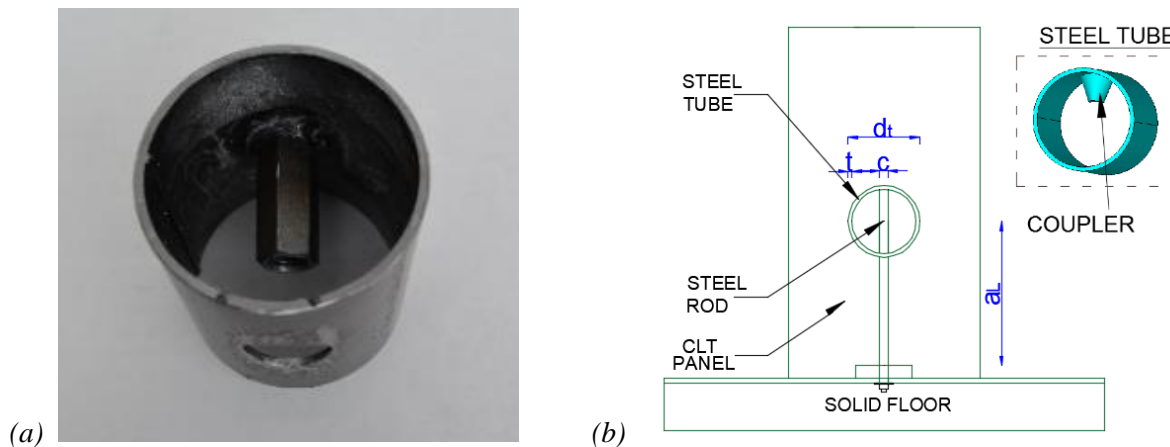
Figure 7-1: (a) Steel tube connector photo (Photo credit Mpidi Bita); and (b) Schematic representation of steel tube detailing

The tubes' performances under quasi static monotonic and cyclic loadings were evaluated with d_t as the only variable. Three different diameters were used: 50.8mm, 76.2mm and 101.6mm; herein these configurations are labelled $Tube_1$, $Tube_2$ and $Tube_3$, respectively. All connections behaved in a ductile manner with no wood failure; and all deformations occurred in the tube, specifically around the area where the coupler was welded to the tube. $Tube_2$ exhibited the best post-yield performance, reached a ductility ratio (μ) of 10, with 1,150kNm as total energy dissipated (U), a

yield force (F_y) of 41kN, an elastic stiffness (k_e) of 15kN/mm, and load-carrying capacity (F_u) of 49kN. These preceding experimental tests showed that the CHSS could be a good option to enhance the performance of mass-timber detailing for disproportionate collapse prevention. Given the observed results, optimisation of the steel tube was required to improve its performance and achieve higher strength, stiffness, and ductility required for horizontal and vertical ties.

7.4 Finite Element Analyses

7.4.1 Overview

Finite Element Analyses (FEA) were conducted using the commercial software package ANSYS to capture material, geometric, and contact nonlinearities. Multiplas (Dynardo, 2016), an ANSYS add-on that applied Grosse's theory (Gross, 2005) to implement orthotropic-boxed values material models, allowed capturing the post yielding behaviour of wood. Multiplas accounts for the interaction of the material strength, elastic stiffness, as well as post yielding behaviour under compression, tension, and shear loadings, in all three orthogonal directions.

The first step was to develop and validate a FE material model to account for the elastic and plastic behaviours of CLT and steel. The second step was to develop a model of Tube$_2$ connection, as this size exhibited the most favourable performance in terms of post-yielding deformations. The FE model was calibrated to capture Tube$_2$'s behaviours in terms of F_y, k_e, F_u, $U,$ and μ. Thereafter, the model was verified by comparing its predictions against the test results for Tube$_1$ and Tube$_3$, only changing the tube diameter. All material properties, as well as boundary conditions, were maintained as defined for Tube$_2$. The third step was to perform a sensitivity analysis using OptiSlang to establish the correlation between input and output parameters. Using the results of the sensitivity analysis, the fourth step was a parameter optimisation to achieve the stated research

objective. In the fifth and last step, a robustness analysis was conducted to evaluate the performance of the optimised connection with respect to uncertainties encountered in the material properties (CLT and steel) and the connection geometry.

7.4.2 CLT Models

The three-dimensional (3D) FE model of the CLT block was developed using parameters of the Multiplas wood material law #33 (Dynardo, 2016). The inputs of the wood elastic properties, for both longitudinal and transverse layers of the CLT, were obtained from CSA-O86 and the wood handbook (Forest Products Laboratory, 2010), corresponding to stress grade E_1. Table 7-1 summarises these elastic parameters: Young's moduli *(E)*, Shear moduli *(G)*, and Poisson ratio *(ν)*, for the longitudinal *(L)* and transverse *(T)* directions of timber. The parameters for the uniaxial compressive strength in the longitudinal and transverse directions, f_L and f_T respectively, as well as the plastic behaviours were determined from testing wood specimens (100×100×100mm) loaded in compression parallel and perpendicular to the grain. Appendix-A3 gives all parameters used to model wood material law #33 in Multiplas.

Table 7-1: Wood elastic material properties for CLT panels

Layer Direction	E_L [MPa]	E_T [MPa]	G_L [MPa]	G_T [MPa]	ν_L [~]	ν_T [~]	f_L [MPa]	f_T [MPa]
Longitudinal	11,000	$E_L/30$	$E_L/16$	$G_L/10$	0.35	0.07	28.9	4.7
Transverse	9,000	$E_L/30$	$E_L/16$	$G_L/10$	0.35	0.07	25.2	3.4

The CLT blocks used for experimental testing had a cross-sectional area of 150×150mm and a thickness of 120mm (Bhat, 2013). The specimens were cut from a 7-ply CLT panel to four layers (32-35-35-18mm). A compression load was applied in two settings: i) using a 25.4×25.4mm square

profile, as shown in Figure 7-2a; and ii) using a 25.4mm diameter bolt, as shown in Figure 7-2b. The configuration was done in such a way to test the influence of bearing profile on the embedment strength (Bhat, 2013). The loads applied using the square profile was predominantly in the vertical direction; whereas the bolt caused direct vertical and horizontal compressive stresses around its circumference. For both configurations, it was assumed that the steel components always remained elastic, and all deformations were a result of wood crushing.

Figure 7-2c and Figure 7-2d show the 3D FE models for the square rod and circular dowel configurations, respectively, constructed using solid modelling approach. The four layers of the CLT block were represented by four separate solids, which were then meshed with 3.5mm long solids to meet their shape requirements and for computational efficiency. The contact surfaces between layers were assumed as fully bonded. The Young's modulus and the Poisson's ratio for the steel, assumed as a linear elastic material, were taken as 200,000MPa and 0.3, respectively. Contact elements with a friction coefficient of 0.3 between the steel bar/bolt and the CLT block avoided penetration between the two components. The analyses were static, considering both material (timber only) and geometric nonlinearities.

(a)   (b)

(c)   (d)
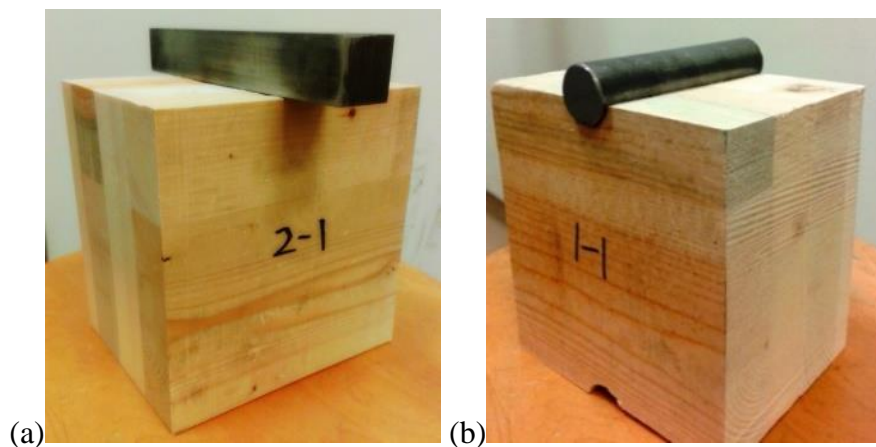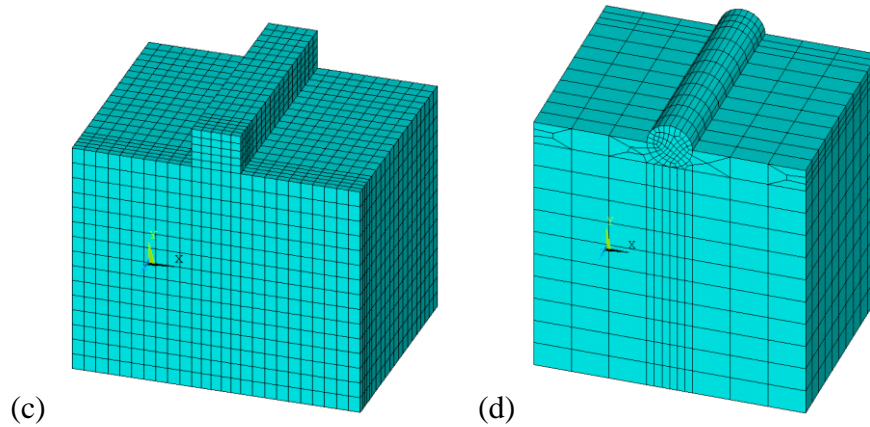
Figure 7-2: CLT test configuration (Bhat, 2013) *(Reprinted with permission): (a) Square rod, and (b)*
Circular dowel; Isometric views of FEM: (c) Square rod, and (d) Circular dowel

7.4.3 CHSS Models

Although steel material properties and behaviours are well documented, small scale testing, as
shown in Figure 7-3a, was conducted to validate the ultimate material strength. The test setup
restrained the bottom side of samples, while a vertical displacement was applied from the top, until
failure. The bone-shape ensured failure to occur at the reduced section, which was 6mm long,
10mm wide, and 3mm thick (net section without edge fillets). Figure 7-3b shows the FEA model
used for material parameter calibration. ANSYS solid modelling approach was considered; the
model constituted of a single solid. A mesh of 1mm was used at the failure surface of the reduced
section to give an acceptable stress distribution.

Welding impacts the mechanical properties of low carbon steel (Sahin, 2005; Talabi et al., 2014);
depending on the process parameters, yield and ultimate strengths are reduced up to 40%. As
shown in Figure 7-4a, the material was affected at the tube-coupler interface, herein labelled 'weld-
coupler' area. The circle shown in Figure 7-4a illustrates the area with different steel properties
between the weld-coupler *(M2)* and the rest of the tube *(M1)*. Figure 7-4b shows the numerical

representation of the CHSS, highlighting the different areas. Herein, the weld-coupler area was assumed perfectly circular, with its centre lying in the middle of the tube.
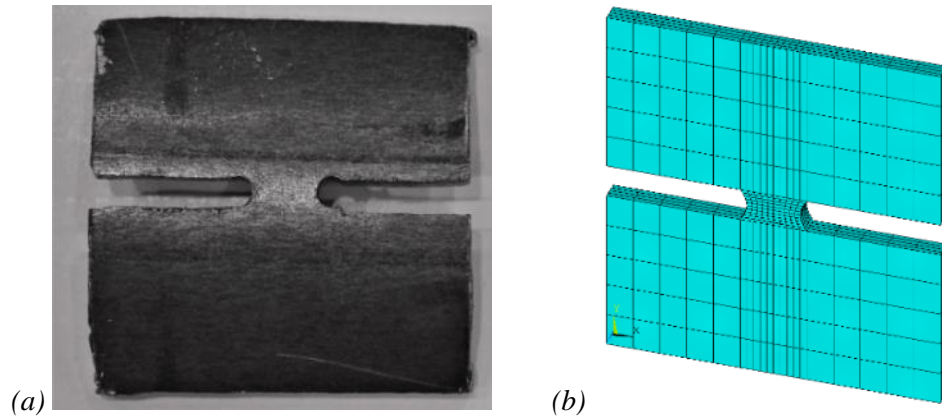
Figure 7-3: Bone-shaped steel specimens: (a) Experiment specimen (Photo credit Mpidi Bita); and (b) FE model specimen
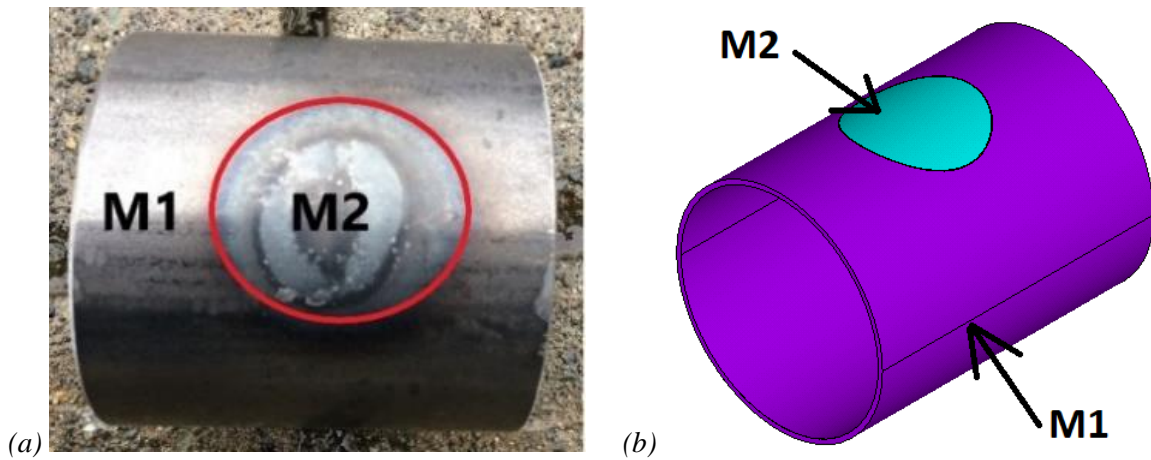
Figure 7-4: Steel tube zones with different material properties: (a) Tested tube (Photo credit Mpidi Bita); and (b) FE model

Since Schneider (Schneider, 2015) did not specifically inspect the welds, it was not possible to determine the weld properties. Rather, 750 numerical analyses were performed using the model described in section 7.4.4 to achieve a good fit between experimental and numerical force-deformation curves for Tube$_2$. The results allowed to calibrate the material properties of *M*2,

defined as a trilinear stress-strain curve with $Tube_2$ dimensions and steel properties (M_1 obtained from testing) kept constant. Table 7-2 gives the input parameters, along with their respective ranges, considered for model calibration. The yield $(\sigma_{y,w})$ and ultimate $(\sigma_{u,w})$ strengths for $M2$ were defined as reduction (Sahin, 2005; Talabi et al., 2014) from the $M1$ steel properties. The failure stress $(\sigma_{F,w})$ was 80% of the selected $\sigma_{u,w}$. Additionally, a range was also defined for the elastic, plastic, and failure moduli $(E_{el,w}, E_{pl,w}, E_{F,w})$ in accordance to the moduli of the tested steel. The weld strength-loss slope $(E_{F,w})$ referred to the negative slope of the stress-strain curve between the maximum stress $(\sigma_{u,w})$ and the stress at failure $(\sigma_{F,w})$.

Table 7-2: Input parameters and ranges for weld-coupler area

Component	Parameters	Ranges [MPa]
Weld-coupler	i) Yield strength $(\sigma_{y,w})$ ii) Ultimate strength $(\sigma_{u,w})$ iii) Elastic modulus $(E_{el,w})$ iv) Plastic modulus $(E_{pl,w})$ v) strength-loss slope $(E_{F,w})$	$(0.60\text{-}0.90) \times \sigma_y$ $(0.75\text{-}0.90) \times \sigma_u$ 200,000 - 240,000 2,000 – 100,000 900 – 100,000

7.4.4 Steel Tube Connection Model

The preceding assumptions for CLT and CHSS were used to construct the 3D FE models of the connection. The geometry was identical to the descriptions of $Tube_2$ from Schneider (Schneider, 2015) with a tube diameter $d = 76.2$mm, tube thickness $t = 3.0$mm, diameter of the weld-coupler area $c = 40$mm and loaded end distance of $a_L = 191$mm. The steel rod transferring the loads from the connection to the supporting floor or foundation below always remained elastic during testing. This capacity-protected part of the connection was not part of the optimisation; therefore, it was not explicitly modelled. From the experimental results, all damage was centralised at the weld-

coupler area. This region was modelled on the tube and therefore, applying a force *(Pa)* directly on this area as a downward vertical displacement was deemed an appropriate simplification. The assumption was that the coupler diameter was the same as the rod diameter (d_r), both idealised in terms of c, as illustrated in Figure 7-1b. Figure 7-5a shows the test configuration, whereas Figure 7-5b shows the model.

The test setup restrained the steel rod on a solid base; and upward displacements were applied from the upper steel fixture. This configuration was idealised in the FE by restraining the CLT panel against all lateral movements at the fixture location, represented by the red dots in Figure 7-5b, and applying a static downward vertical deformation at the weld-coupler area, represented by the arrow in Figure 7-5b. Since the steel tube was the main component affecting the behaviour of the connection, a fine mesh size (5mm element length) was selected for its elements. To reduce convergence problems by allowing a better contact, the same mesh size was selected for the CLT volumes around the tube. A coarser mesh size (20mm element length) was defined for the remaining CLT volumes. The contact formulations between steel and CLT were identical to those described in section 7.4.2.
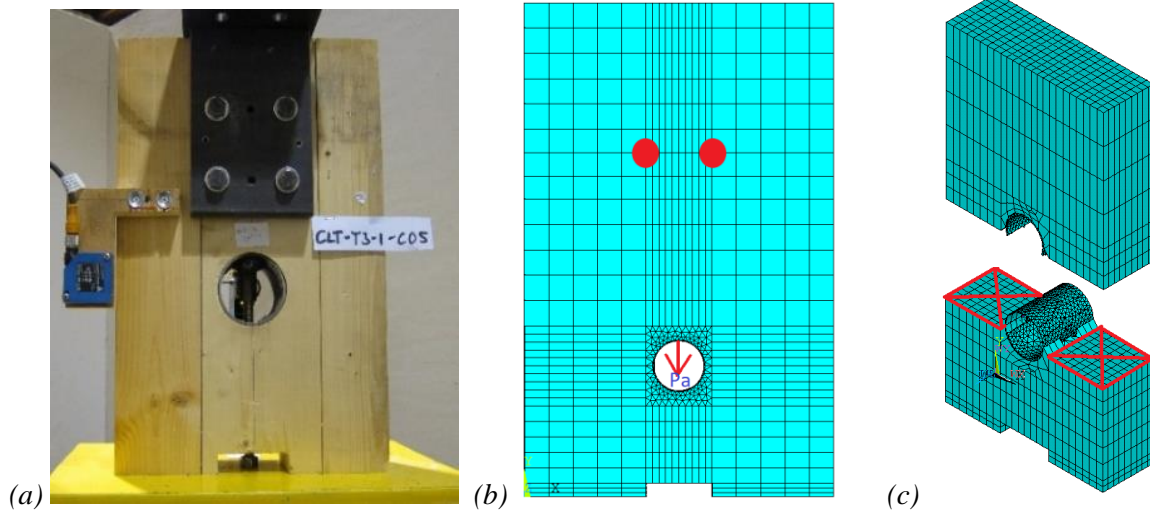
Figure 7-5: (a) Tube test specimen (Schneider, 2015) *(Reprinted with permission); (b) FE model; and (c) CLT net tension failure*

The outputs from the tube FEA were: i) the deformation at the weld-coupler area *(δ_t)*, ii) the corresponding applied force *(Pa)*, and iii) the compressive stresses parallel *(σ_{par})* to the grain of the longitudinal layers of the CLT, around the CHSS. The output curves from *Pa* and δ_t allowed to compute F_y, k_e, F_u, and *μ,* as well *U*, calculated as the area under the *P*-δ_t curve up to the failure displacement, from the equivalent energy elastic plastic (EEEP) method of ASTM E2126 (American Society for Testing and Materials, 2011). Herein, k_e was calculated between $0.1 \times F_u$ and $0.4 \times F_u$ and *μ* was the ratio of the failure displacement, corresponding to $0.8 \times F_u$, and the yield displacement.

7.5 Sensitivity Analysis

A global variance-based sensitivity analysis helps understanding how FEA results are affected by input parameters. In other words, how important the selected variables are with respect to the outputs, expressed in terms of importance factor *(IF),* estimated for every parameters (Dynardo, 2017; Most and Will, 2012). Herein, Latin Hypercube Sampling (LHS) was used to scan the design

space with a sample size of 250 analyses to account for the permutations of input parameters. Metamodel of Optimal Prognosis (MOP) was used to estimate the accuracy of the input-output correlations, expressed in terms of Coefficient of Prognosis *(CoP)*.

The input variables were: i) the tube diameter *(d_t)*; ii) the tube thickness *(t)*; iii) the diameter of the weld-coupler area *(c);* iv) the yield strength *(σ_y)* of the steel tube; v) the ultimate strength *(σ_u)* of the steel tube; and vi) the minimum loaded wood end-distance *(a_L)*. For this analysis, the slopes of the stress-strain curves *(E_{el}, E_{pl}* and *E_F)* defined for the steel tube were kept constant (Mahendran, 1996). Herein, E_F is the steel tube strength-loss slope, defined as the negative slope of the stress-strain curve of the steel between the maximum stress *(σ_u)* and the stress at failure *(σ_F)*. Table 7-3 shows the input parameters used for the sensitivity analysis, along with their respective ranges defined from analyses.

Table 7-3: Input parameters and ranges

Parameters		Sensitivity analysis	Second optimisation
Tube	i) Diameter *(d_t)* (mm)	50-250	150-230
	ii) Thickness *(t)* [mm]	3-15	9-15
	iii) Coupler diameter *(c)* [mm]	25-80	30-80
	iv) Yield strength *(σ_y)* [MPa]	250-800	400-800
	v) Ultimate strength *(σ_u)* [MPa]	$(1.0\text{-}2.0) \times \sigma_y$	$(1.0\text{-}1.6) \times \sigma_y$
CLT	vi) Loaded end-bearing *(a_L)* [mm]	$(2.0\text{-}4.0) \times d_t$	$2.0 \times d_t$

Since it would be unpractical to optimise welds for a given target performance; and it was assumed that the same procedures would lead to similar weld properties. Consequently, no variations were considered for the material models of area *M*2 and the reductions of $\sigma_{y,w}$ and $\sigma_{u,w}$. Also, the same slope of the stress-strain curves ($E_{el,w}$, $E_{pl,w}$ and $E_{F,w}$), obtained after Tube$_2$ calibration, were considered for the sensitivity analyses and subsequent first level of optimisation. Nevertheless, it

should be noted that the uncertainties and variations present in the weld material models were considered in the robustness analysis, as described in section 7.7.

In this study, 3-ply CLT panels with equal layer thickness of 35mm were modelled. Although variations in panel thickness could have a small impact on the connector performance, it was kept constant under the assumption that the rigorous CLT production quality control limit variability. The ranges of the input parameters for sensitivity analysis, as shown in Table 7-3, were identical to those used in the subsequent first optimisation, to account for the *IF* of individual input parameters as well as the *CoP*. In addition, the analysis ensured that a value of $c \leq 0.6 \times d$ was used, to maintain a realistic geometry representation.

For both sensitivity and optimisation analyses, the outputs were the same as for the tube modelling: i) δ_t, ii) *Pa*, and iii) σ_{par}. The output curves from *Pa* and δ_t again allowed to compute F_y, k_e, F_u, μ, and *U*. The constraint for the analyses was the applied stress parallel to the grain of the longitudinal layers of the CLT panels. Threshold for this value, to avoid damage to the CLT panels, was the CSA-O86 value. Herein, for compression parallel to the grain of the longitudinal layers for E_1 CLT (1950Fb- 1.7E Spruce-Pine-Fir (SPF) MSR lumber), σ_{par} should be below the CSA-O86 nominal value of 19.3MPa *($\sigma_{par,max}$)*. In the perpendicular direction, it was assumed that sufficient bearing would be provided considering the location of the hold-downs with respect to the width of the CLT panel. Furthermore, in accordance with CSA-O86, the transverse layers were assumed to not contribute to the resistance against the applied loads; therefore, stresses perpendicular to the grain were not evaluated.

7.6 Tube Optimisation

The primary objective of the research was to optimise the tube connector's geometric and material properties for 3-ply CLT panels to meet a specified target performance, herein the yield force $F_{y,t}$, while maximising: i) the initial stiffness (k_e), ii) the load-carrying capacity (F_u), iii) the dissipated energy (U), and iv) the ductility ratio (μ). The CLT compression stresses (σ_{par}) had to be kept within their elastic limits $(\sigma_{par,max})$.

The research by Schneider (Schneider, 2015) investigated the performance of three randomly selected tube diameters, resulting in a maximum F_y=52kN. Herein, to account for higher hold-down demands, a target yield force $(F_{y,t})$ of 80kN was specified with yielding of the tube as the primary ductile failure mechanism. Applying capacity-based design approach, a 19mm (3/4in) diameter steel rod (d_r) CSA 58W/400W (weldable construction steel with 400MPa yield strength) was selected. The steel rod, which provides a tension capacity of 112kN (40% stronger than $F_{y,t}$) was considered as the secondary ductile failure mechanism. Finally, the required brittle tension capacity of the CLT panel (see Figure 7-5c) was determined as 156kN, 40% stronger than the rod yielding, as recommended in clause 11.9 of CSA-O86. Assuming that tension resistance is provided by the area on one side of the steel tube, a 125mm wide section of 3-ply CLT would be required.

A two-level optimisation was conducted. The first level used the results of the MOP, obtained from the sensitivity analysis. Consequently, the defined ranges were the same as the sensitivity analysis, as shown in Table 7-3. The Evolutionary Algorithm (EA) approach, implemented in OptiSlang (Dynardo, 2017; Most and Will, 2012), was used. The EA searched the design space for possible combinations of input variables to find better approximations for the optimised

responses. Because this analysis was based on the MOP from the sensitivity analysis, no numerical solver was needed. Surrogate models were used to solve 9,900 analyses. However, these surrogate models, which reduce the complexities of the real model, only give an approximation of the true solution, hence the need for validation (Dynardo, 2017). Therefore, a second level of optimisation was required, using the best results of the first optimisation as a reference design, to perform analyses with the numerical solver. Consequently, the ranges of input parameters could be refined to the values shown in the last column of Table 7-3, which were determined after the first optimisation. Since the second optimisation was performed around the pre-optimised model, only 100 analyses were required.

7.7 Variance-based Robustness Analysis

Even with high accuracy in modelling, not all uncertainties encountered can be reduced. An approximation method described as "Variance-Based Robustness Analysis (VBRA)" was used to perform the stochastic analysis (Most and Will, 2012). The VBRA relates uncertainties of the input parameters to the response variabilities. A VBRA was conducted to investigate the effects of uncertainties present in the material properties of timber and steel material models, as well as the geometry of the CHSS and CLT panel, on the variability of the connection performance measured in terms of F_y, F_u, k_e, U, μ, and σ_{par}.

The input random variables or uncertainties related to wood were: i) the E-modulus of the longitudinal layers (E_L), ii) compressive strength parallel to the grain of the longitudinal layers (f_L) of the CLT panel, iii) and the compression parallel to the grain values $(\sigma_{par,max})$. Although wood properties have high variability, the production process of CLT ensures homogeneous end products with less variability (Thelandersson and Larsen, 2003). For European CLT, the coefficient of

variation (*CoV*) ranged from 4% to 10% for E_L, and 7% to 10% for f_L (Jeitler et al., 2016; Joebstl et al., 2006; Steiger and Gulzow, 2009). Since there is no data available on the variability of Canadian CLT, 5% and 10% *CoV* for E_L and f_L, were taken as conservative values.

The uncertainties related to steel *(M1)* were: i) the elasticity modulus *(E_{el})*, ii) the yield strength *(σ_y)*, iii) the plastic modulus *(E_{pl})*, and iv) the ultimate strength *(σ_u)*. *CoV*s of 2%, 10% and 5% were assigned for E_{el}, σ_y and σ_u, respectively based on available information (Hess et al., 2002). The *CoV* for E_{pl} and E_F were assumed as 5%. A *CoV* of 20% was assumed for all *M2* material properties. The probability density functions (PDFs) for all random variables were defined as lognormal to avoid negative outcomes (Hess et al., 2002). For the model geometry, 1% *CoV* was obtained after measuring all specimens tested by Schneider (Schneider, 2015), assuming a uniform PDF.

Table 7-4 summarises the uncertainties considered for the VBRA, along with their respective means and *CoV*s, and distribution types (PDFs). Within the specified ranges, the selection of the realisations of the defined uncertainties was done randomly using the LHS. To stay within realistic boundaries, the analyses ensured that wood properties $E_T \leq E_L$, the panel thicknesses $t_{trans} \leq t_{long}$. In addition, for steel and weld properties $\sigma_u \leq 2 \times \sigma_y$, $\sigma_{u,w} \leq 2 \times \sigma_{y,w}$, $E_{pl} \leq E_{el}$, and $E_{pl,w} \leq E_{el,w}$. A total of 100 samples was sufficient to perform this analysis.

Two Limit State Functions (LSFs) *(g)* were defined for the VBRA: i) $g_1 = F_{y,t} - F_y$, and ii) $g_2 = \sigma_{par,max} - \sigma_{par}$. The analysis dealt with each one separately; failure occurred when $g_i \leq 0$ (i=1,2). A second MOP was obtained from the VBRA to estimate the influence of each random variables on the performance of the connection. Therefore, the correlation between the considered input random variables, obtained from their respective PDFs, was used to estimate the correlation

between the response outputs. This approach resulted to a single compound LSF, used to quantify

the robustness of the model. The VBRA determined whether the optimised connection detailing

was robust (met $F_{y,t}$ without exceeding $\sigma_{par,max}$) or not robust (one or both LSFs violated) in the

presence of the considered uncertainties.

Table 7-4: Random variables for variance-based robustness

	Parameter	PDF	*mean*	*CoV* [%]
CLT	E-value (E_L)	Lognormal	From Table 7-1	5
	Compression par. (f_L)	Lognormal	From Table 7-1	10
	Compression par. $(\sigma_{par,max})$	Lognormal	From CSA-O86	10
Steel	E-elastic (E_{el})	Lognormal	From section 7.4.3	2
	Yield strength (σ_y)	Lognormal	From optimisation	10
	E-plastic (E_{pl})	Lognormal	From section 7.4.3	5
	Ultimate strength (σ_u)	Lognormal	From optimisation	5
	E-failure (E_F)	Lognormal	From section 7.4.3	5
Weld	E-elastic $(E_{el,w})$	Lognormal	From calibration	20
	Yield strength $(\sigma_{y,w})$	Lognormal	From optimisation	20
	E-plastic $(E_{pl,w})$	Lognormal	From calibration	20
	Ultimate strength $(\sigma_{u,w})$	Lognormal	From optimisation	20
	E-failure $(E_{F,w})$	Lognormal	From calibration	20
Geometry	Thickness long (t_{long})	Uniform	From section 7.3	1
	Thickness trans (t_{trans})	Uniform	From section 7.3	1
	Diameter (d_t)	Uniform	From optimisation	1
	Thickness (t)	Uniform	From optimisation	1
	weld-coupler (c)	Uniform	From optimisation	1
	End-bearing (a_L)	Uniform	From optimisation	1

Wood strength parameters are best represented by a Weibull two-parameter distribution (Barrett

and Foschi, 1977; Lam et al., 1997). The histograms obtained from the frequency distribution of

the individual response output were then used to fit their respective PDFs. The values with high

frequency, corresponding to the *mean* of the fitted curves, should match the performance of the

optimised connection (Opt-2), for a robust design. The 5th percentile of the curve $(F_{y,min})$ (Canadian

Standards Association, 2017; Canadian Wood Council, 2011), characterising the resistance of the connection, was calculated as $F_{y,min}=mean-(1.645\times stdv)$, where *stdv* was the standard deviation of all obtained values, for a given response output. The number of standard deviation from *mean* to $F_{y,min}$ represented the sigma-level *(σ_{level})*. With $\sigma_{level} \geq 2.0$ for individual response, it would be safe to assume that the optimised detailing of the tube connection would be resilient with respect to the considered uncertainties (Most and Will, 2012).

7.8 Results and Discussion

7.8.1 CLT Properties

The yield point of the CLT loaded in compression obtained from the FEA, 70kN after less than 1.5mm deformation, agreed with the experimental tests. Figure 7-7 compares the average stress-strain curves obtained from testing clear wood specimens, loaded in compression parallel and perpendicular to the grain, against the numerically obtained stress-strain curves for the CLT block. In the FEA, these curves were computed for the longitudinal layers, where there was compression parallel to the grain; and the transverse layers, which were compressed perpendicular to their grain direction. The FE model adequately captured both elastic and plastic behaviours until failure. Checking the stresses within the wood elements, both longitudinal and transverse layers were in their plastic regions, with strength softening mainly observed in the longitudinal layers. From Figure 7-7, crushing started after 28MPa and 4MPa for the longitudinal and transverse layers, respectively. The constitutive material model by Grosse (Gross, 2005) used in the FEA followed the plastic behaviours of the tested samples.

7.8.2 Steel Properties

Calibration of the numerical models was performed using the trilinear kinematic hardening stress-strain curve as obtained for the steel tube properties *(M1)* to subsequently capture the connection behaviours in terms of post yielding and failure. The average stress-strain curve of the bone-shape specimens obtained during the small-scale experimental testing is given in Appendix A.5. These showed an ultimate strength of 760MPa. The material properties of the steel were then calibrated to match the experimental results of Tube₂. From Figure 7-7, the yield and ultimate strengths were estimated as σ_y=780MPa and σ_u=800MPa, respectively, with an ultimate strain *(ε_u)* of 0.29. The elastic *(E_{el})* modulus was 200,000MPa, with the Poisson 0.3. The plastic modulus *(E_{pl}=51MPa)* was calculated as the slope of the stress-strain curve between the yield and the ultimate strengths. The ultimate strength *(σ_u)* was assumed 2.5% higher than σ_y. The third slope passing through the failure stress *(σ_F=0.80×σ_u)* was estimated to E_F=-1,570MPa.

(a)
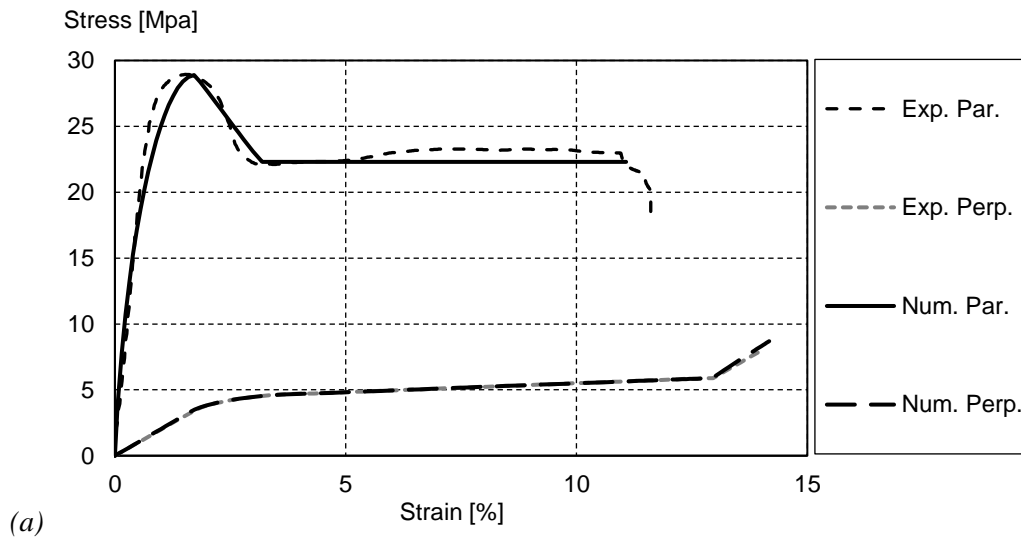
Figure 7-6: Experimental and numerical stress-strain curves for CLT
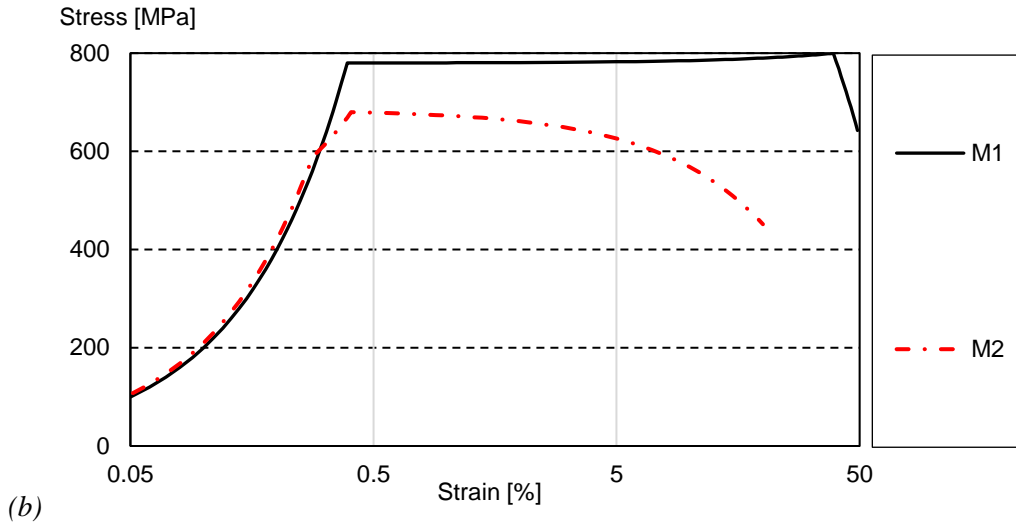
Figure 7-7: Material properties for steel tube (M1) and welded area (M2) (in logarithmic scale)

Table 7-5 shows the material properties obtained after calibration of Tube$_2$ model, with *M*1 and

*M*2 defined for the tube and weld-coupler areas, respectively. The results shown in Table 7-5 and

Figure 7-7 demonstrate that the tube areas with the original steel exhibited large ductility while

the weld area exhibited brittle failure. For the subsequent modelling, it was assumed that welding

reduced the yield and ultimate strengths by 25% and 15%, respectively, and increased the elastic

modulus by 5%. For the plastic modulus, the value of the original steel represented less than 1%

welds value. For the strength-loss slope, the welds were more brittle, representing 74% of the

corresponding value for the original steel.

Table 7-5: Material properties of the tubes

Area	E_{el} [MPa]	σ_y [MPa]	E_{pl} [MPa]	σ_u [MPa]	E_F [MPa]	σ_F [MPa]
*M*1 (Tube)	*200,000*	780	51	800	-1,570	640
*M*2 (weld-coupler)	210,000	588	73,500	*680*	-1,166	*545*

186

7.8.3 Steel Tube Connection

Figure 7-8 compares the experimental and numerical force-deformation curves for the three tube diameters. The calibrated model of Tube$_2$ showed a very good approximation of the behaviour observed during testing. The post yielding behaviour was highly affected by the stress-strain curves of the weld-coupler area, especially the value of the yield strain. It was observed that if the welds yielded at higher strains (for a given $E_{el,w}$ value), bigger strength degradations after yielding point were noted. In this case, strength loss of up to 40% was observed after yielding. Furthermore, the strain hardening of the weld-coupler caused the connection to quickly pick up load after the initial dip, up to the load-carrying capacity. The value of $E_{F,w}$ needed to be in the same range as E_F to avoid sudden failure and convergence problems.

The modified models of Tube$_1$ and Tube$_3$ also resulted in acceptable agreement with the experimental force-deformation curves. The elastic and post yielding behaviours changed, especially for Tube$_1$, where a smaller weld-coupler area was measured, high strength and stiffness degradations were noted after yielding. Further improvement of the numerical results for Tube$_1$ and Tube$_3$ would need re-calibration of material properties, since the welding process was not controlled, and the presence of imperfections could have led to different $M2$ material properties and possibly different dimensions for $M2$. In other words, the procedure explained in section 7.4.3 would have to be repeated for Tube$_1$ and Tube$_3$, separately. This approach was not followed since the obtained force-deformation curves for Tube$_1$ and Tube$_3$, shown in Figure 7-8 and the results summarised in Table 7-6, were also acceptable for the purpose of this study. Tube$_1$ exhibited the highest capacity whereas Tube$_2$ exhibited higher ductility. Nevertheless, as observed by Schneider (Schneider, 2015), the models also confirmed that there was a threshold where buckling of the

steel tube becomes the governing failure mechanism. For Tube$_3$ with the largest tube diameter, smaller yield capacity and ductility were obtained.
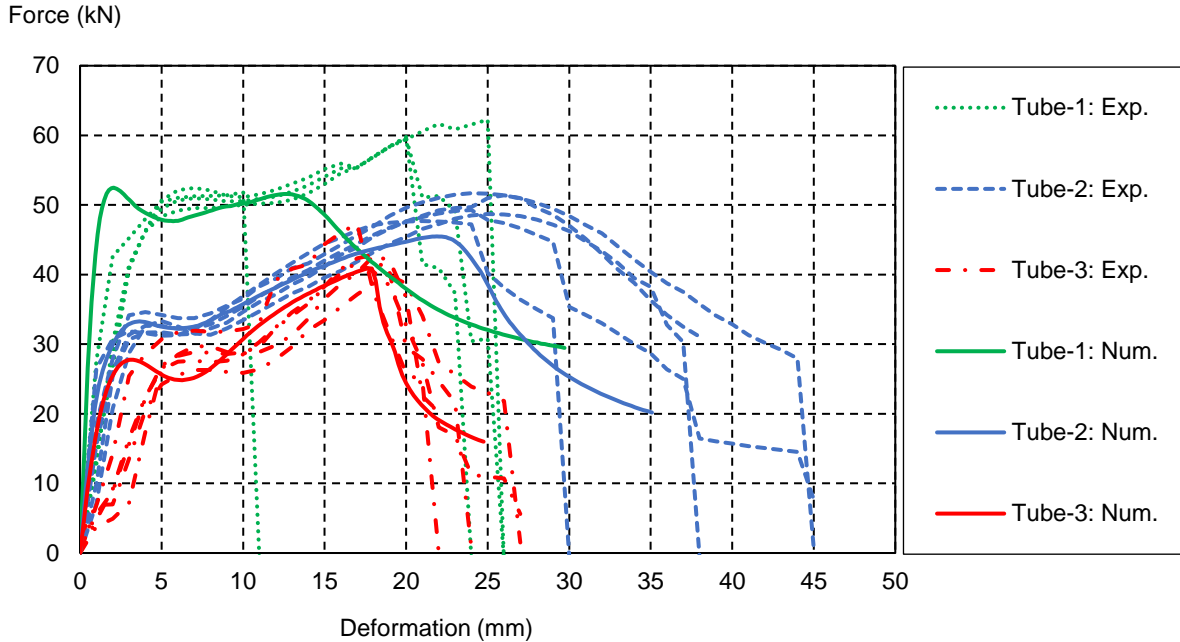
Figure 7-8: Experimental and numerical force-deformation curves for Tubes 1, 2 and 3

Table 7-6: Comparison between experiment and numerical results

Tube		F_y [kN]	k_e [kN/mm]	F_u [kN]	U [kNm]	μ [~]
Tube$_1$	Experiment	52	18	59	1,136	7
	Numerical	52	16	53	850	19
Tube$_2$	Experiment	41	15	49	1,159	10
	Numerical	40	14	46	950	15
Tube$_3$	Experiment	33	13	42	565	4
	Numerical	32	12	41	564	10

Furthermore, as shown Figure 7-9, good agreement was obtained with respect to the failure modes. The observed failures were: i) the buckling of the tube, due to pull down or tension forces on the coupler through the steel rod, and ii) tearing of the welds, due to high stress concentration around

188

its perimeter. However, these results also confirmed the need for a robustness analysis, to account for the uncertainties in the material properties and connection geometry, to develop a robust detailing.

(a) *(b)*

(c)
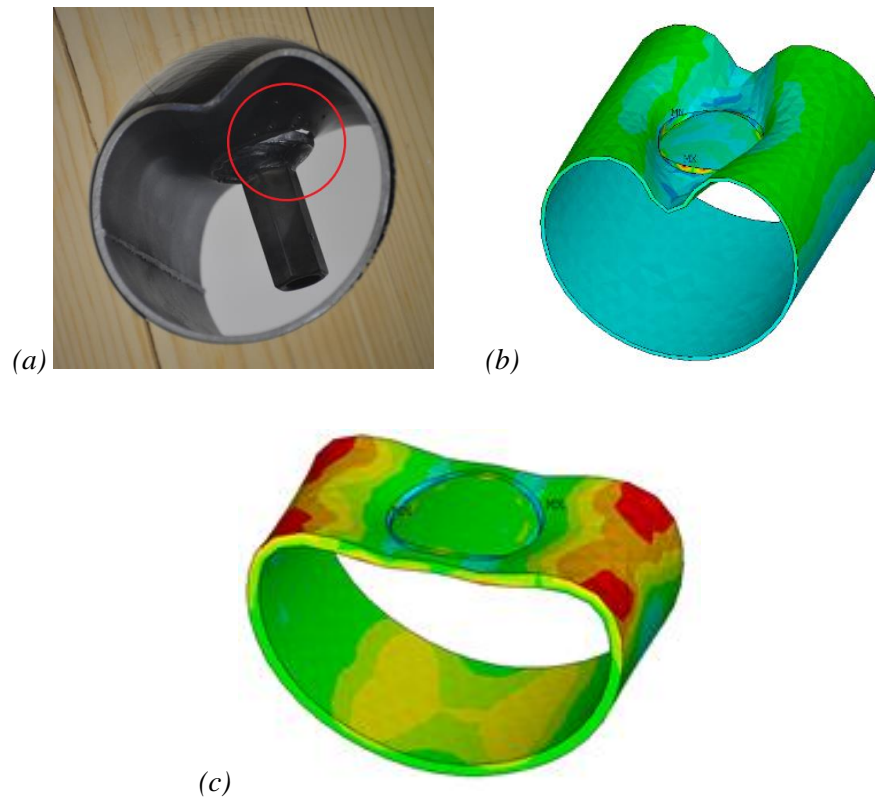
Figure 7-9: Failure modes: (a) Experiment; (b) Tube buckling; and (c) Tearing at weld-coupler

7.8.4 Sensitivity Analysis

The sensitivity analysis was performed to understand how the input variables affect the response of the model, in terms of F_y, k_e, F_u, U, and μ. Given the defined ranges of input parameters, a quarter of all 250 analyses successfully met the constraint ($\sigma_{par} \leq \sigma_{par,max}$). Table 7-7 shows the results of the sensitivity analysis in terms of the individual *CoP*s and total *CoP* for the accuracy of the overall estimation. A positive correlation between t, c, and σ_y, and the output F_y was obtained, whereas d and F_y were negatively correlated. These results confirmed that larger d resulted in

weaker connections due to buckling. Increasing t increased the buckling resistance; nevertheless, this had negative impact on μ as thicker CHSS were stiffer. Furthermore, bigger c increased the tearing surface, and consequently allowing to carry higher loads. The results demonstrated that a_L only affected k_e. Table 7-7 also shows that σ_u (the ultimate and failure strains) had no influence on the responses, except on μ. Satisfying the defined constraint depended on d, with the *CoP* of 53%. A low total *CoP* was obtained for σ_{par} because other parameters influencing the applied compressive stresses on the longitudinal layers, such as the material properties of timber and the geometry of the layers, were kept constant for the sensitivity analysis. F_y was highly sensitive to t, with a *CoP* of 70%. The t also enabled to obtain buckling as the main failure mode of the connection.

Table 7-7: Results of MOP from the sensitivity analysis

Responses	*CoP* Coefficient of Prognosis [%]						Total *CoP* [%]
	d	t	c	a_L	σ_y	σ_u	
F_y	-5	+70	+9	-	+4	-	89
k_e	+46	+42	-	+11	-	-	99
F_u	-6	+72	+10	-	+5	-	95
U	-11	+76	-14	-	+6	-	92
μ	+6	-59	-	-	-15	-9	85
σ_{par}	-53	-	-	-	-	-	53

Although the input parameters were randomly selected, the algorithms implemented in the MoP enabled the estimation of the correlations between the outputs. The results confirmed that d, t and c were the most significant parameters ($CoP \geq 5\%$) to meet the design objective, given their influence on $F_{y,t}$. Although high-strength steel (higher σ_y) would lead to a stronger connection (high F_y and F_u), the simplest approach is to optimise t, c and d to meet $F_{y,t}$ while maximising k_e, U, and μ, and maintaining σ_{par} below $\sigma_{par,max}$. The parameters t, c should be set to their optimum

maximum, whereas d should be kept to its optimum minimum. Although aiming for $F_{y,t}$ would affect the ductility of the connection, it was shown that this approach would lead to a stronger and stiffer connection, with high energy absorption.

7.8.5 First Optimisation

The first level of connection optimisation was done using the results of the MOP, obtained after the sensitivity analysis, with a second constraint added to ensure that the target $F_{y,t}$ was met. The results showed that 93% successful analyses satisfied the two constraints. It was observed that beyond F_y=100kN, buckling of the CHSS was no longer a failure mode. For these cases, tearing around the coupler area became the dominant, see Figure 7-9c. Since this behaviour was not ductile, connection failure occurred shortly after yielding.

Table 7-8 gives the inputs parameters of two distinctive successful designs from the first level of optimisation, labeled Opt-1a and Opt-1b. Their responses, in terms of force-deformation curves, are shown in Figure 7-10. For both models, buckling of the CHSS was the dominant failure mode. Opt-1a reached the highest capacities with yield and load-carrying capacities of 84kN and 92kN, respectively. Although Opt-1a could still be classified as moderately ductile, the energy dissipation was relatively low. Opt-1b provided better performance in terms of k_e, U and μ, although it did not meet the target yield capacity. As shown in Figure 7-10, there is a loss of capacity after yielding, followed by strain hardening up to its load-carrying capacity. This behaviour resulted in higher ductility and energy absorption capability.

Table 7-8: Optimisation results: Input parameters and output responses

Design (Opt-)	Input parameters					Outputs responses				
	d [mm]	t [mm]	c [mm]	σ_y [MPa]	σ_u [Mpa]	F_y [kN]	F_u [kN]	k_e [kN/mm]	U [kNm]	μ [~]
1a	228	11.7	49	410	$1.6 \times \sigma_y$	84	92	14	1,071	5
1b	155	9.5	30	485	$1.1 \times \sigma_y$	64	72	22	1,565	12
2	155	9.5	30	796	$1.2 \times \sigma_y$	85	98	30	2,163	9
3	176	13.5	79	607	$1.2 \times \sigma_y$	120	200	26	-	-

7.8.6 Second Optimisation

Both Opt-1a and Opt-1b were selected as reference designs for the second optimisation to account for their respective positive performances. The ranges of input parameters used for analysis for the second optimisation were then refined as shown in the last column of Table 7-3. The results gave Opt-2 as the optimum design which maximised all responses while meeting all constraints. Table 7-8 shows the dimension of the optimised design Opt-2. The graph in Figure 7-10 compares the obtained solution from the second optimisation (Opt-2) to the force-deformation curves for both experiments (Tube₁, Tube₂, and Tube₃), and the first optimisation (Opt-1a, Opt-1b). Considerable improvements in terms of the overall performances from Schneider (Schneider, 2015) CHSS experiments were noted. Opt-2 combined the positive behaviours from Opt-1a and Opt-1b and provided a resilient connection with higher yield and load-carrying capacities associated with high stiffness, energy dissipation, and ductility. Buckling of the tube and tearing around the weld-coupler area, as observed during testing, were the failure modes. No failure of the CLT occurred as the maximum stress (σ_{par}) was 2.3MPa.
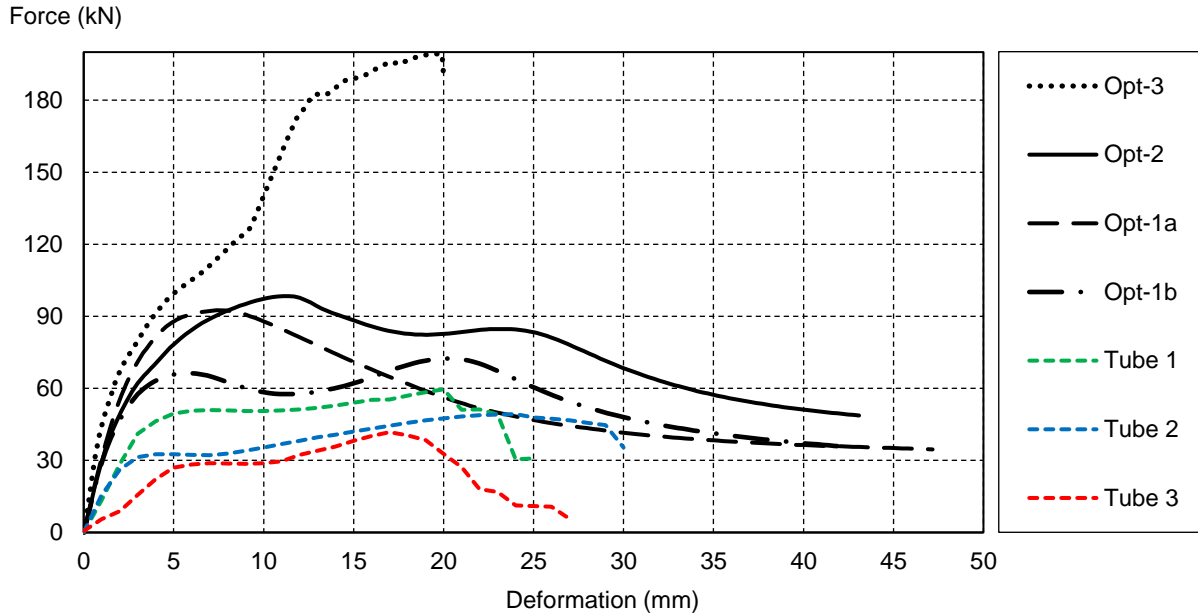
Figure 7-10: Numerical force vs deformation curves for optimised designs

The procedure followed in this study demonstrated how the connection could be optimised for a given target performance. In an attempt to further increase the target yield force $(F_{y,t2})$ to 145kN, a 25.4mm (1in) diameter steel rod would have to be used, as per capacity-based design approach. Optimisation to meet the new target would use the parameter for Opt-3, shown in Table 7-8. From Figure 7-10, albeit reaching $F_{y,t2}$, with F_u=200kN, Opt-3 would have to be classified as brittle with low energy dissipative capability. Figure 7-9c shows the observed failure mode of the CHSS as per Opt-3. Buckling did not occur; the applied deformations at the weld-coupler area only caused tearing around its perimeter. Failure occurred immediately after the applied stress on the steel went beyond σ_y, despite keeping $\sigma_{par} \leq \sigma_{par,max}$.

7.8.7 Robustness Analysis

Given the considered uncertainties, 70% of the 100 analyses successfully met the two defined LSFs. The results of the MOP obtained for the VBRA showed that σ_y, $\sigma_{u,w,}$ and E_L were the most

important random variables ($CoP \geq 5\%$) influencing the performance of the optimised detailing. Table 7-9 quantifies the influence of the uncertainties on these parameters, in terms of CoP, as well as the accuracy of the approximation, in terms of total CoP. From the uncertainties-responses correlations it can be seen that high strength steel (σ_y) and high CLT grade (E_L) should be used to meet the design objective ($F_y \geq 80kN$). This was particularly observed comparing Opt-1b and Opt-2, with the later resulting to higher F_y because of its higher σ_y. Nevertheless, it is worth mentioning that using stronger CHSS would also cause high σ_{par}, hence the importance of having high grade CLT panels to avoid brittle failure.

Table 7-9: Results of MOP from the VBRA

Responses	CoP Coefficient of Prognosis [%]			Total CoP [%]
	σ_y	$\sigma_{u,w}$	E_L	
F_y	+57	-37	+6	96
k_e	-47	+16	+29	97
F_u	+65	-37	-	98
U	+46	-32	+16	95
μ	-66	+35	-	98
σ_{par}	-24	-11	+62	82

With respect to F_y, *mean*=81kN and *sdtv*=3.5kN of the fitted PDF were close to the results of Opt-2 shown in Table 7-8. This gave a $F_{y,min}$ =75kN, corresponding to a σ_{level} =2.1. Therefore, the proposed optimised design was robust in presence of the considered uncertainties. σ_{level} =2.0 was obtained for F_u, with $F_{y,min}$ =85kN, also confirming a robust design. With respect to σ_{par}, obtaining *mean*=0.6MPa and *sdtv*=0.1MPa meant that the optimised design was also robust, given that these would never result to a compression stress higher than $\sigma_{par,max}$. The results of the VBRA proved that regardless the uncertainties present in the material properties as well as its geometry, the optimised connection was robust given the considered LSFs. The results also demonstrated that

the model was robust with respect to μ; with *mean*=9 and *sdtv*=0.9, the connection would be ductile. The model, however, was not as robust with respect to k_e and U, with σ_{level} =1.8 for both output responses. This was mainly characterised by the significant difference between their respective *mean*-values from the fitted curve and the results of Opt-2.

7.9 Steel Tube as Detailing for Disproportionate Collapse Prevention

7.9.1 Detailing for Catenary Action

Requirements for novel floor-to-floor connection detailing were highlighted in both Chapters 3 and 5, for platform-type construction, and chapter 4 for flat-plat construction. Figure 7-11 illustrates how conventional floor-to-floor connections can be improved using steel tubes to enable the floor system to develop catenary action after internal loadbearing removal following abnormal loads. In this detailing, which is applicable for both platform-type and flat-plate construction, steel tubes are placed along the width of the floor at 300mm to 500mm centre, depending on the demands. During large vertical deformations, the steel rods (single or double) transfer tie-force between adjacent floor panels by deforming (buckling) the tubes on either sides. This detailing is exclusively proposed to enhance the axial performance of the floor-to-floor joint; therefore, it is only proposed as an addition to the conventional detailing. Essentially composed of off-the-shelf parts, the simplicity of this detailing has minor impacts on the overall cost of the project.
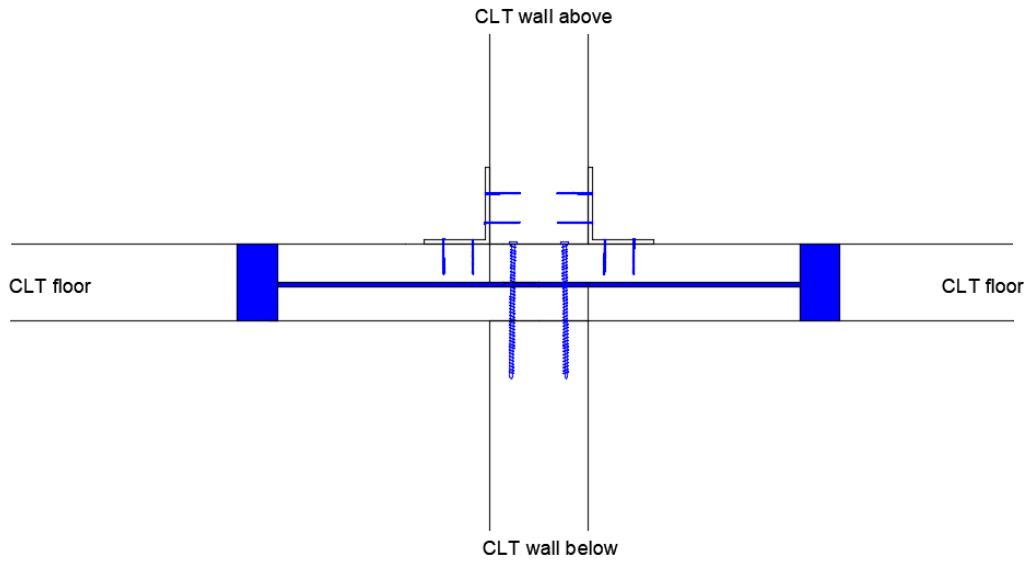
Figure 7-11: Detailing for catenary action for mass-timber platform-type and flat-plate constructions

Figure 7-12 and Figure 7-13 illustrate the first and second steps of the construction sequence, respectively. Given that this is a platform-type construction, the wall below would be installed first. Thereafter the floor panels would be placed on top of the wall, then fastened using STSs. It is worth mentioning that, to minimise the construction time, holes of the same diameter as the steel tubes would be predrilled on the floor panels. At these locations, cuts would also be required to connect the two holes. The predrilled holes and cuts would facilitate the insertion of the steel tubes and rods. The tubes, already connected to the steel rod, would be slotted to their final position. Then, the wall above can be dropped on the CLT floor panel; angle brackets and wood screws or nails would be used to secure the wall in place.

Figure 7-12: Detailing for catenary action for mass-timber platform-type and flat-plate constructions: Construction sequence step 1

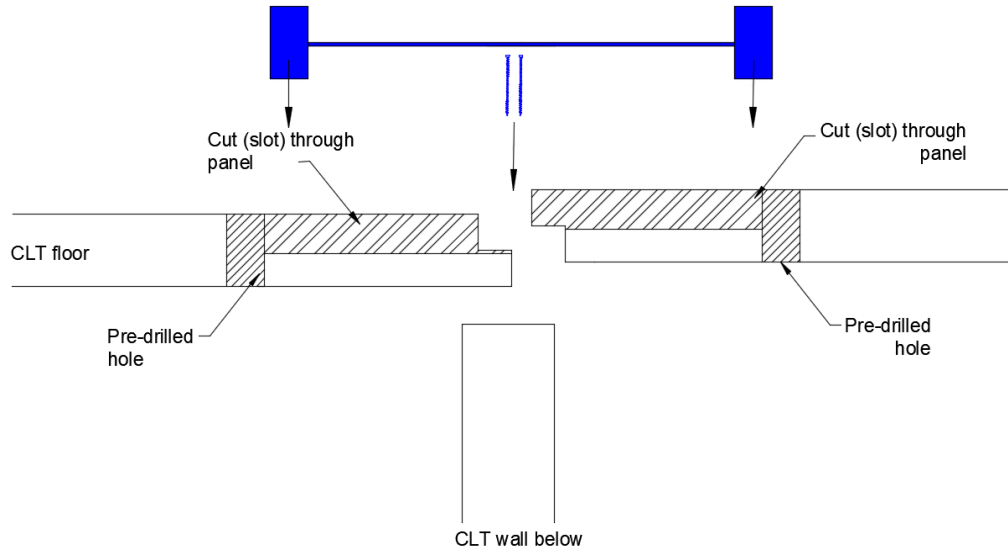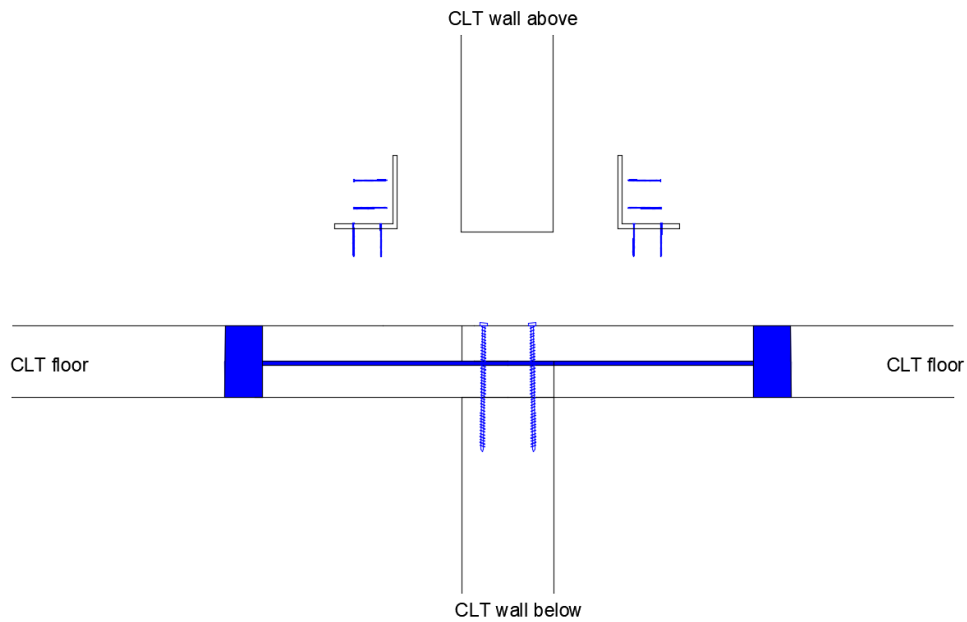*Figure 7-13: Detailing for catenary action for mass-timber platform-type and flat-plate constructions: Construction sequence step 2*

197

7.9.2 Detailing for Hanging Action

Requirements for new column-to-column detailing were highlighted in chapter 4, which studies collapse-resistance mechanisms for flat-plate mass-timber buildings. Figure 7-14 illustrates possible detailing with steel tube connectors designed to enable the floor panels to hang on the column above in the event the column below would be rendered ineffective following abnormal loads. In detailing 1, Figure 7-14a, the HS and SS sections would be designed to transfer vertical gravity loads from the column above to the column below. Mass-timber floor panels would be simply supported on the steel plate, tightened to the column below. Horizontal movements of the floor panels would be restrained by bolts tightened to the column below.

For hanging action, transfer of loads from the floor to the column above entirely would rely on the steel tubes. Herein, strength, stiffness, and ductility of the connection would solely be supplied through deformation of steel tube due to pulling of single or double steel rods. The overdesigned drift-pins would help maintaining HS and SS together during the load transfer.

Alternative design would be proposed by replacing the HS and SS by steel H or W-section. This therefore simplifies the design by eliminating the need for drift pins. Similarly, the detailing can also use squared hollow steel section as illustrated in detailing-2, see Figure 7-14b. Hanging action mechanism works exactly like detailing-1. Nevertheless, the only difference with detailing-1 is that direct load transfer from the column above to the below is done through the squared hollow steel section. Mass-timber floor panels rest on angle brackets, fastened to the below by STSs.
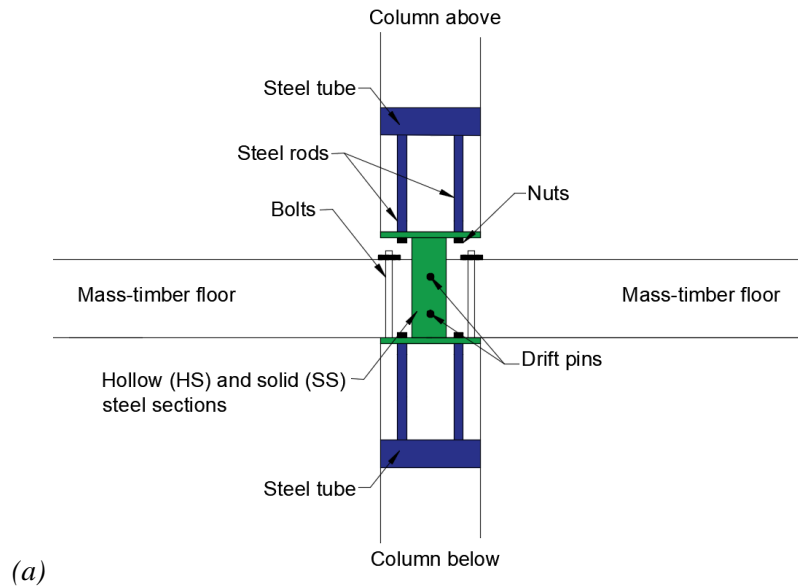
(a)
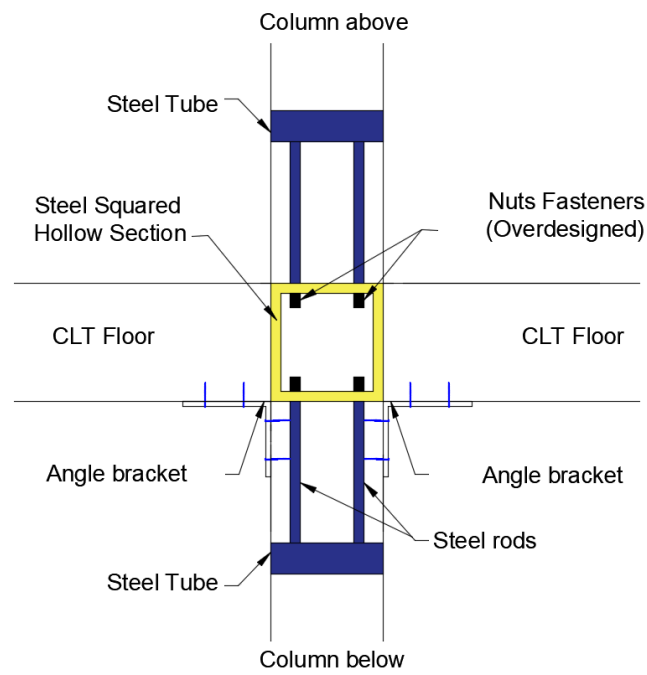
(b)

Figure 7-14: Detailing for hanging action for flat-plate mass-timber building: (a) Detailing-1 with HS and SS sections; (b) Detailing-2 with squared hollow section

Figure 7-15 illustrates the steps required for the construction of the proposed detailing in Figure 7-14b. Given that this is also a platform-type construction, the column below would be installed first. Here, the steel tube and rods would be preinstalled to minimise construction time. Thereafter,

the floor panels can be dropped in place on the angle bracket or steel ledger bolted or screwed to the column below. The floor panels would be held in place using wood screws or STSs. Finally, the column above with preinstalled steel tubes and rods would be dropped and fastened in place using nuts or couplers.
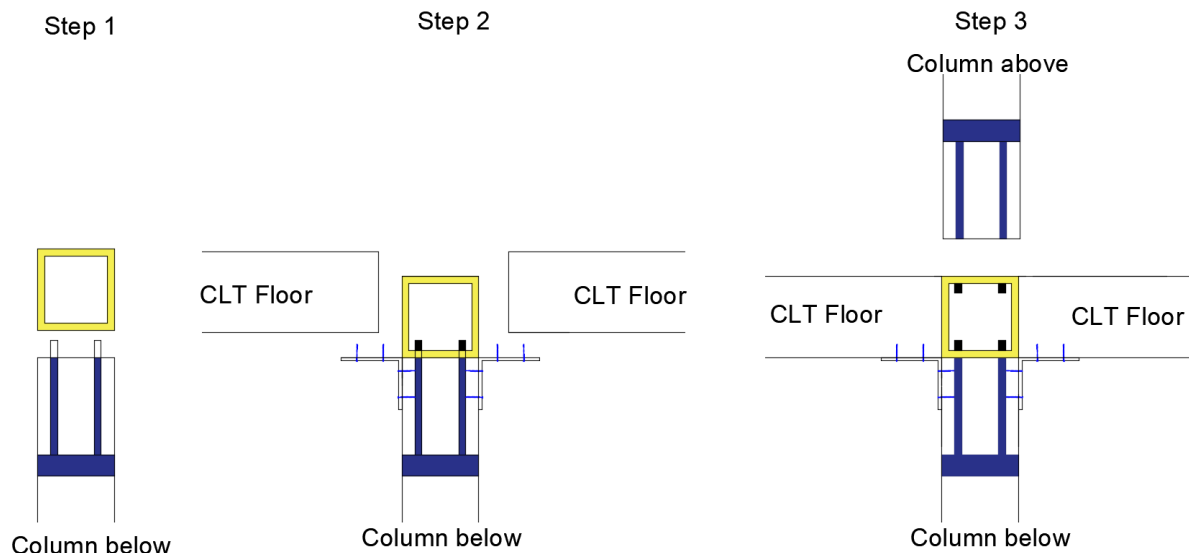
Figure 7-15: Detailing for hanging action for flat-plate mass-timber building: Construction sequence

7.10 Summary

This chapter presented FE analyses of a novel connection composed of steel tube inserted into CLT panel. The concept of capacity-based design was integrated into the detailing in such a way that, to meet the set target yield capacity, the steel component alone was sized to yield while avoiding any damage to the wood. A sensitivity analysis was performed to quantify the input-performance correlations, then the connection was optimised to meet a target yield capacity. Thereafter, a robustness analysis quantified the impacts of uncertainties in the material properties and geometry of the connection. The following conclusion were drawn:

(1) The diameter and thickness of the tube as well as the coupler diameter were the main parameters influencing the yield capacity and overall performance of the connection.

(2) To reach a target yield capacity of 85kN, the optimum design required a tube diameter of 155mm, a tube thickness of 9.5mm, a coupler diameter of 30mm, a steel yield strength of 796MPa, a steel ultimate strength of $1.2 \times \sigma_y$, and loadbearing distance of 2.0 times the tube diameter. These parameters provided a load-carrying capacity of 98kN, an elastic stiffness of 30kN/mm, a total energy dissipated of 2,163kNm, and a ductility of 9.

(3) The optimised connection design was shown to be robust with respect to the uncertainties related to the material properties and geometric parameters.

The steel tube connector provided significant advantages when considering stiffness, ductility, and resilience in addition to the load-carrying capacity. This study illustrated how the tube could be implemented as a detailing to act as horizontal or vertical tie for disproportionate collapse prevention. The procedure followed in this chapter could be used to improve the tube's performance for high strength, stiffness, and ductility. Nevertheless, experimental tests and numerical analyses to confirm the behaviour against disproportionate collapse at component and global levels are still required.

Chapter 8: Experimental Study of Mass-timber floor Systems[6]

8.1 Introduction

Floor systems collapse-resistance mechanisms for mass-timber buildings with platform-type construction are similar to those of precast concrete buildings (Schultz et al., 1977a, 1977b). For laterally restrained reinforced concrete floors, Stevens (2008) estimated that catenary action develops at a deflection between 10% and 20% of *L*. Nonetheless, the brittle nature of wood and the limited deformation capabilities of conventional connections question the feasibility to trigger catenary action in timber buildings (DoD, 2013).

For mass-timber platform-type construction, given the force and deformation demands, catenary action as a collapse-resistance mechanism often dictate the overall connection design. The review of the limited literature on the topic demonstrated that further experimental studies are required to understand the behaviours of connection detailing to develop large deformations for catenary action. (DoD, 2013) gives acceptance criteria for several construction types for concrete and steel buildings; yet no details are given for wood structures. Furthermore, for mass-timber buildings, little experimental data exist on possibilities to develop such large deformations. In addition,

---

thorough investigations are also required to confirm the performance of mass-timber floor systems with novel connection with steel tubes.

Furthermore, as catenary action only occurs at large deformations, associated with nonlinear behaviours, a nonlinearity reduction factor (NF) of 0.67 was proposed for concrete structures (Ruth et al., 2006 and Li et al., 2011). The results obtained from linear static equilibrium are multiplied by NF to obtain more realistic estimations of tie-forces mobilised at large deformation (Li et al.,2011). Nevertheless, the applicability of $NF = 067$ for timber structure is yet to be demonstrated.

8.2 Objectives

The loads applied on the damaged floor system depend on building's type, height, and dimension. Instead of presenting a case study, this chapter rather gives generic solutions to disproportionate collapse prevention for mass-timber buildings. These are residential and office buildings up to ten storeys, with no structural irregularities, typical gridline of 5m × 5m, and 2.4kPa and 1.0kPa floor live and superimposed dead loads as per NBCC (NBCC, 2015).

Using experimental tests, the primary objective of this chapter is to evaluate possible collapse-resistance mechanisms for mass-timber floor systems after internal loadbearing wall removal. This research focuses on the influences of floor-to-floor connection detailing (traditional and novel) and compares their performance using different mass-timber panels, as well as between continuous and discontinuous floor systems. The secondary objective was to propose deflection acceptance criteria to avoid disproportionate collapse for mass-timber floor systems.

8.3 Experimental Investigation

8.3.1 Specimen Description

The tested floor systems were two-span mass-timber panels, simply supported on two external walls. The floor panels were 580mm wide, and the thickness depended on the considered panels, 139mm or 89mm for CLT or LSL and LVL, respectively. The overall span of the floor assembly was 3,960mm measured from the supporting walls' centroid, with 1,980mm as the main single span (*L*). As shown in Figure 8-1, the tests represent internal floor systems with surrounding bays on both sides of the walls. It is worth mentioning that the presented collapse-resistance mechanisms are best-suited for internal floor systems, as demonstrated in chapter 5. The same steel tubes and rods would connect the damaged floor bay to the adjacent undamaged bay. Therefore, an additional 194mm was added to the floor panels to mimic continuation over the supporting walls, resulting to a total floor length of 4,350mm. The assembly height measured 425mm from the base of the external wall to the centroid of the floor panels. The materials and the thicknesses of the walls were matched to the respective mass-timber floor.

Two floor configurations were considered to study the influence of the connection detailing in developing the collapse-resistance mechanism. Configuration 1 idealised discontinuous single span floor segments connected above the removed internal wall using floor-to-floor connections, and continuous floor over the external walls. This configuration was used for assemblies with conventional (see Figure 8-1a) and novel (see Figure 8-1b) connection detailing, which were noted as *C1-Trad* and *C1-Novel*, respectively. Configuration 1 therefore helped to critically appraise the difference between conventional and novel floor-to-floor detailing, given their respective strength, stiffness, and ductility. Configuration 2 see Figure 8-1c, tested for LSL floor assemblies only,

idealised a double span floor system, continuous over the interior walls. This configuration, noted as *C2*, helped to understand the influence of continuity in the floor system, at the location of the removed element, towards developing the resistance mechanisms.
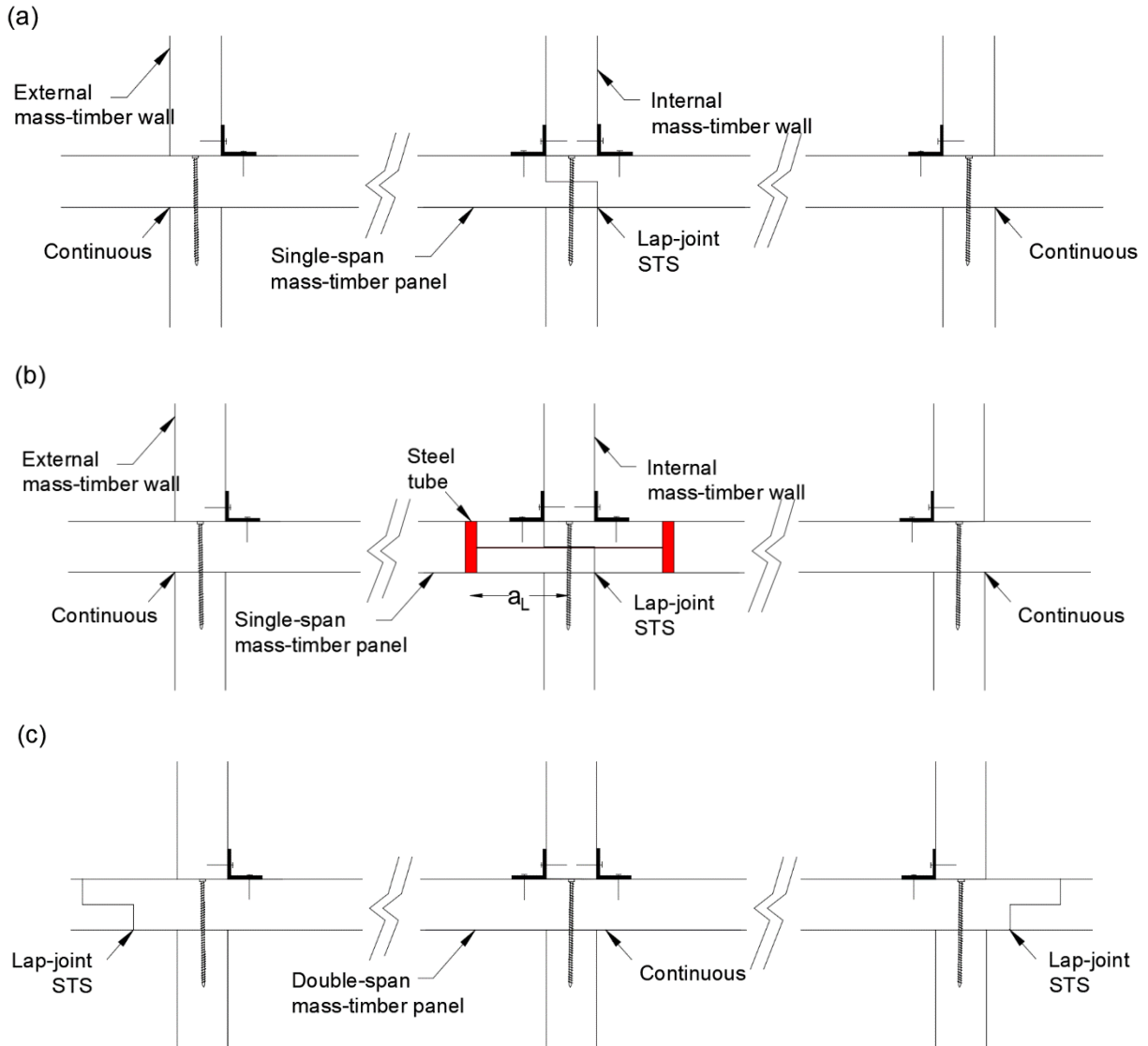
Figure 8-1: Floor system configuration: (a) Discontinuous floor system with conventional connection; (b) Discontinuous floor system with novel connection; and (c) Continuous floor system

The conventional connection was a lap-joint connected by four STSs along the width of the panels, spaced at 150mm centre to satisfy the minimum spacing in accordance to the Canadian product

approval (MyTiCon, 2017). It was anticipated that the screws would also improve the stability of the floor assembly, especially against sideways movements at mid-span during testing. The angle brackets were spaced at 300mm centre, fastened with 18 and 7 ring-shank nails on the wall and floor segments, respectively. Stiffer floor-to-wall detailing ensured that the floor-to-floor connection failed first. Therefore, conclusions on floor system failure would exclusively focus on the floor-to-floor detailing and their contribution to structural integrity. The novel connection placed the steel tubes at 300mm from the centre, with an end-bearing distance (a_L) of 300mm, measured from the centre of the tube to the edge of the panel at the floor-to-floor joint, as shown in see Figure 8-1b. This detailing was expected to enhance the axial performance of the floor-to-floor joint; therefore, it was only an addition to the conventional detailing. The rods were installed at the centroid of the section to not only align with the axial tensile force for catenary action, but also to avoid wood splitting when bending under the applied vertical loads. Table 8-1 gives an overview of the test series.

Table 8-1: Test series overview

Assemblies	Descriptions	Configurations	Specimen -IDs
CLT	Discontinuous floor system with conventional connection	*C1-Trad*	CLT-Trad-01
			CLT-Trad-02
	Discontinuous floor system with novel connection	*C1-Novel*	CLT-Novel-01
			CLT-Novel-02
LVL	Discontinuous floor system with conventional connection	*C1-Trad*	LVL-Trad-01
	Discontinuous floor system with novel connection	*C1-Novel*	LVL-Novel-01
LSL	Discontinuous floor system with conventional connection	*C1-Trad*	LSL-Trad-01
			LSL-Trad-02
	Discontinuous floor system with novel connection	*C1-Novel*	LSL-Novel-01
			LSL-Novel-02
	Continuous floor system	*C2*	LSL-Cont-01
			LSL-Cont-02

8.3.2 Material

The floor systems for this study were constructed using three types of mass-timber panels: CLT, LVL, and LSL. The CLT panels were 5-ply, 35-17-35-17-35mm thick layers, and *E1M4* stress-grade (Structurlam, 2016). The LVL and the LSL panels were 89mm thick, with $2950F_b$-2.0*E* (Louisiana Pacific Corporation, 2018) and 1.55*E* (Weyerhaeuser, 2018) stress-grade, respectively. For the conventional connections, the STSs were 8mm diameter carbon steel SWG ASSY® 3.0 Ecofast, (MyTiCon, 2017); partially threaded 300mm long for the floor-to-wall connections, and

120mm long fully threaded STSs for the floor-to-floor connections. For the floor-to-wall connection, AE116-R angle brackets were fastened with CAN-4×60 ring-shank nails, 60mm long and 4mm diameter (Simpson Strong-Tie, 2017). All mass-timber panels as well as the conventional connector components had Canadian product approvals.

The tube connection consisted of off-the-shelf components, to achieve simple detailing that can be readily adopted for mass-timber floors. The tubes were cold rolled carbon steel, grade B&C, 3mm thick and 76.2mm in diameter (Atlas Tubes, 2018), cut to a length of 89mm and 189mm, corresponding to the thickness of the mass-timber panels. The hexagonal coupling nuts were low carbon steel, with 12.7mm coarse threads diameter, 3mm thick, 45mm long, and 17mm wide. The coupling nut was welded at the centre of the inner surface of the steel tube as shown in Figure 7-1a. The welding process was performed using 0.9mm diameter MIG Wire ER480S-6 (Praxair Inc, 2018). The 12.7mm diameter steel rods, installed on the coupling nut to link the tubes on either side of the connection as shown in Figure 8-2a, had the same material properties as the coupling nut. The mass-timber panels had pre-drilled holes and cuts to facilitate the installation of the steel tubes and rods. First, the tubes were installed to both sides of the rod. Then the connector assembly was placed on top of the mass-timber panels, as shown in Figure 8-2a, and pushed into its final position as illustrated in Figure 8-2b. Figure 8-2c illustrates the schematic of the novel connection detailing.

(a)

(b)
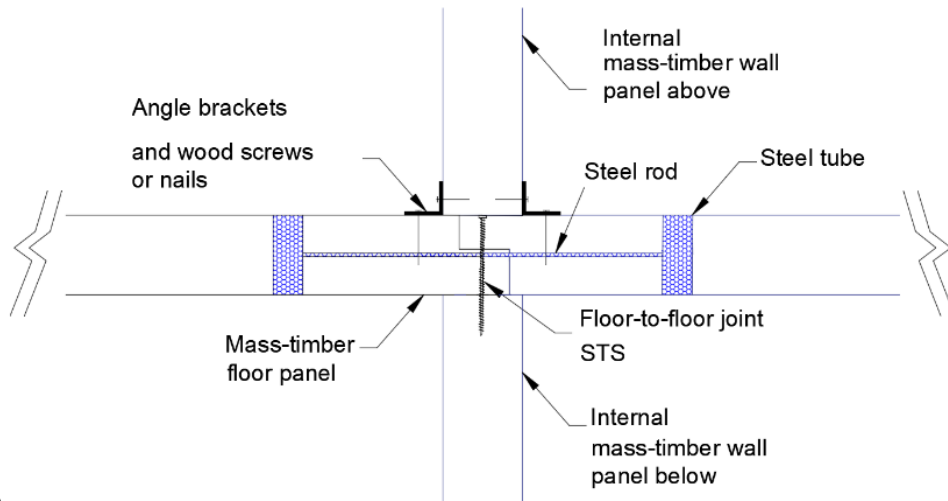
(c)

Figure 8-2: (a) Steel tube inserted in CLT panel; (b) Steel tubes and rods in mass-timber panel; and (c) Schematic representation of the detailing

8.3.3 Test Setup

The test-setup is shown in Figure 8-3. The loads were applied as a displacement at the location of the removed internal wall, similar to preceding tests on precast concrete floor and wall systems (Schultz et al., 1977a; Tohidi, 2015). The floor panels were considered as rigid body bodied with no (longitudinal) axial deformation. The recorded axial deformations were assumed to be exclusively provided by the floor-to-floor connections to estimate the compatibility between axial deformation (δ) and applied deflection (Δ). Furthermore, the test setup guaranteed that the collapse-resistance mechanisms were one-way, along the longitudinal direction of the floor system, without contribution from the transverse direction. The load was applied under displacement control at a rate of 25mm/min. Given there is no guideline for tests related to disproportionate collapse assessment, the loading rate was identical to that by Sadek et al. (2010) who investigated the behaviour of steel moment connections under a column removal scenario. Herein, the actuator applied a vertical downward load on steel bar to distribute the load along the width of the floor panels. The tests were stopped when either the maximum actuator stroke of 250mm or complete system failure were attained.

As shown in Figure 8-3, the floor panels were supported on wall sections in a platform-type system. These walls rested on the laboratory floor on one side and on roller supports on the other side to avoid shear effects and friction. To idealise a platform-type construction without installing any wall segments above the floor, the angle brackets were nailed to the wall below. Under the applied loading, the behaviour of the chosen test setup was assumed to be similar to a configuration with angle brackets nailed onto the walls above the floor.
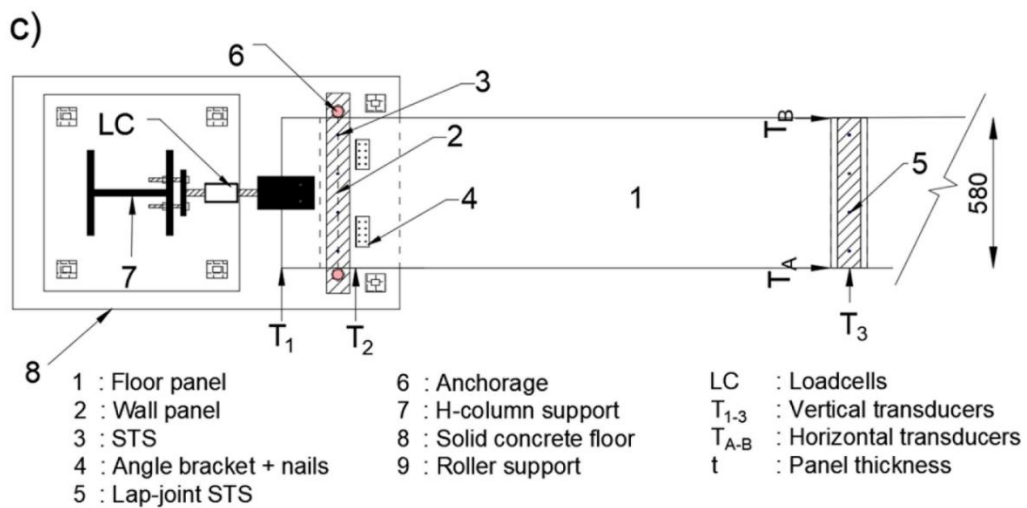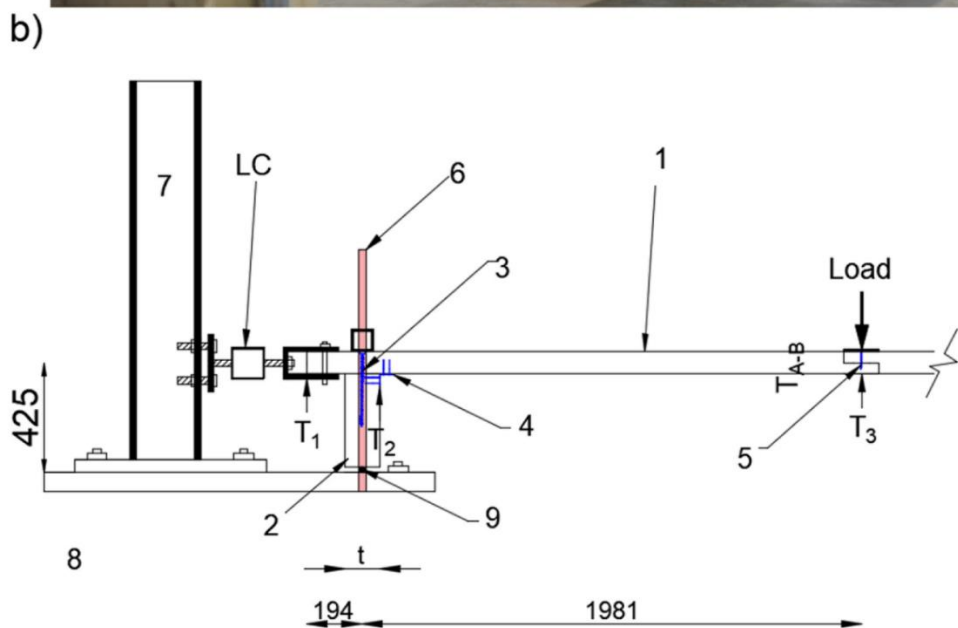
Figure 8-3: Test-setup: (a) Photo, (b) Elevation-view schematic, (c) Plan-view schematic

For disproportionate collapse investigation, previous chapters 3 and 4 demonstrated that removals of ground floor loadbearing elements are generally considered as worst-case scenarios. Since the presented tests are in isolation from its application in real building, the worst-case scenario with a maximum number of floors above the damaged level would have loads sufficiently high to ensure complete clamping of the floor systems to the wall below. Furthermore, this clamping would restrain rotation of the floor panels under the applied mid-span deflection and cause high compressive stresses at the point of rotation. To mimic the worst-case scenario, a full anchorage was applied along the width of the external walls using steel rods anchorage and bar, as illustrated in Figure 8-3, and the anchorage remained constant throughout the duration of the test.

To mimic the bays on either side providing horizontal supports, the floor assembly was laterally restrained. One load cell (LS) was installed on each end of the mass-timber floor system to measure the axial (tie) forces during the different stages of the collapse-resistance mechanisms (as per Figure 2-2). The mid-span deflection at the location of the removed internal wall was recorded using one Linear Variable Differential Transformer (LVDT) (T_3). The T_3 maximum extension was 100mm; since its recordings and those obtained from the actuator stroke were the same, the latter was validated for the initial linear condition. Beyond 100mm, the deflection was only measured by the actuator displacement until the maximum stroke of 250mm.

The recorded actuator stroke was used to define the disproportionate collapse-prevention acceptance criterion for maximum deflection (Δ). The axial displacement (opening) between the floor-to-floor connection during loading was measured by two LVDTs (T_A and T_B), to understand the compatibility between the applied Δ and the horizontal connection deformations (δ). Further LVDTs (T_1 and T_4) and (T_2 and T_5) measured the displacement caused by compression at the point

of floor rotation and the uplift at the end of the floor panels, respectively. These measurements helped validating that the anchorage forces of the same range were applied for all floor assemblies.

8.4 Results

8.4.1 Load-carrying Capacity

Figure 8-4 shows the applied vertical force against mid-span deflection for all tested floor assemblies. For Configuration 1 (*C1*), both traditional and novel floor-to-floor connections, the observed collapse-resistance mechanism followed the load-deformation stages shown in Figure 2-2a: initial condition (stage 1), compressive arching (stage 2), tensile transient stage (stage 3), and catenary action (stage 4). For *C1* assemblies, the behaviour remained linear, stage 1, for $\Delta <$ 20mm, representing 1% of the floor span (L=1,981mm). Table 8-2 includes the elastic bending stiffness values (*EI*), the maximum load during compressing arching (F_{com}), as well as the maximum load-carrying capacity (F_{max}) for all assemblies. *EI* was computed for the elastic part of the force-deflection curves between 5mm and 20mm deflection, and F_{com} was the applied load corresponding to a deflection of 45mm and 70mm for LSL/LVL and CLT, respectively. CLT *C1* assemblies were stiffer than corresponding LVL and LSL assemblies. *C1-Novel* were stiffer than *C1-Trad* for CLT and LSL assemblies, whereas for LVL assemblies was the same.

Table 8-2: Test results

Specimen - ID	EI [10^8 kNmm^2]	F_{com} [kN]	F_{max} [kN]	F_t [kN]
CLT-Trad-01	2.7	8.8	17	23
CLT-Trad-02	3.1	8.9	14	18
CLT-Novel-01	3.5	10.5	32	59
CLT-Novel-02	4.4	9.9	32	67
LVL-Trad-01	1.6	3.3	15	35
LVL-Novel-01	1.6	3.4	26	70
LSL-Trad-01	1.6	3.4	18	46
LSL-Trad-02	1.1	2.5	18	42
LSL-Novel-01	1.8	4.3	55	92
LSL-Novel-02	1.5	3.8	50	98
LSL-Cont-01	6.2	-	33	41
LSL-Cont-02	7.0	-	36	40

With the lap-joint, the effective section depth (d) was taken as half the overall panel thickness: 45mm and 70mm for LSL/LVL and CLT, respectively. Compressive arching, stage 2, was maximum at $\Delta = d$. From Figure 8-4, at $\Delta = d$, there were negligible differences between *C1-Trad* and *C1-Novel*. CLT assemblies had an average maximum load during compressive arching (F_{com} = 9.5kN) than LSL and LVL (F_{com} = 3.5kN) assemblies. At $\Delta = d$, the assemblies maintained their load-carrying capacity; the response was ductile up to $\Delta = 2 \times d$ which highlighted the beginning of the tensile transient stage 3, where the load-carrying capacity increased for all *C1* assemblies.
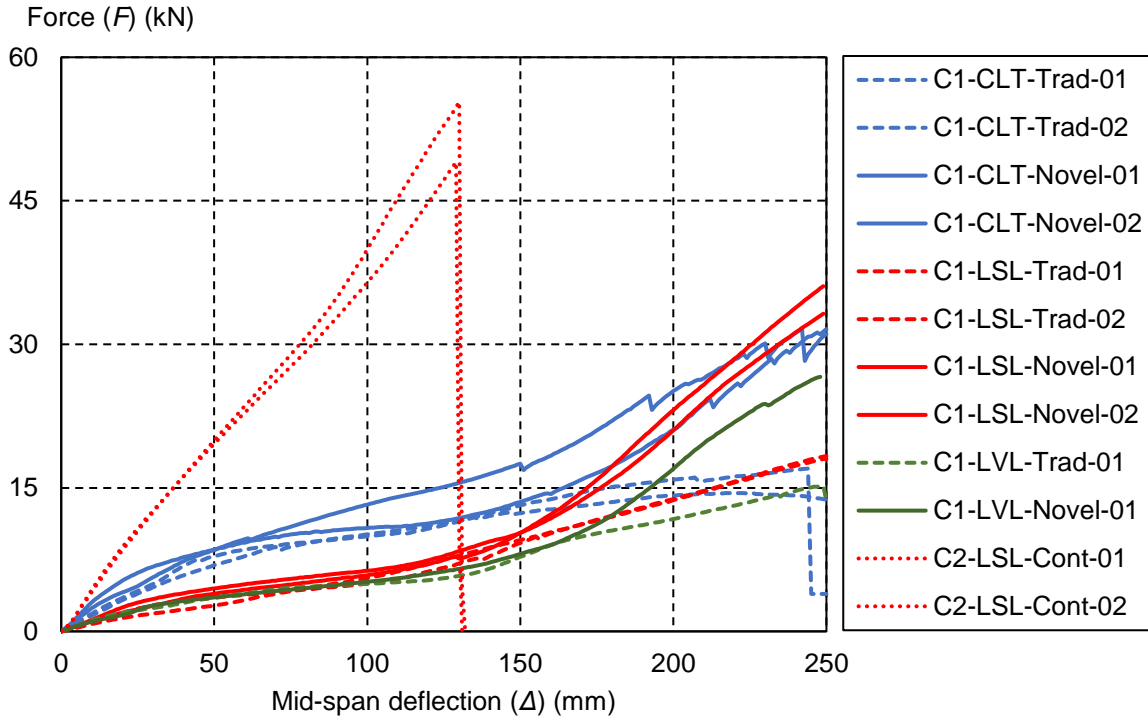
Figure 8-4: Force against applied deflection

At $\Delta = 150$mm or 8% of *L*, the load-carrying capacity for *C1-Trad* assemblies no longer increased. For *C1-Trad,* catenary action (stage 4) could not develop. Nonetheless, behaviour was still ductile until the maximum deflection was applied; with the maximum load $F_{max} \leq 18$kN. Beyond $\Delta = 150$mm, the load-carrying capacity of *C1-Novel* kept increasing; minor wood failure was observed at the maximum deflection of $\Delta = 250$mm or 13% of *L. C1-Novel* assemblies developed catenary action; with F_{max} more than double the values obtained for *C1-Trad*. For both *Novel* and *Trad* assemblies F_{max} was lower for *C1-Novel* LSL assemblies compared to CLT and LSL.

A different load deformation behaviour was observed for *C2* assemblies: the floor system was not able to develop any collapse-resistance mechanism (see Figure 2-2). Comparing the *EI*-values from Table 8-2, the *C2 LSL-Cont* assemblies were stiffer than all *C1* assemblies. The behaviour remained almost linear until brittle failure occurred at $\Delta \leq 130$mm or 6% of *L*. The recorded F_{max}

exceeded 50kN. Double span continuous floor systems were stronger and stiffer than discontinuous floors with floor-to-floor connection; nonetheless, this was in detriment of ductility. After reaching F_{max}, complete failure was observed. The observed F_{max} was in agreement with the analytical estimation for the maximum allowable load of a simply supported $(2{\times}L)$m long and 89mm thick LSL floor panel, with a bending strength of 33.3MPa (Weyerhaeuser, 2018), subjected to a point load (F_{max}).

8.4.2 Axial (tie) Forces

Figure 8-5 shows the curves of the axial tensile force (F_t) against Δ for all tested floor assemblies. F_t was the average tensile force obtained from both ends of the floor assemblies at the loadcells. Table 8-2 gives the maximum tie-force (F_t) for all tested assemblies. As F_t were recorded at the neutral axis of the floor cross-section, the loads during stage 1 ($\Delta \leq 20$mm) were negligible. The compressive forces occurring at the top fibre of the section, during compressive arching, were not recorded. The axial forces at the LCs were recorded at the centroid of the sections where the neglectable tension forces prevent inward floor movements during this stage. For *C1* assemblies, with both traditional and novel connections, it was observed that compressive arching was better developed for CLT assemblies compared to LVL and LSL. This was noted by a larger compressive area, which caused minor wood crushing parallel to the grain of the CLT assemblies, as explained in section 8.4.4.

The recorded F_t were still negligible for LVL and LSL assemblies until the peak of the compressive arching was reached ($\Delta = 45$mm). At this point, the compressive arching reduced while F_t increased, becoming significant at the end of the compressive arching (Δ=89mm and 139mm for LSL or LVL and CLT, respectively). The tensile transient stage 3 was also marked by F_t increase.

Between the maximum compressive arching and the end of the tensile transient stage, $d \leq \Delta \leq$ 150mm, the behaviours were identical for all C_1 assemblies, although F_t was highest for LSL and lowest for LVL assemblies.
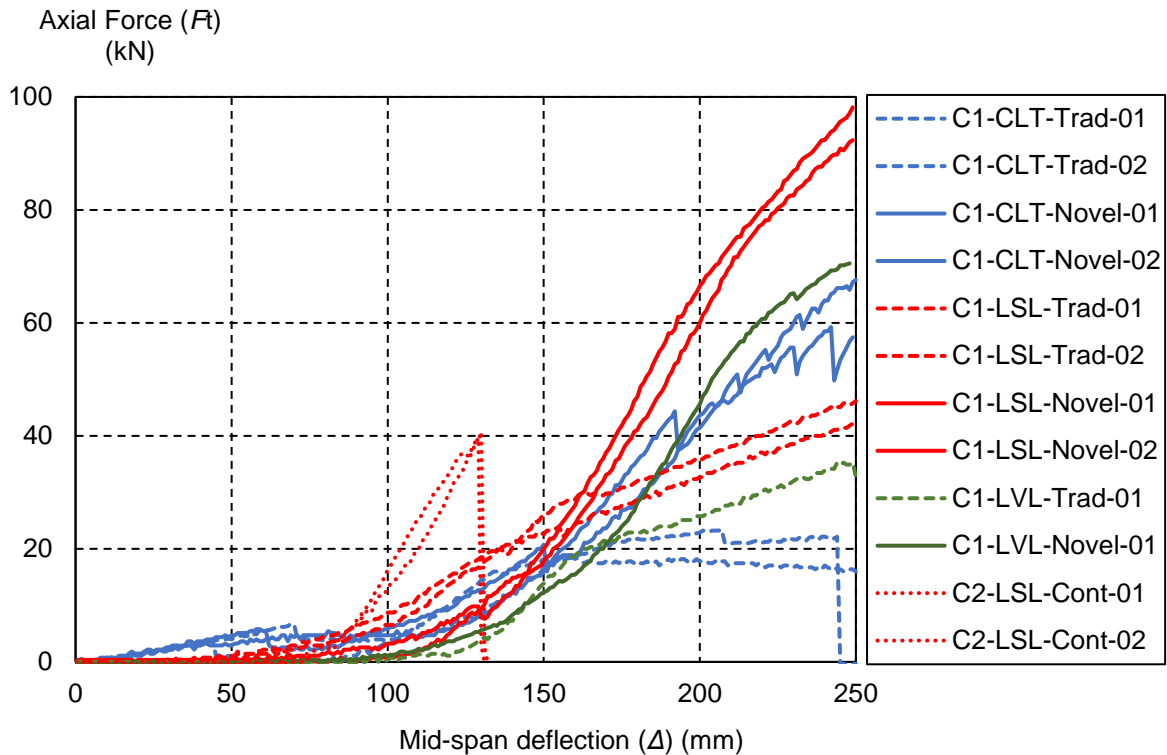
Figure 8-5: Axial tensile force against applied deflection

At $\Delta \geq 150$mm, the difference between assemblies with traditional and novel connection became noticeable. *C1-Trad* assemblies could not develop high axial loads with increase in the applied deflection. Nevertheless, ductile behaviour was noted as the magnitude of F_t was maintained while undergoing axial deformations until $\Delta = 250$mm. When $\Delta \geq 150$mm, for CLT *C1-Trad* assemblies, F_t remained almost constant until maximum Δ was attained. For LVL and LSL *C1-Trad* assemblies, F_t kept increasing, with the highest values noted for the latter, allowing the floor system to remain stable without failure. With *C1-Novel* developing catenary action at stage 4, F_t

increased linearly with increasing Δ. F_t was highest for *C1-Novel* LSL and lowest for *C1-Novel* LVL and CLT assemblies. For *C2* LSL assemblies without floor-to-floor connections, at $\Delta = 89$mm, a significant increase in F_T was noted. This was linear and suddenly dropped at failure ($\Delta = 130$mm). Although a stiffer response was observed, the recorded maximum $F_T = 40$kN was lower than in *C1* assemblies.

8.4.3 Axial Deformation, Compression and Uplift

 The recorded axial deformations (average values from T_A and T_B) at the mid-span floor-to-floor joint are plotted in Figure 8-6 with respect to the applied deflection. At the linear stage 1 ($\Delta \leq 20$mm), the recorded axial deformations were negligible, for all floor *C1* assemblies. For *C1-Trad*, at $d \leq \Delta \leq 150$mm, axial deformation increased linearly with respect to the applied deflection. The highest axial stiffness was observed for CLT specimens, whereas the lowest was observed for LSL assemblies. At $\Delta \geq 150$mm, when the floor assemblies exhibited ductile failure behaviour, the slope of the axial deformation exhibited a further increase. A different behaviour was observed for *C1-Novel* assemblies: after stage 1, the axial stiffness remained linear until the maximum deflection was attained. It must be noted that the observed plateaus at higher deflections were noted due to the extension limits of the transducers. For *C2* assemblies, no mid-span axial deformations were observed.
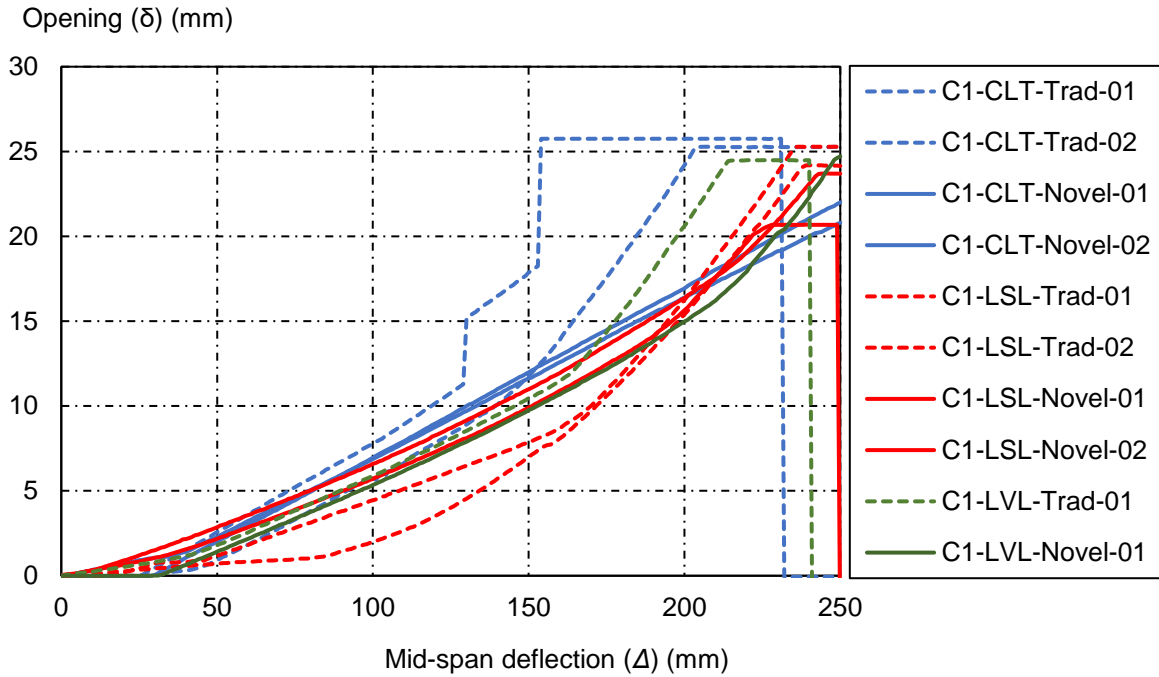
Figure 8-6: Axial deformation at the mid-span against applied deflection

Figure 8-7 shows the recorded compression deformation (average from T_2 and T_5) at the rotation point of the floor system against the applied deflection. The observed compressive deformations were linear with respect to deflection and similar for all floor assemblies. The highest compressive deformations were observed for *C1-Novel* CLT floor assemblies.
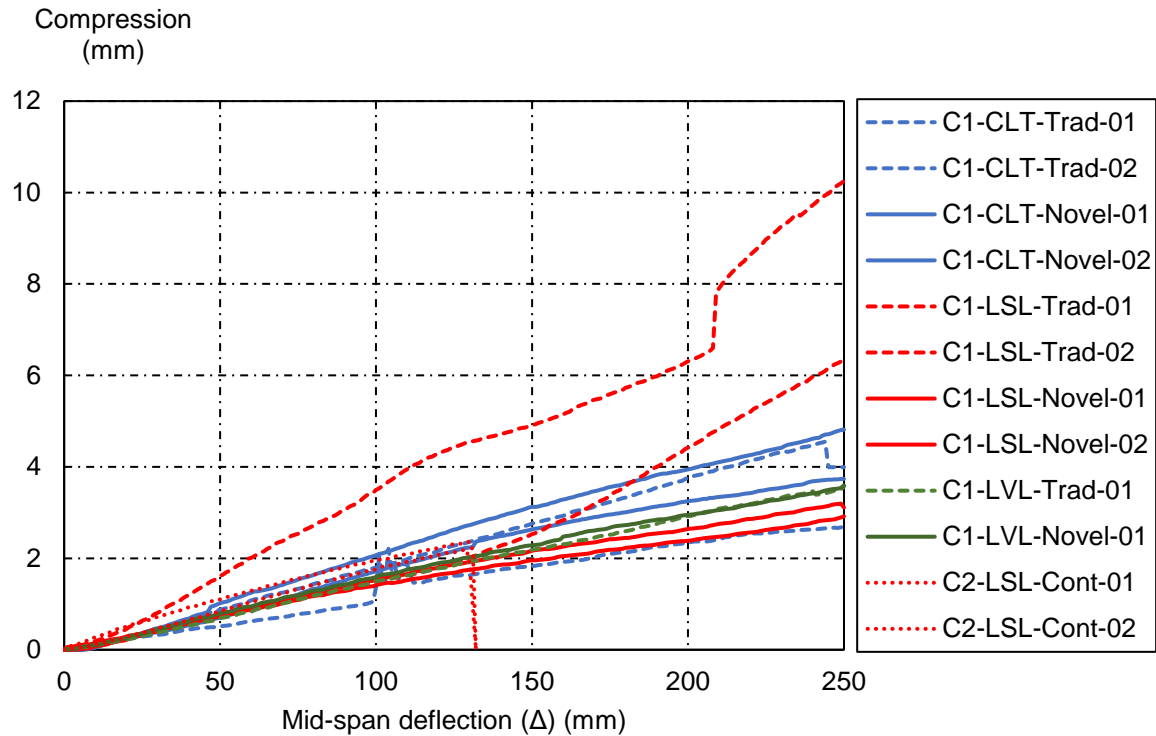
Figure 8-7: Compression at the point of rotation of the floor against applied deflection

Similar observations were made for the uplift (average from T_1 and T_4) at both ends of the floor systems, see Figure 8-8. The graph shows a linear increase of uplift with respect to the applied deflection, for all floor assemblies (*C1* and *C2*).

Friction forces and rotational restraints provided by the transverse steel elements were assumed to have no impact on the results during catenary action and were therefore not measured. However, LVDTs T_1 and T_2 measured the vertical displacement caused by compression at the point of floor rotation and the uplift at the end of the floor panel, respectively. The recorded measurements were linear with respect to the applied mid-span deflection and similar for all tested floor assemblies. Linear behaviour confirmed that full anchorage, providing rotational restraints, was maintained for the duration of the test.
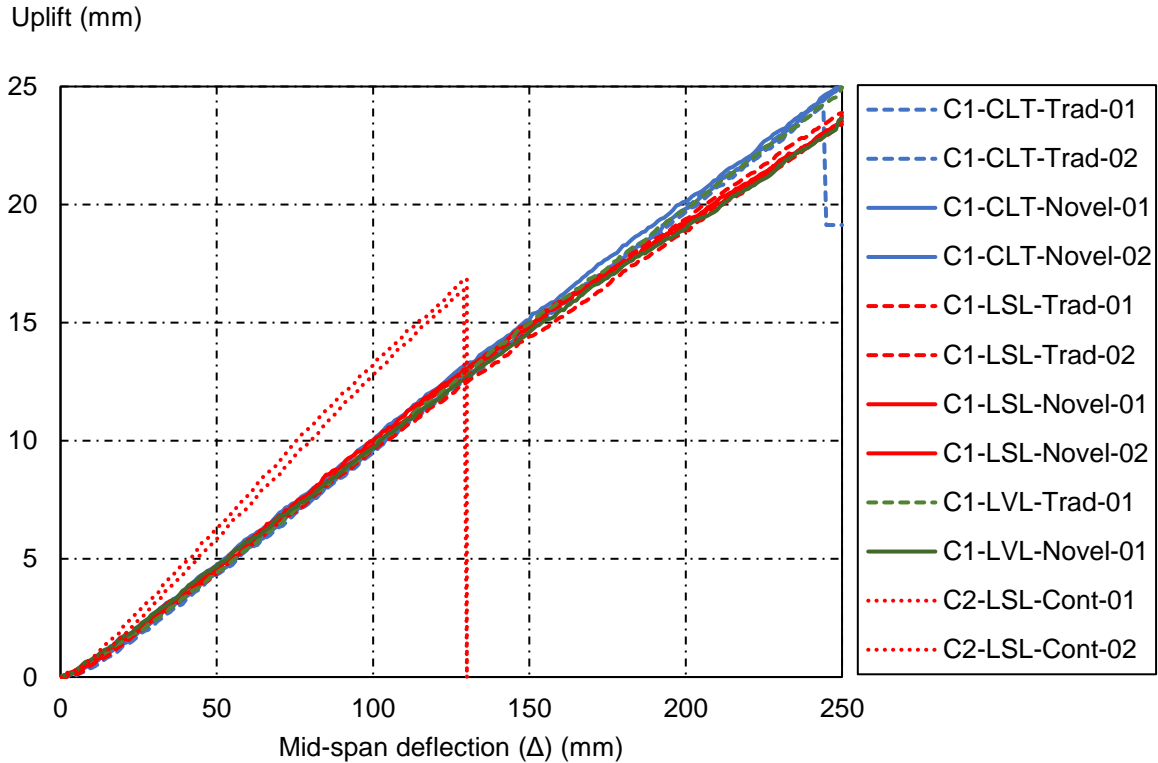
Figure 8-8: Uplift at the end of the floor system against applied deflection

8.4.4 Failure Modes

Figure 8-9 illustrates the failure modes of the floor assemblies observed at mid-span. Figure 8-9a shows the *C1* (for both *Trad* and *Novel*) CLT panels during compressive arching (stage 2) when the behaviour was governed by the compression parallel to the grain strength at the top fibres, noted by wood crushing. However, no damage was observed at the top fibres for LVL and LSL under compressive stresses, as shown in Figure 8-9b. Furthermore, the observed areas in compression were larger for CLT than for LVL or LSL panels. As stated in section 8.4.1, *C1-Trad* did not develop catenary action, this was only noted for *C1-Novel*. Figure 8-9c shows the *C1-Trad* CLT floor assemblies at $\Delta = 150$mm. There was no contact between the two floor segments in the longitudinal direction.

Figure 8-9: Failure modes at mid-span: (a) at Δ = 70mm for C1 CLT assembly; (b) at Δ=45mm for C1 LVL assembly; (c) at Δ=150mm for C1-Trad CLT assembly; (d) at Δ=150mm for C1-Trad LVL assembly; (e) at Δ=250mm for C1-Novel CLT assembly; and (f) at Δ=250mm for C1-Novel LSL assembly

After the maximum compressive arching (Δ = 70mm), separation started to occur between the two floor segments. The lap-joint provided a bearing area of one floor segment on the other and helped to avoid collapse as further axial deformation occurred at the floor-to-floor connection. The gap between the two floor segments in the longitudinal direction linearly increased with deflection. Similar behaviours were observed for *C1-Trad* LVL (see Figure 8-9d) and LSL assemblies.

C1-Novel floor assemblies developed catenary action. Figure 8-9e shows the CLT floor at Δ = 250mm for. The gap between the floor segments was smaller than for *C1-Trad* at Δ = 150mm. For *C1-Novel*, the tube connection held the floor segments together, preventing failure at larger deformations. Although similar behaviour was observed for *C1-Novel* LVL and LSL floor assemblies, at Δ = 250mm, the gap between the floor segments was bigger than in the CLT floors, see Figure 8-9f, although smaller than *C1-Trad*. Figure 8-9g illustrates the brittle failure of the *C2* LSL floor assembly, characterised by pulling of the strands in the longitudinal direction, started at the bottom of the cross-section.

The photo in Figure 8-9h illustrates a *C1-Novel* assembly under maximum deflection. At Δ =250mm, none of the *C1* floor assemblies had failed; the deflection of the floor assemblies was maintained for five minutes without noticeable changes in load. All recorded forces and deformations also remained constant. Negligible failure was observed on the floor assemblies; all mass-timber panels remained undamaged. The observed vertical deformed shape as well as behaviours were identical for all tested *C1* floor assemblies. For continuous double span *C2* floor assemblies, brittle failure was observed at Δ =130mm; the mass-timber panels broke at mid-span and were not able to maintain load beyond that deflection.

8.4.5 Connector Deformations

For all *C1-Trad* floor assemblies, the axial deformation was supplied by the STSs at the floor-to-floor connection. Figure 8-10a shows the shear failure of STSs. The addition of the steel tube, which reduced the gap between the two floor segments at the floor-to-floor connection, also prevented shearing of STSs and only deformations were observed for all *C1-Novel* assemblies, as shown in Figure 8-10b. Deformations were also noted on the steel tubes and rods. The steel rods bent, see Figure 8-10c, while the steel tubes buckled around the welding areas as shown in Figure 8-10d. This buckling, caused by the axial tensile forces keeping the two floor segments together, led to a 7mm deformation on both tubes on either side of the detailing.

Negligible deformations were observed on the floor-to-wall connections (STSs, angle brackets and nails), as shown in Figure 8-10e. The bracket bent at the same angle as the connected floor. At maximum deflection (Δ =250mm), minor bending of the nails was observed on the first row of nails on both floor and wall panels. Figure 8-10f illustrates the compression perpendicular to the grain of the LVL floor panel at the point of rotation, observed for both Trad and Novel floor assemblies. The recorded measurements from T_1 and T_2 were similar and the failure modes shown in Figure 8-10e and 11f applied to all tested *C1* floor assemblies, confirming similar rotational restraints during these tests. For *C2* LSL floor assemblies, the compression during rotation was not noticeable.

Figure 8-10: Failure modes: (a) Shear failure of STSs for C1-Trad; (b) Excessive deformation of STSs for C1-Novel; (c) Deformation of steel tube and rods; (d) Inelastic buckling of steel tube; (e) Deformation of angle brackets; and (f) Compression perpendicular to the grain of mass-timber floor

8.5 Discussion

The experimental tests confirmed that with floor-to-floor connections above the removed internal loadbearing element, mass-timber floor systems can develop load-deflection response similar to that of concrete and steel floor systems. This was noted by an initial linear condition (stage 1),

compressive arching (stage 2), tensile transient (stage 3), and catenary action (stage 4). The linear stage 1 occurred at low deflections; and it was controlled by the bending stiffness of the floor system, influenced by both the E-modulus and the cross-sectional area. Increasing the applied deflection led to stage 2. With the presence of the floor-to-floor connection, no tension developed at the bottom fibres, whereas the top fibres under compression triggered the arching thrust and resisted collapse. For the observed small deformations, the behaviour during compressive arching was ductile; the floor assemblies maintained the load-carrying capacity while undergoing further deformations without failure as shown in Figure 8-5. The maximum capacity at stage 2 was mainly influenced by the effective section depth (half the floor section because of the lap-joint), and the axial stiffness of the connection.

The observed behaviour (see Figure 8-4) of floor assemblies with traditional connections did not extend beyond stage 3 after the compressive arching became zero. Herein, the load-carrying capacity was only influenced by the axial stiffness of the lap-joint STSs connection. It is worth mentioning that floor system collapse-resistance mechanisms cannot rely on stage 2 and 3 alone, given the observed low capacities. Nonetheless, possible improvements for higher capacity at stage 2 could be considered by increasing the floor effective depth (e.g. thicker floor, using butt or spline-joints). With the addition of the novel tube connections, the floor assemblies were able to develop catenary action given the increase of the axial strength and ductility of the connection. At stage 4, the floor system load-carrying capacity linearly increased with the deflection; therefore, catenary action was the ideal collapse-resistance mechanism.

The importance of the floor-to-floor connection was noted when comparing against assemblies with continuous double span. Without discontinuity at the location of the removed loadbearing

element, brittle wood failure was observed due to the applied bending moments at larger deflection. This configuration provided high strength and high stiffness, but also highlighted the problem of continuous floor systems with respect to structural robustness. Structural integrity after element loss cannot be satisfied for continuous floors as these cannot develop collapse-resistance mechanisms that distribute the loads from the damaged to undamaged parts of the building. Consequently, for disproportionate collapse prevention design, continuous double- or triple-span mass-timber floor system is not recommended. The robustness of the tube connections could also be relevant for building rehabilitation. The holes and cuts in the floor panels were bigger than the tubes and rods to facilitate insertion and removal when damaged. Given that the floor panel remained undamaged even after large deflections, they could be re-used after replacing damaged tubes and rods.

This study confirmed that mass-timber panels remained axially rigid when developing collapse-resistance mechanisms. The axial deformations were solely supplied by floor-to-floor connections given that no damage was observed on the floor-to-wall connections. The rotational strength and ductility of the connection, provided by the steel rods, were important during stages 1 and 2. As catenary action only occurred at large deflections, the behaviour of the floor system was exclusively governed by the axial force. Here, the connection was subject to pure tension which required the detailing to be axially strong and ductile to prevent failure. This highlighted the requirement for compatibility between the axial strength and ductility of the overall system; the connection needed to be able to sustain large axial deformations while carrying the large axial forces necessary to prevent floor collapse. In addition, the tests also highlighted compatibility between the axial deformation and the applied deflection. Herein, linear relation could be assumed;

this could be estimated using trigonometry assuming that all axial deformations were supplied by the floor-to-floor connections alone.

Chapter 6 showed that optimised tube detailing can provide the required axial strength, stiffness, and ductility to trigger catenary action. *C1-Novel* assemblies developed catenary action and the load-carrying capacity was increasing linearly with the increase in the applied deflection. As explained in section 2.5.1, F_t could be estimated by linear static equilibrium, assuming a simply supported floor system. When comparing $F_{t,a}$ calculated from linear equilibrium of moments at Δ=250mm against the recorded maximum F_t from *C1-Novel* assemblies given in Table 8-2, an average nonlinear factor (*NF*) of 0.61 was obtained. Multiplying F_t calculated from equilibrium by *NF* would give an estimation of the recorded F_t values during catenary action.

Without floor-to-floor connections, the response of continuous double span mass-timber floor systems solely depended on the bending stiffness and strength of the mass-timber panel. With failure occurring at 130mm; this floor system failed at 6% of *L* deformation without providing any ductility; therefore, the design must specify smaller limits to ensure structural safety. With conventional connection detailing (STS lap-joints), failure occurred at approximately 150mm deflection, or 8% of *L*. In contrast, the floor assemblies with the novel tube connections exhibited no damage at 250mm deflection, representing 13% of *L*. It was possible that larger deflections, such as 285mm (15% of *L*), as recommended in the literature for catenary action, could also be achieved. Therefore, 8% and 15% of *L* can be proposed as acceptance criterion for mass-timber floor systems with conventional and novel floor-to-floor connection, respectively. Conventional connections consist of STSs and angle brackets. Novel connection should have sufficient axial strength and ductility to develop catenary action.

In residential and office buildings, with a typical span of 5m and maximum floor load of 3.4kPa, the floor system should be able to carry 34kN per metre width at the location of the removed element. From the obtained test results, *C1-Trad* assemblies would not have sufficient load-carrying capacity to prevent collapse. While the obtained load-carrying capacity (F_{max}>34kN) for both *C1- Novel* and *C2* assemblies would be adequate, this study demonstrated the importance of ductility. Allowing for larger deflection would reduce the required tie forces: from equilibrium ($M_z = M_r$), *C2* assemblies would require $F_{t,a}$=142kN for 6% of *L* as maximum deflection to prevent disproportionate collapse, whereas *C1-Novel* assemblies would only require 57kN, for 15% of *L* maximum deflection.

8.6 Summary

This chapter presented experimental studies of the collapse-resistance mechanisms of mass-timber floor systems resting on exterior wall panels, with deflection applied at mid-span to idealise internal wall removal. Continuous double span and discontinuous floor systems with conventional and novel connection detailing were tested. The following conclusions are drawn:

(1) The static load-deflection response for mass-timber (CLT, LSL and LVL) floor systems in platform-type construction with floor-to-floor connections is similar to that of concrete and steel systems. With specific connections, the mass-timber floor can trigger both compressive arching and catenary actions as resistance mechanisms against disproportionate collapse.

(2) Continuous double span floor panels are not robust. For conventional connection detailing with STSs, angle-brackets and nails, compressive arching is the only triggered collapse-resistance mechanism and a deflection of 8% of the floor span can be considered as acceptance criterion. Nevertheless, its resistance is low and collapse prevention measures should not rely on it.

(3) The novel tube detailing helps to trigger catenary action as collapse-resistance mechanism. The acceptance criterion for mass-timber floor system where floor-to-floor connections have sufficient axial strength and ductility can be taken as 15% of the floor span.

While the experimental tests were performed on isolated floor assemblies and not complete buildings, this paper provides a generic solution to ensure catenary action for disproportionate collapse prevention for mass-timber floor systems in platform-type construction. Further studies, e.g. finite element modelling and experimental tests at component and building levels, are required to confirm the performance of larger mass-timber systems with tube connectors under large defections.

Chapter 9: Conclusions

9.1 Main Contributions

Within the research presented in this thesis, the structural performance of mid-rise mass-timber buildings for disproportionate collapse prevention following initial damage was investigated. The goal was to develop methods that enable mass-timber buildings to trigger collapse-resistance mechanisms for structural robustness. The specific objectives were: i) perform a state-of-the-art review on current research studies as well as contemporary practice on disproportionate collapse prevention for timber buildings; ii) Assess the structural performance after initial damage of CLT platform-type construction that carry both gravity and lateral loads; iii) assess the structural performance after initial damage of CLT platform-type construction with flat-plate gravity load-resisting system; iv) evaluate possible collapse-resistance mechanisms for CLT platform-type construction, and derive the tie-force requirements for structural integrity; v) develop novel connection detailing, investigate, and optimise its performances against existing experimental test results; and vi) perform experimental testing to investigate the collapse resistance mechanism of mass-timber systems with novel tube connection detailing and compare the performance against floor systems with traditional connections. While achieving the aforementioned objectives, several milestones were reached:

1) In the first part of this research, the contemporary practice on structural design against disproportionate collapse was summarised. This section critically compared available methods and implementation of the existing design codes and guidance for concrete, steel, and timber structures, in Europe, Canada, the USA, and other countries around the world. The results from this part first highlighted the need for direct clauses in building codes to incite structural design against

disproportionate collapse. From comparison against concrete and steel designs, this section demonstrated that there is a need to explore the methods applying engineering judgments, minimum tie-force for structural integrity, and advanced analyses methods to facilitate the design against disproportionate collapse for mass-timber buildings.

2) In the second part of this research, the structural behaviour of a twelve-storey CLT platform-type construction subjected to sudden removal of internal and external ground floor loadbearing walls was investigated. Analyses were carried out at three different structural idealisations, accounting for feasibility and complexity of finite element models to understand their performance at: i) the global; ii) the component; and iii) the connection level. The results demonstrated that the applied forces and deformations required to develop collapse-resistance mechanisms were too large to be supplied by common CLT sizes and connection detailing. From reliability analysis, considered building had a high probability of disproportionate collapse. Furthermore, this section emphasised on the need for sufficient strength, stiffness, and ductility at connection level to ensure structural robustness for mass-timber buildings with platform-type construction for both gravity and lateral load-resisting systems.

3) In the third part of this research, the structural behaviour of a nine-storey flat-plate CLT floor system with GLT columns was investigated. Analyses were carried at global structural level, with all connections between structural components idealised as a set of uniaxial independent spring elements. The results of nonlinear dynamic analyses after ground floor column removals showed that hanging and catenary actions were the ideal collapse-resistance mechanisms. For this new load-path, a parameter sensitivity analysis demonstrated that the axial strength and stiffness of the column-to-column and the rotational capabilities of the floor-to-column, and the axial and shear

capacities of the floor-to-floor connections were the most relevant design parameters. The findings from this section demonstrated that novel connection detailing is required to design CLT buildings with flat-plate construction with negligible probability of disproportionate collapse.

4) In the fourth part of this research, an improved procedure to quantify the minimum longitudinal, transverse and vertical tie-force requirements was presented. This indirect approach for disproportionate collapse prevention solely applied linear-elastic static principles of engineering mechanism to satisfy force and moment equilibriums and ensure CLT platform-type buildings have sufficient strength, stiffness, and ductility to bridge over damaged walls. Herein, cantilever action of the walls and catenary action of the floor panels were identified as the main collapse-resistance mechanisms. For the considered eight-storey case-study building, typical seismic design connection detailing might be adequate to trigger cantilever action with respect to deformation demands. Nonetheless, additional considerations might be required to meet the strength demands estimated to be up to three times the seismic loads. This section also emphasised on the need for novel connection detailing to meet both axial force and deformation demands required for catenary action.

5) In the fifth part of this research, an optimisation procedure which can be applied for a wide range variety of design problems as an aid to optimise existing and novel connections as well as structural systems and assemblies for a given target performance was presented. FE analyses investigated the performance of a novel connection detailing consisting of steel tube and rods inserted in CLT panels. Considering a capacity-based design approach to avoid brittle wood failure, sensitivity analyses of the main parameters of the detailing followed by subsequent optimisation were done to reach a target performance. Subsequently, novel connection detailing

for disproportionate collapse prevention was proposed. Herein, steel tubes were implemented as a floor-to-floor connection to transfer the axial and deformations demands for catenary action, and as column-to-column connector to trigger hanging action.

6) In the sixth part of this research, experimental tests to examine static responses of mass-timber floor systems under the idealised internal wall removal were conducted. Testing was performed on continuous double span, and discontinuous floor assemblies with both conventional and novel steel tube floor-to-floor connection detailing. The results showed low safety level for continuous floor systems as their behaviours depended on the maximum bending resistance of the panels. For assemblies with conventional floor-to-floor connections, without sufficient axial strength and ductility, ductile failure at large deformation was observed after compressive arching. It was shown that the addition of steel tubes and rods enables to trigger catenary action, where the floor systems maintained high load-carrying capacity while undergoing large deflections for disproportionate collapse prevention.

9.2 Future Research

This thesis presented numerical and analytical analyses followed by experimental tests which enabled mass-timber buildings to trigger resistance mechanisms against disproportionate collapse. To safely expand the application of mass-timber constructions to tall buildings as well as post-disaster, military, federal structures, with structural irregularities, areas for further studies were identified from the outcomes of this thesis:

1) Advanced analyses at global level, accounting for both dynamic and nonlinear behaviours, are required. Investigations should focus on the structural responses after element removal for tall and irregular mass-timber buildings with different structural concepts including post-and-beam,

truss, platform-type and balloon wall constructions. Herein, the methodology could consider either a three-level structural idealisation or an idealisation of connections as set of uniaxial spring elements.

2)   Advanced 3D modelling at component level, accounting for both geometric and material nonlinearities, is required. Investigations should focus on the structural behaviours of existing connection detailing to determine realistic axial, shear and rotational stiffness at both elastic and plastic stages as well as the interaction between them. These stiffnesses would then be used to simplify the advanced modelling at global level.

3)   Comparison of the performance between different structural concept for tall mass-timber buildings, with respect to structural robustness, is required. This could come as a design chart or procedure listing the different structural systems from the most to the least robust. This guideline should also include advantages and disadvantages of the considered structural concept for disproportionate collapse prevention given the initial damage.

4)   The tie-force procedure should be extended to account for 3D action of the floor systems, nonlinear geometric and material properties, as well as other structural concepts for mid-rise mass-timber buildings. This could be achieved by advanced 3D modelling of the structural systems at component level, including connection to capture realistic behaviour.

5)   Novel connection detailing with adequate strength, stiffness, and ductility to trigger anticipated collapse-resistance mechanisms for other structural concepts for tall mass-timber buildings need to be developed. The detailing should be practical and economical, based on the capacity-based design approached, to avoid brittle wood failure.

6) Scaled testing for mass-timber floor systems are required, including different floor-to-floor and floor-to-wall connection detailing, floor depths, with and without concrete topping. Focus would be on the contributions of their respective axial and rotational stiffnesses, effective depth, as well as possible composite action with concrete topping.

7) For the different structural concepts for tall mass-timber building, large scale testing of the floor systems is required. The test assemblies should consider adjacent bays surrounding the damaged floors to capture their contributions towards collapse resistance. Initial damage should include static and dynamic element removal at different locations in plan and elevation.

8) Experimental testing and advanced 3D modelling are required to investigate static and dynamic load-displacement responses for different structural concepts with focus on possible compressive arching and catenary action to define acceptance criteria for collapse prevention.

9) A database for all previous disproportionate collapses incidents is required to quantify the probability of extreme events and to identify economic structural design solutions given the probability of the worst-case extreme events.

Bibliography

Abrahamsen, R.B. (2017). Mjostarnet – Construction of an 81m tall timber building. 23. International Holzbau – Forum IHF, Garmisch-Partenkirchen, Germany, Dec. 06-08, 2017.

Abrahamsen, R.B., & Malo, K.A. (2014). Structural design and assembly of "Treet" – a 14-storey timber residential building in Norway. World Conference on Timber Engineering, Quebec City, Canada, Aug. 10-14, 2014.

Ali, M.M., & Moon, K,S. (2011). Structural developments in tall buildings: current trends and future prospects. Architectural Science Review 50 (3): 205-223.

American National Standards Institutes (ANSI). (2018). ANSI/APA PRG 320-2018: Standard for performance-rated cross-laminated timber. 2018th ed. APA-The Engineered Wood Association, Tacoma, USA.

American Society for Testing and Materials (ASTM). (2011). ASTM E 2126-2011. Standard test methods for cyclic (reverse) load test for shear resistance of vertical elements of the lateral force resisting systems for buildings. ASTM, Conshohocken, USA.

ANSYS. (2015). ANSYS mechanical APDL User's manual. © ANSYS.

Arup. (2011). Review of international research on structural robustness and disproportionate collapse. Department for Communities and Local Government, London, UK.

American Society of Civil Engineers (ASCE). (2013). ASCE/SEI 7: Minimum design loads for buildings and other structures. ASCE Standards, Reston, USA.

Atlas Tubes Canada. (2018). "Material test report" <https://www.metalsupermarkets.com/> (July 26, 2018).

Australia/New Zealand Standards (AS/NZS). (2002). AS/NZS 1170.0:2002 Structural design action – General principles. Standards Australia Limited / Standards New Zealand, June 2002.

Baker, J.W., Schubert, M., & Faber, M.H. (2008). On the assessment of robustness. Structural safety 30 (3): 253-267.

Barrett, J.D., & Foschi, R.O. (1977). Shear strength of uniformly loaded dimension lumber. Canadian Journal of Civil Engineering 4 (1): 86-95.

Bartlett, F.M., Hong, H.P., & Zhou, W. (2003). Load factor calibration for the proposed 2005 edition of the National Building Code of Canada: Statistics of loads and load effects. Canadian Journal of Civil Engineering 30 (2): 429-439.

Building Code of British Columbia (BCBC). (2012). Building Code of British Columbia. Office of Housing and Construction Standards, Victoria, Canada.

Bhat, P. (2013). Experimental investigation of connection for the FFTT timber-steel-hybrid system. MASc Thesis, University of British Columbia, Vancouver, Canada.

Brandner, R., Flatscher, G., Ringhofer, A., Schickhofer, G., & Thiel, A. (2016). Cross laminated timber (CLT): overview and development. European Journal of Wood and Wood Products 74 (3): 331-351.

Brett, C., & Lu, Y. (2013). Assessment of robustness of structures: current state of research. Frontiers of Structural and Civil Engineering 7 (4): 356-368.

Buchanan, A., & Abu, A. (2017). Structural design for fire safety. 2nd ed. New York: Wiley Publishing Ltd.

Buchanan, A., Ostman, B., & Frangi, A. (2014). Fire resistance of timber structures. National Institute of Standards and Technology, Gaithersburg, USA.

Byfield, M., Mudalige, W., Morison, C., & Stoddart, E. (2014). A review of progressive collapse research and regulations. Proceedings of the Institution of Civil Engineers – Structures and Buildings 167 (8): 447-756.

Canadian Standards Association (CSA). (2017). Engineering design in wood CSA-O86-14. CSA Group, Mississauga, Canada.

Canadian Wood Council (CWC). (2017). Wood design manual 2017. Canadian Wood Council, Ottawa, Canada.

Canadian Wood Council (CWC). (2011). Introduction to wood design – A learning guide to complement the wood design manual 2011. Canadian Wood Council, Ottawa, Canada.

Casagrande, D., Doudak, G., Mauro, L., & Polastri, A. (2018). Analytical approach to establish the elastic behaviour of multipanel CLT shear walls subjected to lateral loads. Journal of Structural Engineering 144 (2): 04017193. doi:10.1061/(ASCE)ST.1943-541X.0001948.

Ceccotti, A., & Follesa, M. (2006). Seismic behaviour of multi-storey X-Lam buildings. COST action E29 Workshop on Earthquake Engineering on Timber Structures SEI, Coimbra, Portugal, Nov. 9-10, 2016.

Chen, Y-L., Huang, L., Lu, Y-Q., Deng, L., & Tan, H-Z. Assessment of structural robustness under different events according to vulnerability. Journal of performance of constructed facilities 30 (5): 04016004. Doi:10.1061/(ASCE)CF.1943-5509.0000854.

City of Vancouver. (2018). Zero emissions building. < https://vancouver.ca/green-vancouver/zero-emissions-buildings.aspx> (Oct. 25, 2018).

Cormie, D., Mays, G., & Smith, P. (2012). Blast effects on buildings. 2nd ed. London: ICE Publishing

Canadian Standards Association (CSA). (2012). Design and assessment of buildings subjected to blast loading Standard S850. CSA Group, Mississauga, Canada.

Department of Defence (DoD). (2013). UFC 4-023-03. Unified Facility Criteria -Design of buildings to resist progressive collapse. Department of Defence, Washington, DC, USA.

Diestsch, P., & Brandner, R. (2015). Self-tapping screws and threaded rods as reinforcement for structural timber elements – A state-of-the-art report. Construction and Building Materials 97: 78-89.

Driver, R.G. (2014). Canadian disproportionate collapse design provisions and recent research developments. ASCE Structures Congress 2014, Boston, USA, April 3-5, 2014.

Dynardo Dynamic Software and Engineering GmbH. (2017). OptiSlang robust design optimisation (RDO). © DYNARDO GmbH.

Dynardo Dynamic Software and Engineering GmbH. (2016). Multiplas-elastoplastic material modelds for ANSYS: general multisurface plasticity User's manual. © DYNARDO GmbH.

EN 1990. (2010). Basic of structural design. CEN European Committee for Standardisation, Brussels, Belgium.

EN 1991-1-1. (2009). General actions – density, self-weight, imposed loads for buildings. CEN European Committee for Standardisation, Brussels, Belgium.

EN 1991-1-7. (2006). Actions on structures – Part 1-7: Accidental actions. CEN European Committee for Standardisation, Brussels, Belgium.

EN 1995-1-1. (2008). Design of timber structures – Part 1-1: General – common rules and rules for buildings. CEN European Committee for Standardisation, Brussels, Belgium.

Edri, I., Feldgun, V., Karinski, Y.S., & Yankelevsky, D. (2018). The balst load acting on a structure in an internal explosion scenario. ASCE Structures Congress 2018, Fort-Worth, USA, April 19-21, 2018.

Ellingwood, B.R. (2002). Load and resistance factor criteria for progressive collapse design. Georgia Institute of Technology, Atlanta, USA.

Ellingwood, B.R. (2006). Mitigating risk from abnormal loads and progressive collapse. Journal of Performance of Constructed Facilities 20 (4): 315-23. doi:10.1061/ASCE0887-3828200620:4315.

Ellingwood, B.R., & Dusenberry, D.O. (2005). Building design for abnormal loads and progressive collapse. Computer-aided Civil and Infrastructure Engineering 20 (3): 194-205.

Ellingwood B.R., MacGregor, J.G., Galambos, T.V., & Corner, C. (1982). Probability-based load criteria: Load factors and load combination. Journal of the Structural Division 108 (5): 978-997.

Ellingwood, B.R., Smilowitz, R., Dusenberry, D.O., Duthinh, D, Lew, H.S., & Carino, N.J. (2007). Best practices for reducing the potential for progressive collapse in buildings. National Institute of Standards and Technology – Technology Administration – US Department of Commerce, NISTIR 7396.

ETA-06/0106. (2008). Three-dimentaional nailing plate (timber-to-timber/timber-to-concrete or steel angle bracket). European Technical Approval. Deutsches Institut fuer Bautechnik, Berlin, Germany.

ETA-11/0190. (2011). Wurth self-tapping screws. European Technical Approval. Deutsches Institut fuer Bautechnik, Berlin, Germany.

Fast, P., & Jackson, R. (2017). Case study: University of British Columbia's 18-storey tall wood house at Brock Commons. International Association for Bridge and Structural Engineering, IABSE Symposium, Vancouver, Canada, Sept. 21-23, 2017.

Follesa, M. (2015). Seismic design of timber structures – A proposal for revision of Chapter 8 of Eurocode 8. PhD Thesis, Universita degli Studi di Cagliari, Sardinia, Italy.

Forest Products Laboratory. (2010). Wood handbook – Wood as an engineering material. General Technical Report FPL-GTR-190. Centenial edition. Madison: Department of Agriculture, Forest Service, Forest Products Laboratory.

Fragiacomo, M., Dujic, B., & Sustersic, I. (2011). Elastic and ductile design of multi-storey crosslam massive wooden buildings under seismic actions. Engineering Structures 33 (11): 3043-3053.

Frühwald, E., Serrano, E., Toratti, T., Emilsson, A. & Thelandersson, S. (2007). Design of safe timber structures – How can we learn from structural failures in concrete, steel, and timber? (Report TVBK-3053). Lund University, Lund, Sweden.

Frühwald, E.H. (2011). Analysis of structural failures in timber structures: Typical causes for failure and failure modes. Engineering Structures 33 (11): 2978-2982.

Fu, F. (2010). 3-D nonlinear dynamic progressive collapse analysis of multi-storey steel composite frame buildings – Parametric study. Engineering Structures 32 (12): 3974-3980.

Gagnon, S., & Pirvu, C. (2011). CLT handbook: Cross-laminated Timber. FPInnovations, Quebec, Canada.

Gavric, I., Fragiacomo, M. & Ceccotti, A. (2014). Cyclic behaviour of typical metal connectors for cross-laminated (CLT) structures. Materials and Structures. doi.org/10.1617/s11527-014-0278-7.

Gavric, I., Fragiacomo, M. & Ceccotti, A. (2015). Cyclic behaviour of CLT wall systems: Experimental tests and analytical prediction models. Journal of Structural Engineering 141 (11): 04015034. doi:10.1061/(ASCE)ST.1943-541X.0001246.

GCWood. (2017). Green construction through wood program. < https://www.nrcan.gc.ca/forests/federal-programs/gcwood/20046> (Dec. 10, 2018).

General Service Administration (GSA). (2013). Progressive collapse analysis and design guidelines for new Federal office buildings and Major modernisation projects. General Service Administration, Washington, DC, USA.

Gong, Y. (2010). Analysis and design for the resilience of shear connections. Canadian Journal of Civil Engineering 37 (12): 1581-1589.

Google. (2018). Google-Forms. < https://www.google.ca/forms/about/ > (May 20, 2018).

Green, M., & Karsh, E. (2012). Tall wood – The case for tall wood buildings. Wood Enterprise Coalition, Vancouver, Canada.

Grosse M. (2005). Zur numerischen Simulation des physikalisch nichtlinearen Kurzzeittragverhaltens von Nadelholz am Beispile von Holz-Beton-Verbundkonstruktionen (In German). Doctoral Dissertation, Bauhaus University, Weimar, Germany.

Gross, J.L., & McGuire, W. (1983). Progressive collapse resistance design. Journal of Structural Engineering 109 (1). doi.org/10.1061/(ASCE)0733-9445(1983)109:1(1).

Gudmundsson, G.V., & Izzuddin, B.A. (2010). The 'suden column loss' idealisation for disproportionate collapse assessment. The Structural Engineer 88 (6): 22-26.

Hamburger, R. & Whittaker, A. (2004). Design of steel structures for blast-related progressive collapse resistance. Modern Steel Construction 44 (3): 45-51.

Harte, A. & Fragiacomo, M. (2010). COST action E55 – Modelling of the performance of timber structures: 6th workshop. University of Ljubljana, Ljubljana, Slovenia.

Hess, P.E., Bruchman, D., Assakkaf, I.A., & Ayyub, B.M. (2002). Uncertainties in material and geometric strength and load variables. Naval Engineers Journal 114 (2): 139-166.

Hewson, N. (2016). Robustness in Structures. Forest and Wood Products Australia Limited, Melbourne, Australia.

Hochreiner, G., Füssl, J. & Eberhardsteiner, J. (2013). Cross-laminated timber pates subjected to concentrated loading. International Journal for Experimental Mechanics 50 (1): 68-81.

Hoogenboom, P. & Spaan, R. (2005). Shear stiffness and maximum shear stress of tubular members. International Offshore and Polar Engineering Conference, Seoul, Korea, June 19-24, 2005.

Hossain, A., Danzig, I., & Tannert, T. (2016). Cross-laminated timber shear connections with double-angled self-tapping screw assemblies. Journal of Structural Engineering 142 (11): 1-9. doi:10.1061/(ASCE)ST.1943-541X.0001572.

Hossain, A., Popovski, M., & Tannert, T. (2018). Cross-laminated timber connections assembled with a combination of screws in withdrawal and screws in shear. Engineering Structures 168 (1): 1-11.

Huber, J.A.J., Ekevad, M., Berg, S., & Girhammar, U.A. (2018a). Assessment of connections in cross-laminated timber buildings regarding structural robustness. World Conference on Timber Engineering (WCTE), Seoul, South Korea, Aug. 20-23, 2018.

Huber, J.A.J, Ekevad, M., Berg, S., & Girhammar, U.A. (2018b). Structural robustness and timber buildings – A review. Wood Material Science 7 Engineering. doi:10.1080/17480272.2018.1446052.

IStructE. (2010). Practical guide to structural robustness and disproportionate collapse in buildings. The Institution of Structural Engineers, London, UK.

Izzi, M., Casagrande, D., Bezzi, S., Pasca, D., Follesa, M., & Tomasi, R. (2018). Seismic behaviour of cross-laminated timber structures: A state-of-the-art review. Engineering Structures 170 (1): 42-52.

Jeitler, G., Augustin, M., & Schickhofer, G. (2016). Mechanical properties of glied laminated timber and cross laminated timber produced with wood species Birch. World Conference on Timber Engineering (WCTE), Vienna, Austria, Aug. 22-25, 2016.

Jessome, A.P. (1977). Strength and related properties of woods grown in Canada. Eastern Forest Products Laboratory, Ottawa, Canada.

Joebstl, R.A., Bogensperger, T., & Schickhofer, G. (2008). In-plane shear strength of cross laminated timber. International Council for Research and Innovation in Building and Construction. Working Commission W18- Timber Structures, St. Andrews, Canada.

Joebstl, R.A., Bogensperger, T., & Schickhofer, G. (2006). A contribution to the design and system effect of cross laminated timber (CLT). International Council for research and Innovation in Building and Construction. Working Commission W18 – Timber Structures, Florence, Italy.

Kelley, K., Clark, B., Brown, V., & Sitzia, J. (2003). Good practice in the conduct and reporting of survey research. International Journal for Quality in Health Care 15 (3): 261-266.

Khandelwal, K. El-Tawil, S., & Sadek, F. (2009). Progressive collapse analysis of seismically designed steel braced frames. Journal of Constructional Steel research 65 (3): 699-708.

Kirkegaard, P., Sorensen, J.D., Cizmar, D., & Rajcic, V. (2011). System reliability of timber structures with ductile behaviour. Engineering Structures 33 (11): 3093-3098.

Kohler, J. (2006). Reliability of timber structures. PhD Thesis, Swiss Federal Institute of Technology, Zurich, Switzerland.

Krauthammer, T., Hall, R.L., Woodson, S.C., Baylot, J.T, & Hayes, J.R. (2002). Development of progressive collapse analysis procedure and condition assessment for structures. National Workshop on Prevention of Progressive Collapse in Rosemont, Multizards Mitigation Council of the National Institute of Buildin Science, Pennsylvania State University, USA.

Lam, F., Yee, H., Barrett, J.D. (1997). Shear strength of Canadian softwood structural lumber. Canadian Journal of Civil Engineering 24 (3): 419-430.

Lew, H.S. (2003) Best practices guidelines for mitigation of building progressive collapse. Building and Fire Research Laboratory, National Institute of Standards and Technology, Gaithersburg, USA.

Li, Y., Xinzheng, L., Guan, H., & Ye, L. (2011b). An improved tie force method for progressive collapse resistance design of reinforced concrete frame structures. Engineering Structures 33 (10): 2931-2942.

Louisiana Pacific Corporation. (2018). LP SolidStart laminated strand lumber (LSL) and laminated veneer lumber (LVL). <https://lpcorp.com> (Aug. 14, 2018).

Lyu, C., Gilbert, B., Gunala, S., Karampour, H., Underhill, I., Masaeli, M., et al. (2018). Progressive collapse (Robustness) behaviour of mid-rise mass-timber frame buildings. World Conference on Timber Engineering (WCTE), Seoul, South Korea, Aug. 20-23, 2018.

Macleod, I.A. (2014). Modern structural analysis: supplementary information on modelling. London: Thomas Telford Ltd.

Mahendran, M. (1996). The modulus of elasticity of steel – It is 200GPa? 13th International Speciality Conference on Cold-Formed Steel Structures, St Louis, USA, Oct. 17-18, 1996.

Main, J., Bao, Y., Sadel, F., & Lew, H. (2011). Experimental and computational assessment of robustness of steel and reinforced concrete framed buildings. Structures Group, Engineering Laboratory, National Institute of Standards and Technology, Gaithersburg, USA.

Milner, M., Bullock, M., & Pitts, G. (2003). Multi-storey timber frame buildings: A design guide 1st ed. London: BRE.

Moore, D.B. (2005). The UK and European regulations for accidental actions. Prevention of progressive collapse: Report on the July 2005 National Workshop and recommendations for future effort. National Institute of Building Sciences, Washington, DC, USA.

Most, T., & Will, J. (2012). Robustness design optimisation in industrial virtual product development. 5th International Conference on Reliable Engineering Computing, Brno, Czech, June 13-15, 2012.

MyTiCon. (2017). Structural screw -design guide. <https://www.my-ti-con.com> (Oct.25, 2018).

NBCC. (2015). National Building Code of Canada 2015, Canadian Commission on Building and Fire Codes. National Research Council of Canada, Ottawa, Canada.

NBCC. (2010a). National Building Code of Canada 201a, Canadian Commission on Building and Fire Codes. National Research Council of Canada, Ottawa, Canada.

NBCC. (2010b). User's guide-NBC 2010, Structural commentaries (Part 4 of Division B). Ottawa: Canadian Commission of Buildings and Fire Codes, National Research Council Canada.

Olaniyi, A., Rahmn, M., & Hussain, B. (2017). Dynamic response of reinforced concrete bridge piers subjected to combined axial and blast loading. ASCE Structures Congress, Denver, USA, April 6-8, 2017.

Patel, B.R. Progressive collapse analysis of RC buildings using non-linear static and non-linear dynamic method. International Journal of Emerging Technology and Advanced Engineering 4 (9): 503-507.

Pei, S., van de Lindt, J.W., Popovski, M., Berman, J.W., Dolan, J.D., Ricles, J., et al. (2016). Cross-laminated timber for seismic regions: Progress and challenges for research and implementation. Journal of Structural Engineering 142 (4):E2514001. doi:10.1061/(ASCE)ST.1943-541X.0001192.

Pei, S., Popovski, M., & van de Lindt, J.W. (2013). Analytical study on seismic force modification factors for cross-laminated buildings for NBCC. Canadian Journal Civil Engineering 40 (9):887–96.

Peixoto, R. Seif, M., & Vieira, Jr.L.C.M. (2017). Double-shear tests of high-strength structural bolts at elevated temperatures. Fire Safety Journal 94: 8-21.

Popovski, M., Chen, Z., Gafner, B. (2016). Structural behaviour of point supported CLT floor systems. World Conference on Timber Engineering (WCTE), Vienna, Austria, Aug. 22-25, 2016.

Popovski, M., & Gavric, I. (2015). Performance of a 2-story CLT house subjected to lateral loads. Journal of Structural Engineering 142 (4):E4015006. doi:10.1061/(ASCE)ST.1943-541X.0001315.

Praxair Inc. (2018). Praxair's StarGold C-20 and C-25. <https://www.praxair.com> (Sept. 13, 2018).

Ramage, M.H., Burridge, H., Busse-Wicher, M., Fereday, G., Reynolds, T., Shah, D.U., et al. The wood from the trees: The use of timber in construction. Renewable and Sustainable Energy Reviews 68 (1): 333-359.

Rinaldin, G., & Fragiacomo, M. (2016). Non-linear simulation of shaking-table tests on 3- and 7-storey X-Lam timber buildings. Engineering Structures 113:133–48.

Ruth, P., Marchand, K.A., & Williamson, E.B. (2006). Static equivalency in progressive collapse alternate path analysis: reducing conservatism while retaining structural integrity. Journal of Performance of Constructed Facilities 20 (4):349–64. doi:10.1061/(ASCE)0887-3828(2006)20:4(349).

Sadek, F., Main, J., Lew, H., Robert, S., Chiarito, V., & El-Tawil, S. (2011). An Experimental and Computational Study of Steel Moment Connections under a Column Removal Scenario. National Institute of Standards and Technology, Gaithersburg, USA.

Sahin, M. (2005). Joining with friction welding of high-speed steel and medium-carbon steel. Journal of Materials Processing Technology 168 (2):202–210.

Schneider, J. (2015). Conventional and novel timber steel hybrid connections: testing, performance and assessment. PhD Thesis, University of British Columbia, Vancouver, Canada.

Schneider, J., Shen, Y., Stiemer, S.F., & Tesfamariam, S. (2015). Assessment and comparison of experimental and numerical model studies of cross-laminated timber mechanical connections under cyclic loading. Construction and Building Material 77:197–212.

Schneider, J., Tannert, T., Tesfamariam, S., & Stiemer, S.F. (2018). Experimental assessment of a novel steel tube connection in cross-laminated timber. Engineering Structures 177:283–90.

Schultz, D.M., Burnett, E.F.P., & Fintel, M. (1977a). Design and construction of large-panel concrete structures. Report 4: A design approach to general structural integrity. Portland Cement Association, Washington, DC, USA.

Schultz, D.M., Burnett, E.F.P., & Fintel, M. (1977b). Design and construction of large-panel concrete structures. Report 2: A design approach to general structural integrity. Portland Cement Association, Washington, DC, USA.

Shahnewaz, Md., Tannert, T., & Alam, S. (2018). In-plane strength and stiffness of cross-laminated timber shear walls. Buildings 2018, 8,100. doi:10.3390/buildings8080100.

Simpson Strong-Tie. (2017). Straps and Ties | Simpson Strong-Tie. Straps Ties 2017. <https://www.strongtie.com/strapsandties_woodconnectors/category> (Nov. 14, 2017).

SOM. (2013). Timber tower research project. Final Report. Skidmore, Owings & Merrill LLP, Chicago, USA.

Sørensen, J.D. (2011). Framework for robustness assessment of timber structures. Engineering Structures 33 (11):3087–92.

STA. (2017). STA Advice Note 14 - Robustness of CLT structures. London: Structural Timber Association.

Starossek, U. (2006). Progressive collapse of structures: nomenclature and procedures. Structural Engineering International 16 (2):113–117.

Starossek, U., & Haberland, M. (2010). Disproportionate collapse: Terminology and procedures. Journal of Performance of Constructed Facilities 24 (6):519–28. doi:10.1061/(ASCE)CF.1943-5509.0000138.

Steiger, R., & Gulzow, A. (2009). Validity of bending tests on strip-shaped specimens to derive bending strength and stiffness properties of Cross Laminated Timber (CLT). International Council for Research and Innovation in Building and construction. Working Commission W18 - Timber Structures, Dubendorf, Switzerland.

Stevens, D., Crowder, B., Sunshine, D., Marchand, K., Smilowitz, R., Williamson, E., et al. (2011). DoD Research and Criteria for the Design of Buildings to Resist Progressive Collapse. Journal of Structural Engineering 137 (9):870–80. doi:10.1061/(ASCE)ST.1943-541X.0000432.

Stevens, D., Martin, E., Williamson, E.B., Mckay, A., & Marchand, K.A. (2003). Recent developments in progressive collapse design. Protection Engineering Consultants doi:10.1016/0306-2619(86)90066-8.

Stevens, D.J. (2008). Assessment and proposed approach for tie forces in frames and load-bearing wall structures. Protection Engineering Consultants, Texas, USA.

Structurlam. (2016). Crosslam CLT - Technical design guide. < http://www.structurlam.com/wp-content/uploads/2016/10/CrossLam-CLT-CA-Design-Guide-1.pdf> (May 20, 2016).

Stylianidis, P.M. (2011). Progressive collapse response of steel and composite buildings. PhD Thesis. Department of Civil and Environmental Engineering, Imperial College London, UK.

Stylianidis, P.M., Nethercot, D.A., Izzuddin, B.A., & Elghazouli, A.Y. (2016). Study of the mechanics of progressive collapse with simplified beam models. Engineering Structures 117:287–304.

Talabi, S.I., Owolabi, O.B., Adebisi, J.A., & Yahaya, T. (2014). Effect of welding variables on mechanical properties of low carbon steel welded joint. Advances in production Engineering & Management 9 (4): 181-186.

Tannert, T., Follesa, M., Fragiacomo, M., Gonzalez, P., Isoda, H., Moroder, D. et al. (2018). Seismic design of cross-laminated timber buildings. Wood & Fiber 50:3-26.

Tannert, T., & Haukaas, T. (2013). Probabilistic models for structural performance of rounded devetail joints. Journal of Structural Engineering 139 (9):1478–88. Doi.org/10.1061/(ASCE)ST.1943-541X.0000744.

Tavakoli, H.R., Rashidi, A.A., & Abdollahzadeh, G.R. (2012). 3-D Nonlinear Static Progressive Collapse Analysis of Multi-story Steel Braced Buildings. 15th World Conference on Earthquake Engineering (WCEE), Lisboa, Portugal, Sept. 24-28, 2012.

Taylor, D.A. (1975). Progressive collapse. Canadian Journal of Civil Engineering. Doi: http://www.nrcresearchpress.com/doi/pdf/10.1139/l75-047

Thelandersson, S., & Honfi, D. (2009). Behaviour and modelling of timber structures with reference to robustness. COST actions TU0601 and E55 – Modelling of performance of timber structures: 6th Workshop. University of Ljubljana, Ljubljana, Slovenia.

Thelandersson, S., & Larsen, H.J. (2003). Timber engineering. New York: Wiley Publishing Ltd.

Tohidi, M. (2015). Effect of floor-to-floor joint design on the robustness of precast concrete cross wall buildings. PhD Thesis, University of Birmingham, Birmingham, UK.

TRADA. (2009). Worked Example. - 12-storey building of cross-laminated timber (Eurocode 5). Timber Research and Development Association, Buckinghamshire, UK.

Turk, T., Elhady, M.T., Rashed, S., Abdelkhalek, M., Nasef, S.A., Khallaf, A.M., et al. (2018). Quality of reporting web-based and non-web-based survey studies: what authors, reviews and consumers should consider. PLOS One 13. doi:10.1371/journal.pone.0914239.

United Nations. (2014) World Urbanization Prospects: The 2014 revision, highlights (ST/ESA/SER.A/352). <https://www.compassion.com/multimedia/world-urbanization-prospects.pdf> (April 13, 2017).

UN-Habitat. (2008). State of the world's cities 2008/2009 – Harmonious cities. < https://unhabitat.org/books/state-of-the-worlds-cities-20082009-harmonious-cities-2/> (May 18, 2014).

Vaisey, S. (2009). Motivation and justification: A dual-process model of culture in Action. American Journal of Sociology 114 (6):675–1715.

Van Selm, M., & Jankowski, N.W. (2006). Conducting Online Surveys. Quality & Quantity 40: 435-456. https://doi.org/10.1007/s11135-005-8081-8.

Wang, Y., Lin, F., & Gu, X. (2011). Load and resistance factors for progressive collapse resistance design of reinforced concrete building structures. Advances Materials Research 255-260:388–344.

Weigand, J., Bao, Y., & Main, J. (2017). Acceptance criteria for the nonlinear alternative load path analysis of steel and reinforced concrete frame structures. ASCE Structures Congress, Denver, , April 6-8, 2017.

Wells, M.(2011). Tall timber buildings: Applications of solid timber construction in multistory buildings. CTBUH Research paper 2011(1):24–7.

Weyerhaeuser. (2018). TimberStrand LSL beams.<https://www.weyerhaeuser.com> (Oct.14, 2018).

Winter, S., & Kreuzinger, H. (2008). The Bad Reichenhall Ice arena collapse and the necessary consequences for wide span timber structures. World Conference on Timber Engineering (WCTE), Miyakazi, Japan, June 2-5, 2008.

Wood-Works. (2016). Construction advantages sell hotel deveoper on CLT - CLT builds faster and more safely with fewer workers. <http://www.woodworks.org/> (accessed December 10, 2018).

WoodCampusUK. (2017). Architect Andrew Waugh on CLT (Timber| The Building Material of the Future). < https://www.youtube.com/watch?v=22GtgUnmICo> (Aug. 14, 2018).

Wood Solutions. (2018). 21 Reasons why wood is better: Prof. Alex de Rijke. < https://www.woodsolutions.com.au/blog/21-Reasons-Why-Wood-is-Better-Prof-Alex-de-Rijke> (Dec. 13, 2018)

Woschitz, R., & Zotter, J. (2017). High-rise Timber Building HoHo Vienna – The structural Concept. Österreichische Ingenieur- Und Architekten-Seitschrift 162(1-12): 63-68.

Wright, K. B. (2005). Researching Internet-Based Populations: Advantages and Disadvantages of Online Survey Research, Online Questionnaire Authoring Software Packages, and Web Survey Services. Journal of Computer-Mediated Communication 10 (3) JCMC1034. doi.org/10.1111/j.1083-6101.2005.tb00259.x

Yin, Y., & Li, Y. (2010). Seismic collapse risk of light-frame wood construction considering aleatoric and epistemic uncertainties. Structural Safety 32(4):250–261.

Zhang, X., Popovski, M., & Tannert, T. (2018). High-capacity hold-down for mass-timber buildings. Construction and Building Material 164: 688–703.

Zhu, H., Faghani, P., & Tannert, T. (2017). Experimental investigations on timber joints with single glued-in FRP rods. Construction and Building Material 140:167–72.

Appendices

A.1. Modelling of point supported CLT Floor

The FE model of CLT panels were validated against experimental testing performed by Popovski et al. (2016). This was a double span, point supported CLT floor system tested to investigate the structural performance including the stiffness, deformability, load-carrying capacity and the failure mechanisms. The panels were 5-ply CLT, 170mm thick (40-30-30-30-40). As study did not give the material properties of the CLT panels, the following assumptions were made during the model: i) the panels were modelled using four-node shell elements with both membrane and bending stiffness; ii) the cross-section were defined according to the CLT layup, with the top layer longitudinal to the span direction, and the remaining layers oriented crosswise; iii) the elastic material properties on the Table A.1.1 were used for calibration; and iv) the point-supports had no rotation restraints and were modelled using rigid shell elements of the same area as the GLT column below, to avoid stress concentration; v) the load was applied as a displacement, on an area in the centre of the panel, to avoid high stress concentration, as done during the tests. The dimensions in Figure A.1.1 were used to build the model, and the analysis was static linear.

Table A.1.1: Material properties of CLT panels

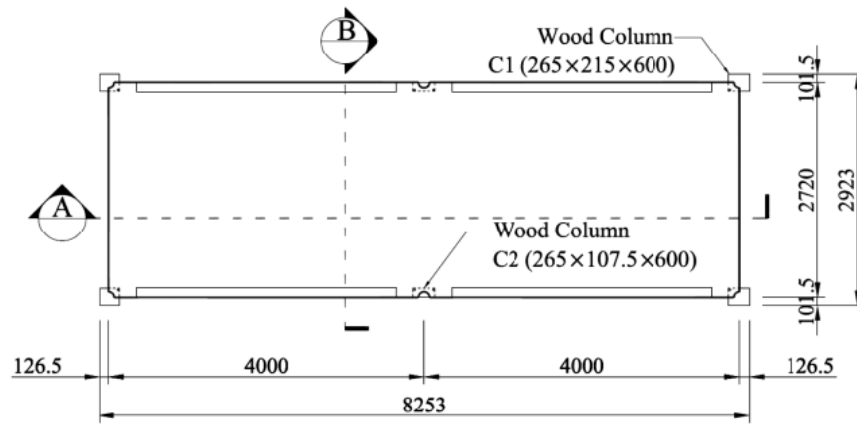| Layer Direction	E_L [MPa]	ET [MPa]	G_L [MPa]	G_T [MPa]	U_L [~]	U_T [~]
Longitudinal (*L*)	12,400	$E_L/30$	$E_L/16$	$G_{LT}/10$	0.35	0.07
Transverse (*T*)	9,000	$E_L/30$	$E_L/16$	$G_{LT}/10$	0.35	0.07

Figure A.1.1: Plan view of the tested point supported CLT floors (Popovski et al., 2016)

Figure A.1.2a illustrates the deformed shape of the point supported CLT floor panel under the applied deformation. Figure A.1.2b shows that the FE model agreed with the experimental tests in terms of load-deformation curves.
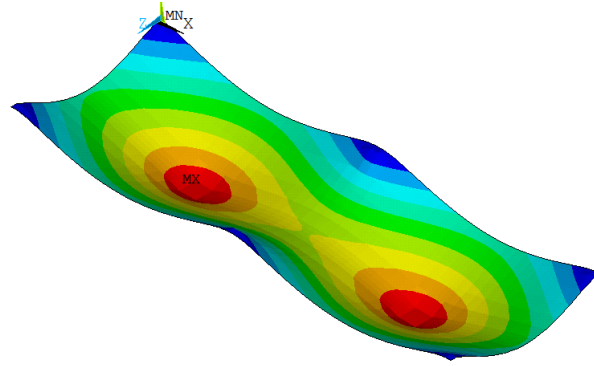
(a)
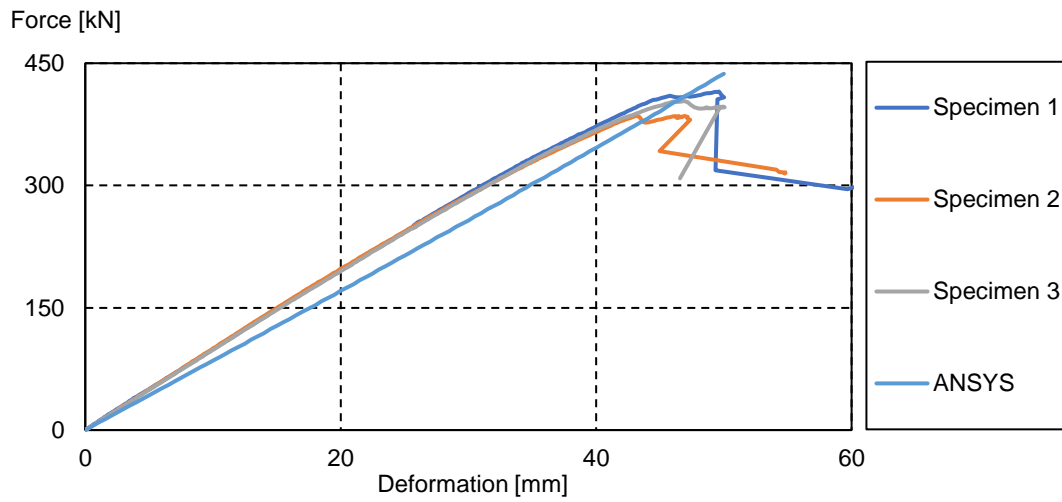
(b)

Figure A.1.2: (a) Deformed shape of the FE model of the point supported CLT floor; and (b) Comparison of load-deflection curves

A.2. Derivation of Tie-force Formulae

A.2.1 Catenary Action

Figure A.2.1.1. illustrates 2D schematic representation of floor catenary action. The horizontal tie-force was derived as follows:

$$F_\mathrm{T} \times \mathit{\Delta} = \frac{w_\mathrm{f} \times L^2}{8} \tag{A.3.1.1}$$

$$F_T = \frac{w_f \times L^2}{8 \times \Delta} \qquad\qquad (A.3.1.2)$$

The compatibility between vertical and horizontal deformations was derived from trigonometry as follows, where $\delta_L = (\delta_s + \delta_m)$ elongation on a single span (L_1) only

$$\delta_L = \sqrt{L_1^2 \times \Delta^2} - L_1 \qquad\qquad (A.3.1.1)$$

$$\delta_L = L_1 \times \left(\sqrt{1 + \left(\frac{\delta_s}{L_1}\right)^2} - 1 \right) \qquad\qquad (A.3.1.2)$$
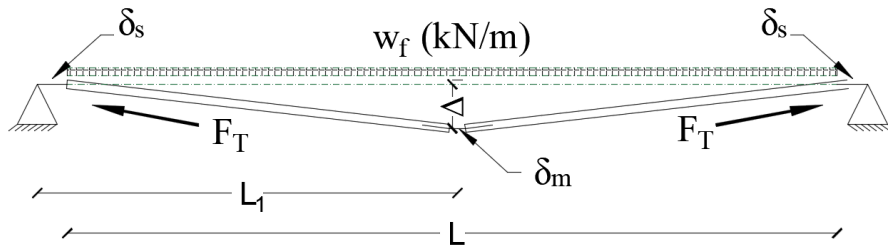

Figure A.2.1.1: 2D Schematic representation of floor catenary action

A.2.2. Cantilever Action

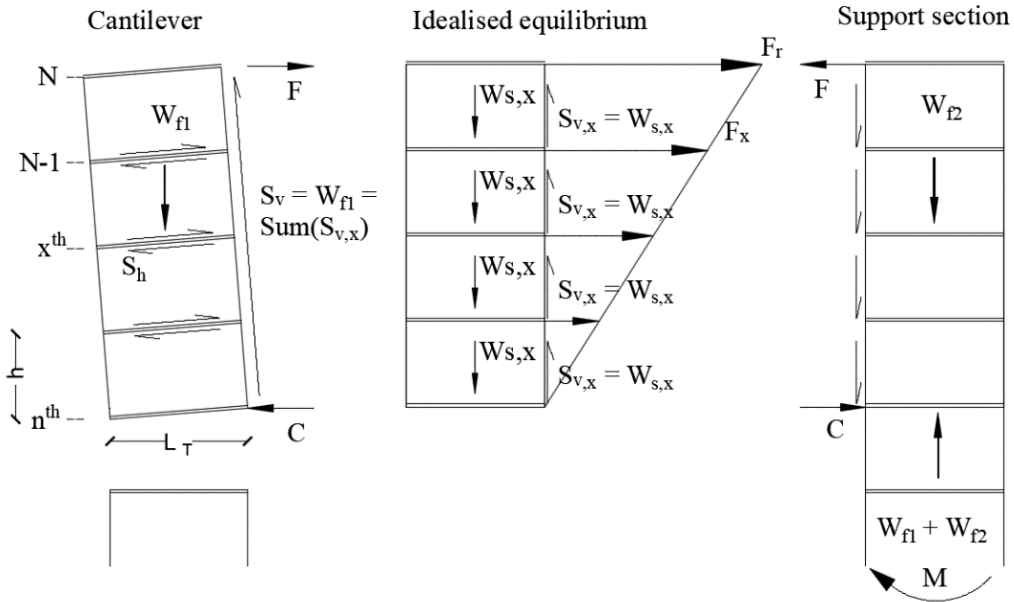Figure A.2.2.1. is a 2D schematic representation of the cantilever action.

Figure A.2.2.1: 2D schematic representation of Cantilever action

The transverse ties, horizontal and vertical shear were derived as follows:

$$W_{f1} = \left(w_s \times (N - n)\right) \times L_T \tag{A.3.2.1}$$

$$F_x = \frac{F_r}{(N - n)} \times (N - i) \tag{A.3.2.2}$$

$$M_A = w_s \times (N - n) \times L_T \times \frac{L_T}{2} \tag{A.3.2.3}$$

$$M_R = \sum_{i=n}^{N} \left(F_r \times \frac{N - i}{N - n}\right) \times (h \times (N - i)) \tag{A.3.2.4}$$

Where (N-n) is the total cantilever, (i-n) is the height of interest within the cantilever, w_s is the floor loads in kN/m, and F_x is the transverse force at the height of interest, F_r is the transverse tie force at the roof, M_A is the applied moment due to the weight of the cantilever about point C, and M_R is the resisting moment provided by the transverse ties. F_r can therefore be found by equating M_A and M_R.

$$F_r = \frac{(N-n)^2 \times w_s \times L_T^2}{2 \times h \times \sum_{i=n}^{N}(N-i)^2} \qquad\qquad \text{(A.3.2.5)}$$

$$F_x = F_r \times \frac{(x-n-1)}{(N-n)} \qquad\qquad \text{(A.3.2.6)}$$

The shear force (S_{hx}) at the horizontal joints between consecutive storey panels is at its lowest value at the top storey (roof) and is of the same magnitude as F_r. This shear value increases by the amount of the force of the transverse tie (F_x) at each level:

$$S_{hx} = \left((N-n) \times \frac{\sum_{i=x}^{N}(i-n)}{\sum_{i=n}^{N}(N-i)^2} \right) \times \frac{w_s \times L_T^2}{2 \times h} \qquad n+1 \leq x \leq N \qquad \text{(A.3.2.7)}$$

$$S_{hx} = \sum_{i=x}^{N} F_r \times \frac{i-n}{N-n} \qquad\qquad n+1 \leq x \leq N \qquad \text{(A.3.2.8)}$$

$$S_{hx} = \sum_{i=n+1}^{N} F_r \times \frac{i-n}{N-n} \qquad\qquad \text{At point } C \text{ only} \qquad \text{(A.3.2.9)}$$

The shear in the vertical joint between the cantilever and the support is distributed uniformly with throughout the height of the cantilever, assuming all storeys have the same weight (w_s). Assuming

the biggest opening at roof level (δ_N) is linearly distributed along the height of the cantilever, the opening at each floor (δ_x) can be estimated using similar triangle analogy.

$$S_v = w_s \qquad\qquad\qquad\qquad\qquad\qquad \text{(A.3.2.10)}$$

$$\delta_x = \frac{x - 1}{N - 1} \times \delta_N \qquad\qquad\qquad\qquad\qquad \text{(A.3.2.11)}$$

A.3. Multiplas Material Properties for Wood

Ansys simulation using Multiplas was calibrated to obtain the same behaviour as experimental testing of wood specimens in compression, shear and tension. The model used Multiplas law #33, described as orthotropic boxed model for wood. Inputs for linear and nonlinear material properties are given from Table A.3.1 to Table A.3.5, all in reference to Figure A.3.1.
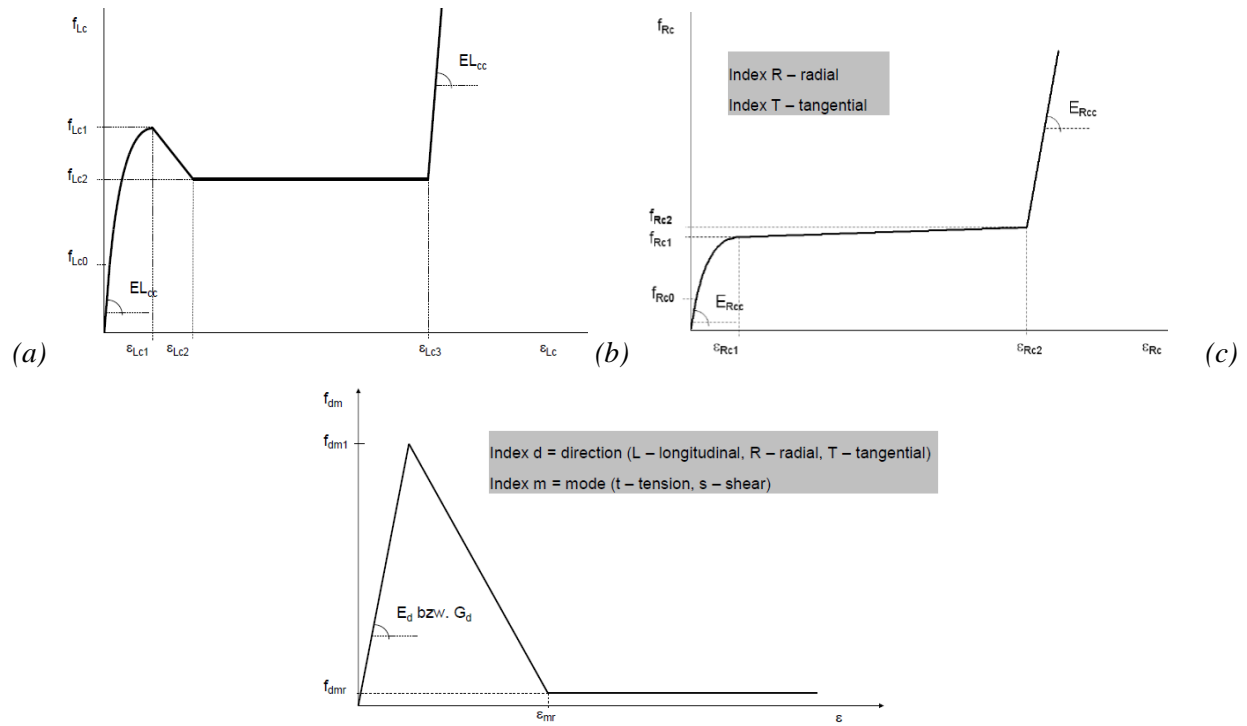
Figure A.3.1: (a) Uniaxial stress-strain curve of timber model in longitudinal compression; (b) Radial or tangential compression; and (c) Shear failure and tensile failure (Dynardo, 2016)

Table A.3.1: Plastic parameters of wood

Parameters description	Values
f_{Lc0}	25.2MPa
f_{Lc2}	22.3MPa
e_{Lc1}	0.017280
e_{Lc2}	0.031416
e_{Lc3}	0.11
f_{Rc0} and f_{Tc0}	3.41MPa
f_{Rc2} and f_{Tc2}	5.89MPa
e_{Rc1}	0.042011
e_{Rc2}	0.128405

Table A.3.2: Initial parameters of wood

Parameters description	Values [MPa]
Uniaxial tensile strength in longitudinal direction (f_{Lt})	20.4
Uniaxial compressive strength in the longitudinal direction (f_{Lc})	28.9
Uniaxial tensile strength in radial/tangential direction (f_{Rt})	5.1
Uniaxial compressive strength in radial/tangential direction (f_{Rc})	4.7
Radial/longitudinal or Tangential/longitudinal shear strength (f_{RLs})	8.7
Radial/tangential or Tangential/radial shear strength (f_{RTs})	5.6

Table A.3.3: Hardening/softening parameters longitudinal compression

Parameters description	Range
Relative stress level at start of initial hardening (Ω_{LC0})	f_{Lc0}/f_{Lc}
Hardening variable (plastic strain) at longitudinal compressive strength (κ_{LC1})	$e_{Lc1}-f_{Lc}/E_L$
Relative stress level in ideal plastic domain (Ω_{LC1})	f_{Lc2}/f_{Lc}
Hardening variable (plastic strain) defining start of the ideal plastic domain (κ_{LC2})	$e_{Lc2} - \Omega_{Lc2} \times f_{Lc}/E_L$
Hardening variable (plastic strain) defining end of ideal plastic domain (κ_{LC3})	$e_{Lc3} - \Omega_{Lc2} \times f_{Lc}/E_L$

Table A.3.4: Hardening/softening parameters radial or tangential compression

Parameters description	Range
Relative stress level at start of initial hardening (Ω_{LC0})	f_{Rc0}/f_{Rc}
Hardening variable (plastic strain) at radial compressive strength (κ_{RC1})	$e_{Rc1} - f_{Rc}/E_R$
Relative stress level at the end of plastic domain (Ω_{RC2})	f_{Rc2}/f_{Rc}
Hardening variable (plastic strain) defining end of plastic domain (κ_{RC2})	$e_{Rc2} - \Omega_{Rc2} \times f_{Rc}/E_R$

Table A.3.5: Shear/tensile strength softening parameters

Parameters description	Range
Relative residual longitudinal or radial or tangential tensile strength (Ω_{Ltr}) and (κ_{Ltr})	0.01 and $5 \times f_{Lt}/E_L$
Relative residual radial/longitudinal or radial/tangential or tangential/longitudinal or tangential/radial shear strength (Ω_{RLsr}) and (κ_{RLsr})	0.01 and $5 \times f_{RLs}/G_{RL}$

A.4. Connection Material Properties

A.4.1. Spline Self-tapping screws Connections

The experimental data used to calibrate the spring elements representing STSs in a spline connection were obtained from Hossain et al. (2016). The surface spline joint shown in Figure A.4.1.1a. The connection was tested on 5 Ply CLT panels. The slots for the plywood were 25mm deep and 40mm wide. The screws were ASSY Ecofast STSs, 100mm long. Figure A.4.1.1b shows the experimental setup for a single shear plane. Each tested connection was composed of six STSs to meet the spacing requirements of the Canadian product approval (CCMC 13677-R).
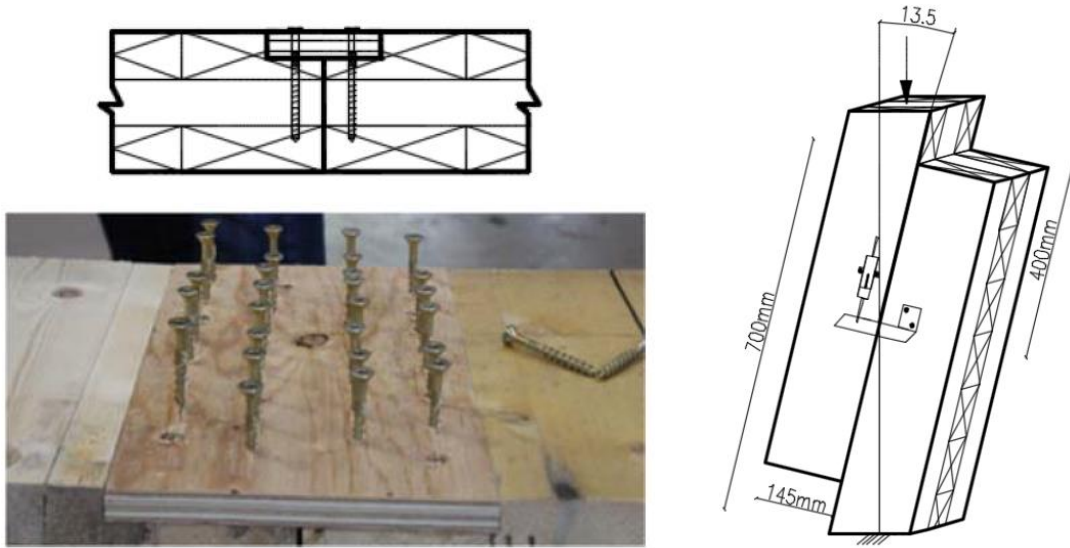
Figure A.4.1.1: (a) Surface spline joints with STSs in shear ; and (b) Test setup specimens with one shear plane (Hossain et al., 2016)(Reprinted with permission)

Figure A.4.1.2 shows the average shear test results obtained by Hossain et al. (2016). These results were used to obtain the Equivalent Energy Elastic Plastic (EEEP) curve. The yield force and displacement from the EEEP curve were used as inputs for the spring elements representing surface spline connections, in the FE modelling. For the FE model, these values were divided by the total number of fasteners (six) in order to obtain the behaviour of a single shear.
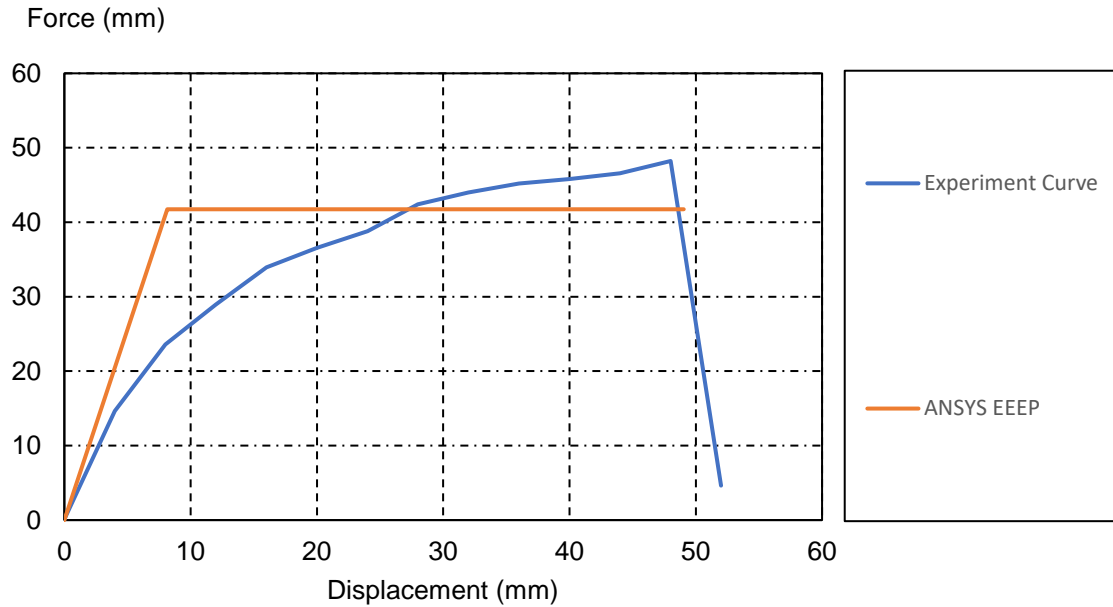
Figure A.4.1.2: Force against the applied deformation curves: Experimental results (Hossain et al., 2016) against EEEP curve used in Ansys model

A.4.2. Angle Brackets and Nails Connections

For the angle brackets, the test results were obtained from experimental testing by Gavric et al. (2013). The considered connection was angle bracket 100×100×90×3, used to connect CLT wall on CLT floors. To connect the bracket to the wall panel, eight 4×60mm annular ring nails were used. To connect the bracket to the floor panel, six 4×60mm annular ring nails and two 4×60mm HBS screws were used. The test setup loaded the connection in shear. Figure A.4.2.1 shows the test results along with the EEEP curve used as input values for the spring elements in the FE model to represent angle bracket and nail connections.
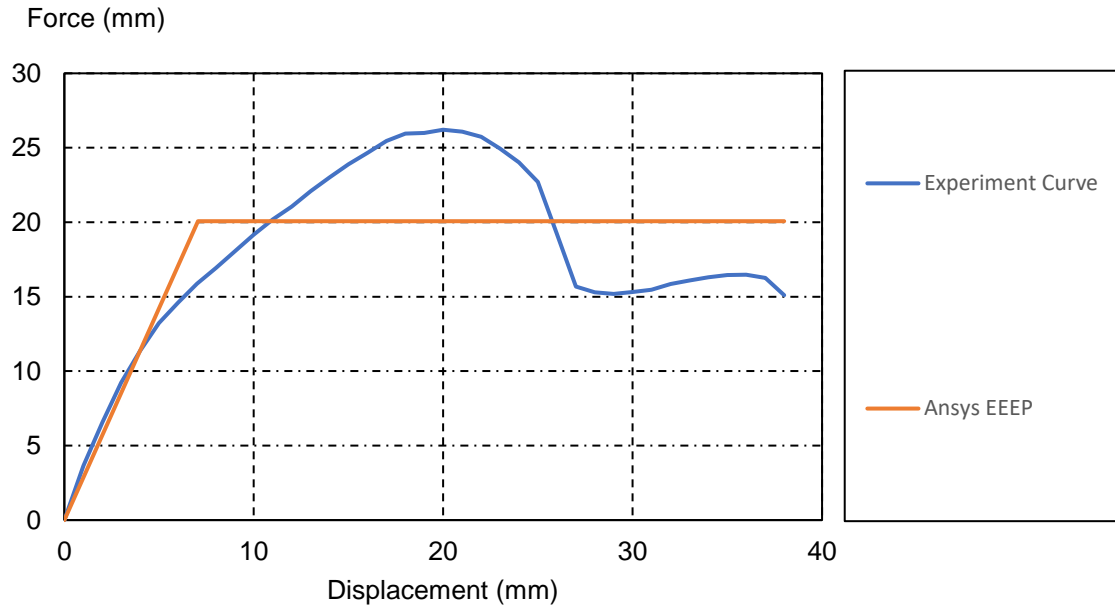
Figure A.4.2.1: Force against the applied deformation curves: Experimental results (Gavric et al., 2016) against EEEP curve used in Ansys model

A.5. Bone-shape Steel Specimens: Test Results

Figure A.5 illustrates the average stress-strain curve of the tested bone-shape steel specimens. The

result shows that the specimens were not ductile, with an ultimate strength of 760MPa
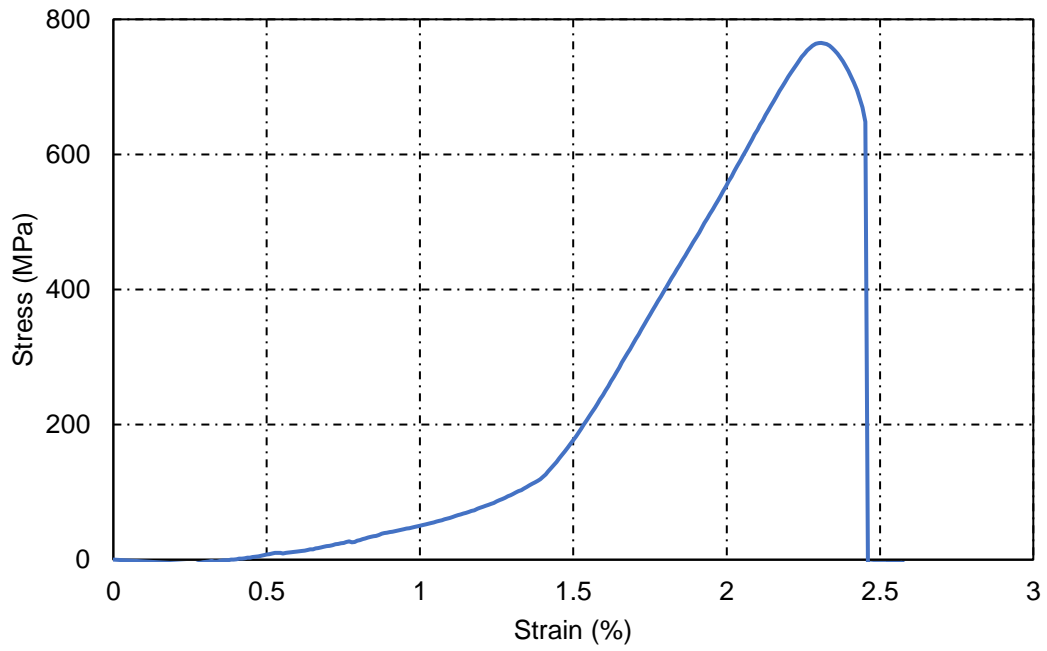
Figure A.5: Experimental results of bone-shape steel specimens: Stress vs Strain curve